

Annual Report

2012-2013

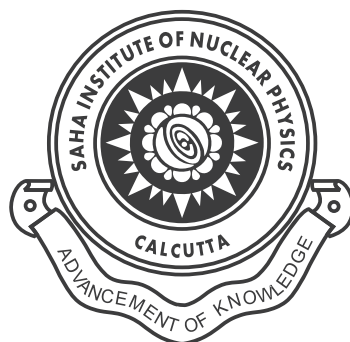


Saha Institute of Nuclear Physics
Kolkata

Saha Institute of Nuclear Physics

Annual Report

2012–2013



Saha Institute of Nuclear Physics
1/AF Bidhan Nagar, Kolkata 700 064
India

Tel: (33) 2337-5345-49 (5 lines)
Fax: (33)-2337-4637
<http://www.saha.ac.in>

Editorial Team

Prof Milan Kumar Sanyal
Prof Palash Baran Pal
Prof Abhijit Chakrabarti
Prof Maitryee Saha Sarkar
Prof Tapas Kumar Chini
Prof Munna Sarkar
Prof Suchandra Dutta
Shri Amit Kumar Saha
Shri Jeevan Shaw

Creation

Prof Abhijit Chakrabarti
Shri Amit Kumar Saha

Photographs

Shri Pradip Das

Cover Design & Printed at
Sailee Press Pvt Ltd

Published by

Registrar, SINP
on behalf of
Centre for Advanced Research & Education
Saha Institute of Nuclear Physics

January 11, 2014

Contents

Foreword	7
From the Desk of the Editorial Team	9
1 Biophysical Sciences including Chemistry	11
1.1 Summary of Research Activities of Divisions	11
1.1.1 Biophysics	11
1.1.2 C&MB	11
1.1.3 Chemical Sciences	12
1.1.4 Structral Genomics	13
1.2 Research Activities	13
1.2.1 Biophysics	13
1.2.2 C&MB	16
1.2.3 Chemical Sciences	21
1.2.4 Structral Genomics	33
1.3 Developmental Work	35
1.4 Publications	36
1.4.1 Publications in Books/Monographs & Edited Volumes	36
1.4.2 Publications in Journal	36
1.5 Ph D Awarded	41
1.6 Seminars/Lectures given in Conference/Symposium/Schools	41
1.7 Honours and Distinctions	43
1.8 Teaching elsewhere	43
1.9 Miscellany	43
2 Condensed Matter Physics including Surface Physics and NanoScience	45
2.1 Summary of Research Activities of Divisions	45
2.1.1 Applied Material Science	45
2.1.2 Experimental Condensed Matter Physics	46
2.1.3 Surface Physics	46
2.1.4 Theoretical Condensed Matter Physics	48
2.2 Research Activities	50
2.2.1 Applied Material Science	50
2.2.2 Experimental Condensed Matter Physics	56
2.2.3 Surface Physics	59
2.2.4 Theoretical Condensed Matter Physics	67
2.3 Developmental Work	73

2.4	Publications	73
2.4.1	Books/Monographs Publications & Edited Volumes	73
2.4.2	Publications in Journal	74
2.5	Ph D Awarded	79
2.6	Seminars/Lectures given in Conference/Symposium/Schools	79
3	Experimental Nuclear and Particle Physics	83
3.1	Summary of Research Activities of Divisions	83
3.1.1	Applied Nuclear Physics	83
3.1.2	High Energy Nuclear and Particle Physics	84
3.1.3	Nuclear Physics	86
3.2	Research Activities	87
3.2.1	Applied Nuclear Physics	87
3.2.2	High Energy Nuclear and Particle Physics	90
3.2.3	Nuclear Physics	92
3.3	Developmental Work	96
3.4	Publications	101
3.4.1	Books/Monographs Publications & Edited Volumes	101
3.4.2	Publications in Journals	101
3.5	Seminars/Lectures given in Conference/Symposium/Schools	112
3.6	Teaching elsewhere	114
4	Plasma Physics	115
4.1	Summary of Research Activities of Divisions	115
4.1.1	Plasma Physics	115
4.2	Research Activities	116
4.2.1	Plasma Physics	116
4.3	Developmental Work	122
4.4	Publications	122
4.4.1	Publications in Journal	122
4.5	Seminars/Lectures given in Conference/Symposium/Schools	124
4.6	Teaching elsewhere	125
5	Theoretical Physics	127
5.1	Summary of Research Activities of Divisions	127
5.1.1	Astroparticle Physics and Cosmology	127
5.1.2	Theory	129
5.2	Research Activities	132
5.2.1	Astroparticle Physics and Cosmology	132
5.2.2	Theory	136
5.3	Developmental Work	150
5.3.1	Astroparticle Physics and Cosmology	150
5.4	Publications	150
5.4.1	Publications in Books/Monographs & Volumes Edited	150
5.4.2	Publications in Journal	150
5.5	Ph D Awarded	155
5.6	Seminars/Lectures given in Conference/Symposium/Schools	155
5.7	Honours and Distinctions	157

5.8	Teaching elsewhere	158
5.9	Miscellany	158
5.10	Computational Science	158
5.11	Summary of Research Activities of Divisions	158
5.11.1	Computational Science	158
5.11.2	Research Activities	159
5.11.3	Developmental Work	161
5.11.4	Publications in Journal	161
5.11.5	Seminars/Lectures given in Conference/Symposium/Schools	162
6	Research Fellows/Visiting Fellows/Research Associates	163
7	Facilities	167
7.1	Centre for Advanced Research & Education	167
7.1.1	The Post-M Sc Associateship Course	169
7.1.2	Summer Students' Programme	172
7.1.3	Under Graduate Students' Programme	173
7.2	Electron Micorscope Facility	173
7.3	Library	173
7.4	Central Workshop	175
8	Administration	177
8.1	Governing Council	177
8.2	Audited Accounts	178
8.3	Balancesheet	178
8.4	Income & Expenditure Account for the year ended March 31, 2013	179
8.5	Receipts & Payments for the year ended March 31, 2013	180
8.6	Purchase Section	180
8.7	Members of the Institute [As on March 31, 2013]	181
9	External Collaborators	187
10	Index	191

Foreword

I am extremely happy to write the foreword of this annual report. It is obvious from large numbers of quality publications from our institute that setting up of state-of the art laboratories over XIth Plan Period and Science Review process with national and international experts has started giving us results. Particularly noteworthy contributions from our institute was on (a) determining the density content of symmetry energy and neutron skin, (b) common origin of fermion mixing and geometrical CP violation (c) fixed-energy sandpiles belonging generically to directed percolation. We have signed an agreement with Cavendish Laboratory, University of Cambridge for joint-PhD program to initiate collaboration between our institutes. In this program, two scientists from each side will be guides of a jointly selected student, who will work 50% time in each institute and PhD degree will be given by Cambridge University. Cambridge Commonwealth Trust has agreed to support five students initially in next three years, for their stay in Cambridge, to promote this Saha-Cambridge Scholarship program.

SINP has developed an Indian Beamline at Photon Factory Synchrotron, KEK, Japan and 15 research institutes from India have already used this beamline. This beamline has been opened for international use on 16th March, 2013. In this beamline one can carry out (a) Powder diffraction from (nano) materials as a function of temperature and high-pressure to perform phase transition studies (b) Reflectivity and diffuse scattering from solid and liquid surfaces decorated with nano particles and buried interfaces of nano-structured materials (c) Small angle x-ray scattering (SAXS) experiments - both in transmission and reflection geometry. SINP has also become the nodal institute for Indian access to PETRA-III synchrotron at DESY, Germany.

SINP has contributed significantly in LHC activities at CERN through CMS and ALICE collaborations. SINP contribution in the search of Higgs-Boson at CMS has received considerable attention particularly in gamma-gamma channel.

We have organized two major international conferences, namely 'Surface X-ray and Neutron Scattering (SXNS-12)' and 'Conference on Electron Microscopy (EMSI)'. We have brought back the first horizontal microscope of Asia developed by the faculty members of our institute and kept it in the auditorium for general display to inspire school and college students who visit regularly our institute.

SINP has also organized special session on 'Strategic Science' during 100th Indian Science Congress involving Defence Research & Development Organisation, Department of Space and Department of Atomic Energy.

Prof Milan K Sanyal
Director

January 11, 2014

From the Desk of the Editorial Team

This annual report contains activities of Saha Institute of Nuclear Physics (SINP) from April 2012 till March 2013. The nature of research work and developmental activities carried out during this period for a multi-disciplinary institute like ours is wide in spectrum. Like in previous reports, we stuck to the policy of accommodating the accomplished research work by collecting the research papers published by our institute members during this period in journals enlisted in the ISI Web of Science. Each document in the research activities section for each of the five major areas of research pursued in the Institute contains title of the paper, summary of the work as described in the abstract, and list of authors for each paper. This time, we have been also able to publish research highlights from the voluntary inputs of various faculty members. Towards this, a short summary of on-going research and/or developmental work, not published anywhere else, have been included in the report. The list of publications also contains papers published in journals outside the list of the ISI Web of Science. Needless to say that research at SINP, like research at any other academic institute, is enriched by collaboration across the boundaries of divisions and institutes. Accordingly, the authors' lists on many of the research activities include researchers belonging to other institutes. At the end of the report, names and affiliations of collaborators have been enlisted. For convenience of reference, the names of external collaborators are marked with dagger (†) in the research activities section. In addition to the work that appeared in this annual report, there is a huge body of contributions in the form of oral presentations and posters by research students, post-doctoral fellows and faculty members in different national and international symposia, workshops and schools including DAE symposia. Those could not be included due to constraints of space. We have only included lists of invited talks in this report. The editorial team apologizes if any important information has been left out despite the sincerest efforts; and wishes to thank all the institute members for their inputs, support and feedback during the course of collection of information and editing process for making of this Annual Report 2012-'13.

January 11, 2014
Kolkata



Prof. J Narlikar receiving memento from the Director after delivering the 50th Saha Memorial Lecture, April 5, 2012



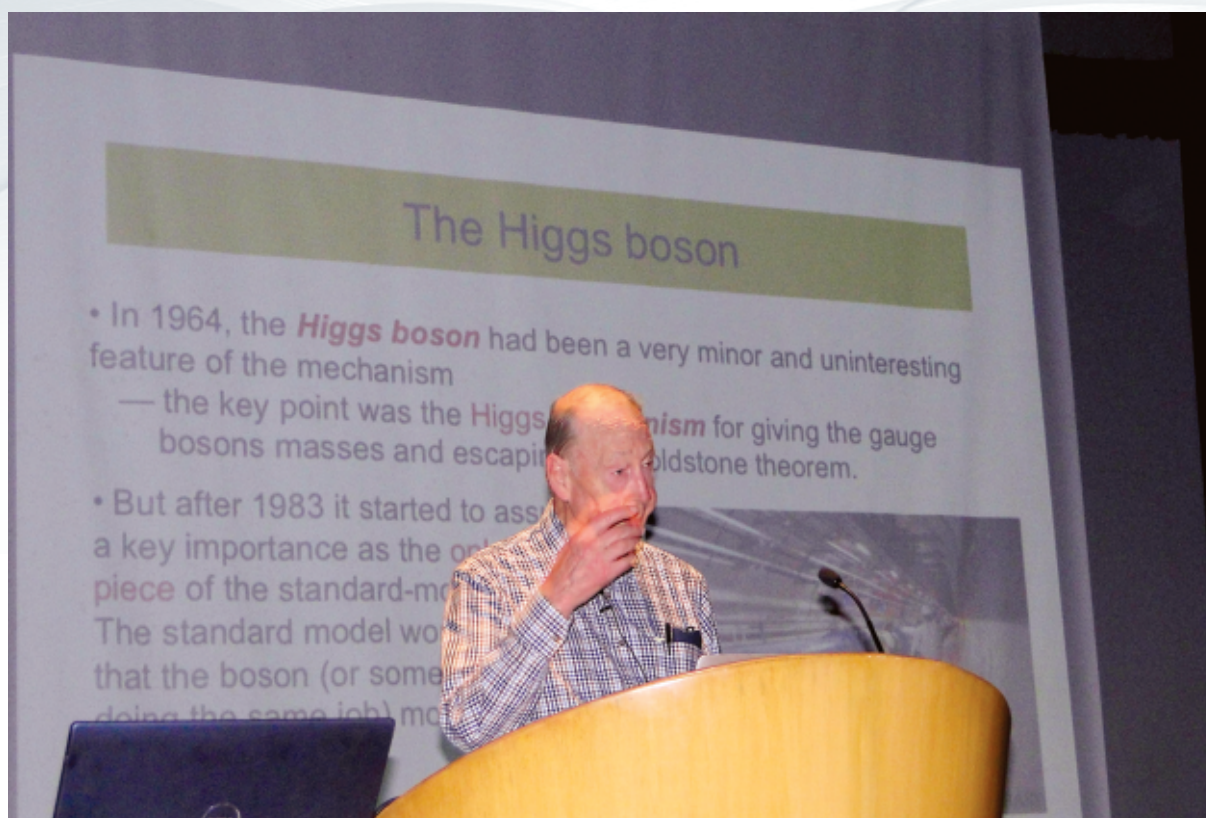
Dignitaries from DAE participating in an Outreach Programme at SINP on the occasion of 100th year of Indian Science Congress, January 6, 2013



Dr. Arunava Sengupta speaking on cancer awareness, organized by CARE, October 5, 2012



Prof. C N R Rao delivering lecture in the symposium on Frontiers of Materials Science on February 10, 2013



Third R N Tagore Lecture delivered by Prof. T W B Kibble on December 7, 2012



School students visiting SINP pavilion in 16th National Exhibition, Baguihati, Kolkata, September 9, 2012



Dr. R K Sinha, Chairman, Atomic Energy Commission and Chairman, Governing Council of SINP, with Prof. M K Sanyal, in a SINP Laboratory visit, February 2, 2013



Prof. Amit Ghosh delivering lecture on 63rd Foundation Day, January 11, 2013

Chapter 1

Biophysical Sciences including Chemistry

1.1 Summary of Research Activities of Divisions

1.1.1 Biophysics

In the areas of chemical and structural biology studies on the recognition of multiple stranded DNA (Quadruplex) and putative anticancer agents from plant source have shown that one such agent, ellipticine binds to DNA with a 3:2 stoichiometry in terms of ellipticine: DNA. It also inhibits the telomerase activity. These results indicate an additional/alternate mode of action of this compound under in vivo condition. The list of bivalent metal ion containing enzymes as a binder to the anticancer drug mithramycin, has been expanded to include metallo beta-lactamase, enzyme used by a class of drug resistant bacteria. Structural biology and biophysical studies on lamins whose mutations are responsible for cardiomyopathy, include examination of the effect of point mutations on the structure and function of lamin A by applying a range of biophysical and cell biological techniques. This elucidated that homotypic interaction between the lamin A proteins are altered as a sequel to the mutations which in turn modifies the network structure of the nuclear scaffold. Studies on the chemical biology of chromatin including the epigenetic regulation of chromatin structure have been done in the following areas. Dual binding modes, i.e. the ability to bind both chromosomal DNA and core histone(s), for DNA-binding ligands like ethidium bromide and propidium iodide have been demonstrated. Post translational modification of histone tails functions as a signal platform to recruit effector modules or readers to local chromatin which then dictate the on or off state of the underlying genes. Sp110 is a nuclear body protein harbouring the chromatin binding modules and exhibiting a strong affinity for chromatin. Its preferential site of interaction onto chromatin has been identified. An altered expression of this candidate in RNA and protein level upon differentiation of neuroblastoma cell lines and mouse primary neuron culture has also been noticed.

1.1.2 C&MB

The major goals of the work carried out in the division was to understand the key biological processes using tools for three dimensional (3-D) structure determination and cell and molecular biology. As a part of the general goal, during April 2012 to March 2013, 3-D structures various proteins like Psu from bacteriophage P4, involves in transcription termination in bacteria and thermostable mutant of pro-papain were solved. It is revealed that Psu exists as a knotted homodimer

and is first of its kind in nature. Structure of Psu provides mechanistic views on how Psu folds and reassembles. On the other hand, overall structure of mature part of protease pro-papain was found to be similar to those of other members of the family. Result obtained explains the bimolecular stepwise autocatalytic activation mechanism by limited proteolysis of the zymogen of papain at the molecular level. In addition, 3-D structures of two engineered winged bean chymotrypsin inhibitor (WCI) complexed with Bovine trypsin (BPT) namely L65R-WCI:BPT and F64Y/L65R-WCI:BPT show that the inhibitory loop of these engineered inhibitors are recognized and rigidified properly at the enzyme active site like other strong trypsin inhibitors. Cloning, expression, purification, crystallization and preliminary X-ray analysis of a fructokinase and two low-molecular-weight protein tyrosine phosphatases (VcLMWPTP-1 and VcLMWPTP-2) from *Vibrio cholerae* O395 have been reported. It has been shown that expression of recombinant human cathepsin K is increased by codon optimization. Computational algorithm has been developed to explain protein-protein interactions based on the electrostatic complementarity and surface (or shape) complementarity of interior residues. It was confirmed by site-directed mutagenesis that RXL-like cyclin-binding (Cy) motif dependent interaction of LdHAT1 with LdCyc1 is essential for its phosphorylation at a canonical Cdk target site by the kinase complex. Phosphorylation of LdHAT1 by the S-phase kinase inhibits its H4K10 acetylation activity, implicating a mechanism of periodic regulation of histone acetylation during cell cycle progression. Thirty six interacting partners of HYPK was identified. Various experimental and computation analysis of the interacting partners of HYPK reveal that HYPK together with its interacting partners involve in several biological processes like protein folding, response to unfolded protein, cell cycle regulation, apoptosis and regulation of transcription. Analysis of the validated targets of altered miRNAs in Huntingtons disease reveals that they might be involved in apoptosis, differentiation and development, fatty acid, cholesterol, lipid, glucose, and carbohydrate metabolism, cell cycle and growth and transcription regulation. Besides, micro RNA 125b has been shown to involve in cell cycle regulation by targeting MDA1 protein.

1.1.3 Chemical Sciences

The members of Chemical Sciences Division are currently engaged in research encompassing different areas in Chemical Sciences. A two colour Single molecule FRET imaging set up for real time monitoring of complex macromolecular systems has been developed. Computational studies for a new mechanism for the diol formation catalyzed by formic acid has been initiated to show the important mechanistic ramifications for how the gas phase hydrolysis of carbonyl compounds, which is the forbidden process in presence of single water molecule in our atmosphere, can be catalyzed by organic acids in the atmosphere. Radioactivity generation in Accelerator Driven Subcritical Systems employing Pb, Pb-alloy and W has been determined and analysed. Uncertainty and inaccuracy in Volumetric Modulated Arc Therapy Delivery has been evaluated. Preformed copper complexes of two membrane fusion inducing painkillers viz. Piroxicam and Meloxicam have been effectively used as membrane anchors to bridge apposing vesicles to induce fusion with enhanced efficacy than the bare drugs and lead the process to completion. This provides a simple and effective strategy where molecular recognition and strength of interaction between the partners has no role. An integrated experimental and theoretical study has been carried out to establish Hydrogen bond sensitivity and excimer formation of N- containing heterocyclic compounds in micro heterogeneity of binary mixtures and confined media. Modes of interactions of a cyanine dye with proteins have been investigated using spectroscopy, crystallography and theoretical docking study. In addition, applications of conducting polymer based nano materials in biosensing and in developing energy storage devices, single molecule and ensemble spectroscopic studies of protein folding, misfolding

and aggregation and different areas of nuclear chemistry, radiochemistry and green chemistry are also being executed.

1.1.4 Structural Genomics

Structural Genomics Division has been carrying out research in the area of Disease Biology focussing on two major disorders the hematological and neurological. The widely prevalent disease of Eastern India, HbE-thalassemia, along with sickle cell anemia and leukemia are being studied as model for hematological disorders while Alzheimers, Huntingtons, and the Prion diseases are being studied for the neurodegenerative diseases. Differential proteomics studies have been done using clinical samples of cerebrospinal fluid, plasma, urine, red cells, cell extracts and platelets. Hundreds of proteins from these different tissue types are annotated and 10-15 proteins are identified to be differentially expressed in diseases. Redox regulators and chaperone proteins have been found to be up-regulated in hemoglobin disorders. Studies in cell proliferation and differentiation have implicated the roles of self renewal pathways and cross talk between signaling pathways in chronic to blast transformation of CD34+ CML stem cells isolated from patients. Moreover, we have established that cytoplasmic sequestration of the cell cycle inhibitor, p27 led to its interaction with polycomb group of genes (Bmi1, EZH2) and activation of the Rho/Rac GTPase pathway resulting in actin depolymerization which, in turn, caused cellular egression/mobilization from the bone marrow. Currently this pathway is also being investigated to understand the process of metastasis in epithelial cancer. Late onset but eventually fatal neurodegenerative disorders are all caused by altered metabolism of individual proteins that interfere with normal cellular homeostasis. The normal life cycle of a protein, characterized by its biogenesis, trafficking and degradation, are compromised in these disorders resulting in misfolding, misprocessing or mislocalization of the proteins. Most likely, the aberrant protein can then engage in atypical interactions and ultimately lead to a series of unknown events culminating in cell death. The major focus of our research in Alzheimers disease (AD) is to study the downstream pathogenesis of the disease, mediated through AICD and its adaptor network. AICD possesses conserved motifs that are now known to interact with cytosolic adaptor proteins and these interactions in turn affect different signaling pathways. We have shown that Grb2, one such adaptor, interacted with AICD in late endosomal compartments. The excess protein, thus entrapped, could be degraded by autophagy. With Prion disease as a model system, we plan to simultaneously pursue two broad facets: first, understanding the significance of the ESCRT machinery and the endo-lysosomal pathway in PrP-mediated (Prion protein) neurodegenerative diseases. This will aim to provide a molecular explanation for how the loss of function mutation of Mahogunin results in Prion disease like phenotype of spongiform neurodegeneration. Secondly, we also aim to explore how the various essential molecular components that are regulated during endoplasmic reticular stress (ER stress) and aging, both of which manifest in late onset neurodegenerative diseases.

1.2 Research Activities

1.2.1 Biophysics

1.2.1.1 Contrasting binding of fisetin and daidzein in gamma-cyclodextrin nanocavity

Steady state and time resolved fluorescence along with anisotropy and induced circular dichroism (ICD) spectroscopy provide useful tools to observe and understand the behavior of the therapeutically important plant flavonoids fisetin and daidzein in gamma-cyclodextrin (gamma-CDx)

nanocavity. Benesi-Hildebrand plots indicated 1:1 stoichiometry for both the supramolecular complexes. However, the mode of the binding of fisetin significantly differs from daidzein in gamma-CDx, as is observed from ICD spectra which is further confirmed by docking studies. The interaction with gamma-CDx proceeds mainly by the phenyl ring and partly by the chromone ring of fisetin whereas only the phenyl ring takes part for daidzein. A linear increase in the aqueous solubility of the flavonoids is assessed from the increase in the binding of the flavonoids with the gamma-CDx cavity, which are determined by the gradual increase in the ICD signal, fluorescence emission as well as increase in fluorescence anisotropy with increasing (gamma-CDx). This confirms gamma-CDx as a nanovehicle for the flavonoids fisetin and daidzein in improving their bioavailability.

Biswapathik Pahari, Bidisha Sengupta, Sandipan Chakraborty, Pradeep K Sengupta

1.2.1.2 Double plasmonic profile of tryptophan-silver nano-crystals-Temperature sensing and laser induced antimicrobial activity

Surface plasmon resonance (SPR) for spherical shaped silver nanoparticles showing double maxima at ~ 390 nm and ~ 520 nm respectively is reported. Self assembly of silver nanoparticles grown on tryptophan template leads to emergence of equal intensity double plasmon resonance (EIDPR). While for rod shaped nano-forms such double plasmon is explainable but for spherical shaped forms, such double plasmon can be explained on the basis of bidirectional formation of silver cluster in which attachment of silver at two nitrogen atom locations of tryptophan molecule seems to be obligatory. The absence of double resonance in case of silver nanoclusters formed with other amino acids or N-acetyl L-tryptophanamide (NATA), where bidirectional -NH_2 attachment is not possible, validates the proposed EIDPR mechanism. Electron micrograph of EIDPR particle indicates a bi-periodic fringe pattern indicating unusual crystalline property. Apart from sensing tryptophan, the double plasmon peaks are sensitive to temperature. Furthermore, the particle can be used as a smart killing agent showing bactericidal activity only upon exposure to low power laser.

Sarita Roy, Soumen Basak, Pulak Ray, Anjan Kr Dasgupta

1.2.1.3 A revisit of the mode of interaction of small transcription inhibitors with genomic DNA

One class of small molecules with therapeutic potential for treatment of cancer functions as transcription inhibitors via interaction with double-stranded DNA. Majority of the studies of the interaction with DNA have so far been reported under conditions nonexistent in vivo. Inside the cell, DNA is present in the nucleus as a complex with proteins known as chromatin. For the last few years we have been studying the interaction of these DNA-binding small molecules at the chromatin level with emphasis on the drug-induced structural alterations in chromatin. Our studies have shown that at the chromatin level these molecules could be classified in two broad categories: single-binding and dual-binding molecules. Single-binding molecules access only DNA in the chromatin, while the dual-binding molecules could bind to both DNA and the associated histone(s). Structural effects of the DNA-binding molecules upon chromatin in light of the above broad categories and the associated biological implications of the two types of binding are discussed.

Dipak Dasgupta, Parijat Majumder, Amrita Banerjee

1.2.1.4 A critical study on the interactions of hesperitin with human hemoglobin: Fluorescence spectroscopic and molecular modeling approach

Hesperitin, a ubiquitous bioactive flavonoid abundant in citrus fruits is known to possess antioxidant, anti-carcinogenic, hypolipidemic, vasoprotective and other important therapeutic properties. Here we have explored the interactions of hesperitin with normal human hemoglobin (HbA), using steady state and time resolved fluorescence spectroscopy, far UV circular dichroism (CD) spectroscopy, combined with molecular modeling computations. Specific interaction of the flavonoid with HbA is confirmed from flavonoid-induced static quenching which is evident from steady state fluorescence as well as lifetime data. Both temperature dependent fluorescence measurements and molecular docking studies reveal that apart from hydrogen bonding and van der Waals interactions, electrostatic interactions also play crucial role in hesperitin-HbA interactions. Furthermore, electrostatic surface potential calculations indicate that the hesperitin binding site in HbA is intensely positive due to the presence of several lysine and histidine residues.

Sandipan Chakraborty†, Sudip Chaudhuri, Biswapathik Pahari...Pradeep K Sengupta et al

1.2.1.5 Binding and antioxidant properties of therapeutically important plant flavonoids in biomembranes: Insights from spectroscopic and quantum chemical studies

Plant flavonoids are emerging as novel therapeutic drugs for free radical mediated diseases, for which cell membranes mainly serve as targets for lipid peroxidation and related deleterious effects. Screening and characterization of these ubiquitous, therapeutically potent polyphenolic compounds require a clear understanding regarding their binding and possible locations in membranes, as well as quantitative estimates of relevant parameters such as partition coefficients, antioxidant and radical scavenging capacities. In this article we present perspectives emphasizing novel uses of the exquisitely sensitive 'two color' intrinsic fluorescence of plant flavonoids (which arise due to highly efficient photoinduced excited state intramolecular proton transfer (ESIPT) reactions) to explore their binding to model biomembranes consisting of phosphatidylcholine liposomes. Extension of such studies to natural biomembranes of relevant interest is also exemplified. Spectrophotometric assays reveal that typical mono- as well as poly-hydroxy substituted flavonoids have remarkable inhibitory actions on lipid peroxidation, and are significantly more potent antioxidants (2.5-4 times higher) compared to the reference compound Trolox (an water soluble derivative of vitamin E). The structure-activity relationships emerging from such studies are consistent with theoretical predictions based on quantum chemical computations.

Pahari, Biswapathik, Sandipan Chakraborty, Sudip Chaudhuri, Bidisha Sengupta, Pradeep K Sengupta

1.2.1.6 Structural studies of arginine induced enhancement in the activity of T7 RNA polymerase

Addition of arginine enhances the activity of the enzyme T7 RNA polymerase. Different methods have been employed to understand the enhancement in the light of arginine induced alteration of the tertiary structure. The increase in activity of the enzyme reaches a maximum value around a concentration of 125 mM arginine. Fluorescence, circular dichroism and dynamic light scattering studies indicate an alteration in the tertiary structure of the enzyme. Enthalpy change as a function

of input concentration of arginine to a fixed concentration of the enzyme ($5 \mu\text{M}$) shows a dip at 100 mM concentration of arginine. Differential scanning calorimetric studies of the denaturation of the enzyme in absence and presence of arginine indicates arginine induced destabilization of the C-terminal domain of the enzyme. Structural alterations induced by arginine have been compared with those induced by the denaturant guanidine hydrochloride.

Sudipta Pal, Mili Das, Dipak Dasgupta

1.2.1.7 Association of aureolic acid antibiotic, chromomycin A3 with Cu^{2+} and its negative effect upon DNA binding property of the antibiotic

Here we have examined the association of an aureolic acid antibiotic, chromomycin A3 (CHR), with Cu^{2+} . CHR forms a high affinity 2:1 ($\text{CHR}:\text{Cu}^{2+}$) complex with dissociation constant of $0.08 \times 10^{-10} \text{ M}^{-2}$ at 25°C , pH 8.0. The affinity of CHR for Cu^{2+} is higher than those for Mg^{2+} and Zn^{2+} reported earlier from our laboratory. CHR binds preferentially to Cu^{2+} in presence of equimolar amount of Zn^{2+} . Complex formation between CHR and Cu^{2+} is an entropy driven endothermic process. Difference between calorimetric and van't Hoff enthalpies indicate the presence of multiple equilibria, supported from biphasic nature of the kinetics of association. Circular dichroism spectroscopy show that $[\text{CHR}_2:\text{Cu}^{2+}]$ complex assumes a structure different from either of the Mg^{2+} and Zn^{2+} complex reported earlier. Both $[\text{CHR}_2:\text{Mg}^{2+}]$ and $[\text{CHR}_2:\text{Zn}^{2+}]$ complexes are known to bind DNA. In contrast, $[\text{CHR}_2:\text{Cu}^{2+}]$ complex does not interact with double helical DNA, verified by means of Isothermal Titration Calorimetry of its association with calf thymus DNA and the double stranded decamer (5'-CCGGCGCCGG-3'). In order to interact with double helical DNA, the (antibiotic)₂ : metal (Mg^{2+} and Zn^{2+}) complexes require a isohelical conformation. Nuclear Magnetic Resonance spectroscopy shows that the Cu^{2+} complex adopts a distorted octahedral structure, which cannot assume the required conformation to bind to the DNA. This report demonstrates the negative effect of a bivalent metal upon the DNA binding property of CHR, which otherwise binds to DNA in presence of metals like Mg^{2+} and Zn^{2+} . The results also indicate that CHR has a potential for chelation therapy in Cu^{2+} accumulation diseases. However cytotoxicity of the antibiotic might restrict the use.

Shibojyoti Lahiri, Toshifumi Takao†, Pukhrambam Grihanjali Devi, Saptarni Ghosh, Ayanjeet Ghosh, Amrita Dasgupta, Dipak Dasgupta

1.2.2 C&MB

1.2.2.1 The First Structure of Polarity Suppression Protein, Psu from Enterobacteria Phage P4, Reveals a Novel Fold and a Knotted Dimer

Psu is a capsid decoration protein of bacteriophage P4 and acts as an antiterminator of Rho-dependent transcription termination in bacteria. So far, no structures have been reported for the Psu protein or its homologues. Here, we report the first structure of Psu solved by the Hg^{2+} single wavelength anomalous dispersion method, which reveals that Psu exists as a knotted homodimer and is first of its kind in nature. Each monomer of Psu attains a novel fold around a tight coiled-coil motif. CD spectroscopy and the structure of an engineered disulfide-bridged Psu derivative reveal that the protein folds reversibly and reassembles by itself into the knotted dimeric conformation without the requirement of any chaperone. This structure would help to explain the functional properties of the protein and can be used as a template to design a minimal peptide fragment that

can be used as a drug against Rho-dependent transcription termination in bacteria.

Ramanuj Banerjee, Seema Nath, Amitabh Ranjan, Susmita Khamrui, Bibhusita Pani, Ranjan Sen, Udayaditya Sen

1.2.2.2 Identification of HYPK-Interacting Proteins Reveals Involvement of HYPK in Regulating Cell Growth, Cell Cycle, Unfolded Protein Response and Cell Death

Huntingtin Yeast Two-Hybrid Protein K (HYPK) is an intrinsically unstructured huntingtin (HTT)-interacting protein with chaperone-like activity. To obtain more information about the function(s) of the protein, we identified 27 novel interacting partners of HYPK by pull-down assay coupled with mass spectrometry and, further, 9 proteins were identified by co-localization and co-immunoprecipitation (co-IP) assays. In neuronal cells, (EEF1A1 and HSPA1A), (HTT and LMNB2) and (TP53 and RELA) were identified in complex with HYPK in different experiments. Various Gene Ontology (GO) terms for biological processes, like protein folding (GO: 0006457), response to unfolded protein (GO: 0006986), cell cycle arrest (GO: 0007050), anti-apoptosis (GO: 0006916) and regulation of transcription (GO: 0006355) were significantly enriched with the HYPK-interacting proteins. Cell growth and the ability to refold heat-denatured reporter luciferase were decreased, but cytotoxicity was increased in neuronal cells where HYPK was knocked-down using HYPK antisense DNA construct. The proportion of cells in different phases of cell cycle was also altered in cells with reduced levels of HYPK. These results show that HYPK is involved in several biological processes, possibly through interaction with its partners.

Kamalika Roy Choudhury, Swasti Raychaudhuri, Nitai P Bhattacharyya

1.2.2.3 Expression of recombinant human cathepsin K is enhanced by codon optimization

A synthetic codon-optimized gene encoding human procathepsin K has been cloned in Escherichia coli using pET28a+ vector. The recombinant His-tagged fusion protein was expressed as inclusion body, solubilized in urea and purified by metal affinity chromatography. The purified protein was refolded by dilution technique, concentrated and finally purified by gel-filtration chromatography. The expressed protein was confirmed by Western blot analysis with human cathepsin K specific antibody. We have obtained 140 mg purified and refolded protein from 1 L bacterial culture which is the highest (nearly three times higher) yield reported so far for a recombinant human procathepsin K. The protease could be autocatalytically activated to mature protease at lower pH in presence of cysteine protease specific activators. The recombinant protease showed gelatinolytic and collagenolytic activities as well as activity against synthetic substrate Z-FR-AMC with a K_m value of $5 \pm 2.7 \mu\text{M}$ and the proteolytic activity of the enzyme could be blocked by cysteine protease inhibitors E-64, leupeptin and MMTS.

Sumana Roy, JK Dattagupta, Sampa Biswas

1.2.2.4 Cloning, expression, purification, crystallization and preliminary X-ray analysis of a fructokinase from *Vibrio cholerae* O395

Fructokinase (FK), one of the crucial enzymes for sugar metabolism in bacterial systems, catalyses the unidirectional phosphorylation reaction from fructose to fructose 6-phosphate, thereby allowing parallel entry of fructose into glycolysis beside glucose. The *cscK* gene from *Vibrio cholerae* O395 coding for the enzyme FK has been cloned, overexpressed in *Escherichia coli* BL21 (DE3) and purified using Ni-NTA affinity chromatography. Crystals of *V. cholerae* FK (Vc-FK) and its cocrystal with fructose, adenosine diphosphate (ADP) and Mg^{2+} were grown in the presence of polyethylene glycol 6000 and diffracted to 2.45 and 1.75 Å resolution, respectively. Analysis of the diffraction data showed that both crystal forms have symmetry consistent with space group P21212, but with different unit-cell parameters. Assuming the presence of two molecules in the asymmetric unit, the Matthews coefficient for the apo Vc-FK crystals was estimated to be $2.4 \text{ Å}^3 \text{ Da}^{-1}$, which corresponds to a solvent content of 48%. The corresponding values for the ADP- and sugar-bound Vc-FK crystals were $2.1 \text{ Å}^3 \text{ Da}^{-1}$ and 40%, respectively, assuming the presence of one molecule in the asymmetric unit.

Rakhi Paul, Seema Nath, Udayaditya Sen

1.2.2.5 Mechanism(s) of Alteration of Micro RNA Expressions in Huntington's Disease and Their Possible Contributions to the Observed Cellular and Molecular Dysfunctions in the Disease

To identify the mechanism of deregulation of micro RNAs (miRNAs) altered in Huntington's disease (HD) and their possible contributions to the altered cellular and molecular functions observed in the disease, we analyzed the altered miRNAs in the postmortem brains of HD patients. There are 54 miRNAs differentially expressed in HD brains of which 30 are upregulated and 24 downregulated. Some of these miRNAs were also altered in various models of the disease. Regulation of these miRNAs was attributed to transcription factors and the host genes to which these miRNAs reside. We observed that transcription regulators TP53, E2F1, REST, and GATA4 together could regulate expressions of 26 miRNAs in HD. Altered expressions of 13 intronic miRNAs were correlated with the expressions of their host genes. From literature, we further collected 287 experimentally validated targets of miRNAs upregulated in HD, while 304 validated targets of downregulated miRNAs in HD. Analysis of these validated target genes of altered miRNAs by gene ontology (GO) revealed that these genes are significantly enriched in GO terms belonging to (1) apoptosis, (2) differentiation and development, (3) fatty acid, cholesterol, lipid, glucose, and carbohydrate metabolism, (4) cell cycle and growth, and (5) transcription regulation. Experimental evidences that these processes are altered in HD are provided from published reports. In conclusion, altered miRNAs in HD might target many genes and may contribute to the altered cellular and molecular functions observed in HD.

Mithun Sinha, Saikat Mukhopadhyay, Nitai P Bhattacharyya

1.2.2.6 The structure of a thermostable mutant of pro-papain reveals its activation mechanism

Papain is the archetype of a broad class of cysteine proteases (clan C1A) that contain a pro-peptide in the zymogen form which is required for correct folding and spatio-temporal regulation of prote-

olytic activity in the initial stages after expression. This study reports the X-ray structure of the zymogen of a thermostable mutant of papain at 2.6 Å resolution. The overall structure, in particular that of the mature part of the protease, is similar to those of other members of the family. The structure provides an explanation for the molecular basis of the maintenance of latency of the proteolytic activity of the zymogen by its pro-segment at neutral pH. The structural analysis, together with biochemical and biophysical studies, demonstrated that the pro-segment of the zymogen undergoes a rearrangement in the form of a structural loosening at acidic pH which triggers the proteolytic activation cascade. This study further explains the bimolecular stepwise autocatalytic activation mechanism by limited proteolysis of the zymogen of papain at the molecular level. The possible factors responsible for the higher thermal stability of the papain mutant have also been analyzed.

Sumana Roy, Debi Choudhury, Pulakesh Aich, Jiban K Dattagupta, Sampa Biswas

1.2.2.7 The histone acetyl transferase LdHAT1 from *Leishmania donovani* is regulated by S-phase cell cycle kinase

Histone acetyl transferases (HATs) are important histone modifiers that affect critical cellular processes like transcription, DNA replication and repairs through highly dynamic chromatin remodelling. Our earlier studies recognized LdHAT1 as a substrate of the S-phase cell cycle kinase LdCyc1-CRK3 from *Leishmania donovani*. Here, we confirm through site-directed mutagenesis that RXL-like cyclin-binding (Cy) motif dependent interaction of LdHAT1 with LdCyc1 is essential for its phosphorylation at a canonical Cdk target site by the kinase complex. LdHAT1 acetylates K10 residue of a peptide derived from *L. donovani* histone H4 N-terminal tail. Interestingly, phosphorylation of LdHAT1 by the S-phase kinase inhibits its H4K10 acetylation activity, implicating an important mechanism of periodic regulation of histone acetylation during cell cycle progression.

Anup Kumar Maity, Partha Saha

1.2.2.8 Cloning, purification, crystallization and preliminary X-ray analysis of two low-molecular-weight protein tyrosine phosphatases from *Vibrio cholera*

Low-molecular-weight protein tyrosine phosphatases (LMWPTPs) are small cytoplasmic enzymes of molecular weight ~18 kDa that belong to the large family of protein tyrosine phosphatases (PTPs). Despite their wide distribution in both prokaryotes and eukaryotes, their exact biological role in bacterial systems is not yet clear. Two low-molecular-weight protein tyrosine phosphatases (*VcLMWPTP-1* and *VcLMWPTP-2*) from the Gram-negative bacterium *Vibrio cholerae* have been cloned, overexpressed, purified by Ni²⁺-NTA affinity chromatography followed by gel filtration and used for crystallization. Crystals of *VcLMWPTP-1* were grown in the presence of ammonium sulfate and glycerol and diffracted to a resolution of 1.6 Å. *VcLMWPTP-2* crystals were grown in PEG 4000 and diffracted to a resolution of 2.7 Å. Analysis of the diffraction data showed that the *VcLMWPTP-1* crystals had symmetry consistent with space group P3₁ and that the *VcLMWPTP-2* crystals had the symmetry of space group C2. Assuming the presence of four molecules in the asymmetric unit, the Matthews coefficient for the *VcLMWPTP-1* crystals was estimated to be 1.97 Å³ Da⁻¹, corresponding to a solvent content of 37.4%. The corresponding values for the *VcLMWPTP-2* crystals, assuming the presence of two molecules in the asymmetric

unit, were $2.77\text{\AA}^3\text{ Da}^{-1}$ and 55.62%, respectively.

Seema Nath, Ramanuj Banerjee, Susmita Khamrui, Udayaditya Sen

1.2.2.9 Role of remote scaffolding residues in the inhibitory loop pre-organization, flexibility, rigidification and enzyme inhibition of serine protease inhibitors

Canonical serine protease inhibitors interact with cognate enzymes through the P3-P2' region of the inhibitory loop while its scaffold hardly makes any contact. Neighboring scaffolding residues like Arginines or Asparagine shape-up the inhibitory loop and favor the resynthesis of cleaved scissile bond. However, role of remote scaffolding residues, which are not involved in religation, was not properly explored. Crystal structures of two engineered winged bean chymotrypsin inhibitor (WCI) complexed with Bovine trypsin (BPT) namely L65R-WCI:BPT and F64Y/L65R-WCI:BPT show that the inhibitory loop of these engineered inhibitors are recognized and rigidified properly at the enzyme active site like other strong trypsin inhibitors. Chimeric protein ETIL-WCIS, having a loop of *Erythrina caffra* Trypsin Inhibitor, Ell on the scaffold of WCI, was previously shown to behave like substrate. Non-canonical structure of the inhibitory loop and its flexibility are attributed to the presence of smaller scaffolding residues which cannot act as barrier to the inhibitory loop like in Ell Double mutant A76R/L115Y-(ETIL-WCIS), where the barrier is reintroduced on ETIL-WCIS, shows regaining of inhibitory activity. The structure of A76R/L115Y-(ETIL-WCIS) along with L65R-WCI:BPT and F64Y/L65R-WCI:BPT demonstrate here that the lost canonical conformation of the inhibitory loop is fully restored and loop flexibility is dramatically reduced. Therefore, residues at the inhibitory loop interact with the enzyme playing the primary role in recognition and binding but scaffolding residues having no direct interaction with the enzyme are crucial for rigidification event and the inhibitory potency. B-factor analysis indicates that the amount of inhibitory loop rigidification varies between different inhibitor families.

Sudip Majumder, Susmita Khamrui, Jhimli Dasgupta, Jiban K Dattagupta, Udayaditya Sen

1.2.2.10 Self-Complementarity within Proteins: Bridging the Gap between Binding and Folding

Complementarity, in terms of both shape and electrostatic potential, has been quantitatively estimated at protein-protein interfaces and used extensively to predict the specific geometry of association between interacting proteins. In this work, we attempted to place both binding and folding on a common conceptual platform based on complementarity. To that end, we estimated (for the first time to our knowledge) electrostatic complementarity (E-m) for residues buried within proteins. E-m measures the correlation of surface electrostatic potential at protein interiors. The results show fairly uniform and significant values for all amino acids. Interestingly, hydrophobic side chains also attain appreciable complementarity primarily due to the trajectory of the main chain. Previous work from our laboratory characterized the surface (or shape) complementarity (S-m) of interior residues, and both of these measures have now been combined to derive two scoring functions to identify the native fold amid a set of decoys. These scoring functions are somewhat similar to functions that discriminate among multiple solutions in a protein-protein docking exercise. The performances of both of these functions on state-of-the-art databases were comparable if not better than most currently available scoring functions. Thus, analogously to interfacial residues of protein chains associated (docked) with specific geometry, amino acids found

in the native interior have to satisfy fairly stringent constraints in terms of both S-m and E-m. The functions were also found to be useful for correctly identifying the same fold for two sequences with low sequence identity. Finally, inspired by the Ramachandran plot, we developed a plot of S-m versus E-m (referred to as the complementarity plot) that identifies residues with suboptimal packing and electrostatics which appear to be correlated to coordinate errors.

Sankar Basu, Dhananjay Bhattacharyya, Rahul Banerjee

1.2.2.11 miR-125b promotes cell death by targeting spindle assembly checkpoint gene MAD1 and modulating mitotic progression

The spindle assembly checkpoint (SAC) is a 'wait-anaphase' mechanism that has evolved in eukaryotic cells in response to the stochastic nature of chromosome-spindle attachments. In the recent past, different aspects of the SAC regulation have been described. However, the role of microRNAs in the SAC is vaguely understood. We report here that Mad1, a core SAC protein, is repressed by human miR-125b. Mad1 serves as an adaptor protein for Mad2 - which functions to inhibit anaphase entry till the chromosomal defects in metaphase are corrected. We show that exogenous expression of miR-125b, through downregulation of Mad1, delays cells at metaphase. As a result of this delay, cells proceed towards apoptotic death, which follows from elevated chromosomal abnormalities upon ectopic expression of miR-125b. Moreover, expressions of Mad1 and miR-125b are inversely correlated in a variety of cancer cell lines, as well as in primary head and neck tumour tissues. We conclude that increased expression of miR-125b inhibits cell proliferation by suppressing Mad1 and activating the SAC transiently. We hypothesize an optimum Mad1 level and thus, a properly scheduled SAC is maintained partly by miR-125b.

S Bhattacharyya†, S Nath†, J Ghose, NP Bhattacharyya et al

1.2.3 Chemical Sciences

1.2.3.1 Simultaneous production and separation of no-carrier-added ^{111}In , ^{109}Cd from alpha particle induced silver target

A natural silver foil was bombarded by 30 MeV α -particles which produced ^{111}In , ^{109}Cd and ^{106m}Ag in the target matrix. ^{111}In and ^{109}Cd were separated from the Ag target matrix employing ion-exchange chromatography and liquid-liquid extraction (LLX). In the chromatographic separation, the active solution containing the NCA products were adsorbed in the column containing Dowex 50 and were eluted with HNO_3 . Bulk silver and ^{109}Cd were sequentially eluted with 1 M HNO_3 . After complete elution of Cd-109 and the bulk, ^{111}In was eluted with 1.5 M HNO_3 . In the LLX, the NCA ^{111}In was extracted to 1% HDEHP (di-2(ethylhexyl)phosphoric acid) from 10^{-2} M HNO_3 solution, leaving cadmium and bulk silver quantitatively in the aqueous phase. The NCA ^{109}Cd was separated from the bulk Ag by precipitating Ag as AgCl . NCA ^{111}In was stripped back quantitatively from HDEHP phase using 8 M HNO_3 .

Moumita Maiti, Kaustab Ghosh, Susanta Lahiri

1.2.3.2 Excimer of 9-Aminoacridine Hydrochloride Hydrate in Confined Medium: An Integrated Experimental and Theoretical Study

We aim to find out the extent of stability of the excimer of 9-aminoacridine hydrochloride hydrate (9AA), a prospective PDT drug, in different confined media with varying cavity size. When confined in cetyltrimethyl ammonium bromide micelles, although at low concentration of 9AA, only a single distinct peak (λ_{max} at 460 nm) with a shoulder at 485 nm is observed in steady-state fluorescence spectrum, yet with increase in concentration the peak and the shoulder merge with simultaneous emergence of another peak at 535 nm, which is assigned to excimer. Similar behavior is also observed in Triton-X, crown ether, α -cyclodextrin, β -cyclodextrin, and homogeneous aqueous medium. The formation of excimer, which reflects the extent of confinement of 9AA, is maximum in β -cyclodextrin followed by others. Steady-state and time-resolved fluorescence studies along with TRES and TRANES analyses coupled with anisotropy data and transient absorption studies reveal the presence of monomer-dimer equilibrium of 9AA in the excited state. Molecular modeling indicates that the structure of excimer is stabilized by locking of the two monomeric species via four hydrogen bonds formed between the amino-H and imino-N of 9AA monomers, whereas the dimer in the ground state has only two such hydrogen bonds.

Piyali Mitra, Brojati Chakraborty†, Dhananjay Bhattacharyya, Samita Basu

1.2.3.3 Species dependent extraction of ^{99}Mo

The liquid-liquid extraction profile of molybdenum has been studied with di-(2-ethylhexyl) phosphoric acid from different HCl media. The careful study of extraction profile clearly indicates various species of molybdenum at different acid strengths, which have been interpreted with reference to established data.

Swadesh Mandal, Ajoy Mandal, Susanta Lahiri

1.2.3.4 Separation of no-carrier-added $^{113,117m}\text{Sn}$ and $^{113m,114m}\text{In}$ from alpha particle irradiated natural cadmium target

A natural cadmium foil was irradiated by 42 MeV α -particles to produce $^{113,117m}\text{Sn}$, $^{111,113m,114m}\text{In}$ simultaneously in the target matrix. After the complete decay of short lived radionuclides, long-lived NCA products were separated sequentially from the bulk cadmium by liquid-liquid extraction using di-(2-ethylhexyl)phosphoric acid (HDEHP) dissolved in cyclohexane as organic phase and HCl as aqueous phase. At the optimum condition, 10^{-2} M HCl and 5% HDEHP, NCA In along with NCA Sn radionuclides (75%) were separated from the bulk Cd resulting to high separation factors of 2.7×10^4 (D_{In}/D_{Cd}) and 500 (D_{Sn}/D_{Cd}), respectively. The NCA In was stripped back completely to the aqueous phase by 6 M HCl leaving NCA Sn in the HDEHP phase with a separation factor (D_{Sn}/D_{In}) of 3.94×10^6 .

K Ghosh, M Maiti, S Lahiri

1.2.3.5 Cloud point extraction of ^{99}Mo with Triton X-114

This paper reports the cloud point extraction (CPE) extraction behaviour of ^{99}Mo in non-ionic Triton X-114 (TX-114), sodiumdodecyl sulphate (SDS) + TX-114 and sodium diethyldithiocarbamate (DDTC) + TX-114. The high extraction of ^{99}Mo observed in all the CPE systems in pH 5 or less. The extent of extraction was almost unchanged with addition of SDS and DDTC in TX-114. Extraction behaviour was also studied in presence of common salts. It was observed the presence of salts dramatically decreased the amount of molybdenum extraction in the surfactant-rich phase.

Swadesh Mandal, Susanta Lahiri

1.2.3.6 An improved method for determination of Be-7 in mosses

We have measured Be-7 activity in moss samples collected from in and around Mumbai, India. The use of heavily shielded Compton suppressor system is more efficient than the conventional gamma spectroscopic system for detection of Be-7. The Be-7 accumulation capacities of mosses are more than other plant samples. Therefore monitoring of young moss samples by Compton suppressor system is an excellent tool for determination of atmospheric fallout of Be-7. A positive bias in the high altitude samples has been observed which might be due to any of the two reasons (i) higher cosmic ray flux in the high altitude or (ii) high pollution in the lower altitude area ultimately inhibits uptake of Be-7.

Moumita Maiti, Santosh R Tiwari, Nilesch B Dubey, Hemlata Bagla, Susanta Lahiri

1.2.3.7 Application of PEG based aqueous biphasic systems in extraction and separation of no-carrier-added ^{183}Re from bulk tantalum

No-carrier-added (nca) rhenium isotopes ($^{182,182m,183}\text{Re}$) were produced by irradiation with 30 MeV alpha particles on natural tantalum target. The short-lived $^{182,182m}\text{Re}$ were allowed to decay and long-lived nca ^{183}Re was separated from bulk tantalum matrix by aqueous biphasic system (ABS) using 2 M solutions of nine different salts, namely, Na_2SO_4 , Na_2SO_3 , NaHSO_3 , $\text{Na}_2\text{S}_2\text{O}_3$, Na_2HPO_4 , Na_2CO_3 , Na-citrate, Na-tartrate, and $(\text{NH}_4)_2\text{SO}_4$ as salt rich phases against 50% (w/w) PEG-4000 as polymer rich phase at room temperature. The influence of temperature and thermodynamic parameters Delta H degrees and Delta S degrees were obtained for the partition of ^{183}Re and tantalum in these systems. Nca ^{183}Re was extracted in high amount in polymer rich phases irrespective of the salt rich phases. Bulk tantalum showed tendency to remain in salt rich phases. ABSs with PEG-4000 polymer rich phase in combination with Na_2SO_4 , Na_2SO_3 , NaHSO_3 , Na_2HPO_4 , Na_2CO_3 , Na-citrate and Na-tartrate as salt rich phases at basic pH and at ambient temperature (27° C) offered single-step separation between nca ^{183}Re and bulk Ta. When $\text{Na}_2\text{S}_2\text{O}_3$ and $(\text{NH}_4)_2\text{SO}_4$ were used as salt rich phase, slight extraction of bulk tantalum was observed in PEG-4000 rich phase. The dynamic dissociation constant of ^{183}Re -PEG-4000 complex was measured by dialysis of the PEG-rich phase against de-ionised water. The $k_{\text{dissociation}}$ value was found as low as 0.0185 min^{-1} . Therefore, it is possible to have pure ^{183}Re in de-ionized water immediately after the dialysis.

B Dutta, S Lahiri, BS Tomar†

1.2.3.8 An improved non-destructive method of potassium determination

The simplest non-destructive method of potassium determination is to co-relate the fixed abundance of naturally occurring ^{40}K with the total amount of potassium. Earlier this relationship was applied by measuring the β^- activity of ^{40}K in a sample by Geiger counter. However, merely this simple linear relationship has been applied through gamma spectrometric measurement of ^{40}K activity, might be due to the huge interference of the ^{40}K background. We have demonstrated that heavily shielded Compton Suppressor System reduces the background in such extent that the total amount of K in a sample can be measured by measuring the area of the ^{40}K photo peak (at 1460.82 keV). The developed method requires neither chemical treatment of the sample like dissolution or digestion, nor irradiation of the sample in a nuclear reactor and therefore truly follows green chemistry principles, minimizing the chemicals and hazards. The method has been validated using NIST SRMs. The developed method was compared with WDXRF and ICPOES measurement.

Moumita Maiti, Ajoy Mandal, Susanta Lahiri

1.2.3.9 Manganese-incorporated iron(III) oxide-graphene magnetic nanocomposite: synthesis, characterization, and application for the arsenic(III)-sorption from aqueous solution

High specific surface area of graphene (GR) has gained special scientific attention in developing magnetic GR nanocomposite aiming to apply for the remediation of diverse environmental problems like point-of-use water purification and simultaneous separation of contaminants applying low external magnetic field (<1.0 T) from ground water. Fabrication of magnetic manganese-incorporated iron(III) oxide ($\text{Mn}_x^{2+}\text{Fe}_{2-x}^{3+}\text{O}_4^{2-}$) (IMBO)-GR nanocomposite is reported by exfoliating the GR layers. Latest microscopic, spectroscopic, powder X-ray diffraction, BET surface area, and superconducting quantum interference device characterizations showed that the material is a magnetic nanocomposite with high specific surface area ($280\text{ m}^2\text{ g}^{-1}$) and pore volume ($0.3362\text{ cm}^3\text{ g}^{-1}$). Use of this composite for the immobilization of carcinogenic As(III) from water at 300 K and pH ~ 7.0 showed that the nanocomposite has higher binding efficiency with As(III) than the IMBO owing to its high specific surface area. The composite showed almost complete ($>99.9\%$) As(III) removal ($\leq 10\text{ }\mu\text{g L}^{-1}$) from water. External magnetic field of 0.3 T efficiently separated the water dispersed composite ($0.01\text{ g}/10\text{ mL}$) at room temperature (300 K). Thus, this composite is a promising material which can be used effectively as a potent As(III) immobilizer from the contaminated groundwater ($>10\text{ }\mu\text{g L}^{-1}$) to improve drinking water quality.

Debabrata Nandi, Kaushik Gupta, Arup Kumar Ghosh, Amitabha De, Sangam Banerjee, Uday Chand Ghosh

1.2.3.10 Radioactivity generation in Pb target by protons-A comparative study from MeV to GeV

In an Accelerator Driven Subcritical System (ADSS), choice of the target is decided by several factors like neutron yield, heat generation, ease of cooling, possibility of fire hazard, generation of chemically toxic elements and radioactive nuclides, running cost of the accelerator, etc. ^{208}Pb is one of the probable targets for an ADSS. In the present work, we have estimated induced activity in a ^{208}Pb target by primary proton beam in the energy range of 20 MeV up to 2.0 GeV using reaction model codes ALICE-91, TALYS-1.2, EMPIRE-2.19 and QMD. The energy range studied

spans the entire energy interval used for target property study to practical application of an ADSS. At several hundreds of MeV, some of the major contributors to induced activity are projectile-like fragments, such as, H-3. The maximum activity produced is of the order of 10^6 - 10^7 MBq over the whole energy range. Some chemically toxic elements like Xe, Hg are also formed in significant amount.

Maitreyee Nandy, Chirashree Lahiri

1.2.3.11 Study of the average charge states of ^{188}Pb and $^{252,254}\text{No}$ ions at the gas-filled separator TASCA

The average charge states of ^{188}Pb and $^{252,254}\text{No}$ ions in dilute helium gas were measured at the gas-filled recoil separator TASCA. Hydrogen gas was also used as a filling gas for measurements of the average charge state of ^{254}No . Helium and hydrogen gases at pressures from 0.2 mbar to 2.0 mbar were used. A strong dependence of the average charge state on the pressure of the filling gases was observed for both, helium and hydrogen. The influence of this dependence, classically attributed to the so-called "density effect", on the performance of TASCA was investigated. The average charge states of ^{254}No ions were also measured in mixtures of helium and hydrogen gases at low gas pressures around 1.0 mbar. From the experimental results simple expressions for the prediction of average charge states of heavy ions moving in rarefied helium gas, hydrogen gas, and in their mixture were derived.

J Khuyagbaatar, D Ackermann, LL Andersson, S Lahiri, M Maiti et al

1.2.3.12 Neutron ambient dose equivalent from 5 MeV/u $^{10,11}\text{B}$, $^{12,13}\text{C}$ and $^{16,18}\text{O}$ projectiles incident on a thick Al target

The neutron ambient dose equivalent has been measured from $^{10,11}\text{B}$, $^{12,13}\text{C}$, $^{16,18}\text{O}$ projectiles of energy 5 MeV/amu incident on a thick Al target at 0 degrees, 30 degrees, 60 degrees and 90 degrees with respect to the beam direction using a conventional dose equivalent meter. The calculated results obtained using previously reported empirical relations do not reproduce the experimental data. The results obtained from the PACE nuclear reaction code are closer to the experimental data as compared to the various empirical expressions. The ratio of the increase in the dose rates when the projectile is changed from the lighter to the heavier isotopes is fairly reproduced by most of the empirical formulations and the PACE code. A previously reported relation for the slope parameter is used to predict the directional distribution of the neutron dose for the projectiles used in this study. The calculated doses are lower than the experimental results in the forward directions but agree within the uncertainties at the backward directions. A new set of projectile-based parameters have been derived from the present experimental data which can be used in an empirical formulation.

C Sunil, AA Shanbhag, M Nandy et al

1.2.3.13 Synthesis of molybdenum nanoparticle by in situ γ -radiation

This paper reports the synthesis of various types of molybdenum nanoparticles using in-situ minuscule amount of radioactivity. The radioisotope ^{99}Mo was introduced into the solution of (i)

10^{-5} M ammonium molybdate and (ii) mixture of 10^{-5} M ammonium molybdate and anionic surfactant sodiumdodecyl sulphate (SDS). The molybdate ions were changed to nanoparticles due to radiolysis initiated by gamma-irradiation in both the cases. The transmission electron microscopic images showed 4-15 nm size nanoparticles with spherical shape in ammonium molybdate solution. However, the aggregation of nanoparticles could not be avoided in this case. The addition of SOS to the solution helped to obtain 10-60 nm size of spherical molybdenum nanoparticle and 2-10 nm wire like molybdenum nanoparticle. Interpretation of spectral data advocates that the molybdenum nanoparticles might be in MoO_3 form.

Swadesh Mandal, Susanta Lahiri

1.2.3.14 Observation of superparamagnetism to flux closure behaviour in ZnO nanoparticle agglomerates

In this paper we have tried to understand the nature of magnetism in ZnO nanoparticle samples with an intrinsic 50 ppm trace of Fe impurity. When the samples are annealed we observe formation of nanoparticle agglomerates and the size increases with annealing temperature. When the sample is annealed at 600 degrees C we observe superparamagnetic behaviour, and the magnetic hysteresis along with the coercive field below the blocking temperature is almost independent of the cooling field. When the sample is annealed at 900 degrees C we observe reduction of saturation magnetization but the magnetic hysteresis and the coercive field are now dependent on the cooling field, indicating magnetic correlation and ordering within the agglomerated nanograins. We propose a simple model that explains the reduction of magnetization as being due to a vortex-state-like flux closure formation.

B Ghosh, M Sardar, S Lahiri, S Banerjee

1.2.3.15 Prototropic Interactions of Pyrimidine Nucleic Acid Bases with Acridine: A Spectroscopic Investigation

In this article, we have investigated the interactions of three pyrimidine nucleic acid bases, cytosine (C), thymine (T), and uracil (U) with acridine (Acr), an N-heterocyclic DNA intercalator, through the changes in photophysics of Acr inside SDS micelles. Fluorescence of AcrH^{+*} at 478 nm and its lifetime are quenched on addition of C, T, and U, while a concomitant increment of Acr^* is observed only with C. However, the relative amplitude of Acr^* increases with a simultaneous decrease in AcrH^{+*} only with C. The fluorescence quenching of AcrH^{+*} is explained by photoinduced electron transfer (PET), while changes in the relative contributions of Acr^* and AcrH^{+*} with C are due to associated excited-state proton transfer (ESPT). The rate of electron transfer (k_{ET}) is maximum for T, followed by U and C. The associated ESPT from AcrH^{+*} is the reason behind the reduced efficiency of PET with C. The lack of proton transfer with T and U as well as the higher k_{ET} for T compared to U are explained by keto-enol tautomerization and subtle changes in the structure and geometry of the pyrimidine bases.

Manas Kumar Sarangi, Ankita Mitra, Samita Basu

1.2.3.16 Functionalized polyaniline nanowires for biosensing

Conducting polymers and related nanomaterials are widely used for different biosensing applications. In the present work gold nanoparticles (AuNP) incorporated polyaniline nanowires (PAN-NW) were used for fabrication of a novel biosensing platform. PAN-NW with AuNP (8-10 nm) was treated with β -mercaptoethylamine (MEA) that leads to the formation of the NH_2 functionalized PAN-AuNP in dispersed form. Immobilizing the functionalized dispersion on the Pt electrode makes a biosensing platform suitable for attachment of different biomolecules via NH_2 functionality and sensing of the target elements in turn. Efficiency of the system as oligonucleotide (dA-dT) sensor was examined by immobilizing a single stranded oligonucleotide (ssdA) and monitoring its hybridization with target nucleotide (ssdT) following cyclic voltammetry (CV), differential pulse voltammetry (DPV) and electrochemical impedance spectroscopy (EIS) techniques. The system works well even at concentrations as low as 10^{18} M (of target nucleotide) and produces substantially large peak current (mA) in DPV. On the other hand it produces a huge change in impedance at low frequencies (EIS), after hybridization with complementary strand.

Rupali Gangopadhyay, Ankan Dutta Chowdhury, Amitabha De

1.2.3.17 Label free polyaniline based impedimetric biosensor for detection of E. coli O157:H7 Bacteria

A new and simple method for label free, rapid and inexpensive impedimetric sensing of Escherichia coli O157:H7 (a highly infectious and potentially fatal food and water borne pathogen) using antibody-antigen binding method based on covalently linked antibody on a conducting Polyaniline (PANI) film surface is reported. Electrochemical impedance spectroscopy (EIS) was used to test the sensitivity and effectiveness of the sensor electrode by measuring the change in impedance values of electrodes before and after incubation with different concentrations of bacteria. An equivalent electrical circuit model has also been proposed to explain the sensing mechanism. As small concentration as 10^2 CFU mL^{-1} of E. coli O157:H7 were successfully detected on the Au/PANI/Glu/antibody sensor with the upper detection limit of 10^7 CFU mL^{-1} . The specificity of the sensor has been tested by comparing with two other strains of similar bacteria and found to be satisfactory. The mechanism of the detection is very simple and rapid, giving it a major advantage over DNA based techniques and other secondary antibody based labeled methods.

Ankan Dutta Chowdhury, Amitabha De, Chirosree Roy Chaudhuri et al

1.2.3.18 Polypyrrole-titanium(IV) doped iron(III) oxide nanocomposites: Synthesis, characterization with tunable electrical and electrochemical properties

Titanium(IV)-doped synthetic nanostructured iron(III) oxide (NITO) and polypyrrole (PPy) nanocomposites was fabricated by in situ polymerization using FeCl_3 as initiator. The polymer nanocomposites (PNCs) and pure NITO were characterized by X-ray diffraction, Fourier transform infrared spectroscopy, scanning electron microscopy, electron dispersive X-ray spectroscopy, transmission electron microscopy, etc. Thermo gravimetric and differential thermal analyses showed the enhancement of thermal stability of PNCs than the pure polymer. Electrical conductivity of the PNCs had increased significantly from 0.793×10^{-2} S/cm to 0.450 S/cm with respect to the PPy, and that had been explained by 3-dimensional variable range hopping (VRH) conduction

mechanisms. In addition, the specific capacitance of PNCs had increased from 147 F/g to 176 F/g with increasing NITO content than that of pure NITO (26 F/g), presumably due to the growing of mesoporous structure with increasing NITO content in PNCs which reduced the charge transfer resistance significantly.

Nandi, Debabrata, Arup Kumar Ghosh, Kaushik Gupta, Amitabha De et al

1.2.3.19 Photophysical properties of an environment sensitive fluorophore 1-keto-6,7-dimethoxy-1,2,3,4-tetrahydrocarbazole and its excited state interaction with N,N-dimethylaniline: A spectroscopic investigation

Photophysical properties of a fluorophore 1-keto-6,7-dimethoxy-1,2,3,4-tetrahydrocarbazole (KTHC-67) have been studied in a number of organic solvents. The profile of the fluorescence spectrum and the wavelength at which fluorescence intensity maximizes are found to vary with the nature of the solvent. The photophysics of KTHC-67 is much more influenced by the hydrogen bond donor and acceptor abilities of the solvents rather than their polarity of the solvent. Excited state interactions of KTHC-67 with N,N-dimethylaniline (DMA) have also been investigated in three homogeneous solvents, acetonitrile (ACN), dimethyl sulphoxide (DMSO) and ethanol (EtOH). Photoinduced electron transfer from DMA to KTHC-67 is evident from the subsequent changes in the fluorescence intensity, fluorescence lifetime and transient absorbance of KTHC-67 in presence of DMA.

Amrit Krishna Mitra, Sujay Ghosh, Suchandra Chakraborty, Manas Kumar Sarangi, Chandan Saha, Samita Basu

1.2.3.20 Production of long-lived Al-26 and Na-24 from neutron interaction in Al target

The excitation functions of (n, 2n) and (n, a) reactions for the production of long-lived radio nuclides Al-26 and Na-24 from Al-27 have been calculated for 1-20 MeV neutrons. The excitation functions of these reactions are calculated using the codes ALICE-91, EMPIRE-2.19 and TALYS-1.0. The codes account for the major nuclear reaction mechanisms, including direct, pre-equilibrium and compound nuclear ones. The excitation functions of these isotopes have been compared graphically with the evaluated nuclear data file and available experimental data. The results are more or less agreeing up to which energy the experimental data are available whereas ALICE code largely under predicts the data in the energy range 1-20 MeV.

PK Saran, Maitreyee Nandy, PK Sarkar et al

1.2.3.21 Angular distribution of the ambient neutron dose equivalent from incidence of alpha particles on thick Al target

In this study, the measured data of angular distribution of neutron dose equivalent due to neutrons arising from the bombardment of 19.8 and 30 MeV alpha particles on a thick aluminium target has been reported. These measurements have been carried out at the BARC-TIFR Pelletron Linac Accelerator Facility using neutron dose equivalent meters popularly known as REM meters. The neutron dose equivalent values measured at a distance of 1 m from the target at various angles

relative to the incident beam direction are presented here. The values are compared with those predicted by the empirical formulation of Clapier & Zaidins.

AA Shanbhag, SP Tripathy, GS Sahoo, M Nandy et al

1.2.3.22 Nickel(II)-Schiff base complex recognizing domain II of bovine and human serum albumin: Spectroscopic and docking studies

It has been spectroscopically monitored that a mononuclear nickel(II)-Schiff base complex [NiL]center dot CH₃OH = NSC exhibits greater binding affinity for bovine serum albumin (BSA) than that of its human counterpart (HSA). Moreover the modes of binding of NSC with the two serum albumins also differ significantly. Docking studies predict a relatively rare type of 'superficial binding' of NSC at domain IIB of HSA with certain mobility whereas for BSA such phenomena has not been detected. The mobile nature of NSC at domain IIB of HSA has been well correlated with the spectroscopic results. It is to be noted that thermodynamic parameters for the NSC interaction also differ for the two serum albumins. Occurrence of energy transfer between the donor (Trp of BSA and HSA) and acceptor (NSC) has been obtained by means of Forster resonance energy transfer (FRET). The protein stability on NSC binding has also been experimented by the GuHCl-induced protein unfolding studies. Interestingly it has been found that NSC-HSA interaction enhances the protein stability whereas NSC-BSA binding has no such impact. Such observations are indicative of the fact that the conformation of NSC is responsible in recognizing the two serum albumins and selectively enhancing protein stability.

Aurkie Ray, Banabithi Koley Seth, Uttam Pal, Samita Basu

1.2.3.23 Oxidative Interaction between OxyHb and ATP: A Spectroscopic Study

The binding mode between oxyhemoglobin (oxyHb) and adenosine triphosphate (ATP) has been studied using absorption and fluorescence spectroscopy. OxyHb forms a ground state complex with ATP supported by five isosbestic points which appear in absorption spectra of oxyHb in buffer solution on addition of ATP. Moreover, the changes in absorption spectra suggest an oxidative interaction between the particular interacting systems. The binding constant has been determined from the quenching of fluorescence of oxyHb in the presence of a varied concentration of ATP, and that is $3.8 \times 10^3 \text{ M}^{-1}$ at 25 degrees C. The negative changes in entropy and enthalpy indicate that the binding is enthalpy driven and the hydrogen bond and van der Waals (stacking) interactions play a major role. The oxygen affinity of oxyHb decreases with simultaneous formation of metHb in the presence of ATP. ATP-induced structural changes have been affirmed using both circular dichroism spectroscopy and synchronous fluorescence. A theoretical docking study gives the molecular details about the binding site of ATP in oxyHb.

Mousumi Banerjee, Abhijit Chakrabarti, Samita Basu

1.2.3.24 Separation of nca ^{123,124,125,126}I from alpha particle induced the natural anti-mony trioxide target

Natural Sb₂O₃ target was irradiated with 29.4 MeV α beam to produce no-carrier-added (nca) ^{123,124,125,126}I radionuclides. Attempt has been made to separate nca iodine from bulk antimony

oxide by solvent extraction using CCl_4 , solid-liquid extraction using Dowex 1 as anion exchanger, and by precipitation methods using different precipitating agents like HCl , AgNO_3 , Na_2S and Zn powder. Only the solvent extraction method was found suitable for separation of nca iodine from bulk antimony target.

Swadesh Mandal, Ajoy Mandal, Susanta Lahiri

1.2.3.25 Studies on dynamic dissociation constant of ^{99}Mo -insulin complex

In this article we studied the dynamic dissociation constant (k_d) of ^{99}Mo complexed with insulin molecule at various pH. The k_d values were determined by dialysis technique against deionised water. The $T_{1/2}$ of the molybdenum-insulin complexes were found to be 6.41, 5.25 and 3.5 h at pH 5, 6 and 7 respectively. The half-lives indicate that insulin may act as good carrier of ^{99}Mo to the intestine and may be useful in the field of nuclear medicine.

Swadesh Mandal, Susanta Lahiri

1.2.3.26 The Binding of a Hydroxy-9,10-anthraquinone CuII Complex to Calf Thymus DNA: Electrochemistry and UV/Vis Spectroscopy

Anthracyclines are broad-spectrum antibiotics that are used against several human cancers. Hydroxy-9,10-anthraquinone compounds closely resemble anthracycline antibiotics from a structural and functional viewpoint. High cost and aspects of toxicity introduce limitations on its use. On complex formation the toxicities of anthracyclines decrease. A close analogue is sodium 1,4-dihydroxy-9,10-anthraquinone-2-sulphonate (AS), which is a comparatively cheaper molecule and resembles a good number of anthracycline derivatives. It forms a complex with CuII , $[\text{Cu}(\text{AS})_2]$. The complex interacts with calf thymus DNA that was studied by UV/Vis spectroscopy and cyclic voltammetry. The experimental data obtained from the two techniques was analyzed for binding constant and size of the binding site. These results not only corroborate each other but also justify earlier data obtained using fluorescence spectroscopy. An important aspect to this study was that nonlinear curve fitting, which is usually applied for analyzing DNA interaction using fluorescence and absorption spectroscopy, was used for the first time to analyze the interaction of the complex with DNA using cyclic voltammetry by monitoring the change in the reduction peak current (I_p). The DNA binding data provides an insight into a probable mode of action of the hydroxy-9,10-anthraquinones within cells as modification of DNA that leads to cell death is an important aspect in cancer research.

Partha S Guin, Parikshit C Mandal, Saurabh Das

1.2.3.27 Purification and characterization of a new alkali-thermostable lipase from *Staphylococcus aureus* isolated from *Arachis hypogaea* rhizosphere

An extracellular lipase (EC 3.1.1.3), SAL-PP1, from *Staphylococcus aureus* isolated from *Arachis hypogaea* rhizosphere was purified and characterized. The enzyme was purified using PALL'S Microsep centrifugal device (10 kD cut off), hydrophobic interaction (phenyl sepharose CL-4B column) and Superose-12 gel filtration chromatography and found to have a molecular mass of around 49

kDa. The gene fragment encoding the part of the catalytic site of the SAL-PP1 lipase was sequenced and the deduced amino acid sequence shows 93% identity with that of SEL3. SAL-PP1 showed activity against long acyl-chain triglycerides, various p-nitrophenyl esters and phospholipids. The enzyme shows high stability and activity after incubation with various metal ions (retained >90% activity in presence of Ca^{2+} , Na^+ , Cu^{2+} , Mg^{2+} , Fe^{2+} , or Hg^{2+} at 10 mM), organic solvents (retained >80% activity in presence of acetonitrile, ethanol, DMSO, methanol, isopropanol, toluene, or ethylene glycol at 10 mM), detergents (retained >70% activity in Triton X-100, Tween 80, or sodium deoxycholate at 10 mM) and irreversible inhibitors (retained >77% activity in presence of PMSF, leupetin, or beta-mercaptoethanol, at 1 mM). Thermal inactivation studies revealed a temperature dependent unfolding of secondary structure of protein. SAL-PP1 showed maximal activity and stability at pH 8.0 and pH 9.0, respectively. The alkali-thermostability, organic solvent-tolerance and broad substrate specificity of this enzyme may have potential implications in detergent formulations, biotransformation, industries, and medicine.

Prodipta Sarkar†, Shinji Yamasaki†, Soumen Basak et al

1.2.3.28 Prototropic Interactions of Pyrimidine Nucleic Acid Bases with Acridine: A Spectroscopic Investigation

In this article, we have investigated the interactions of three pyrimidine nucleic acid bases, cytosine (C), thymine (T), and uracil (U) with acridine (Acr), an N-heterocyclic DNA intercalator, through the changes in photophysics of Acr inside SDS micelles. Fluorescence of AcrH^{+*} at 478 nm and its lifetime are quenched on addition of C, T, and U, while a concomitant increment of Acr^* is observed only with C. However, the relative amplitude of Acr^* increases with a simultaneous decrease in AcrH^{+*} only with C. The fluorescence quenching of AcrH^{+*} is explained by photoinduced electron transfer (PET), while changes in the relative contributions of Acr^* and AcrH^{+*} with C are due to associated excited-state proton transfer (ESPT). The rate of electron transfer (k_{ET}) is maximum for T, followed by U and C. The associated ESPT from AcrH^{+*} is the reason behind the reduced efficiency of PET with C. The lack of proton transfer with T and U as well as the higher k_{ET} for T compared to U are explained by ketoenol tautomerization and subtle changes in the structure and geometry of the pyrimidine bases.

Manas Kumar Sarangi, Ankita Mitra, Samita Basu

1.2.3.29 Production and separation of no-carrier-added ^{73}As and ^{75}Se from ^7Li irradiated germanium oxide target

This work reports for the first time ^7Li -induced accelerator based production of $^{71,72,73,74}\text{As}$, $^{75,76,77}\text{Br}$ and $^{73,75}\text{Se}$ radionuclides in their no-carrier-added (nca) state. After the decay of all short-lived radionuclides ^{75}Se and ^{73}As were only existing radionuclides in germanium oxide target, which were subsequently separated by liquid-liquid extraction (LLX) using trioctylamine (TOA) dissolved in cyclohexane as liquid ion exchanger. The presence of stable germanium in various fractions was examined by Inductively Coupled Plasma Optical Spectrometry (ICP-OES). At 0.1 M TOA and 10 M HCl concentration, ^{75}Se and stable Ge were extracted into the organic phase leaving ^{73}As in the aqueous phase. The bulk Ge was stripped back to the aqueous phase by 1 M NaOH, keeping ^{75}Se in the organic phase. Therefore complete separation between ^{73}As , ^{75}Se and

bulk Ge was achieved.

Ajoy Mandal, Susanta Lahiri

1.2.3.30 Thermally stable polypyrrole-Mn doped Fe(III) oxide nanocomposite sandwiched in graphene layer: Synthesis, characterization with tunable electrical conductivity

We have manifested a novel approach to fabricate metal oxide supported conducting polypyrrole (PPy) nanocomposites which are sandwiched by graphene layers with regular surface morphology. This method is based on the electrostatic interactions of positively charged surfactant micelles and negatively charged graphene oxide sheets followed by reduction. The prepared composites including pure materials are characterized by X-ray diffraction, Raman spectroscopy, Fourier transform infrared spectroscopy, scanning electron microscopy, transmission electron microscopy, atomic force microscopy etc. Enhanced thermal stability of this hybrid composite is ascribed to the more compact structure of PPy reinforced by metal oxide nanoparticles inserted between thermally stable graphene layers. These hybrid composites exhibit significant increase in electrical conductivity from 7.93×10^{-3} S/cm to 2.9 S/cm with respect to pure PPy, and that can be tuned to 50.9 S/cm with variation of Mn doped Fe(III) oxide nanoparticles loading. The hybrid composites behave like semiconductor and follow 3D variable range hopping model through the whole range of experimental temperature (50–300 K).

Debabrata Nandi, Kaushik Gupta†, Arup Kumar Ghosh†, Amitabha De, Nihar Ranjan Ray, Uday Chand Ghosh†

1.2.3.31 Reduced Graphene Oxide/Ethylene Vinyl Acetate Co-polymer Composite with Improved Thermal Stability and Flame Retardancy

Graphene based polymer composites have emerged as a frontier field of research in recent years. Mechanical, thermal and electrical properties are reported to be significantly improved on addition of this carbonaceous material in polymers. On the other hand ethylene vinyl acetate copolymer is an important conventional polymer to be used in different fields. But poor thermal stability and weak flame retardancy limit the use of this polymer in wider fields. The present investigation therefore, reports the fabrication of reduced graphene oxide GR/EVA composites at varying wt % of GR content by solution mixing method to improve the above properties. XRD and SEM are employed to study the morphology of the composites. Thermal stability and flame retardancy of the composites were studied by thermogravimetric (TG) analysis and limiting oxygen index (LOI) test respectively. Under identical condition composite shows better thermal stability and an increase of similar to 70% of LOI value in the composite with only 0.75% of GR content than that of pristine EVA.

Debabrata Nandi†, Atanu Talukdar, Uday Chand Ghosh†, Amitabha De, Satyaban Bhunia, Arup Kumar Ghosh†

1.2.3.32 Hydrogen Bond Sensitive Probe 5-Methoxy-1-keto-1,2,3,4-tetrahydro Carbazole in the Microheterogeneity of Binary Mixtures and Reverse Micelles

The structure and dynamics of water under confinement differ drastically from its bulk behavior and show a considerable degree of inhomogeneity due to disruption in its hydrogen bonding (H-bonding)

network. We attempt to probe such a microheterogeneous environment of reverse micelles (RMs) as well as binary mixtures of acetonitrile water and ethanol water by a H-bond sensitive probe 5-methoxy-1-keto-1,2,3,4-tetrahydro carbazole (MTC). Photophysical properties (quantum yield, lifetime, λ_{max}) of MTC in the excited states are found to be extremely sensitive to the changes in the H-bonding of its immediate local environment. We observe huge Stoke's shifts in the λ_{max}^{em} of MTC with variation in the solvent environment, as we increase the polarity inside the nanopool of RMs and the mole fractions of water in the binary mixtures. We are able to effectively sense the subtle changes in the H-bonding network inside RMs with an increase in w_0 and the formation of self-aggregated microclusters inside the binary mixtures, by measuring the photophysical variations in steady state and time-resolved fluorescence of MTC. An iso-emissive point in the time-resolved area normalized spectra of MTC inside RMs suggests the presence of two distinct emissive species of MTC, (a) MTC* and (b) H-bonded MTC, h-MTC*, which are expected to be predominant in nonaqueous and aqueous media, respectively. The variations in the nature and type of the H-bonding in such self-assemblies and clusters with changes in aqueous environment are very well characterized by the photophysics of two isomers of MTC.

Manas Kumar Sarangi, Amrit Krishna Mitra, Chaitrali Sengupta, Sujay Ghosh, Suchandra Chakraborty, Chandan Saha, Samita Basu

1.2.4 Structural Genomics

1.2.4.1 Identical RNA-Protein Interactions in Vivo and in Vitro and a Scheme of Folding the Newly Synthesized Proteins by Ribosomes

A distinct three-dimensional shape of rRNA inside the ribosome is required for the peptidyl transfer activity of its peptidyltransferase center (PTC). In contrast, even the in vitro transcribed PTC RNA interacts with unfolded protein(s) at about five sites to let them attain their native states. We found that the same set of conserved nucleotides in the PTC interact identically with nascent and chemically unfolded proteins in vivo and in vitro, respectively. The time course of this interaction, difficult to follow in vivo, was observed in vitro. It suggested nucleation of folding of cytosolic globular proteins vectorially from hydrophilic N to hydrophobic C termini, consistent with our discovery of a regular arrangement of cumulative hydrophobic indices of the peptide segments of cytosolic proteins from N to C termini. Based on this observation, we propose a model here for the nucleation of folding of the nascent protein chain by the PTC.

Debasis Das, Dibyendu Samanta, Salman Hasan...Abhijit Chakrabarti et al

1.2.4.2 Rotaviral Enterotoxin Nonstructural Protein 4 Targets Mitochondria for Activation of Apoptosis during Infection

Viruses have evolved to encode multifunctional proteins to control the intricate cellular signaling pathways by using very few viral proteins. Rotavirus is known to express six nonstructural and six structural proteins. Among them, NSP4 is the enterotoxin, known to disrupt cellular Ca^{2+} homeostasis by translocating to endoplasmic reticulum. In this study, we have observed translocation of NSP4 to mitochondria resulting in dissipation of mitochondrial membrane potential during virus infection and NSP4 overexpression. Furthermore, transfection of the N- and C-terminal truncated NSP4 mutants followed by analyzing NSP4 localization by immunofluorescence microscopy identified the 61-83-amino acid region as the shortest mitochondrial targeting signal. NSP4 exerts its

proapoptotic effect by interacting with mitochondrial proteins adenine nucleotide translocator and voltage-dependent anion channel, resulting in dissipation of mitochondrial potential, release of cytochrome c from mitochondria, and caspase activation. During early infection, apoptosis activation by NSP4 was inhibited by the activation of cellular survival pathways (PI3K/AKT), because PI3K inhibitor results in early induction of apoptosis. However, in the presence of both PI3K inhibitor and NSP4 siRNA, apoptosis was delayed suggesting that the early apoptotic signal is initiated by NSP4 expression. This proapoptotic function of NSP4 is balanced by another virus-encoded protein, NSP1, which is implicated in PI3K/AKT activation because overexpression of both NSP4 and NSP1 in cells resulted in reduced apoptosis compared with only NSP4-expressing cells. Overall, this study reports on the mechanism by which enterotoxin NSP4 exerts cytotoxicity and the mechanism by which virus counteracts it at the early stage for efficient infection.

Rahul Bhowmick, Umesh Chandra Halder, Shiladitya Chattopadhyay...Oishee Chakrabarti, et al

1.2.4.3 Biophysical studies with AICD-47 reveal unique binding behavior characteristic of an unfolded domain

APP intracellular C-terminal domain (AICD-47), generated upon γ -secretase cleavage of amyloid precursors protein (APP), bears the signature of a classical intrinsically unstructured domain (IUD). Comparing the recent crystal structures of AICD-47 peptides bound to its different adaptors such as protein-tyrosine-binding domain-2 (PTB2) of Fe65 and Src homology 2 (SH2) domain of growth factor receptor binding protein 2 (Grb2), the "conformational switching" of AICD-47 becomes evident. In order to understand different binding processes undertaken by this flexible molecule, upon recognizing different interfaces resulting in different 3D conformations, spectroscopic and calorimetric studies have been done. CD spectroscopy has revealed an overall random coil like structure in different pHs while TFE (2'-2'-2'-trifluoro ethanol) and HFIP (Hexa fluoro isopropanol) induced α -helicity to a certain extent. Binding of Tyr phosphorylated AICD-47 (P AICD-47) to Grb2-SH2 domain was carried out by a favorable enthalpic change ($\Delta H = -197.5 \pm 6.2$ kcal mole⁻¹ at 25° C) and an unfavorable entropic contribution ($\Delta S = -631$ cal mol⁻¹ deg⁻¹ at 25° C). Alternative conformation of AICD-47 in different biological contexts is another remarkable feature of IUDs which presumably has definitive roles in regulating Alzheimers disease phenotype.

Samir Das, Saptarni Ghosh, Dipak Dasgupta, Udayaditya Sen, Debashis Mukhopadhyaya

1.2.4.4 Notch1 intracellular domain increases cytoplasmic EZH2 levels during early megakaryopoiesis

Notch pathway is a well known player in the development of lymphoid lineage. However, its role in the myeloid lineage has remained ambiguous. We looked into the effect of Notch1 on the megakaryocytic lineage commitment and found an increase in megakaryocyte specific lineage markers upon transfection with Notch1 intracellular domain (NICD). This effect was mediated by Akt whereby constitutive activation of Akt increased the megakaryocyte markers while inhibition of Akt signalling reduced these marker levels. Along with the change in differentiation status, NICD induced initiation of early megakaryopoiesis was accompanied by increased cytoplasmic EZH2 expression. This process was found to be Akt dependent and inhibition or over expression of Akt lead to concurrent changes in EZH2 levels. To elucidate the function of EZH2 in the cytoplasm, novel

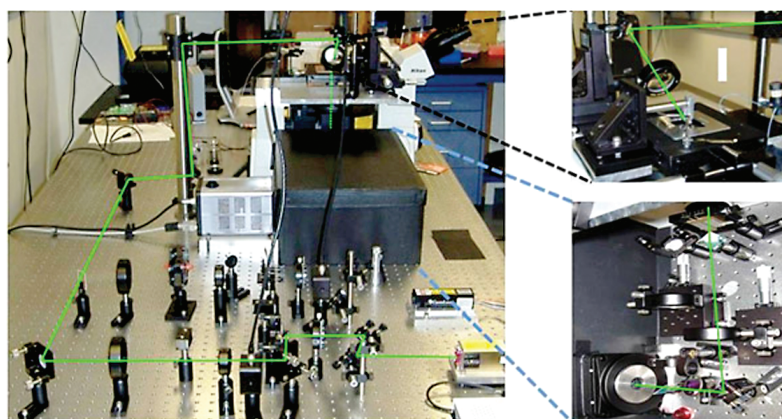
cytoplasmic interactors of EZH2 were identified by Co-IP followed by MALDI MS/MS based protein identification and thus PDIA1 and LIMK1 were identified. Interaction of EZH2 with LIMK1 changed the activity of cofilin (a downstream target of LIMK1) towards actin filaments thereby leading to lower filamentous actin content within these cells. Thus Notch1 not only induces early megakaryopoiesis but also prepares these cells for subsequent morphological changes.

A Roy, NP Basak, S Banerjee

1.3 Developmental Work

1.3.0.5 Single Molecule FRET imaging system

Recent advances in single-molecule detection and single-molecule spectroscopy at room temperature by laser-induced fluorescence offer new tools for the study of individual macromolecules under physiological conditions. In Chemical Sciences division, we have successfully developed a total internal reflection fluorescence (TIRF) based Single molecule fluorescence resonance energy transfer (smFRET) imaging system to examine a multitude of phenomena.

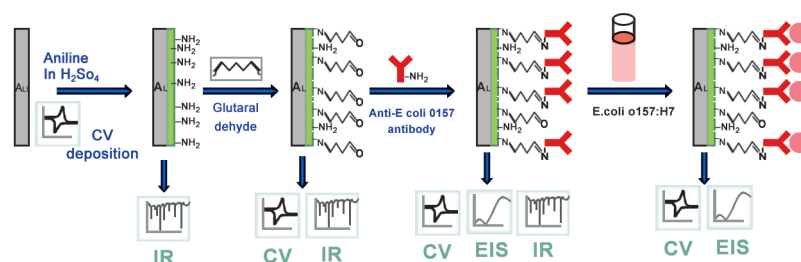


This home-built smFRET system can create super-resolution images with a resolution of 10 to 20 nanometer. The advantages of this system are to relay conformational states, conformational dynamics, and activity of single biological molecules to physical observables in real time, unmasked by ensemble averaging. Distributions and time trajectories of these observables can therefore be measured during a reaction without the impossible need to synchronize all the molecules in the ensemble.

Padmaja Prasad Mishra

1.3.0.6 Sensing Bacteria Using Antibody Linked PANI

We have developed a new and simple method for label free, rapid and inexpensive impedimetric sensing of E.Coli O157:H7 bacteria using antibodyantigen binding method based on covalently linked antibody on a Conducting Polyaniline (PANI) film.



The sensing procedure which may be an easy substitute of ELISA in pathogen detection is fabricated by covalent immobilization of E.Coli O157:H7 antibody. Electrochemical impedance spectroscopy (EIS) was used to test the sensitivity and effectiveness of the sensor by measuring the change in impedance values of electrodes before and after incubation with different concentration of bacteria from 10² CFU mL⁻¹ to 10⁷ CFU mL⁻¹.

Amitava De

1.4 Publications

1.4.1 Publications in Books/Monographs & Edited Volumes

1.4.1.1 Books Edited

Maitreyee Nandy

Accelerator and Radiation Physics, Narosa Publishing House Pvt Ltd, Eds: PK Sarkar, Samita Basu, Maitreyee Nandy, (2013) ISBN: 978-81-8487-182-1

1.4.1.2 Publications in Monographs

Maitreyee Nandy

Maitreyee Nandy, C Sunil, Estimation of induced activity in an ADSS facility in Tech Open access book Radioactive Waste (2012) ISBN: 978-953-51-0551-0

1.4.2 Publications in Journal

Ajoy Mandal, Susanta Lahiri, Production and separation of no-carrier-added ⁷³As and ⁷⁵Se from ⁷Li irradiated germanium oxide target, *Radiochimica Acta*, **100** (2012) 865

A Manikandan, B Sarkar, M Nandy et al, Evaluation of Velocity Dependent Positional Error of Dynamic Multi Leaf Collimator During VMAT Delivery Using a Well Defined Mathematical Function, *Medical Physics* **39** (2012) 3714

Ankan Dutta Chowdhury, Amitabha De, Chirosree Roy Chaudhuri et al, Label free polyaniline based impedimetric biosensor for detection of E. coli O157:H7 Bacteria, *Sensors and Actuators B* **171** (2012) 916

Anup Kumar Maity, Partha Saha, The histone acetyl transferase LdHAT1 from *Leishmania donovani* is regulated by S-phase cell cycle kinase, *FEMS Microbiology Letters* **336**(2012) 57

A Roy, NP Basak, S Banerjee, Notch1 intracellular domain increases cytoplasmic EZH2 levels during early megakaryopoiesis, *Cell Death & Disease* **3** (2012) Art No:e380

B Dutta, S Lahiri, BS Tomar, Application of PEG based aqueous biphasic systems in extraction and separation of no-carrier-added Re-183 from bulk tantalum, *Radiochimica Acta* **101** (2013) 19

B Ghosh, M Sardar, S Lahiri, S Banerjee, Observation of superparamagnetism to flux closure behaviour in ZnO nanoparticle agglomerates, *Journal of Physics-Condensed Matter* **24** (2012) Art No: 366002

Biswapathik Pahari, Bidisha Sengupta, Sandipan Chakraborty, Pradeep K Sengupta, Contrasting binding of fisetin and daidzein in gamma-cyclodextrin nanocavity, *Journal of Photochemistry and Photobiology* **B118** (2013) 33

B Pahari, S Chakraborty, S Chaudhuri, B Sengupta, PK Sengupta, Binding and antioxidant properties of therapeutically important plant flavonoids in biomembranes: Insights from spectroscopic and quantum chemical studies, *Chemistry and Physics of Lipids* **165** (2012) 488

B Sarkar, M Nandy, A Manikandan et al, Estimation of Uncertainty in Dose Delivery Due to MLC Position Inaccuracies by Inverse Derivative Method During Volumetric Modulated Arc Therapy Delivery by Elekta Beam Modulator, *Medical Physics* **39** (2012) 3715

C Sunil, A Shanbhag, M Nandy et al, Neutron ambient dose equivalent from 5 MeV/u $^{10,11}\text{B}$, $^{12,13}\text{C}$ and $^{16-18}\text{O}$ projectiles incident on a thick Al target, *Radiation Measurements* **47** (2012) 1035

Debabrata Nandi†, Atanu Talukdar, Uday Chand Ghosh†, Amitabha De, Satyaban Bhunia, Arup Kumar Ghosh†, Reduced Graphene Oxide/Ethylene Vinyl Acetate Co-polymer Composite with Improved Thermal Stability and Flame Retardancy, *J Polym Mater* **29** (2012) 401

Debabrata Nandi, Kaushik Gupta†, Arup Kumar Ghosh†, Amitabha De, Nihar Ranjan Ray, Uday Chand Ghosh†, Thermally stable polypyrrole- Mn doped Fe(III) oxide nanocomposite sandwiched in graphene layer: synthesis, characterization with tunable electrical conductivity, *Chemical Engineering Journal* **220** (2013) 107

Debasis Das, Dibyendu Samanta, Salman Hasan et al, Identical RNA-Protein Interactions in Vivo and in Vitro and a Scheme of Folding the Newly Synthesized Proteins by Ribosomes, *Journal of Biological Chemistry* **287** (2012) (2012) 37508

Dipak Dasgupta, Parijat Majumder, Amrita Banerjee, A revisit of the mode of interaction of small transcription inhibitors with genomic DNA, *Journal of Biosciences* **37** (2012) 475

Kamalika Roy Choudhury, Swasti Raychaudhuri, Nitai P Bhattacharyya, Identification of HYPK-

Interacting Proteins Reveals Involvement of HYPK in Regulating Cell Growth, Cell Cycle, Unfolded Protein Response and Cell Death, PLOS One **7** (2012) Art No: e51415

K Ghosh, M Maiti, S Lahiri, Separation of no-carrier-added ^{113}Sn , ^{117m}Sn and ^{113n}In , ^{114m}In from alpha particle irradiated natural cadmium target, Journal of Radioanalytical and Nuclear Chemistry **295** (2013) 865

Maitreyee Nandy, Chirashree Lahiri, Radioactivity generation in Pb target by protons - A comparative study from MeV to GeV, 0, Indian Journal of Pure & Applied Physics **50** (2012) 761

Manas Kumar Sarangi, Ankita Mitra, Samita Basu, Prototropic Interactions of Pyrimidine Nucleic Acid Bases with Acridine: A Spectroscopic Investigation, Journal of Physical Chemistry **B116** (2012) 10275

Mithun Sinha, Saikat Mukhopadhyay, Nitai P Bhattacharyya, Mechanism(s) of Alteration of Micro RNA Expressions in Huntington's Disease and Their Possible Contributions to the Observed Cellular and Molecular Dysfunctions in the Disease, Euromolecular Medicine **14** (2012) 221

Moumita Maiti, Ajoy Mandal, Susanta Lahiri, An improved non-destructive method of potassium determination, Applied Radiation and Isotopes **71** (2013) 37

Moumita Maiti, Kaustab Ghosh, Susanta Lahiri, Simultaneous production and separation of no-carrier-added ^{111}In , ^{109}Cd from alpha particle induced silver target, Journal of Radioanalytical and Nuclear Chemistry **295** (2013) 1945

Moumita Maiti, Santosh R Tiwari, Nilesch B Dubey, et al, An improved method for determination of Be-7 in mosses, Journal of Radioanalytical and Nuclear Chemistry **295** (2013) 1443

Mousumi Banerjee, Abhijit Chakrabarti, Samita Basu, Oxidative Interaction between OxyHb and ATP: A Spectroscopic Study, Journal of Physical Chemistry **B116** (2012) 6150

Partha S Guin, Parikshit C Mandal, Saurabh Das, The Binding of a Hydroxy-9,10-anthraquinone CuII Complex to Calf Thymus DNA: Electrochemistry and UV/Vis Spectroscopy, Chempluschem **77** (2012) 361

Piyali Mitra, Brotati Chakraborty, Dhananjay Bhattacharyya, Samita Basu, Excimer of 9-Aminoacridine Hydrochloride Hydrate in Confined Medium: An Integrated Experimental and Theoretical Study, Journal of Physical Chemistry **A117** (2013) 1428

PK Saran, Maitreyee Nandy, PK Sarkar et al, Production of long-lived Al-26 and Na-24 from neutron interaction in Al target, Indian Journal of Pure & Applied Physics **50** (2012) 509

Priyanka Saha, Debasis Das, Sumana Roy, Arunabha Chakrabarti et al, Effect of gamma irradiation on metallothionein protein expression in *Plantago ovata* Forsk, International Journal of Radiation Biology **89** (2013) 88

Prodipta Sarkar, Shinji Yamasaki, Soumen Basak et al, Purification and characterization of a new alkali-thermostable lipase from *Staphylococcus aureus* isolated from *Arachis hypogaea* rhizosphere,

Process Biochemistry **47** (2012) 858

Rahul Bhowmick, Umesh Chandra Halder, Shiladitya Chattopadhyay, Oishee Chakrabarti et al, Rotaviral Enterotoxin Nonstructural Protein 4 Targets Mitochondria for Activation of Apoptosis during Infection, *Journal of Biological Chemistry* **287** (2012) 35004

Rakhi Paul, Seema Nath, Udayaditya Sen, Cloning, expression, purification, crystallization and preliminary X-ray analysis of a fructokinase from *Vibrio cholerae* O395, *Acta Crystallographica* **F68** (2012) 1564

Ramanuj Banerjee, Seema Nath, Amitabh Ranjan, et al, The First Structure of Polarity Suppression Protein, Psu from Enterobacteria Phage P4, Reveals a Novel Fold and a Knotted Dimer, *Journal of Biological Chemistry* **287** (2012) 44667

Rupali Gangopadhyay†, Ankan Dutta Chowdhury, Amitabha De, Functionalised Polyaniline Nanowires: A Prospective Biosensing Platform, *Asian Journal of Chemistry* **25** (2013) S369

Rupali Gangopadhyay†, Ankan Dutta Chowdhury, Amitabha De, Functionalized polyaniline nanowires for biosensing, *Sensors and Actuators* **B171** (2012) 777

Samir Das, Saptarni Ghosh, Dipak Dasgupta, Udayaditya Sen, Debashis Mukhopadhyaya, Biophysical studies with AICD-47 reveal unique binding behavior characteristic of an unfolded domain, *Biochemical and Biophysical Research Communications* **425** (2012) 201

Sandipan Chakraborty, Sudip Chaudhuri, Biswapathik Pahari...Pradeep K Sengupta et al, A critical study on the interactions of hesperitin with human hemoglobin: Fluorescence spectroscopic and molecular modeling approach, *Journal of Luminescence* **132** (2012) 1522

Sankar Basu, Dhananjay Bhattacharyya, Rahul Banerjee, Self-Complementarity within Proteins: Bridging the Gap between Binding and Folding, *Biophysical Journal* **102** (2012) 2605

Sarita Roy, Soumen Basak, Pulak Ray et al, Double plasmonic profile of tryptophan-silver nano-crystals-Temperature sensing and laser induced antimicrobial activity, *Photonics and Nanostructures-Fundamentals and Applications* **10** (2012) 506

S Bhattacharjya†, S Nath†, J GhoseNP Bhattacharyya et al, miR-125b promotes cell death by targeting spindle assembly checkpoint gene MAD1 and modulating mitotic progression, *Cell Death Differ* **3** (2013) 430

Seema Nath, Ramanuj Banerjee, Susmita Khamrui, et al, Cloning, purification, crystallization and preliminary X-ray analysis of two low-molecular-weight protein tyrosine phosphatases from *Vibrio cholerae*, *Acta Crystallographica* **F68** (2012) 1204

Shibojyoti Lahiri, Toshifumi Takao, Pukhrambam Grihanjali Devi, Saptarni Ghosh, Ayanjeet Ghosh, Amrita Dasgupta, Dipak Dasgupta, Association of aureolic acid antibiotic, chromomycin A3 with Cu²⁺ and its negative effect upon DNA binding property of the antibiotic, *Biometals* **25** (2012) 435

Shibojyoti Lahiri, Toshifumi Takao, Pukhrambam Grihanjali Devi, Saptarni Ghosh, Ayanjeet

Ghosh, Amrita Dasgupta, Dipak Dasgupta, Association of aureolic acid antibiotic, chromomycin A3 with Cu²⁺ and its negative effect upon DNA binding property of the antibiotic, *Biometals* **25** (2012) 435

Shiladitya Chattopadhyay, Trayambak Basak, Kant Mukti, Oishee Chakrabarti et al, Identification of Cellular Calcium Binding Protein Calmodulin as a Regulator of Rotavirus A Infection during Comparative Proteomic Study, *PLOS ONE* **8** (2013) Art No:e56655

Sudip Majumder, Susmita Khamrui, Jhimli Dasgupta et al, Role of remote scaffolding residues in the inhibitory loop pre-organization, flexibility, rigidification and enzyme inhibition of serine protease inhibitors, *Biochimica et Biophysica Acta-Proteins and Proteomics* **1824** (2012) 882

Sudipta Pal, Mili Das, Dipak Dasgupta, Structural studies of arginine induced enhancement in the activity of T7 RNA polymerase, *Biochemical and Biophysical Research Communications* **421** (2012) 27

Sumana Roy, JK Dattagupta, Sampa Biswas, Expression of recombinant human cathepsin K is enhanced by codon optimization, *Process Biochemistry* **47** (2012) 1944

Sutapa Saha, Suchismita Halder, Dipankar Bhattacharya, Debashis Banerjee, Abhijit Chakrabarti, Fractional precipitation of plasma proteome by ammonium sulphate: case studies in leukemia and thalassemia. *J Proteomics Bioinformatics* **5** (2012) 163

Swadesh Mandal, Ajoy Mandal, Susanta Lahiri, Separation of nca ^{123,124,125,126}I from alpha particle induced the natural antimony trioxide target, *Journal of Radioanalytical and Nuclear Chemistry* **292** (2012) 579

Swadesh Mandal, Ajoy Mandal, Susanta Lahiri, Species dependent extraction of ⁹⁹Mo, *Journal of Radioanalytical and Nuclear Chemistry* **295** (2013) 861

Swadesh Mandal, Susanta Lahiri, Cloud point extraction of ⁹⁹Mo with Triton X-114, *Journal of Radioanalytical and Nuclear Chemistry* **295** (2013) 1361

Swadesh Mandal, Susanta Lahiri, Studies on dynamic dissociation constant of ⁹⁹Mo-insulin complex, *Journal of Radioanalytical and Nuclear Chemistry* **292** (2012) 859

Swadesh Mandal, Susanta Lahiri, Synthesis of molybdenum nanoparticle by in situ gamma-radiation, *Applied Radiation and Isotopes* **70** (2012) 2340

TK Mandal, NS Das, Testicular gametogenic and steroidogenic activities in chlorpyrifos insecticide-treated rats: a correlation study with testicular oxidative stress and role of antioxidant enzyme defence systems in Sprague-Dawley rats, *Andrologia* **44** (2012) 102

1.5 Ph D Awarded

Brotati Chakraborty [Samita Basu], A study of photoinduced interactions of some acridine derivatives with organic amines and macromolecules of biological relevance, Jadavpur University, December 2012

Manas Kumar Sarangi [Samita Basu], Photo-physical and magnetic field effect studies on electron / proton transfer among biologically important molecules in homogenous and heterogeneous media, University of Calcutta, February 2013

Sutapa Saha [Abhijit Chakrabarti], Proteomic Study in a Hematological Malignancy: B-cell Acute Lymphoblastic Leukemia, Homi Bhabha National Institute (HBNI) April 2012

1.6 Seminars/Lectures given in Conference/Symposium/Schools

Amitabha De

1. Covalently linked to Polyaniline-Gold Nanocomposite for low level Glucose detection, Fifth International Conference on Electroactive Polymers (ICEP 2012), Organized by Indian Society of Electroactive Polymers, BHU, Varanasi, India, Nov 4-9, 2012

Samita Basu

1. Electrons in Molecular Orbitals: Absorption and Emission, DST JBNSTS INSPIRE Science Camp, JBNSTS, Kolkata, Jul 11, 2012
2. Excited State Properties of Molecules, Academic Staff College, Department of Chemistry, Calcutta University, Aug 25, 2012
3. A spectroscopic approach for the determination of modes of interactions of small molecules with proteins in vitro, National Symposium on Recent Palestrae in Photosciences, Banaras Hindu University, Varanasi, Sep 3-4, 2012
4. Magnetodynamics in Photoinduced Electron Transfer: Enhancement of Exciplex Fluorescence / Free ion Formation, National Fluorescence Workshop: Fluorescence Methods in Single Molecule Spectroscopy, SINP & IICB, Kolkata, Dec 3-7, 2012
5. Magnetic field effect on photoinduced chemical reactions, Professor PK Bose Memorial Lecture for the year 2011 in the 49th Annual Convention of Chemists held at Bhopal, Madhya Pradesh organized by Indian Chemical Society, Kolkata, Dec 12-14, 2012
6. Significance of magnetic field effect in distance-dependent photoinduced electron transfer reactions Seminar in IIT Bombay, Dec 21, 2012
7. Excited State Properties: Photophysical and Photochemical Behavior of Acridine, Academic Staff college, Department of Chemistry, Jadavpur University, Jan 05, 2013
8. Laser flash photolysis with magnetic field effect: an efficient tool to identify photoinduced electron transfer embedded with other excited state interactions, National Seminar on "Recent Trends in Chemical Sciences" (RETICS-2013), School of Chemistry, Sambalpur University, Sambalpur, Mar 16-17, 2013

Susanta Lahiri

1. Alternative production routes and new separation methods for no-carrier-added ^{163}Ho , the Fu-

ture of Neutrino Mass Measurements: Terrestrial, Astrophysical, and Cosmological Measurements in the Next Decade (ν Mass13), by Susanta Lahiri, Moumita Maiti, Zoltan Szucs and Sandor Takacs, Milano, Italy, Feb 4-7, 2013

2. ^{163}Ho , Collaboration meeting on Electron Capture Holmium Neutrino (ECHO), by Susanta Lahiri, Moumita Maiti, Zoltan Szucs, Sandor Takacs, Johannes Gutenberg Universitat Mainz, Jan 21, 2013

3. Chemistry of Lead Bismuth Loop, Kick off meeting for lead bismuth loop, CERN, Switzerland, May 10, 2012

4. ICP-state of the art instruments for trace analysis, Thematic Workshop on Trace Element analysis and Radiological Sciences, Manipal University, Imphal, Mar 12-14, 2013

5. Neutrino mass measurement and radiochemistry, Susanta Lahiri and Moumita Maiti, Nuclear and Radiochemistry Symposium, NUCAR-2013, RD University, Jabalpur, Feb 19-23, 2013

Maitreyee Nandy

1. Nuclear Reaction Models - Source Term Estimation for Safety Design in Accelerators, DAE-BRNS Theme Meeting on Physics Aspects of Accelerator Radiation Protection, BARC Training School Hostel, Anushaktinagar, Mumbai, Feb 20-22, 2013

2. Environmental Radioactivity Analysis at Kolkata after Fukushima Accident, by Banhi Chatterjee, Abhijit Bisoi, Dibyadyuti Pramanik, Sudatta Ray, Aditya Priyant, Maitreyee Saha Sarkar, Maitreyee Nandy, 12th International Conference on Radiation Shielding (ICRS-12), organized by the Atomic Energy Society of Japan at Nara Prefectural New Public Hall, Nara, Japan, Sep 2-7, 2012

3. Radiation Environment - Assessment, Measurement and its Impact, International conference RADENVIRON 2012, Babasaheb Bhimrao Ambedkar University, Lucknow, Uttar Pradesh, India, Apr 12-14, 2012

4. Radiation in Space Biological Effects, 14 day Workshop in Fundamentals of Space Science and Technology, KalpanaChawla Centre for Space and Nano-Sciences and Ramkrishna Mission Vivekananda Institute, Kolkata, Jun 2012

Abhijit Chakrabarti

1. Eryptosis in Hemoglobinopathy, 81st Annual Meeting of Society of Biological Chemists (I) & Symposium on Chemistry & Biology, Two Weapons against Disease, Science City, Kolkata, Nov 8-11, 2012

2. Differential expression of red cell proteins in hemoglobinopathy, International Symposium on Proteomics beyond IDs..and Fourth Annual Meeting of Proteomics Society (India), CSIR-National Chemical Laboratory, Pune, Nov 22-24, 2012

3. Membrane asymmetry and Spectrin interactions with aminophospholipids : implications in hematological disease, Indo-US Meeting on Structure, Dynamics and Mechanics of Biological Membranes, Department of Chemical Engineering, Indian Institute of Science, Bengaluru, Dec 29-31, 2012

4. Clinical proteomics in hemoglobin disease, 100th Indian Science Congress, University of Calcutta, Kolkata, Jan 3-7, 2013

5. Lecture on Footprints of Life in C K Majumdar Memorial Summer Workshop in Physics 2012, organized jointly by Indian Association of Physics Teachers (Regional Council 15) and SN Bose National Centre for Basic Sciences, June 20, 2012

Kaushik Sengupta

Nuclear Lamins & Laminopathies: Understanding the Complex Circuitry, TIFR, Mumbai, June 2012

Chandrima das

Recognition of specific epigenetic modifications by the reader domains of CBP and ZMYND8, 16th Transcription Assembly Meeting, Kolkata, Mar 3-5, 2013

1.7 Honours and Distinctions

Avik Basu

Avik Basu has been awarded with the Nehru-Fullbright Fellowship to work in the laboratory of Dr. David Speicher, Wistar Institute, University of Pennsylvania, USA during July 2012 March 2013

Chandrima Das

Ramalingaswami Fellowship awarded for 2011-2012 from Department of Biotechnology (DBT) was activated from April 2012

1.8 Teaching elsewhere

Samita Basu

M Sc (Inorganic Chemistry special), Spectroscopy, University of Calcutta
M Sc (Physical Chemistry special), Photochemistry, Midnapore College, Vidyasagar University, West Bengal

1.9 Miscellany

Samita Basu

Professor PK Bose Memorial Award, Indian Chemical Society, December 2012

Kaushik Sengupta

DBT-CREST award, DBT, Govt of India, 2012

KNOW YOUR ENVIRONMENT: Science Camp for undergraduate students, Nov 8-10, 2012, Organized by Saha Institute of Nuclear Physics Under the auspicious of the project TULIP

A three days residential science camp was organized for the undergraduate students on Know your environment during Nov 8-10, 2012



Total 50 undergraduate students from different colleges mainly located at the adjacent districts of Kolkata, like Howrah, Hooghly, North 24 Pgs, South 24 pgs participated in the event. Nine resource persons delivered lectures on various aspects of environment. The program also included laboratory demonstration. The program was highly successful as the participants went home with promise to keep the environment safe to the best of their ability.

Chapter 2

Condensed Matter Physics including Surface Physics and NanoScience

2.1 Summary of Research Activities of Divisions

2.1.1 Applied Material Science

Calf-thymus DNA, spin-coated from pristine and 500mM NaCl solutions in water, show formation of well defined thin films. The X-ray reflectivity studies reveal pristine film consists of three layers i.e. lateral stacks of three layers of DNA molecules whereas the salted film has lesser thickness ~ 1.5 times of DNA chain width, indicating enhanced lateral entanglement. Pressure area isotherm of a stearic acid monolayer is recorded and the corresponding image viewed using a Brewster Angle Microscope. Au nanoparticles have been introduced into the monolayer at two different concentrations. The changes in the pressure area isotherm of the system as it progressively changes from a complex to a simpler two dimensional liquid have been studied. The relationship between the change in viscosity of a solution of 50 g asphaltene in 100 ml toluene and the methyl to methylene (CH_3/CH_2) ratio of the asphaltene, when exposed to ultrasonic irradiation, has been studied. The asphaltene used was extracted from refinery sedimentation. Adopting Fourier transform infrared spectroscopy (FTIR) and viscosity measurement as the probing tools, it is found that the viscosity initially decreases but eventually it starts to increase with prolonged duration of ultrasound irradiation. Viscosity decrease is accompanied by an increase in CH_3/CH_2 ratio, which, however, is reversed as the viscosity starts rising in the latter period of irradiation. Thus a clear correspondence exists between the two, viz. when asphaltene is exposed to ultrasonic irradiation its viscosity is inversely proportional to its CH_3/CH_2 ratio. The accuracy of the photo-acoustic (PA) technique to assess blood oxygen saturation (SO_2) using two laser beams was examined theoretically. A Monte Carlo technique was used to simulate 2D tissue configurations, and the PA signals from many red blood cells (RBCs) were constructed by summing the signals emitted by the individual cells. The level of oxygenation of each cell was assumed to be identical in a configuration. The cellular oxygenation state defined the blood oxygen saturation (SO_2) and also controlled the PA signal amplitude. The PA amplitude was observed to vary linearly with blood SO_2 . It was nearly 4.6 times less and 8.2 times greater at $\text{SO}_2=100\%$ than that of 0% for the 600 and 1064 nm incident optical radiations, respectively. The

blood SO_2 was estimated using the PA amplitudes generated at these wavelengths. The estimated values matched perfectly with that of the actual SO_2 confirming the suitability of the PA technique to determine blood SO_2 noninvasively.

2.1.2 Experimental Condensed Matter Physics

The state of art of major capital equipments like cryogen free room temperature bore 9T for grain oriented, magnetocaloric effect studies, Custom built UHV Versatile thin film deposition set-up to fabricate high performance magnetic/nonmagnetic hybrid nano-structure, SQUID VSM for magnetic properties, Thermal expansion, thermal transport experimental systems have been installed. Phase transition and magnetoelectronic phase separation in La-Sr-Co-O single crystals, Giant magnetocaloric effect in antiferromagnetic R-Mn-O crystals, Vortex dynamics and second magnetization peak in Pr-Fe-As-O-F superconductor, the Hall coefficient and magnetic susceptibility of NaCoO_2 as functions of magnetic field and temperature have been experimentally studied. Using NMR field sweep magnet, the nature of spin trimer and 3d spin dynamics in $\text{Ca}_3\text{Cu}_2\text{Ni}(\text{PO}_4)_4$ was studied using ^{31}P NMR, Anisotropic spin-fluctuations in SmCoPO revealed by ^{31}P NMR measurement. The effect of interfacial hydrogen bonding on the behavior of the freezing/melting processes in two organoliquids, namely, ethylene glycol $[(\text{CH}_2\text{OH})_2]$ and isopropanol $[\text{CH}_3\text{CH}(\text{OH})\text{CH}_3]$, confined in nanopores of ZSM-5 zeolite has been investigated using the positron annihilation spectroscopy (PAS) and nuclear magnetic resonance (NMR) techniques. Further Evidence of a structural phase transition in superconducting $\text{SmFeAsO}_{1-x}\text{F}_x$ from ^{19}F NMR have been investigated.

Electronic transport properties of a Kondo lattice CeNi_9Si_4 at low temperature under pressure, Electronic transport minimum in SmCuAs_2 at low temperature with structural anomalies and Unusual pressure response of electronic transport properties of a Kondo insulator CeRu_4Sn_6 have been investigated. The possible Spin Glass like transition for the AFM nano particles in the limit of spin correlation length $\sim 10\text{-}20\text{nm}$ of Ni-Cr-O have been studied.

Scaling of non-Ohmic conduction in strongly correlated systems and Evidence of exchange bias effect and surface spin glass ordering in electron doped $\text{Sm}_{0.09}\text{Ca}_{0.91}\text{MnO}_3$ nanomanganites have been investigated.

Griffiths phase behavior has been observed in in some of the new antiferromagnetic intermetallic ternary 1-1-2 type of Sn based compounds. New intermetallic full Heusler alloys with valence electron count 24 has been synthesized to study the occurrence of possible large ZT. Large volume collapse has been observed in polymorphic antiperovskite compounds under annealing. Soft magnetic materials with high Curie temperature (400K) have been synthesized and investigated. New compounds of 2-1-3 type of intermetallics have also been synthesized for studying possible geometrically frustrated magnetism.

2.1.3 Surface Physics

Research activities of the Surface Physics Division encompass the physical and chemical methods of growing low-dimensional structures with tunable morphology and mechanical/electrical/magnetic/optical properties, epitaxial growth of semiconductor quantum structures and their applications in micro-nano technology. Modifications of materials using medium and low-energy ion beams, such as fabrication of decorated and modified surfaces as growth templates, synthesis of quantum dot-composites for photonic/plasmonic applications, etc. are also active areas of our ongoing research. The division has also been involved in the growth of magnetic and photonic structures through nano-manipulation and self-assembly, development of polymer-based photovoltaics and other molecular electronic systems and study of their morphology-transport cor-

relations. Glimpses of some important activities are given in the following.

Morphological and structural characterizations of Molecular Beam epitaxy (MBE) - grown Si/Ge superlattice structures are extensively being done using simultaneous analysis of x-ray reflectivity and x-ray diffraction data. Consistent analysis of the data collected in the Indian Beamline at Photon Factory Synchrotron (KEK, Japan) allows for the determination of electron density and strain profiles as a function of depth in the multilayer stacks.

Light emission and ultraviolet (UV) photoconductivity characteristics of ZnO nanorods (NRs) fabricated using a facile, cost-effective, and catalyst-free thermal decomposition route under varying reaction temperatures have been studied. The morphological and structural studies reveal the formation of homogeneous quality nanorods in large scale at the highest reaction temperature of 600°C. The luminescence feature of the nanorods is dominated by the defect related emission over the typical band edge emission. The variation of band-edge and native defect-related emission response of the samples has been correlated to the morphology and microstructure. In photoconductivity studies, the *IV* characteristics of the ZnO NRs prepared at different reaction temperatures in dark and under UV illumination ($\lambda = 365$ nm) follow the power law. An enhanced ultraviolet photodetection has been observed in the nanorods fabricated at the highest reaction temperature of 600°C. The sample exhibits UV photosensitivity value (photo-to-dark current ratio) of around 1.18×10^3 , which is much higher in magnitude compared to that of the samples prepared at lower reaction temperatures. The enhanced photoconductivity has been assigned to the development of uniformity and homogeneity of the nanorods.

Periodic ripple formation on GaAs sputtered by 60 keV Ar ions at an angle of 60° over a large range of ion doses from 1×10^{17} to 1×10^{19} ions/cm² have been studied under Atomic Force Microscopy (AFM). Initially in the dose range between 1×10^{17} and 4×10^{17} ions/cm², only very small roughness is formed on the surface and from the dose of 5×10^{17} ions/cm², the ripples start to form and attain a well-defined structure at a dose around 9×10^{17} ions/cm², remain stable and then from a dose of 4×10^{18} ions/cm², the ripple structures become very rough, periodicity breaks down and step-like features become prominent all over the surface. Parameters like rms roughness, ripple wavelength, amplitude etc. are measured from the AFM image analysis.

Localized surface plasmon (LSP) modes on individual tilted gold nanodecahedron sitting on a silicon substrate have been studied by cathodoluminescence (CL) spectroscopy and imaging in a field emission gun (FEG) scanning electron microscope (SEM). We experimentally resolve three distinct LSP modes in the far-field radiation acquired via CL. The experimental spectra and intensity maps of plasmon modes are in excellent agreement with the spectra and 2D-CL image obtained from finite difference time domain (FDTD) simulations. Detail analysis reveals the signature of a quadrupolar surface plasmon mode in addition to the two dipolar modes along azimuthal and polar direction of the decahedron. The experimental method and the theoretical formalism presented here provide useful insight into the plasmonic behavior of complex shaped metal nanoparticle supported by a high index substrate.

Irradiation of crystalline muscovite mica samples by 500 eV Ar⁺ ions at different incident angles can induce significant surface morphological variations. A periodic ripple pattern of nano-dimensions forms in the angle window 47 degrees-70 degrees. On the other hand, tilted conical protrusions develop on the surface at grazing incidence angles around 80 degrees. From the derivative of the topographic images the distribution of the side-facet slopes in the ion incidence plane are measured, which is found to be strongly related to the pattern morphology. Additionally, it has been shown that, for the ripple structures, the base angles can be tuned by changing the ion fluence. An asymmetric sawtooth profile of the ripples obtained at low fluence is transformed to a symmetrical triangular profile at high fluence. As the slopes are found to be small, the pattern formation is not provoked by the gradient-dependent erosion mechanism rather it is the general effect of the

curvature-dependent sputtering phenomena.

Electronic structure of low dimensional materials such as MoS_2 and MoSe_2 has been studied using Angle-resolved Photoemission Spectroscopic (ARPES) studies and the noble metal over layers on such materials have been explored. These studies have been supported by ab-initio band structural calculations which provide a good description of the electronic structure of such materials. In-plane dispersions of quantum well (QW) states originating from the electron confinement of Ag sp electrons within the MoS_2 band gap region are investigated by means of angle-resolved photoemission spectroscopy (ARPES). A number of QW resonances have been observed in the ARPES spectra in a binding energy range lying outside the MoS_2 energy gap which is required for full confinement of the Ag sp electrons. In spite of having the expected free electron-like behavior, these QW states show a significant increase of in-plane effective mass with increasing binding energy due to the hybridization of Ag sp electrons with the MoS_2 valence bands. The binding energy dependence of the bottom of the QW states ($k_{\parallel} = 0$) as a function of the Ag film thickness has been analyzed. The well-established phase accumulation model has been applied for calculating the phase shifts of electrons at the boundaries. Our observations show that the total phase shift behaves differently for energies above and below the MoS_2 valence band maxima, due to the hybridizations being different in nature. The structure plot calculated considering the different quantum number dependent total phase shifts provides a good description of the experimental observations.

The hydrophilic/hydrophobic nature of the Cl-passivated Ge (001) surface is investigated directly by contact angle (CA) measurement and indirectly by growing nickel arachidate Langmuir-Blodgett (LB) films on the Cl-passivated Ge(001) surface. Passivation of Ge (001) surface by Cl atoms is confirmed by X-ray photoelectron spectroscopy measurement. CA measurements show that the Cl-passivated Ge (001) surface has intermediate wettability, i.e., the surface has intermediate hydrophilic/hydrophobic behavior. Structural information obtained from the deposited LB films by using X-ray reflectivity and atomic force microscopy analysis shows that the surface is homogeneous and hydrophilic (similar to 85%), although very few effectively hydrophobic (similar to 15%) regions are present. Structural study in molecular level thus helps to identify the surface nature in nanometer level, which is not possible by simple macroscopic CA measurement. Specific electrostatic and dispersive effects of Cl atoms are possibly responsible for such hydrophilic-like nature of the Cl-passivated Ge (001) surface.

Nanowires of polypyrrole have exhibited switching transition that reduces the resistance of the wires by several orders of magnitude under certain bias around and below 30 K temperature. Here, we have shown that by incorporating gold in these polypyrrole nanotubes using a cost effective template based single-step chemical synthesis technique, this novel resistance switching transition could be extended beyond liquid nitrogen temperature (>90 K) to make this phenomena technologically relevant. The single step synthesis technique, reported here, provides us uniform mixing of gold and polypyrrole during the formation of composite-nanotubes; with appropriate choice of materials, this synthesis technique can be extended to form nanotubes of other metal-polymer composites.

2.1.4 Theoretical Condensed Matter Physics

Thermoelectric effects in strongly correlated systems and effect of strong correlations in band insulators are being studied. In high T_c superconductors a wide ranging connection between the doping dependence of the transition temperature T_c and the room temperature thermopower has been observed. A universal correlation between these two quantities exists with the thermopower vanishing at optimum doping. An interpretation of this universality has been provided in terms of a possible underlying quantum critical point (QCP) at T_c . Central to the viewpoint is the recently noted Kelvin formula relating the thermopower to the density derivative of the entropy. The effect

of strong correlations in a band insulator has also been studied and interesting antiferromagnetic (AFM) and ferrimagnetic Half metallic phases seen to arise as an effect of strong correlations in a band insulator. A simple tight-binding band insulator with two bands in the presence of an on-site Coulomb repulsion, the Hubbard U is studied. At half filling, with increasing U , there occurs a first order transition between the paramagnetic band insulator and an AFM phase at some threshold U_1 . Inside the AFM phase, a half metal phase appears at U_2 greater than U_1 beyond which the system becomes an AFM Mott insulator. In the doped case, turning on U results in a continuous transition from paramagnetic metal to ferri-magnetic half metal followed by a first order transition, at a higher value of U , to the para-magnetic metal again. Many of the transition metal oxides have both strong electron-phonon (e-ph) and strong electron-electron (e-e) interaction and can be studied using the Hubbard-Holstein model. An effective Hamiltonian for the one-dimensional Hubbard-Holstein model has been derived and the phase diagram at various fillings obtained. As e-e interaction is increased, the system transits from an antiferromagnetic cluster to a correlated nearest-neighbor singlet phase. It has been explicitly demonstrated that superfluidity and charge-density-wave (CDW) occur mutually exclusively with CDW manifesting itself only at one-third filling. In the area of mesoscopic systems, it has been shown analytically that the conductance of a mesoscopic ring comes across an absolute minimum when the strengths of Rashba and Dresselhaus spin-orbit interactions are equal. The way of estimating the strength of Dresselhaus spin-orbit interaction has been also been suggested. Generation of a pure spin current is a major challenge to the physicists even today. A quantum device has been recently suggested which behaves like a spin filter. Scientists have shown that the transport properties of a single benzene molecule changes drastically under the influence of dephasing mechanism. The development of a second quantized formalism for finding the distribution of persistent current in a quantum network is made. Investigation on bipolaron formation in the Holstein-Hubbard and Frohlich-Hubbard model on a 1-d lattice is done exactly. The role of extended electron-electron interaction on the effective mass and stability of bipolarons were also studied. The properties of fermions and bosons in a 3-d optical lattice under anisotropic harmonic trap have been investigated. The Drude weight shows very interesting behavior under anisotropic trap. Possible experiments to verify the theoretical predictions have been investigated. Scientists are actively involved in understanding possible universality classes of absorbing phase transition (APT). There has been a long debate on whether APT can be discontinuous. Recent provision of an example and explanation with exact results indicated that APT can occur discontinuously. In models with additional conserved fields, where APT is known to have unusual critical behaviour, it has been shown that the flow to generic universality class (namely directed percolation or DP) is observed, once conservation is broken. In a very recent work it has been also shown that the fixed energy sandpile models (claimed in the literature to form an independent universality class) actually belong to DP class. A coarse-grained effective two-dimensional hydrodynamic theory as a theoretical model for a coupled system of a fluid membrane and a thin layer of a polar active fluid in its ordered state that is anchored to the membrane has been constructed. It is shown that such a system is prone to generic instabilities through the interplay of nonequilibrium drive, polar order and membrane fluctuation. In a related problem, they elucidated the visco-elastic properties of an active gel by studying the dynamics of a small tracer particle inside it. They showed that the diffusion coefficient can depend on system size (L) and diverges as L approaches an instability threshold. Direct Numerical Simulations and shell model studies on binary fluid mixture that velocity and concentration gradient structure functions exhibit multiscaling and extended self-similarity. In contrast to the well-known passive scalar turbulence problem, concentration structure functions show simple scaling. The XY model out of equilibrium by introducing a non-zero noise cross-correlation of amplitude D_x in a stochastic Langevin description has been derived. The quantum annealing algorithms for more general

classes of multi-variable optimisation problems further developed. The two-fractal overlap model of earthquake dynamics has been extended further to the cases of dry friction and discussed them extensively in a recent review appeared in *Reviews in Modern Physics* 2012. The kinetic exchange models for income and wealth distributions in societies have been further developed and extended for the cases collective opinion formations in the societies.

2.2 Research Activities

2.2.1 Applied Material Science

2.2.1.1 Reinforcing effect of nanosilica on the properties of natural rubber/reclaimed ground rubber tire vulcanizates

In this investigation, incorporation of silica into natural rubber (NR)-reclaim rubber (RR) blend system was carried out by sol-gel technique at various sol-gel reaction temperatures. The effect of RR on silica reinforcement, hitherto unexplored, was studied for different NR/RR blend systems. The degree of reinforcement of sol-gel vulcanizates by equilibrium swelling method indicates that the reinforcing efficiency of the in situ generated silica by sol-gel technique increases with increasing reclaim rubber content. The reinforcing efficiency, tensile properties and thermal stability of sol gel vulcanizates (SGV) prepared at 50 degrees C become maxima as compared to SGV prepared at 30 degrees C and 70 degrees C. The amount of silica incorporated by sol-gel technique was determined by thermogravimetry analysis. It indicates that the thermal stability increases with silica content. Attenuated total reflection study indicates that RR forms bond with silica particles due to the presence of active functional site on RR. Scanning electron microscopy studies further indicate the coherency and homogeneity in the silica filled NR/RR vulcanizates. The microwave diagnosis of different SGVs was also carried out and the frequency dependence of dielectric permittivity (ϵ') and loss (ϵ'') were measured.

Debapriya De, Prabir Kr Panda, Madhusudan Roy, Satyaban Bhunia, Abu Ismail Jaman

2.2.1.2 Variation in glass transition temperature of polymer nanocomposite films driven by morphological transitions

We report the variation of glass transition temperature in supported thin films of polymer nanocomposites, consisting of polymer grafted nanoparticles embedded in a homopolymer matrix. We observe a systematic variation of the estimated glass transition temperature T_g , with the volume fraction of added polymer grafted nanoparticles. We have correlated the observed T_g variation with the underlying morphological transitions of the nanoparticle dispersion in the films. Our data also suggest the possibility of formation of a low-mobility glass or gel-like layer of nanoparticles at the interface, which could play a significant role in determining T_g of the films provided.

Sivasurender Chandran, JK Basu, MK Mukhopadhyay

2.2.1.3 Computational Investigation on the Photoacoustics of Malaria Infected Red Blood Cells

A computer simulation study on the possibility of using photoacoustic (PA) technique to differentiate intraerythrocytic stages of malarial parasite is reported. This parasite during its development substantially converts hemoglobin into hemozoin. This conversion is expected to alter the cellular absorption leading to changes in the PA emission of a red blood cell (RBC) at certain incident optical wavelengths. The PA signals from blood samples corresponding to ring, trophozoite and schizont stages were computed and compared with that of normal blood. A Monte Carlo algorithm was implemented generating random locations of RBCs in 3D to simulate blood samples. The average PA amplitude for wide bandwidth signals decreases for 434 nm incident radiation, but increases for 700 nm as the parasite matures. The spectral power at 7.5 MHz for the blood sample at the schizont stage compared to the normal blood is nearly reduced by 6 dB and enhanced by 22 dB at those incident wavelengths, respectively. Bandlimited signals for transducers of 15 and 50 MHz center frequencies were studied and found to exhibit similar characteristics. The presence of hemozoin inside the cells was examined and an excellent estimation was made. The simulation results suggest that intraerythrocytic stages of malarial parasite may be assessed using the PA technique. Citation: Saha RK, Karmakar S, Roy M (2012) Computational Investigation on the Photoacoustics of Malaria Infected Red Blood Cells.

Ratan K Saha, Subhajit Karmakar, Madhusudan Roy

2.2.1.4 Photoacoustic ultrasound spectroscopy for assessing red blood cell aggregation and oxygenation

Red blood cell (RBC) aggregation and oxygenation are important markers for a variety of blood disorders. No current technique is capable of simultaneously measuring aggregation/oxygenation levels noninvasively. We propose using photoacoustic ultrasound spectroscopy (PAUS) for assessing both phenomena. This technique relies on frequency-domain analysis of the PA signals by extracting parameters such as the ultrasound spectral slope and the midband fit. To investigate the effect of hematocrit, aggregation, and oxygenation levels on PAUS parameters, a Monte Carlo-based theoretical model and an experimental protocol using porcine RBCs were developed. The samples were illuminated at 750 and 1064 nm and changes in the PAUS parameters were compared to the oxygen-dependent optical absorption coefficients to assess the oxygenation level. Good agreement between the theoretical and experimental spectral parameters was obtained for the spectral slope of the nonaggregated spectra (similar to 0.3 dB/MHz). The experimental midband fit increased by similar to 5 dB for the largest aggregate size. Based on the analysis of the PA signals, the oxygen saturation level of the most aggregated sample was <20% greater than the nonaggregated sample. The results provide a framework for using PA signals' spectroscopic parameters for monitoring the aggregation and oxygenation levels of RBCs.

Eno Hysi, Ratan K Saha, Michael C Kolios

2.2.1.5 Thermal Decomposition of Molecular Materials $N(n-C_4H_9)(4)[(MFe^{III})-Fe^{II}(C_2O_4)(3)](\infty)$, $M-II = Zn, Co, Fe$

Thermal decomposition of oxalate-based molecular precursors, namely $N(n-C_4H_9)(4)[(ZnFe^{III})-Fe^{II}(C_2O_4)(3)](\infty)$, $N(n-C_4H_9)(4)[(CoFe^{III})-Fe^{II}(C_2O_4)(3)](\infty)$, and $N(n-C_4H_9)(4)[(MnFe^{III})-Fe^{II}(C_2O_4)(3)](\infty)$, were studied.

[(FeFeIII)-Fe-II (C₂O₄)(3)] (infinity), abbreviated as BuZnFe, BuCoFe, and BuFeFe, respectively, are studied using thermogravimetry (TG) in the temperature range from similar to 300 K to similar to 675 K at multiple heating rates. This study also deals with how the thermal decomposition of the complexes proceed stepwise through a series of intermediate reactions. The effect of the divalent metal M-II on the nature of thermal decomposition of the complexes, reflected in their TG profiles in terms of number of steps involved, is reported in this study. The temperature range of thermal decomposition steps for BuZnFe, BuCoFe, and BuFeFe with the same heating rates are studied systematically. Two different isoconversional methods, namely an improved iterative method and a model-free method are employed to calculate the kinetic parameters, and thus the most probable reaction mechanism of thermal decomposition is determined. Based on kinetic parameters, the important thermodynamic parameters such as the changes of entropy, enthalpy, and Gibbs free energy are estimated for the activated complex formation from the precursors. Considering the mass loss during the different thermal decomposition steps of BuZnFe, BuCoFe, and BuFeFe, observed in the thermogravimetry profiles, the overall reactions of the thermal decompositions are demonstrated.

Ashis Bhattacharjee, Debasis Roy, Madhusudan Roy

2.2.1.6 Charge storage properties of InP quantum dots in GaAs metal-oxide-semiconductor based nonvolatile flash memory devices

Metal organic vapor phase epitaxially grown 5nm InP quantum dots (QDs) were embedded as charge storage elements between high-k control and tunneling dielectric layers in GaAs metal-oxide-semiconductor based nonvolatile memory devices. The QDs trap more electrons resulting in a large memory window (6.3V) along with low leakage due to Coulomb blockade effect. 16.5% charge loss was found even after 105s indicating its good charge storing potential. The programming and erasing operations were discussed with proposed band diagram.

Souvik Kundu†, Nripendra N Halder†, Pranab Biswas†...S Chakraborty

2.2.1.7 Comparative analysis of stability and toxicity profile of three differently capped gold nanoparticles for biomedical usage

Nowadays gold nanoparticle (GNP) is increasingly being used in drug delivery and diagnostics. Here we have reported a comparative analysis of detailed stability and toxicity (in vitro and in vivo) profile of three water soluble spherical GNPs, having nearly similar size, but the surfaces of which were modified with three different capping materials aspartic acid (GNPA), trisodium citrate dihydrate (GNPC) or bovine serum albumin (GNPB). Spectral analyses on the stability of these GNPs revealed that depending on the nature of capping agents, GNPs behave differently at different environmental modalities like wide range of pH, high salt concentrations, or in solutions and buffers of biological usage. GNPB was found to be extremely stable, where capped protein molecule successfully maintained its secondary structure and helicity on the nanoparticle, whereas colloidal stability of GNPA was most susceptible to altered conditions. In vitro cytotoxicity of these nanoparticle formulations in vitro were determined by water soluble tetrazolium and lactate dehydrogenase assay in human fibroblast cell line (MRC-5) and acute oral toxicity was performed in murine model system. All the GNPs were non-toxic to MRC-5 cells. GNPC had slight hepatotoxic and nephrotoxic responses. Hepatotoxicity was also evident for GNPA treatment. Present study established that there is a correlation between capping material and stability together with toxicity

of nanoparticles. GNPB was found to be most biocompatible among the three GNPs tested.

Sumistha Das, Nitai Debnath, Shouvik Mitra, Alokmay Datta, Arunava Goswami

2.2.1.8 Thermal

degradation of a molecular magnetic material: $N(n-C_4H_9)_4[(FeFeIII)-Fe-II(C_2O_4)_3](a)$

Thermal degradation of a mixed-valence oxalate based molecular material $N(n-C_4H_9)_4[(FeFeIII)-Fe-II(C_2O_4)_3](a)$ was investigated by thermogravimetric (TG) analysis. Considering the mass loss at each step of TG profile, possible step-wise thermal degradation reaction pathways of the precursor material are proposed which indicate the formation of hematite and magnetite as the solid end product of the degradation reaction. The IR spectroscopy and powder X-ray diffraction (XRD) studies of the thermally degraded samples supplement the proposed reaction pathways.

A Bhattacharjee, D Roy, M Roy

2.2.1.9 Interface studies on high-k/GaAs MOS capacitors by deep level transient spectroscopy

An experimental analysis has been performed in high-k/GaAs MOS devices to investigate the slow and fast interface traps (D_{it}) using high frequency capacitance-voltage and deep level transient spectroscopic (DLTS) measurements. Prior to deposition of high-k gate dielectric, an ultrathin layer of ZnO was deposited on GaAs by metalorganic chemical vapor deposition. The number of slow interface traps was found to be $2.80 \times 10^{11} \text{ cm}^{-2}$, whereas the fast interface trap density was measured to be $1.80 \times 10^{11} \text{ eV}^{-1} \text{ cm}^{-2}$. The activation energy, capture cross section, and concentration of majority carrier traps were measured to be 0.30 eV, $5.70 \times 10^{-19} \text{ cm}^2$, and $4.93 \times 10^{15} \text{ cm}^{-3}$, respectively. Combining conventional DLTS with insufficient-filling, the trap location was found to be at 0.14 eV. Therefore, the traps are not exactly at the interface of GaAs and high-k but in the GaAs surfaces very close to the interfaces. According to the trap energy level position, D_{it} was found to be $5.3 \times 10^{11} \text{ eV}^{-1} \text{ cm}^{-2}$. The leakage current is found to reduce in ZnO passivated devices due to an increase in valance band offset by 0.49 eV. Such an improvement is due to a higher surface potential resulting from the wide bandgap of ZnO.

Souvik Kundu, Yelagam Anitha, Supratic Chakraborty, Pallab Banerji

2.2.1.10 On the use of photoacoustics to detect red blood cell aggregation

The feasibility of detecting red blood cell (RBC) aggregation with photoacoustics (PAs) was investigated theoretically and experimentally using human and porcine RBCs. The theoretical PA signals and spectra generated from such samples were examined for several hematocrit levels and aggregates sizes. The effect of a finite transducer bandwidth on the received PA signal was also examined. The simulation results suggest that the dominant frequency of the PA signals from non-aggregated RBCs decreases towards clinical frequency ranges as the aggregate size increases. The experimentally measured mean spectral power increased by similar to 6 dB for the largest aggregate compared to the non-aggregated samples. Such results confirm the theoretical predictions

and illustrate the potential of using PA imaging for detecting RBC aggregation.

Eno Hysi, Ratan K Saha, Michael C Kolios

2.2.1.11 Role of ultra thin pseudomorphic InP layer to improve the high-k dielectric/GaAs interface in realizing metal-oxide-semiconductor capacitor

In this article, we report GaAs metal-oxide-semiconductor (MOS) capacitors with a metal organic chemical vapor deposited ultrathin (1.5nm) pseudomorphic InP interface passivation layer (IPL) and a thin (5nm) ZrO₂ high-k dielectric. Reduction of the surface states on InP passivated GaAs surfaces was observed from the photoluminescence study. The x-ray photoelectron spectra confirmed the dramatic reduction of GaAs native oxides (Ga-O and As-O) from the interface of ZrO₂ and p-GaAs, implying that the Fermi level at the high-k/GaAs interface can be unpinned with good interface quality. As a result, very low values of interface trap density ($1.11011\text{cm}^2\text{eV}^{-1}$) and hysteresis (8.21mV) were observed. The same was done for directly deposited ZrO₂ on GaAs surface to understand the efficacy of InP interface passivation layer on GaAs MOS devices. A systematic capacitance-voltage and current density-voltage studies were performed on both Al/ZrO₂/InP/p-GaAs and Al/ZrO₂/p-GaAs structures. It was found that insertion of 1.5nm InP ultrathin layer in-between ZrO₂ and GaAs improves the essential parameters of GaAs MOS such as dielectric constant, frequency dispersion, leakage current, etc. The dielectric reliability has been studied with constant voltage stressing. A very small flatband voltage shift with stress time was observed in InP passivated GaAs MOS capacitors.

Souvik Kundu†, Nripendra N Halder†, Pranab Biswas†...S Chakraborty

2.2.1.12 Xylene-Capped Luminescent Silicon Nanocrystals: Evidence of Supramolecular Bonding

We report capping of silicon (Si) nanocrystals (NCs) via xylene attachment to the surface of oxide etched, luminescent, core/shell nanostructures of Si/Si-oxide in colloidal suspension. The core/shell nanostructures of Si/Si-oxide are formed by controlled oxidation of mechanically milled crystalline Si, which is subsequently etched in aqueous hydrofluoric acid to remove the oxide shell. Xylene attachment is confirmed by peak splitting and shifting in the Fourier transform infrared spectra for the xylene-treated samples in colloidal suspensions as well as for samples deposited on solid substrates like ZnSe. Structural investigations and spectroscopic evidence suggest that capping of Si NCs is associated with the formation of weak supramolecular bonds with the antibonding electrons of xylene. Therefore, we successfully achieve the much desired attachment of methyl groups onto the surface of luminescent Si NCs by a very weak physical bond with minimal modification of the surface chemistry of the NCs.

Arun Kumar Mandal, Mallar Ray, Indrajith Rajapaksa, Smita Mukherjee, Alokmay Datta

2.2.1.13 Phase separation in crowded micro-spheroids: DNA-PEG system

Living cells are characterized as micro-vesicles encapsulating highly crowded macromolecular media, including DNA. To probe the intrinsic property of such crowded systems in a micro-closed

environment, we observed a mixture of DNA and hydrophilic polymer, PEG within an aqueous micro-spheroid. It was found that the mixture causes phase-segregation by depositing DNA near the spheroid surface, whereas corresponding bulk solution sustains isotropic phase. After the phase segregation, DNA molecules in the condensed phase exhibit time evolution to an ordered state. This surface-mediated segregation is discussed in terms of the depletion effect under micro-confinement.

Nupur Biswas, Masatoshi Ichikawa, Alokmay Datta et al

2.2.1.14 Validity of a theoretical model to examine blood oxygenation dependent optoacoustics

A theoretical model investigating the dependence of optoacoustic (OA) signal on blood oxygen saturation (SO₂) is discussed. The derivations for the nonbandlimited and bandlimited OA signals from many red blood cells (RBCs) are presented. The OA field generated by many RBCs was obtained by summing the OA field emitted by each RBC approximated as a fluid sphere. A Monte Carlo technique was employed generating the spatial organizations of RBCs in two-dimensional. The RBCs were assumed to have the same SO₂ level in a simulated configuration. The fractional number of oxyhemoglobin molecules, confined in a cell, determined the cellular SO₂ and also defined the blood SO₂. For the nonbandlimited case, the OA signal amplitude decreased and increased linearly with blood SO₂ when illuminated by 700 and 1000 nm radiations, respectively. The power spectra exhibited similar trends over the entire frequency range (MHz to GHz). For the bandlimited case, three acoustic receivers with 2, 10, and 50 MHz as the center frequencies were considered. The linear variations of the OA amplitude with blood SO₂ were also observed for each receiver at those laser sources. The good agreement between simulated and published experimental results validates the model qualitatively.

Ratan K Saha, Subhajit Karmakar, Eno Hysi, Madhusudan Roy, Michael C Kolios

2.2.1.15 Polymer entanglement - A barrier to nanoparticles aggregation

Au metal nanoparticles embedded in polymer matrices aggregate at elevated temperatures overcoming the barrier induced by entanglement of polymer chains. The temperature required for nanoparticle agglomeration depends on the polymer chain length, providing a measure of the potential barrier induced by entanglement of polymer chains. For higher chain lengths a non-linear dependence of the aggregation temperature with molecular weight was found. These results suggest that, in addition to the role of nanoparticle-polymer interactions, polymer-polymer interactions influence the aggregation of the nanoparticles.

Nupur Biswas, Alokmay Datta

2.2.2 Experimental Condensed Matter Physics

2.2.2.1 Evidence of a structural phase transition in superconducting $\text{SmFeAsO}_{1-x}\text{F}_x$ from ^{19}F NMR

We report resistivity, magnetization and ^{19}F NMR results in a polycrystalline sample of $\text{SmFeAsO}_{0.86}\text{F}_{0.14}$. The resistivity and magnetization data show a sharp drop at 48 K indicating a superconducting transition. The nuclear spinlattice rate ($1/T_1$) and spinspin relaxation rate ($1/T_2$) clearly show the existence of a structural phase transition near 163 K in the sample, which also undergoes a superconducting transition. This finding creates interest in exploring whether this is unique for Sm based systems or is also present in other rare-earth based 1111 superconductors.

M Majumder, K Ghoshray, C Mazumdar, A Poddar, A Ghoshray et al

2.2.2.2 Scaling of non-Ohmic conduction in strongly correlated systems

Abstract: A new scaling formalism is used to analyze nonlinear I-V data in the vicinity of metal-insulator transitions (MIT) in five manganite systems. An exponent, called the nonlinearity exponent, and an onset field for nonlinearity, both characteristic of the system under study, are obtained from the analysis. The onset field is found to have an anomalously low value corroborating the theoretically predicted electronically soft phases. The scaling functions above and below the MIT of a polycrystalline sample are found to be the same but with different exponents which are attributed to the distribution of the MIT temperatures. The applicability of the scaling in manganites underlines the universal response of the disordered systems to electric field.

D Talukdar, Nandit†, UN, A Poddar, P Mandal, KK Bardhan

2.2.2.3 Spin trimers in $\text{Ca}_3\text{Cu}_2\text{Ni}(\text{PO}_4)(4)$

The nature of spin trimer and 3d spin dynamics in $\text{Ca}_3\text{Cu}_2\text{Ni}(\text{PO}_4)(4)$ is studied using ^{31}P NMR measurements. The data are obtained by replacing one of the Cu ions by a Ni ion in the one dimensional spin trimer compound $\text{Ca}_3\text{Cu}_3(\text{PO}_4)(4)$. The NMR spectrum suggests the presence of two types of magnetically inequivalent phosphorous atoms, as in the parent compound. This reveals the presence of only one type of trimer, Cu2-Ni-Cu2, rather than of three types, Cu2-Cu1-Cu2, Cu2-Cu1-Ni and Ni-Cu1-Ni, as indicated by neutron scattering. Hence, the ground state of $\text{Ca}_3\text{Cu}_2\text{Ni}(\text{PO}_4)(4)$ appears to be a quintet. These results also explain the magnetic susceptibility behavior, which indicates no reduction in the net spin of the trimer in $\text{Ca}_3\text{Cu}_2\text{Ni}(\text{PO}_4)(4)$, as expected for $J(\text{Ni-Cu}) = -0.85$ meV compared to the value $J(\text{Cu-Cu}) = -4.74$ meV derived from neutron scattering. The spin lattice relaxation rate suggests that the three magnon mediated scattering process dominant in $\text{Ca}_3\text{Cu}_2\text{Ni}(\text{PO}_4)(4)$ is reduced in $\text{Ca}_3\text{Cu}_2\text{Ni}(\text{PO}_4)(4)$.

M Ghosh, K Ghoshray

2.2.2.4 Anisotropic Spin-Fluctuations in SmCoPO Revealed by ^{31}P NMR Measurement

^{31}P NMR spectral features in polycrystalline SmCoPO reveal an axially symmetric local magnetic field. At low temperature, the anisotropy of the internal magnetic field increases rapidly, with

K_{ab} increasing faster than that of K_c . The dominant contribution to this anisotropy arises from Sm-4*f* electron contribution over that of Co-3*d*. The intrinsic width 2β deviates from linearity with respect to bulk susceptibility below 170 K due to the enhancement of $(1/T_2)$ dynamic, which along with the continuous increase of anisotropy in the internal magnetic field is responsible for the wipe out effect of the NMR signal, well above T_C . $1/T_1$ shows large anisotropy confirming a significant contribution of Sm-4*f* electron spin fluctuations to $1/T_1$, arising from indirect RKKY type exchange interaction indicating a non-negligible hybridization between Sm-4*f* orbitals and the conduction band, over the itinerant character of the Co-3*d* spins. This anisotropy originates from the orientation dependence of (q, γ) . The 3*d*-spin fluctuations in the *ab*-plane is 2D FM in nature, while along the *c*-axis, a signature of a weak AFM spin fluctuations superimposed on weak FM spin-fluctuations even in a field of 7 T and far above T_N is observed. The enhancement of this AFM fluctuations of the Co-3*d* spins along *c*-axis, at further low temperature is responsible to drive the system to an AFM ordered state. 2012 The Physical Society of Japan

Mayukh Majumder, Kajal Ghoshray, Amitabha Ghoshray et al

2.2.2.5 Colossal piezoresistance effect in $\text{Sm}_{0.55}(\text{Sr}_{0.5}\text{Ca}_{0.5})_{0.45}\text{MnO}_3$ single crystal

We have investigated the effect of uniaxial pressure (*P*) on electrical resistivity along the *ab* plane and *c* axis in a single crystal of $\text{Sm}_{0.55}(\text{Sr}_{0.5}\text{Ca}_{0.5})_{0.45}\text{MnO}_3$. A huge piezoresistance (PR-10⁷% at *P*=90MPa) and a remarkable increase (at the rate of -79K/GPa) of metal-insulator transition temperature (TMI) have been observed for *P* applied along the *c* axis, while TMI decreases at the rate of -77K/GPa for *P* perpendicular to the *c* axis. These values of PR and dT_{MI}/dP are much larger than those observed in other perovskite and bilayer manganites. Such colossal PR and large value of dT_{MI}/dP may be utilized for various technological applications.

D Mohan Radheep†, P Sarkar†, S Arumugam†, P Mandal

2.2.2.6 Giant magnetocaloric effect in magnetically frustrated EuHo_2O_4 and EuDy_2O_4 compounds

We have investigated the magnetic and magnetocaloric properties of EuHo_2O_4 and EuDy_2O_4 by magnetization and heat capacity measurements down to 2K. These compounds undergo a field-induced antiferromagnetic to ferromagnetic transition and exhibit a huge entropy change. For a field change of 0-8T, the maximum magnetic entropy and adiabatic temperature changes are 30 (25) Jkg⁻¹K⁻¹ and 12.7 (16) K, respectively, and the corresponding value of refrigerant capacity is 540 (415) Jkg⁻¹ for EuHo_2O_4 (EuDy_2O_4). These magnetocaloric parameters also remain large down to lowest temperature measured and are even larger than that for some of the potential magnetic refrigerants reported in the same temperature range. Moreover, these materials are highly insulating and exhibit no thermal and field hysteresis, fulfilling the necessary conditions for a good magnetic refrigerant in the low-temperature region.

A Midya, N Khan, D Bhoi, P Mandal

2.2.2.7 Hall effect in the metallic antiferromagnet Na_xCoO_2 ($0.72 \leq x \leq 0.90$)

Abstract: We have investigated the magnetic and magnetotransport properties of Na_xCoO_2 single crystals in the heavily doped region ($0.72 \leq x \leq 0.90$). Both the Hall coefficient (R-H) and the susceptibility (χ) exhibit strong temperature dependence in the antiferromagnetic (AFM) as well as in the paramagnetic (PM) states. As the AFM ordering sets in, below $T_N = 21$ K, R-H decreases sharply with T down to similar to 10 K and then increases rapidly. The temperature and field dependence of R-H indicates the emergence of a weak ferromagneticlike phase below 10 K. In the AFM state, R-H scales linearly with χ . The observed T dependence of R-H in the PM state has been discussed in light of the theoretical model proposed for strongly correlated electrons in a triangular lattice.

P Mandal, P Choudhury†

2.2.2.8 Anomalous thermal expansion of Sb_2Te_3 topological insulator

We have investigated the temperature dependence of the linear thermal expansion along the hexagonal c axis (ΔL), in-plane resistivity (ρ), and specific heat (C_p) of the topological insulator Sb_2Te_3 single crystal. ΔL exhibits a clear anomaly in the temperature region 204–236 K. The coefficient of linear thermal expansion α decreases rapidly above 204 K, passes through a deep minimum at around 225 K, and then increases abruptly in the region 225–236 K. α is negative in the interval 221–228 K. The temperature dependence of both α and C_p can be described well by the Debye model from 2 to 290 K, excluding the region around the anomaly in α .

P Dutta, D Bhoi, A Midya, N Khan, P Mandal et al

2.2.2.9 Magnetoelectronic phase separation in $\text{La}_{1-x}\text{Sr}_x\text{CoO}_3$ single crystals: Evidence from critical behavior

We have investigated the critical behavior of ferromagnetic $\text{La}_{0.75}\text{Sr}_{0.25}\text{CoO}_3$ and $\text{La}_{0.79}\text{Sr}_{0.21}\text{CoO}_3$ single crystals from the bulk magnetization measurements around their Curie temperature (T_C). The detailed analysis of the dc magnetization data using different techniques such as the Kouvel-Fisher, the Arrott-Noaks, and critical isotherm plots yield the critical exponents of $\beta = 0.362 \pm 0.002$, $\gamma = 1.304 \pm 0.006$, and $\delta = 4.75 \pm 0.01$ with $T_C = 213.93 \pm 0.02$ K for $\text{La}_{0.75}\text{Sr}_{0.25}\text{CoO}_3$ and $\beta = 0.491 \pm 0.004$, $\gamma = 1.217 \pm 0.003$, and $\delta = 3.51 \pm 0.01$ with $T_C = 187.67 \pm 0.01$ K for $\text{La}_{0.79}\text{Sr}_{0.21}\text{CoO}_3$, characterizing these second-order phase transitions. For both the crystals, the scaling of the magnetization data above and below T_C obtained using the respective critical exponents and the consistency in the values of the critical exponents determined by different methods confirm that the calculated exponents are unambiguous and intrinsic. The obtained values of exponents suggest that for $\text{La}_{0.75}\text{Sr}_{0.25}\text{CoO}_3$ the transition falls into the three-dimensional Heisenberg universality class of the near-neighbor interaction as proposed for double-exchange systems, whereas in the case of $\text{La}_{0.79}\text{Sr}_{0.21}\text{CoO}_3$ the transition is characterized by mean-field-like values of the critical exponents. We have also estimated the reduced critical amplitudes and observed that for $\text{La}_{0.75}\text{Sr}_{0.25}\text{CoO}_3$ they fall well within the range of the Heisenberg model prediction for spin $S > 1/2$, whereas for $\text{La}_{0.79}\text{Sr}_{0.21}\text{CoO}_3$ they are found to be shifted toward the mean-field values. The deviation of the critical exponents from 3D Heisenberg values toward mean-field ones is attributed to the presence of magnetoelectronic phase inhomogeneity in the $x=0.21$ single crystal. The detailed analysis of the specific-heat data in the vicinity of T_C for the $x=0.33$, 0.25, and 0.21 samples

also supports the phase separation scenario at around $x=0.21$.

N Khan, P Mandal, K Mydeen† et al

2.2.2.10 Effect of annealing on the structural, topographical and optical properties of sol-gel derived ZnO and AZO thin films

A comparative study of the physical properties of undoped Zinc Oxide (ZnO) and Al doped Zinc Oxide (AZO) thin films were performed as a function of annealing temperature. The structural properties were analyzed using X-ray diffraction and the recorded patterns indicated that the crystallinity of the films always enhanced with increasing annealing temperature while it degrades with Al doping. The topographical modification of the films due to heat treatment was examined by atomic force microscopy which revealed that annealing roughened the surface of all the films; however the AZO films always exhibited smoother morphology than ZnO. Study of the optical properties by UV-Visible spectrophotometer demonstrated that the transmittance was gradually diminished with the rise in annealing temperature. In addition, a notable increase in the optical band gap was also observed for the AZO films.

J Sengupta, RK Sahoo, CD Mukherjee

2.2.3 Surface Physics

2.2.3.1 Quantum well states in Ag thin films on MoSi₂(0001) surfaces

In-plane dispersions of quantum well (QW) states originating from the electron confinement of Ag *sp* electrons within the MoS₂ band gap region are investigated by means of angle-resolved photoemission spectroscopy (ARPES). A number of QW resonances have been observed in the ARPES spectra in a binding energy range lying outside the MoS₂ energy gap which is required for full confinement of the Ag *sp* electrons. In spite of having the expected free electron-like behavior, these QW states show a significant increase of in-plane effective mass with increasing binding energy due to the hybridization of Ag *sp* electrons with the MoS₂ valence bands. The binding energy dependence of the bottom of the QW states ($k_{\parallel} = 0$) as a function of the Ag film thickness has been analyzed. The well-established phase accumulation model has been applied for calculating the phase shifts of electrons at the boundaries. Our observations show that the total phase shift behaves differently for energies above and below the MoS₂ valence band maxima, due to the hybridizations being different in nature. The structure plot calculated considering the different quantum number dependent total phase shifts provides a good description of the experimental observations.

SK Mahatha; Krishnakumar SR Menon

2.2.3.2 Effect of Al doping on microstructure and optical band gap of ZnO thin film synthesized by successive ion layer adsorption and reaction

Thin films of pure and aluminum-doped zinc oxide (AZO) were deposited on glass substrates from ammonium zincate bath following a chemical dipping technique called successive ion layer adsorption and reaction (SILAR). Characterization techniques such as X-ray diffraction (XRD), scanning electron microscopy (SEM) and energy-dispersive X-rays (EDX) were used to investigate the effect

of Al doping on the microstructure of AZO films. Particle size analysis using X-ray line broadening shows marginally increasing trend with increasing Al impurity. The average particle size for pure ZnO is 22.75 nm. It increases to 24.26 nm for 1% AZO film and 25.13 nm for 2% AZO film. Incorporation of Al was confirmed from elemental analysis using EDX. SEM micrograph shows that pure ZnO particles are spherical shaped. However, AZO films show particles with off-spherical shape with compact interconnected grains. The value of band gap for pure ZnO is 3.229 eV and it increases to 3.29 eV for 1% AZO indicating a blue-shift for 1% AZO film. However, for 2% AZO film, a decrease in band gap compared to pure ZnO is observed indicating a red-shift of fundamental absorption edge. Electrical resistance shows an initial decrease with increasing Al content. With further enhancement of Al incorporation, the resistance increases.

S Mondal, SR Bhattacharyya, P Mitra

2.2.3.3 Electronic structure investigation of MoS₂ and MoSe₂ using angle-resolved photoemission spectroscopy and ab initio band structure studies

Angle-resolved photoemission spectroscopy (ARPES) and ab initio band structure calculations have been used to study the detailed valence band structure of molybdenite, MoS₂ and MoSe₂. The experimental band structure obtained from ARPES has been found to be in good agreement with the theoretical calculations performed using the linear augmented plane wave (LAPW) method. In going from MoS₂ to MoSe₂, the dispersion of the valence bands decreases along both $\kappa \parallel$ and $\kappa \perp$, revealing the increased two-dimensional character which is attributed to the increasing interlayer distance or c/a ratio in these compounds. The width of the valence band and the band gap are also found to decrease, whereas the valence band maxima shift towards the higher binding energy from MoS₂ to MoSe₂.

SK Mahatha, KD Patel, Krishnakumar SR Menon

2.2.3.4 Magnetodielectric effect in composites of nanodimensional glass and CuO nanoparticles

Nanocomposites comprising CuO particles of average diameter 21 nm coated with 5 nm silica glass containing iron ions were synthesized by a chemical route. An ion exchange reaction at the nano-glass/CuO interface produced iron-doped CuO with copper ion vacancies within the nanoparticles. Room temperature ferromagnetic-like behavior was observed in the nanocomposites. This was ascribed to uncompensated spins contributed by Fe ions with associated copper ion vacancies. A rather high value of magnetodielectric parameter in the range 16-26% depending on the measuring frequency was exhibited by these nanocomposites at a magnetic field of 10 KOe. This was caused by a magnetoresistance of 33% in the iron doped CuO nanoparticles. The experimental results were fitted to the Maxwell-Wagner Capacitor model developed by Catalan. These materials will be suited for magnetic sensor applications.

Dhriti Ranjan Saha, Manabendra Mukherjee, Dipankar Chakravorty

2.2.3.5 Polarization dependence of angle-resolved photoemission spectroscopy of graphite

We have used variable polarization synchrotron radiation to map the valence band electronic structure of graphite by angle-resolved photoemission spectroscopy (ARPES). The experimental results with two orthogonal linear polarization of light signifies the contribution of either even or odd symmetry with respect to the crystal mirror plane towards the photoemission intensity. The sigma(1) and sigma(2) valence bands show odd reflection symmetry while the pi valence band shows even symmetry with respect to the mirror plane. The measured ARPES spectrum using left and right circular polarized lights shows asymmetry in intensity around M point of the Brillouin zone, which ultimately mimicking different partial wave character of sigma(1) and sigma(3) bands.

SK Mahatha, Krishnakumar SR Menon

2.2.3.6 Effect of added salt on morphology of ultrathin polyelectrolyte films

Morphological evolution of polyelectrolyte ultrathin films as a function of externally added monovalent salt concentration and its correlation with the solution state morphology have been studied using dynamic light scattering (DLS) and tapping mode AFM. DLS data shows the presence of two different dynamical modes of relaxation in the solution state. Films are prepared from aqueous solution of poly(sodium-4-styrenesulfonate) (NaPSS) with different concentration of added NaCl on the hydrophilic silicon substrate using spin coating technique. Smooth and featureless surface morphology for salt free NaPSS films become rough with addition of salt and beyond a critical salt concentration DLA like fractal structures are formed on the films. Comparison of the surface morphology with slow mode dynamics in DLS establishes the presence of multichain polyelectrolyte clusters in the DLA pattern formed on the surface of the films. Compositional analysis of the films

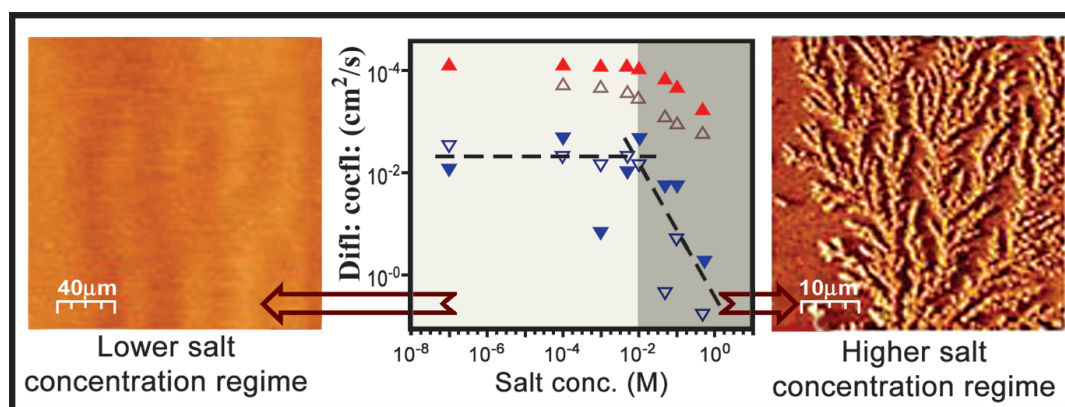


Figure Caption: Change of diffusion coefficient of chains in solution and surface morphology in spin coated polyelectrolyte film with addition of NaCl

shows an accumulation of excess NaCl on the DLA structures with the increase of salt concentration. Our results show that the DLA patterns are primarily formed by the excess salt ions on their solidification during spin coating and multichain polyelectrolyte clusters nucleate on the preformed

nuclei leading to the resultant surface morphology.

Tanusree Samanta, M Mukherjee

2.2.3.7 Hydrophilic-like wettability of Cl-passivated Ge(001) surface

The hydrophilic/hydrophobic nature of the Cl-passivated Ge(001) surface is investigated directly by contact angle (CA) measurement and indirectly by growing nickel arachidate Langmuir-Blodgett (LB) films on the Cl-passivated Ge(001) surface. Passivation of Ge(001) surface by Cl atoms is confirmed by X-ray photoelectron spectroscopy measurement. CA measurements show that the Cl-passivated Ge(001) surface has intermediate wettability, i.e., the surface has intermediate hydrophilic/hydrophobic behavior. Structural information obtained from the deposited LB films by using X-ray reflectivity and atomic force microscopy analysis shows that the surface is homogeneous and hydrophilic (similar to 85%), although very few effectively hydrophobic (similar to 15%) regions are present. Structural study in molecular level thus helps to identify the surface nature in nanometer level, which is not possible by simple macroscopic CA measurement. Specific electrostatic and dispersive effects of Cl atoms are possibly responsible for such hydrophilic-like nature of the Cl-passivated Ge(001) surface.

JK Bal, Sarathi Kundu, S Hazra

2.2.3.8 Exact compositional analysis of SiGe alloys by matrix effect compensated MCs⁺-SIMS

SiGe alloy, owing to its high electron and hole mobility, has potential applications in high-speed microelectronic device technology. The optimization of such technology requires the precise determination of Ge concentration in the full range of composition and the understanding and control of the Ge-Si interdiffusion phenomenon. The most appropriate analytical technique with highest detection sensitivity (similar to subparts per billion) for measuring elemental concentration is secondary ion mass spectrometry (SIMS). However, strong compositional dependence of secondary ion yield, i.e. "matrix effect," has always made SIMS quantification extremely difficult. A procedure for the accurate quantification of Ge concentration in molecular beam epitaxy (MBE)-grown Si_{1-x}Ge_x (0 < x < 0.72) alloys based on MCs⁺-SIMS approach has been proposed. The "matrix effect" is shown to be completely suppressed for all Ge concentrations irrespective of impact Cs⁺ ion energies. The novel methodology has successfully been applied for direct quantitative composition analysis of Si/Ge multilayer structure.

Biswajit Saha, Purushottam Chakraborty, Hubert Gnaser, Manjula Sharma, Milan K Sanyal

2.2.3.9 Hybrid nanotubes: Single step formation of homogeneous nanotubes of polypyrrole-gold composites and novel switching transition of resistance beyond liquid nitrogen temperature

Nanowires of polypyrrole have exhibited switching transition that reduces the resistance of the wires by several orders of magnitude under certain bias around and below 30 K temperature. Here, we have shown that by incorporating gold in these polypyrrole nanotubes using a cost effective

template based single-step chemical synthesis technique, this novel resistance switching transition could be extended beyond liquid nitrogen temperature (>90 K) to make this phenomena technologically relevant. The single step synthesis technique, reported here, provides us uniform mixing of gold and polypyrrole during the formation of composite-nanotubes; with appropriate choice of materials, this synthesis technique can be extended to form nanotubes of other metal-polymer composites.

Abhisakh Sarma, Milan K Sanyal, Atikur Rahman, Biswarup Satpati

2.2.3.10 Role of metal ions in growth and stability of Langmuir-Blodgett films on homogeneous and heterogeneous surfaces

Structure and stability of cadmium arachidate (CdA) Langmuir-Blodgett (LB) films on homogeneous (i.e., OH-, H-passivated Si(001) substrates) and heterogeneous (i.e., Br-passivated Si(001) substrates) surfaces were studied using X-ray reflectivity and atomic force microscopy techniques and compared with those of nickel arachidate (NiA) LB films. While on OH-passivated Si, an asymmetric monolayer (AML) structure starts to grow, on H-passivated Si, a symmetric monolayer (SML) of CdA forms, although for both the films, pinhole-type defects are present as usual. However, on heterogeneous Br-passivated Si substrates, a combination of AML, SML, shifted SML and SML on top of AML (i.e., AML/SML), all types of structures are found to grow in such a way that, due to the variation of heights in the out-of-plane direction, ring-shaped in-plane nanopatterns of CdA molecules are generated. Probably due to stronger head-head interactions and higher metal ion-carboxylic ligand bond strength for CdA molecules compared to NiA, easy flipping of SML on top of another preformed SML, i.e. a SML/SML structure formation was not possible and as a result a wave-like modulation is observed for the CdA film on such heterogeneous substrate. The presence of hydrophilic/hydrophobic interfacial stress on the heterogeneous substrate thus modifies the deposited molecular structure so that the top surface morphology for a CdA film is similar to monolayer buckling while that for NiA film is similar to monolayer collapse.

JK Bal, Sarathi Kundu, S Hazra

2.2.3.11 Inhomogeneous band bending on MoS₂(0001) arising from surface steps and dislocations

We study the observed inhomogeneous band bending effects on cleaved MoS₂(0001) single-crystal surfaces. Both Mo 3d and S 2p core levels were found to shift to lower binding energy in regions of the MoS₂ crystal with high step densities, as suggested by spot splitting of the LEED (low energy electron diffraction) pattern. Surface electronic band structure measurements also reveal a rigid shift of the valence bands in these regions, resulting from local Fermi level pinning effects. A surface electric field gradient on the MoS₂ crystals caused by the charged dislocations from the regions of high step densities generated by the cleaving process is found to explain most of the experimental observations.

SK Mahatha, Krishnakumar SR Menon

2.2.3.12 Probing Higher Order Surface Plasmon Modes on Individual Truncated Tetrahedral Gold Nanoparticle Using Cathodoluminescence Imaging and Spectroscopy Combined with FDTD Simulations

We report the spatial maps of the localized surface plasmon resonances associated photon emission in a truncated tetrahedral gold nanoparticle on a silicon substrate. Site-specific cathodoluminescence spectroscopy and imaging in a scanning electron microscope shows stronger photon emission in the visible range near the tips of the particle in contact with the substrate compared to the edges of the particle. Strong local field variations on a length scale as short as 19 nm are resolved. We also perform FDTD simulations of both the spectra and, for the first time, the full cathodoluminescence images. Excellent agreement is obtained with the experimental results, and the detailed information available from the simulated results makes it possible to identify the signature of out-of-plane higher order modes in the truncated tetrahedral gold particle.

Pabitra Das, Tapas Kumar Chini, James Pond

2.2.3.13 Symmetric and asymmetric collision effects on the formation of singly and doubly-charged ions in sputtering process

Measurements of Si^{2+} and Si^+ ions sputtered due to bombardment of 3-5 keV Ar^+ ions on silicon substrate have been performed for understanding exact charge-state formation mechanisms. Examination on the penetration depth dependence of incident particle on secondary ion formation has been performed. A closure look at the energetics of the secondary ions from their kinetic energy distributions suggests that Si^+ ions are predominantly formed in the upper surface layer and Si^{2+} ions are produced due to target-target symmetric collision-induced Si 2p shell vacancy creation following the Auger electron emission. Furthermore, the increase in the oxygen-induced impurity in the silicon substrate enables us to explore the gradual transition from the dominating symmetric to asymmetric collision channel for production of Si^{2+} ions.

S Mondal, H Gnaser, P Chakraborty

2.2.3.14 Role of metal ions of Langmuir-Blodgett film in hydrophobic to hydrophilic transition of HF-treated Si surface

Hydrophobic to hydrophilic transition of HF-treated Si surface strongly depends upon the metal ions, which are present in the headgroups of the deposited Langmuir-Blodgett (LB) film. Structure of LB films studied by X-ray reflectivity technique and chemical analysis of LB film-substrate interfaces studied by X-ray photoelectron spectroscopy combinedly suggest that the partial transition or partial oxidation of the HF-treated Si surface takes place under the subphase water but further transition or oxidation is possible only in the presence of metal ions. Electrovalent and covalent natures of the metal ions tune this transition or oxidation. Ni ions, for which bonding with headgroups are electrovalent in nature, are favorable for such transition/oxidation and as a result, complete transition/oxidation takes place when nickel arachidate LB film is deposited. On the other hand, Cd ions, for which bonding with headgroups show covalent nature, is not favorable for such transition and can not oxidize the underlying H-passivated Si substrate totally when cadmium arachidate LB film is deposited on such HF-treated Si surface. This ion-specific hydrophobic to hydrophilic transition is visualized by X-ray reflectivity, contact angle and X-ray photoelectron

spectroscopy measurements.

JK Bal, Sarathi Kundu, S Hazra

2.2.3.15 Nanopatterning of mica surface under low energy ion beam sputtering

Irradiation of crystalline muscovite mica samples by 500 eV Ar⁺ ions at different incident angles can induce significant surface morphological variations. A periodic ripple pattern of nano-dimensions forms in the angle window 47 degrees-70 degrees. On the other hand, tilted conical protrusions develop on the surface at grazing incidence angles around 80 degrees. From the derivative of the topographic images the distribution of the side-facet slopes in the ion incidence plane are measured, which is found to be strongly related to the pattern morphology. Additionally, it has been shown that, for the ripple structures, the base angles can be tuned by changing the ion fluence. An asymmetric sawtooth profile of the ripples obtained at low fluence is transformed to a symmetrical triangular profile at high fluence. As the slopes are found to be small, the pattern formation is not provoked by the gradient-dependent erosion mechanism rather it is the general effect of the curvature-dependent sputtering phenomena.

A Metya, D Ghose, SA Mollick, A Majumdar

2.2.3.16 Optimized luminescence properties of Mn doped ZnS nanoparticles for photovoltaic applications

Mn²⁺ doped ZnS nanoparticles (ZnS:Mn²⁺ NPs) are non-toxic systems known for their attractive light emitting properties. This paper discusses the luminescence properties of ZnS:Mn²⁺ NPs prepared by wet chemical synthesis with the objective of using them as down-shifters. A modification of the incident solar spectrum inducing improved exploitation of the UV region was expected to increase the efficiency of single junction cells with an optimal absorber band gap around 1.1 eV. The potential of ZnS:Mn²⁺ NPs as down-shifters was therefore demonstrated on both Si and Cu(In, Ga)Se-2 solar cells.

Alessia Le Donne, Sourav Kanti Jana, Sangam Banerjee et al

2.2.3.17 Irradiation effects of 6 MeV electron on electrical properties of Al/Al₂O₃/n-Si MOS capacitors

The influence of 6 MeV electron irradiation on the electrical properties of Al/Al₂O₃/n-Si metal-oxide-semiconductor (MOS) capacitors has been investigated. Using rf magnetron sputtering deposition technique, Al/Al₂O₃/n-Si MOS capacitors were fabricated and such twelve capacitors were divided into four groups. The first group of MOS capacitors was not irradiated with 6 MeV electrons and treated as virgin. The second group, third group and fourth group of MOS capacitors were irradiated with 6 MeV electrons at 10 kGy, 20 kGy, and 30 kGy doses, respectively, keeping the dose rate ~ 1 kGy/min. The variations in crystallinity of the virgin and irradiated MOS capacitors have been compared from GIXRD (Grazing Incidence X-ray Diffraction) spectra. Thickness and in-depth elemental distributions of individual layers were performed using Secondary Ion Mass Spectrometry (SIMS). The device parameters like flat band voltage (V-FB) and interface trap density (D-it) of virgin and irradiated MOS capacitors have been calculated from C vs V and G/ω vs

V curve, respectively. The electrical properties of the capacitors were investigated from the $\tan \delta$ vs V graph. The device parameters were estimated using C-V and G/ω -V measurements. Poole-Frenkel coefficient (β PF) of the MOS capacitors was determined from leakage current (I)-voltage (V) measurement. The leakage current mechanism was proposed from the β PF value.

P Laha, I Banerjee, A Bajaj, P Chakraborty et al

2.2.3.18 Effect of thermal modification on swelling dynamics of ultrathin polymer films

Swelling dynamics of spin coated ultrathin polyacrylamide films, annealed at the onset of thermal degradation temperature (220° C) of polyacrylamide have been studied using in situ X-ray reflectivity technique to understand the effects of thermal modification of the polymer to their swelling dynamics. The results are compared with those of thermally annealed unmodified films from our previous study. Significant changes in swelling dynamics and swellability of the modified films are observed. The swellability of the modified films was greatly reduced compared to the annealed ones. The swelling dynamics of the films are analyzed with a model where the dynamical behavior for the swelling was expressed in terms of combination of two independent components namely "free" and "restricted". Analyses of the results show that the effect of thermal modification can be clearly observed in the free component whereas it was not distinguishable for the dynamics of attached component. The study of mass uptake behavior of solvent molecules shows that this process was dependent on film thickness and was non-Fickian in nature. Comparison of the diffusion coefficients of water to that of the free component of the polymer chains shows that for thinner films swelling was controlled by the solvent uptake whereas for the thicker ones the two processes are independent.

Mojammel H Mondal, M Mukherjee

2.2.3.19 Spectroscopy and Imaging of Plasmonic Modes Over a Single Decahedron Gold Nanoparticle: A Combined Experimental and Numerical Study

Employing cathodoluminescence (CL) spectroscopy and imaging in a field emission gun (FEG) scanning electron microscope (SEM), we study localized surface plasmon (LSP) modes on individual tilted gold nanodecahedron sitting on a silicon substrate. We experimentally resolve three distinct LSP modes in the far-field radiation acquired via CL. The experimental spectra and intensity maps of plasmon modes are in excellent agreement with the spectra and 2D-CL image obtained from finite difference time domain (FDTD) simulations. Detail analysis reveals the signature of a quadrupolar surface plasmon mode in addition to the two dipolar modes along azimuthal and polar direction of the decahedron. The experimental method and the theoretical formalism presented here provide useful insight into the plasmonic behavior of complex shaped metal nanoparticle supported by a high index substrate.

Pabitra Das, Tapas Kumar Chini

2.2.3.20 Copper(I) Hydroxyapatite Catalyzed Sonogashira Reaction of Alkynes with Styrenyl Bromides. Reaction of cis-Styrenyl Bromides Forming Unsymmetric Diynes

An efficient Sonogashira coupling of terminal alkynes and styrenyl bromides has been achieved under the catalysis of hydroxyapatite-supported copper(I). The trans-styrenyl bromides produce the usual trans-enyne products, whereas the cis-styrenyl bromides lead to unsymmetric 1,3-diynes by the cross coupling of terminal alkyne and the alkyne generated from the cis-styrenyl bromide. A series of trans-enynes and unsymmetric 1,3-diynes have been synthesized by this protocol.

Debasree Saha, Tanmay Chatterjee, Manabendra Mukherjee, C Ranu Brindaban

2.2.3.21 In Situ X-ray Reflectivity Study of Polystyrene Ultrathin Films Swollen in Carbon Dioxide

We report here original in situ X-ray reflectivity (XRR.) studies of thin films isothermally exposed to CO₂ as a function of CO₂ pressure starting from ambient pressure up to its supercritical state. Swelling of polystyrene confined films is investigated by this technique. Cycling through the supercritical state of CO₂, the PS films show an irreversible behavior that is analyzed in terms of CO₂ uptake that depends on $P-g(h)$ (the pressure at which the film crosses thickness dependent $T-g(h)$). We evidence that this pressure is indeed thickness dependent and that CO₂ can be up taken in the film in a condensed state as soon as $P > P-g(h)$. We also evidence that the content of CO₂ stored inside the film after depressurization can be determined by a careful analysis of the electron density of the film.

M Souheib Chebil, G Vignaud, Y Grohens, MK Sanyal et al

2.2.4 Theoretical Condensed Matter Physics

2.2.4.1 Anomalous behavior of the diffusion coefficient in thin active films

Inspired by recent experiments in cell biology, we elucidate the visco-elastic properties of an active gel by studying the dynamics of a small tracer particle inside it. In a stochastic hydrodynamic approach for an active gel of finite thickness L , we calculate the mean square displacement of a particle. These particle displacements are governed by fluctuations in the velocity field. We characterize the short-time behavior when the gel is a solid as well as the limit of long times when the gel becomes a fluid and the particle shows simple diffusion. Active stresses together with local polar order give rise to velocity fluctuations that lead to characteristic behaviors of the diffusion coefficient that differ fundamentally from those found in a passive system: the diffusion coefficient can depend on system size and diverges as L approaches an instability threshold. Furthermore, the diffusion coefficient becomes independent of the particle size in this case.

Abhik Basu, Jean-Francois Joanny, Frank Juelicher et al

2.2.4.2 Instabilities and diffusion in a hydrodynamic model of a fluid membrane coupled to a thin active fluid layer

We construct a coarse-grained effective two-dimensional (2d) hydrodynamic theory as a theoretical model for a coupled system of a fluid membrane and a thin layer of a polar active fluid in its ordered state that is anchored to the membrane. We show that such a system is prone to generic instabilities through the interplay of nonequilibrium drive, polar order and membrane fluctuation. We use our model equations to calculate diffusion coefficients of an inclusion in the membrane and show that their values depend strongly on the system size, in contrast to their equilibrium values. Our work extends the work of S. Sankararaman and S. Ramaswamy (Phys. Rev. Lett., 102, 118107 (2009)) to a coupled system of a fluid membrane and an ordered active fluid layer. Our model is broadly inspired by and should be useful as a starting point for theoretical descriptions of the coupled dynamics of a cell membrane and a cortical actin layer anchored to it.

N Sarkar, A Basu

2.2.4.3 Restricted exclusion processes without particle conservation flows to directed percolation

Absorbing phase transitions in restricted exclusion processes are characterized by simple integer exponents. We show that this critical behaviour flows to the directed percolation (DP) universality class when particle conservation is broken suitably. The same transition, when studied using the average density as the controlling parameter, yields critical exponents quite different from DP; we argue that these exponents are actually related to DP by a scaling factor $1/\beta(\text{DP})$. These conclusions also apply to conserved lattice gas in one dimension.

Urna Basu, PK Mohanty

2.2.4.4 Active-to-absorbing-state phase transition in the presence of fluctuating environments: Weak and strong dynamic scaling

We investigate the scaling properties of phase transitions between survival and extinction (active-to-absorbing-state phase transition, AAPT) in a model that by itself belongs to the directed percolation (DP) universality class, interacting with a spatiotemporally fluctuating environment having its own nontrivial dynamics. We model the environment by (i) a randomly stirred fluid, governed by the Navier-Stokes (NS) equation, and (ii) a fluctuating surface, described either by the Kardar-Parisi-Zhang (KPZ) or the Edward-Wilkinson (EW) equations. We show, by using a one-loop perturbative field theoretic setup that, depending upon the spatial scaling of the variance of the external forces that drive the environment (i.e., the NS, KPZ, or EW equations), the system may show weak or strong dynamic scaling at the critical point of active-to-absorbing-state phase transitions. In the former case AAPT displays scaling belonging to the DP universality class, whereas in the latter case the universal behavior is different.

Niladri Sarkar, Abhik Basu

2.2.4.5 Integer quantum Hall effect in a lattice model revisited: Kubo formalism

We investigate numerically the integer quantum Hall effect (IQHE) in a two-dimensional square lattice with non-interacting electrons in presence of disorder and subjected to uniform magnetic field in a direction perpendicular to the lattice plane. We employ nearest-neighbor tight-binding Hamiltonian to describe the system, and obtain the longitudinal and transverse conductivities using Kubo formalism. The interplay between the magnetic field and disorder is also discussed. Our analysis may be helpful in studying IQHE in any discrete lattice model.

Paramita Dutta, Santanu K Maiti, SN Karmakar

2.2.4.6 Magneto-transport in a quantum network: evidence of a mesoscopic switch

We investigate magneto-transport properties of a θ shaped three-arm mesoscopic ring where the upper and lower sub-rings are threaded by Aharonov-Bohm fluxes ϕ_1 and ϕ_2 , respectively, within a non-interacting electron picture. A discrete lattice model is used to describe the quantum network in which two outer arms are subjected to binary alloy lattices while the middle arm contains identical atomic sites. It is observed that the presence of the middle arm provides localized states within the band of extended regions and lead to the possibility of switching action from a high conducting state to a low conducting one and vice versa. This behavior is justified by studying persistent current in the network. Both the total current and individual currents in three separate branches are computed by using second-quantized formalism and our idea can be utilized to study magnetic response in any complicated quantum network. The nature of localized eigenstates are also investigated from probability amplitudes at different sites of the quantum device.

Srilekha Saha, Santanu K Maiti, SN Karmakar

2.2.4.7 Study of cooperative breathing-mode in molecular chains

Using a controlled analytic nonperturbative treatment that accounts for the quantum nature of the phonons, we derive a model that generically describes the cooperative breathing-mode at strong electron-phonon interaction in one-band one-dimensional systems. The effective model involves a next-nearest-neighbor hopping (that dominates over the nearest-neighbor hopping at strong coupling) and a nearest-neighbor repulsion that is significantly enhanced due to incompatibility of neighboring dilations/compressions. At non-half-filling, upon tuning the electron-phonon coupling, the system undergoes a period-doubling second-order quantum phase transition from a Luttinger liquid to a conducting commensurate charge-density-wave state: a phenomenon absent in both the Holstein model and the t-V model. Using fidelity to study the nature of the quantum phase transition, we find that the fidelity susceptibility shows a superextensive power law divergence as well as a remarkable scaling behavior; both together establish a second-order transition.

Ravindra Pankaj, Sudhakar Yarlagadda

2.2.4.8 Spin Hall effect in a kagome lattice driven by Rashba spin-orbit interaction

Using four-terminal Landauer-Büttiker formalism and Green's function technique, in this present paper, we calculate numerically spin Hall conductance (SHC) and longitudinal conductance of a

finite size kagome lattice with Rashba spin-orbit (SO) interaction both in the presence and absence of external magnetic flux in clean limit. In the absence of magnetic flux, we observe that depending on the Fermi surface topology of the system SHC changes its sign at certain values of Fermi energy. Unlike the infinite system (where SHC is a universal constant $\pm \frac{e}{8}\pi$), here SHC depends on the external parameters like SO coupling strength, Fermi energy, etc. We show that in the presence of any arbitrary magnetic flux, periodicity of the system is lost and the features of SHC tend to get reduced because of elastic scattering. But again at some typical values of flux ($\phi = \frac{1}{2}, \frac{1}{4}, \frac{3}{4}, \dots$, etc.) the system retains its periodicity depending on its size and the features of spin Hall effect (SHE) reappears. Our predicted results may be useful in providing a deeper insight into the experimental realization of SHE in such geometries.

Moumita Dey, Santanu K Maiti, SN Karmakar

2.2.4.9 Correlated singlet phase in the one-dimensional Hubbard-Holstein model

We show that a nearest-neighbor singlet phase results (from an effective Hamiltonian) for the one-dimensional Hubbard-Holstein model in the regime of strong electron-electron and electron-phonon interactions and under nonadiabatic conditions ($t\omega(0) < 1$). By mapping the system of nearest-neighbor singlets at a filling $N\text{-}p/N$ onto a hard-core-boson (HCB) t - V model at a filling $N\text{-}p/(N - N\text{-}p)$, we demonstrate explicitly that superfluidity and charge density wave (CDW) occur mutually exclusively with the diagonal long range order manifesting itself only at one-third filling. Furthermore, we also show that the Bose-Einstein condensate (BEC) occupation number $n(0)$ for the singlet phase, similar to the $n(0)$ for a HCB tight binding model, scales as root N ; however, the coefficient of root N in the $n(0)$ for the interacting singlet phase is numerically demonstrated to be smaller.

Sahinur Reja, Sudhakar Yarlagadda, Peter B Littlewood

2.2.4.10 Fixed-Energy Sandpiles Belong Generically to Directed Percolation

Fixed-energy sandpiles with stochastic update rules are known to exhibit a nonequilibrium phase transition from an active phase into infinitely many absorbing states. Examples include the conserved Manna model, the conserved lattice gas, and the conserved threshold transfer process. It is believed that the transitions in these models belong to an autonomous universality class of nonequilibrium phase transitions, the so-called Manna class. Contrarily, the present numerical study of selected (1+1)-dimensional models in this class suggests that their critical behavior converges to directed percolation after very long time, questioning the existence of an independent Manna class.

Mahashweta Basu, Urna Basu, Sourish Bondyopadhyay, PK Mohanty et al

2.2.4.11 Conserved mass models with stickiness and chipping

We study a chipping model in a one-dimensional periodic lattice with continuous mass, where a fixed fraction of the mass is chipped off from a site and distributed randomly among the departure site and its neighbours; the remaining mass sticks to the site. In the asymmetric version the chipped

off mass is distributed among the site and the right neighbour, whereas in the symmetric version the redistribution occurs among the two neighbours. The steady state mass distribution of the model is obtained using a perturbation method for both parallel and random sequential updates. In most cases, this perturbation theory provides a steady state distribution with reasonable accuracy.

Sourish Bondyopadhyay, PK Mohanty

2.2.4.12 Statistical physics of fracture, friction, and earthquakes

The present status of research and understanding regarding the dynamics and the statistical properties of earthquakes is reviewed, mainly from a statistical physical viewpoint. Emphasis is put both on the physics of friction and fracture, which provides a microscopic basis for our understanding of an earthquake instability, and on the statistical physical modelling of earthquakes, which provides macroscopic aspects of such phenomena. Recent numerical results from several representative models are reviewed, with attention to both their critical and their characteristic properties. Some of the relevant notions and related issues are highlighted, including the origin of power laws often observed in statistical properties of earthquakes, apparently contrasting features of characteristic earthquakes or asperities, the nature of precursory phenomena and nucleation processes, and the origin of slow earthquakes, etc.

Hikaru Kawamura, Takahiro Hatano, Naoyuki Kato, Soumyajyoti Biswas, Bikas K Chakrabarti

2.2.4.13 Physics of metal-correlated barrier with disorder-metal heterostructure

A metal-disordered and correlated barrier metal heterostructure is studied at half-filling using unrestricted Hartree Fock method. The corresponding clean system has been shown to be an insulator for any finite on site correlation. Interestingly we find that introduction of explicit disorder induces an inhomogeneous, plane dependent, modulated spin and charge order. There is a metal insulator transition at a critical value of disorder. The critical value corresponds to the point at which disorder kills the gap at half filling due to onsite correlation and completely destroys the plane dependent antiferromagnetic order. The wavefunctions are found to delocalize by increasing disorder, thus rendering the system metallic.

Sanjay Gupta, Tribikram Gupta

2.2.4.14 Fermions in anisotropic harmonic trap

We study a few properties of fermions in an anisotropic harmonic trap in absence as well as in presence of an optical lattice. The density of states (DOS) and specific heat of the fermions are studied for different anisotropies. Analytical expressions for the DOS in a strongly anisotropic harmonic trap are derived. For a particular combined potential, where the fermions are hopping in a 3D lattice under a 2D harmonic potential, the Drude weight of the fermionic system is evaluated. The Drude weight is found to be flat in a wide range of fermion concentrations where it is almost temperature independent.

AN Das, S Sil

2.2.4.15 Magneto-transport in a binary alloy ring

Magneto-transport properties are investigated in a binary alloy ring subjected to an Aharonov-Bohm (AB) flux ϕ within a single-band non-interacting tight-binding framework. In the first part, we expose analytically the behavior of persistent current in an isolated ordered binary alloy ring as functions of electron concentration N_e and AB flux ϕ . While, in the second part of the Letter, we discuss electron transport properties through a binary alloy ring attached to two semi-infinite one-dimensional metallic electrodes. The effect of impurities is also analyzed. From our study we propose that under suitable choices of the parameter values the system can act as a p-type or an n-type semiconductor.

Paramita Dutta, Santanu K Maiti, SN Karmakar

2.2.4.16 Magnetic response in a zigzag carbon nanotube

Magnetic response of interacting electrons in a zigzag carbon nanotube threaded by a magnetic flux is investigated within a Hartree-Fock mean field approach. Following the description of energy spectra for both non-interacting and interacting cases we analyze the behavior of persistent current in individual branches of a nanotube. Our present investigation leads to a possibility of getting a filling-dependent metal-insulator transition in a zigzag carbon nanotube.

Paramita Dutta, Santanu K Maiti, SN Karmakar

2.2.4.17 Spin diffusion in the one-dimensional classical Heisenberg model

The problem of spin diffusion is studied numerically in the one-dimensional classical Heisenberg model using a deterministic odd-even spin precession dynamics. We demonstrate that spin diffusion in this model is normal in the infinite-temperature limit and one obtains a long-time diffusive tail in the decay of the autocorrelation function. Some variations of the model with different coupling schemes and anisotropy are also studied and we find normal diffusion in all of them. A systematic finite-size analysis also suggests normal diffusive spreading of spin fluctuations, contrary to previous claims of anomalous diffusion. We also briefly discuss spin diffusion in this model at finite temperatures.

Debarshee Bagchi

2.2.4.18 Thermally driven classical Heisenberg model in one dimension

We study thermal transport in a classical one-dimensional Heisenberg model employing a discrete-time odd-even precessional update scheme. This dynamics equilibrates a spin chain for any arbitrary temperature and finite value of the integration time step Δt . We rigorously show that in presence of driving, the system attains local thermal equilibrium, which is a strict requirement of Fourier law. In the thermodynamic limit, heat current for such a system obeys Fourier law for all temperatures, as has been recently shown [A. V. Savin, G. P. Tsironis, and X. Zotos, Phys. Rev. B 72, 140402(R) (2005)]. Finite systems, however, show an apparent ballistic transport which crosses over to a diffusive one as the system size is increased. We provide exact results for current and

energy profiles in zero- and infinite-temperature limits.

Debarshee Bagchi, PK Mohanty

2.2.4.19 Stability of Holstein and Frohlich bipolarons

We have investigated bipolaron formation in the Holstein-Hubbard and the Frohlich-Hubbard model on a discrete one-dimensional lattice. Phonon enriched basis has been generated by exploiting the idea of the Lang-Firsov transformation, which results in better convergence in the strong coupling regime. The incorporation of the finite-range electron-phonon (e-ph) interaction reduces the bipolaron effective mass. We systematically increase the spatial extent of the e-ph interaction to study the effect of the long-range tail of the Frohlich model. The electron-electron (e-e) interaction also plays a crucial role in lowering the effective mass for both the Holstein and the Frohlich bipolarons. In the presence of the extended e-e interaction, the intersite S1 Holstein bipolaron becomes unstable, while the effective mass of the Frohlich bipolaron becomes significantly reduced for both the spin singlet and triplet cases.

Monodeep Chakraborty, BI Min, Atisidipankar Chakrabarti, AN Das

2.2.4.20 Disorder induced phase transition in kinetic models of opinion dynamics

We propose a model of continuous opinion dynamics, where mutual interactions can be both positive and negative. Different types of distributions for the interactions, all characterized by a single parameter p denoting the fraction of negative interactions, are considered. Results from exact calculation of a discrete version and numerical simulations of the continuous version of the model indicate the existence of a universal continuous phase transition at $p = p(c)$ below which a consensus is reached. Although the order-disorder transition is analogous to a ferromagnetic-paramagnetic phase transition with comparable critical exponents, the model is characterized by some distinctive features relevant to a social system.

Soumyajyoti Biswas, Arnab Chatterjee, Parongama Sen

2.3 Developmental Work

2.4 Publications

2.4.1 Books/Monographs Publications & Edited Volumes

BK Chakrabarti

BK Chakrabarti, A Chakraborti, SR Chakraborty & A Chatterjee, *Econophysics of Income & Wealth Distributions*, (Cambridge University Press, Feb 2013)

Biswarup Satpati

T Ghosh and B Satpati, *Template Synthesis and Characterizations of Nickel Nanorods*, AIP Conf Proc **1447** (2012) 405

2.4.2 Publications in Journal

A Bhattacharjee, D Roy, M Roy, Thermal degradation of a molecular magnetic material: $N(n-C_4H_9)_4[(FeFeIII)-Fe-II(C_2O_4)(3)](a)$, Journal of Thermal Analysis and Calorimetry **109** (2012) 1423

Abhik Basu, Jean-Francois Joanny, Frank Juelicher, et al, Anomalous behavior of the diffusion coefficient in thin active films, New Journal of Physics **14** (2012) Art No: 115001

Abhisakh Sarma, Milan K Sanyal, Atikur Rahman et al, Hybrid nanotubes: Single step formation of homogeneous nanotubes of polypyrrole-gold composites and novel switching transition of resistance beyond liquid nitrogen temperature, Journal of Applied Physics **112** (2012) Art No: 044304

Alessia Le Donne†, Sourav Kanti Jana†, Sangam Banerjee et al, Optimized luminescence properties of Mn doped ZnS nanoparticles for photovoltaic applications, J Appl Phys **113** (2013) 014903

A Metya, D Ghose, SA Mollick et al, Nanopatterning of mica surface under low energy ion beam sputtering, Journal of Applied Physics **111** (2012) Art No: 074306

A Midya, N Khan, D Bhoi, P Mandal, Giant magnetocaloric effect in magnetically frustrated $EuHo_2O_4$ and $EuDy_2O_4$ compounds, Appl Phys Lett **101** (2012) 132415

AN Das, S Sil, Fermions in anisotropic harmonic trap, Physics Letters **A376** (2012) 1698

Anna Kozakiewicz, Binita Ghosh, Purushottam Chakraborty et al, Ion beam synthesized colloidal silver nanoclusters in crystalline sapphire as third-order optical material, IEEE Photonics Journal **4** (2012) 205

Arun Kumar Mandal†, Mallar Ray†, Indrajith Rajapaksa†, Smita Mukherjee, Alokmay Datta, Xylene-Capped Luminescent Silicon Nanocrystals: Evidence of Supramolecular Bonding, Journal of Physical Chemistry **C116** (2012) 14644

Ashis Bhattacharjee, Debasis Roy, Madhusudan Roy, Thermal Decomposition of Molecular Materials $N(n-C_4H_9)_4[(MFeIII)-Fe-II(C_2O_4)(3)]_\infty$, $M-II = Zn, Co, Fe$, International Journal of Thermophysics **33** (2012) 2351

Biswajit Saha, Purushottam Chakraborty, Hubert Gnaser et al, Exact compositional analysis of SiGe alloys by matrix effect compensated MCs⁺-SIMS, Applied Physics **A108** (2012) 671

Debapriya De, Prabir Kr Panda, Madhusudan Roy, Satyaban Bhunia, Abu Ismail Jaman, Reinforcing effect of nanosilica on the properties of natural rubber/reclaimed ground rubber tire vulcanizates, Polymer Engineering and Science **53** (2013) 227

Debarshee Bagchi; PK Mohanty, Thermally driven classical Heisenberg model in one dimension, Physical Review **B86** (2012) Art No: 214302

Debarshee Bagchi, Spin diffusion in the one-dimensional classical Heisenberg model, Physical Re-

view **B87** (2013) Art No: 075133

Debasree Saha; Tanmay Chatterjee; Manabendra Mukherjee et al, Copper(I) Hydroxyapatite Catalyzed Sonogashira Reaction of Alkynes with Styrenyl Bromides. Reaction of cis-Styrenyl Bromides Forming Unsymmetric Dienes, *Journal of Organic Chemistry* **77** (2012) 9379

Dhriti Ranjan Saha, Manabendra Mukherjee, Dipankar Chakravorty, Magnetodielectric effect in composites of nanodimensional glass and CuO, nanoparticles, *Journal of Magnetism and Magnetic Materials* **324** (2012) 4073

D Mohan Radheep†, P Sarkar†, S Arumugam†, P Mandal, Colossal piezoresistance effect in $\text{Sm}_{0.55}(\text{Sr}_{0.5}\text{Ca}_{0.5})_{0.45}\text{MnO}_3$ single crystal, *Appl Phys Lett* **102** (2013) 092406

D Talukdar, UN Nandi†, A Poddar, P Mandal, KK Bardhan, Scaling of non-Ohmic conduction in strongly correlated systems, *Physical Review* **B86** (2012) Art No: 165104

Eno Hysi, Ratan K Saha, Michael C Kolios, On the use of photoacoustics to detect red blood cell aggregation, *Biomedical Optics Express* **3** (2012) 2326

Eno Hysi, Ratan K Saha, Michael C Kolios, Photoacoustic ultrasound spectroscopy for assessing red blood cell aggregation and oxygenation, *Journal of Biomedical Optics* **17** (2012) Art No: 125006

Hikaru Kawamura, Takahiro Hatano, Naoyuki Kato, Soumyajyoti Biswas, Bikas K Chakrabarti, Statistical physics of fracture, friction, and earthquakes, *Reviews of Modern Physics* **84** (2012) 839

JK Bal, Sarathi Kundu, S Hazra, Hydrophilic-like wettability of Cl-passivated Ge(001) surface, *Chemical Physics* **406** (2012) 72

JK Bal, Sarathi Kundu, S Hazra, Role of metal ions in growth and stability of Langmuir-Blodgett films on homogeneous and heterogeneous surfaces, *European Physical Journal* **E35** (2012) Art No: 79

JK Bal, Sarathi Kundu, S Hazra, Role of metal ions of Langmuir-Blodgett film in hydrophobic to hydrophilic transition of HF-treated Si surface, *Materials Chemistry and Physics* **134** (2012) 549

J Sengupta, RK Sahoo, CD Mukherjee, Effect of annealing on the structural, topographical and optical properties of sol-gel derived ZnO and AZO thin films, *Materials Letters* **83** (2012) 84

Mahashweta Basu, Urna Basu, Sourish Bondyopadhyay, et al, Fixed-Energy Sandpiles Belong Generically to Directed Percolation, *Physical Review Letters* **109** (2012) Art No: 015702

Mayukh Majumder, Kajal Ghoshray, Amitabha Ghoshray et al, Anisotropic Spin-Fluctuations in SmCoPO Revealed by ^{31}P NMR Measurement, *Journal of the Physical Society of Japan* **81** (2012) Art No: 054702

M Ghosh, K Ghoshray, Spin trimers in $\text{Ca}_3\text{Cu}_2\text{Ni}(\text{PO}_4)_4$, *Low Temperature Physics* **38** (2012)

645

M Majumder, K Ghoshray, C Mazumdar, A Poddar, A Ghoshray et al, Evidence of a structural phase transition in superconducting $\text{SmFeAsO}_{1-x}\text{F}_x$ from ^{19}F NMR, *Journal of Physics: Condensed Matter* **25** (2013) 025701

Mojammel H Mondal; M Mukherjee, Effect of thermal modification on swelling dynamics of ultrathin polymer films, *Polymer* **53** (2012) 5170

Monodeep Chakraborty; BI Min; Atisidipankar Chakrabarti et al; Stability of Holstein and Frohlich bipolarons, *Physical Review* **B85** (2012) Art No: 245127

Moumita Dey, Santanu K Maiti, SN Karmakar, Spin Hall effect in a kagome lattice driven by Rashba spin-orbit interaction, *Journal of Applied Physics* **112** (2012) Art No: 024322

M Souheib Chebil; G Vignaud; Y Grohens, MK Sanyal et al, In Situ X-ray Reflectivity Study of Polystyrene Ultrathin Films Swollen in Carbon Dioxide, *Macromolecules* **45** (2012) 6611

Niladri Sarkar, Abhik Basu, Active-to-absorbing-state phase transition in the presence of fluctuating environments: Weak and strong dynamic scaling, *Physical Review* **E86** (2012) Art No: 021122

N Khan, P Mandal, K Mydeen† et al, Magnetoelectronic phase separation in $\text{La}_{1-x}\text{Sr}_x\text{CoO}_3$ single crystals: Evidence from critical behavior, *Physical Review* **B85** (2012) Art No: 214419

N Sarkar, A Basu, Instabilities and diffusion in a hydrodynamic model of a fluid membrane coupled to a thin active fluid layer, *European Physical Journal* **E35** (2012) Art No: 115

Nupur Biswas, Alokmay Datta, Polymer entanglement - A barrier to nanoparticles aggregation, *Chemical Physics Letters* **531** (2012) 177

Nupur Biswas, Masatoshi Ichikawa, Alokmay Datta et al, Phase separation in crowded microspheroids: DNA-PEG system, *Chemical Physics Letters* **539** (2012) 157

Pabitra Das, Tapas Kumar Chini, James Pond, Probing Higher Order Surface Plasmon Modes on Individual Truncated Tetrahedral Gold Nanoparticle Using Cathodoluminescence Imaging and Spectroscopy Combined with FDTD Simulations, *Journal of Physical Chemistry* **C116** (2012) 15610

Pabitra Das; Tapas Kumar Chini, Spectroscopy and Imaging of Plasmonic Modes Over a Single Decahedron Gold Nanoparticle: A Combined Experimental and Numerical Study, *Journal of Physical Chemistry* **C116** (2012) 25969

Paramita Dutta, Santanu K Maiti, SN Karmakar, Integer quantum Hall effect in a lattice model revisited: Kubo formalism, *Journal of Applied Physics* **112** (2012) Art No: 044306

Paramita Dutta; Santanu K Maiti; SN Karmakar, Magnetic response in a zigzag carbon nanotube, *European Physical Journal* **B85** (2012) Art No: 126

Paramita Dutta, Santanu K Maiti, SN Karmakar, Magneto-transport in a binary alloy ring, *Physics Letters* **A376** (2012) 1567

P Dutta, D Bhoi, A Midya, N Khan, P Mandal et al, Anomalous thermal expansion of Sb_2Te_3 topological insulator, *Appl Phys Lett* **100** (2012) 251912

P Laha†; I Banerjee; A Bajaj; P Chakraborty† et al, Irradiation effects of 6 MeV electron on electrical properties of $\text{Al}/\text{Al}_2\text{O}_3/\text{n-Si}$ MOS capacitors, *Radiation Physics and Chemistry* **81** (2012) 1600

P Mandal; P Choudhury†, Hall effect in the metallic antiferromagnet Na_xCoO_2 ($0.72 \leq x \leq 0.90$), *Physical Review* **B86** (2012) Art No: 094423

Ratan K Saha, Subhajit Karmakar, Eno Hysi et al, Validity of a theoretical model to examine blood oxygenation dependent optoacoustics, *Journal of Biomedical Optics* **17** (2012) Art No: 055002

Ratan K Saha, Subhajit Karmakar, Madhusudan Roy, Computational Investigation on the Photoacoustics of Malaria Infected Red Blood Cells, *PLOS ONE* **7** (2012) Art No:e51774

Ravindra Pankaj, Sudhakar Yarlagadda, Study of cooperative breathing-mode in molecular chains, *Physical Review* **B86** (2012) Art No: 035453

RP Maiti, S Dutta, M Mukherjee et al, Magnetic and dielectric properties of sol-gel derived nanoparticles of double perovskite Y_2NiMnO_6 , *Journal of Applied Physics* **112** (2012) Art No: 044311

Sahinur Reja, Sudhakar Yarlagadda, Peter B Littlewood, Correlated singlet phase in the one-dimensional Hubbard-Holstein model, *Physical Review* **B86** (2012) Art No: 045110

Sanjay Gupta, Tribikram Gupta, Physics of metal-correlated barrier with disorder-metal heterostructure, *Solid State Communications* **152** (2012) 878

Sivasurender Chandran, JK Basu, MK Mukhopadhyay, Variation in glass transition temperature of polymer nanocomposite films driven by morphological transitions, *Journal of Chemical Physics* **138** (2013) Art No: 014902

SK Mahatha, KD Patel, Krishnakumar SR Menon, Electronic structure investigation of MoS_2 and MoSe_2 using angle-resolved photoemission spectroscopy and ab initio band structure studies, *Journal of Physics-Condensed Matter* **24** (2012) Art No: 475504

SK Mahatha, Krishnakumar SR Menon, Inhomogeneous band bending on $\text{MoS}_2(0001)$ arising from surface steps and dislocations, *Journal of Physics-Condensed Matter* **24** (2012) Art No: 305502

SK Mahatha, Krishnakumar SR Menon, Polarization dependence of angle-resolved photoemission spectroscopy of graphite, *Surface Science* **606** 1705

SK Mahatha, Krishnakumar SR Menon, Quantum well states in Ag thin films on $\text{MoS}_2(0001)$ surfaces, *Journal of Physics-Condensed Matter* **25** (2013) Art No: 115501

S Mondal, SR Bhattacharyya, P Mitra, Effect of Al doping on microstructure and optical band gap of ZnO thin film synthesized by successive ion layer adsorption and reaction, *Pramana-Journal of Physics* **80** (2013) 315

Soumyajyoti Biswas; Arnab Chatterjee†; Parongama Sen†; Disorder induced phase transition in kinetic models of opinion dynamics, *Physica* **A391** (2012) 3257

Sourish Bondyopadhyay, PK Mohanty, Conserved mass models with stickiness and chipping, *Journal of Statistical Mechanics-Theory and Experiment* (2012) Art No: P07019

Souvik Kundu, Nripendra N Halder, D Biswas S Chakraborty, Role of ultra thin pseudomorphic InP layer to improve the high-k dielectric/GaAs interface in realizing metal-oxide-semiconductor capacitor, *Journal of Applied Physics* **112** (2012) Art No:034514

Souvik Kundu, Nripendra N Halder, Pranab Biswas et al, Charge storage properties of InP quantum dots in GaAs metal-oxide-semiconductor based nonvolatile flash memory devices, *Applied Physics Letters* **101** (2012) Art No: 212108

Souvik Kundu, Yelagam Anitha, Supratic Chakraborty, Pallab Banerji, Interface studies on high-k/GaAs MOS capacitors by deep level transient spectroscopy, *Journal of Vacuum Science & Technology* **B30** (2012) Art No: 051206

Srilekha Saha, Santanu K Maiti, SN Karmakar, Magneto-transport in a quantum network: evidence of a mesoscopic switch, *European Physical Journal* **B85** (2012) Art No: 283

S Sain, J Bhattacharjee, M Mukherjee, et al, Microstructural, magnetic and optical characterizations of nanocrystalline $\text{Zn}_{1-x}\text{Mn}_x\text{O}$ dilute magnetic semiconductors synthesized by mechanical alloying, *Journal of Alloys and Compounds* **519** (2012) 112

Subhendu Mondal, Hubert Gnaser, Purushottam Chakraborty, Symmetric and asymmetric collision effects on the formation of singly and doubly-charged ions in sputtering process, *European Physical journal* **D66** (2012) 197

Sumistha Das, Nitai Debnath, Shouvik Mitra, Alokmay Datta et al, Comparative analysis of stability and toxicity profile of three differently capped gold nanoparticles for biomedical usage, *Biometals* **25** (2012) 1009

Tanusree Samanta, M Mukherjee, Effect of added salt on morphology of ultrathin polyelectrolyte films, *Polymer* **53** (2012) 5393

Urna Basu, PK Mohanty, Restricted exclusion processes without particle conservation flows to directed percolation, *EPL* **99** (2012) Art No: 66002

2.5 Ph D Awarded

Prosenjit Sarkar [Prabhat Mandal], Influence of quenched disorder on magnetic and electronic phase transition in $\text{Sm}_{1-x}\text{Sr}_x\text{MnO}_3$ close to half-doping, Jadavpur University, March 12, 2013

Biswajit Saha [Purushottam Chakraborty], Secondary Emission of MCsn^+ Molecular Ions and its Applications in Compositional Analysis of MBE Grown Si-Ge Structures, University of Calcutta, September 2012

2.6 Seminars/Lectures given in Conference/Symposium/Schools

Milan K Sanyal

1. Metallic behaviour of polymer nanowires, International Conference on Functional Oxides and New Carbon Materials (CFOCM-2012), S. N. Bose National Centre for Basic Sciences -Kolkata, May 6 - 8, 2012
2. Ordering of hydrophobic soft-matter on water surface, Physiques Dartement, Universitdu Maine, Le Mans, France, July 12, 2012
3. Crystallization of nanostructures on water surface, 12th International Conference on Surface X-ray and Neutron Scattering, Kolkata, July 25, 2012
4. Study of spin-vortex structures in gadolinium stearate Langmuir-Blodgett films with polarized neutron reflectivity, Indo-US Workshop, Jawaharlal Nehru Centre for Advanced Scientific Research, Bangalore, September 6-7, 2012
5. Synchrotron X-ray Scattering techniques to probe formation and ordering of nano-materials, Physics Colloquium, Bhabha Atomic Research Centre Mumbai, 20 Sept. 2012
6. Neutron reflectivity studies of chemical and magnetic structures in Langmuir-Blodgett films, Bragg Institute Seminar, Sydney, October 15. 2012
7. Ordering of nanostructures on water surface, Australian National University, Canberra, October 18, 2012
8. Formation and ordering of nanomaterials probed with micron/nano-meter-sized x-ray beams an evolving research fiel, International Conference on Emerging Advanced Nanomaterials (ICEAN2012), Brisbane, October 22, 2012
9. Novel resistance-switching transition in polypyrrole nanowires synthesized in membrane-pores, University of Melbourne, Australia, October 25, 2012
10. Synchrotron x-ray scattering and SIMS studies of MBE grown Si-Ge multilayer film, University of Auckland, Newzealand, October 26, 2012
11. Formation and ordering of nanomaterials probed with micron/nano-meter-sized synchrotron x-ray beam, National University of Singapore, November 1, 2012
12. Synchrotron x-ray scattering studies of nanostructure-formation at interface, 57th DAE-Solid State Physics Symposium, IIT Mumbai, December 3 7, 2012
13. Synchrotron x-ray scattering techniques with micron-sized beams to probe formation of nano-materials at interfaces an evolving research field, Winter School 2012 on Frontiers of Materials Science, Jawaharlal Nehru Centre for Advanced Scientific Research, Bangalore, December 8, 2012
14. Neutron reflectivity studies of chemical and magnetic structures in Langmuir-Blodgett films, International Symposium on Neutron Scattering, Bhabha Atomic Research Centre Mumbai, Jan-

uary 14-17, 2013

15. Low-dimensional Physics and Ordering in Nano-structured Material, Colloquium Physical Research Laboratory, Ahmedabad, January 30, 2013
16. Formation and ordering of nanoparticles at interface, International Symposium on Molecular Organization and Complexity: A Chemical Perspective, Saha Institute of Nuclear Physics, Kolkata, February 6, 2013
17. Synchrotron x-ray scattering studies of nanostructure-formation at buried interfaces, Prof. C. N. R. Rao Prize Lecture in Advanced Materials, Material Research Society Meeting, Indira Gandhi Centre for Atomic Research, Kalpakkam, February 11, 2013
18. Novel resistance-switching transition in polypyrrole nanowires synthesized in membrane-pores, Nano India 2013, Thiruvananthapuram, February 20, 2013
19. Probing Low-dimensional Ordering in Nano-structured Materials, Anil Kumar Memorial Lecture, Indian Institute of Science, Bangalore, March 22, 2013

Barnana Pal

Monte-Carlo Study on Lennard-Jones Clusters, 1st International Conference on Frontiers in Computational Physics: Modeling the Earth System, organized by ELSEVIER, National Center for Atmospheric Research, Boulder, CO, USA, Dec 16-20, 2012

Purushottam Chakraborty

1. National Seminar on Recent Trends in Advanced Materials, Physics Department, Manipur University, India, Mar 26, 2013
2. One Day seminar on Experimental Techniques in Condensed matter Physics, Physics Department, Jadavpur University, India, Mar 21, 2013
3. UGC - Refresher Course on Analytical Instruments: Techniques and Applications, Department of Instrumentation Science, Jadavpur University, India, Feb 25-Mar 16, 2013
4. Short Term Training Program on Physics of Materials, National Institute of Technical Teachers' Training & Research (NITTTR), Kolkata, India, Jan 28-Feb 1, 2013
5. ISOLDE Workshop on Solid State Physics and Users Meeting, CERN, Geneva, Switzerland, Dec 17-19, 2012
6. 10th Asian International Seminar on Atomic and Molecular Physics (AISAMP10), Academia Sinica, Taipei, Taiwan, Oct 23-30, 2012
7. International Workshop on the Modification and Analysis of Materials for Future energy Sources (Energy 2012), Madrid, Spain, Sept 17-20, 2012
8. 19th International Workshop on Inelastic Ion-Surface Collisions (IISC-19), Max Planck Institute for Plasma Physics, Munich, Germany, Sept 16-21, 2012
9. 12th International Conference on Surface X-rays and Neutron Scattering (SXNS-12), Hyatt Regency, Kolkata, India, Jul 25-28, 2012

Alokmay Datta

1. Liquid-like Films. 14th International Conference on Organized Molecular Films ICOMF14 (LB14) Paris, Jul 10-13, 2012
2. Structure and Forces in Soft Materials under Nanoscale Confinement Seminar@Elettra, Elettra, Trieste, Italy, Dec 17, 2012

BK Chakrabarti

1. Fracture Propagation in Heterogeneous Media, SINTEF Petroleum Research, Trondheim, Norway, Aug 2012
2. Stochastic Strategies in Kolkata Paise Restaurant Problems & Minority Games, Ecole Central Paris, Paris, France, Sept 2012
3. (a) Interface Depinning Models & Fracture Front Propagation & (b) Conference Summary, Institute of Mathematical Sciences, Chennai, Jan 2013

Y Sudhakar

1. Strong multiferroicity and giant magnetoelectric effect in (Insulator)/(LaMnO₃)_n/(SrMnO₃)_n/(Insulator) heterostructure, International conference on Correlated Oxides: novel quantum states, device physics and energy technologies, Cambridge Univ, Mar-Apr 2012
2. Modeling multiferroicity in manganite heterostructures by including cooperative electron-phonon interaction, the discussion meeting, entitled 'New functionalities in electronic and magnetic materials', SSCU, IISc, Oct 18-20, 2012

Chapter 3

Experimental Nuclear and Particle Physics

3.1 Summary of Research Activities of Divisions

3.1.1 Applied Nuclear Physics

Research conducted at the Applied Nuclear Physics Division during 2012-2013 can be broadly classified in four categories: exploration of atomic and molecular structure and reaction dynamics using x-rays of various types and origin; investigation on the structure, evolution and phase transition of nanomaterials, crystalline materials, soft matter and bio-materials; development, characterization and optimization of radiation detectors; and model based simulation.

Sequential inner shell multiple ionization of Krypton using ion time of flight spectroscopy at photon energies in the vicinity of L-edge was studied using femtosecond X-ray pulses at the Linac Coherent Light Source at Stanford, USA. The results highlight the role of a resonant ionization pathway involving multiple excitations and autoionization. Fragmentation and ionization of complex molecules (methylselenol) by femtosecond and intense X-ray pulses are explored by coincident ion momentum spectroscopy. Attempts are made at explaining the findings in the light of Coulomb explosion model. Indication of an ultrafast charge redistribution of the inner shell ionized Selenium atom was also observed. Production of inner shell ionization in heavy elements, such as Gold, by electron impact at energies 15 to 40 keV was investigated. These studies have their importance in the quantitative trace element analysis. The characteristic L X-rays yields were measured and converted to L-shell ionization cross section using the known atomic relaxation parameters and the fluorescence yield. Comparison of data with quantum mechanical (DWBA) and other model based estimates indicate the need for better understanding of the many electron wave functions. Positron annihilation studies of different class of materials, such as nanosemiconductors, nanospinels, graphene, etc. were done and the new results were communicated. Systematic investigation of the Positronium life time of soft materials, nanocomposites synthesized by chemical route, has revealed structural modification due to subtle changes in the chemical composition. Nanocrystalline phase of zinc oxide has also been studied with radioactive ion beam using ^{111m}Cd (half-life = 48.5 min) and Perturbed Angular Correlation (PAC) method at CERN/ISOLDE facility. In the PAC spectroscopy labora-

tory, identification of phase transition in crystalline metal and metal oxides were done over a wide range of temperatures using ^{181}Hf as the probe nuclei. These studies manifest many interesting results including the coexistence of defects and their propagation through annealing of the materials. Our divisional scientists are also continuing with their involvement in the research planning, simulation and development of radiation detectors for the RD-51 collaboration in CERN, and also in the proposed India-based Neutrino Observatory (INO) as part of the national multi-institutional collaboration. Simulation of detector performance and design optimization of various grid based gaseous detectors, micropattern gaseous detectors (MPGD), RPC and TPC detectors are successfully done by the scientists involved. These detectors are employed in various high energy physics experiments, dark matter search experiments conducted at various national and international labs as collaboration initiative. A dedicated MPGD laboratory has been set up and experiments are routinely carried out. Members of our division are concentrating on various phenomena associated with visual perception, where the models are inspired mainly by vision. These studies are supplemented by suitable cognitive science experiments. An equipped laboratory has been set up for the purpose.

3.1.2 High Energy Nuclear and Particle Physics

The High Energy Nuclear and Particle Physics division is involved in two major experiments at the Large Hadron Collider (LHC), CERN. LHC has delivered a vast amount of data during 2012-13 initially with proton beams colliding at centre of mass energy of 8 TeV and then with proton beam colliding with lead ions. The two experiments, ALICE and CMS collected data with a very high efficiency and members of the HENPP division of SINP took active parts in the data collection, data analysis and extracting important physics results from these experiments. During the period 2012-13, more than 120 physics results were published in international refereed journal from these two experiments.

The institute has been a member of the ALICE collaboration since 1997 and is responsible for the Muon Spectrometer which is used to study heavy quark formation at the extreme forward angles in proton-proton as well as heavy ion collisions. The SINP team was involved in the development of the front-end electronics chip, fabrication of the second tracking station of the Muon Spectrometer and development of the di-muon high level trigger. The group is now taking part in the run coordination and data quality assurance tests. The group has carried out the analysis of v as well as $\psi(1S)$ and $\psi(2S)$ in proton-proton and heavy ion collisions. The institute has become a member of the CMS collaboration in early 2011 and has made a strong presence in the experiment from the very beginning taking major responsibilities in offline software and online data quality monitoring. The group is participating in the upgrade project of the hadron calorimeter and has successfully made part of the back end electronics of the future calorimeter system. They have been tested in real running condition and has been approved for fabrication after a rigorous technical evaluation. The group has participated in the calibration of the calorimeters and investigated effects of particle induced noise in the detector. One of the most important results in the field of High Energy physics is the discovery of the Higgs boson. The group has participated in the analysis of Higgs boson search in a number of channels and contributed significantly in this discovery. The group also participated in the search of dark matter, investigation of the theory of strong interaction and search for compositeness in the lepton sector.

In addition to these two major experiments, the group has also contributed to phenomenological studies of anisotropic plasma and heavy quark energy loss. It has also made studies of excited nuclei using low energy heavy ion experiments. The current theory of strong interaction, Quantum Chromo Dynamics (QCD), predicts that at very high temperatures and energy densities, quarks

and gluons are no longer confined inside the hadrons and they would exist in the form of free quarks and gluons, a state called Quark Gluon Plasma (QGP). Within the first few microseconds of the birth of the Universe, the temperature and energy density was extremely high and the primordial state of matter was a system of QGP. Thus, to understand the evolution of our Universe during its infancy, we need to create and study the formation of QGP in the laboratory. This can be done by colliding two heavy nuclei at very high energies. In the LHC heavy-ion programme, Lead beams collide at energies up to 30 times higher than in previous laboratory experiments. In these heavy-ion collisions, matter is heated to more than 100,000 times the temperature at the centre of the Sun over a tiny volume of the size of a nucleus and for an infinitesimally short instant. We then observe this QGP state as it reverts to hadronic matter through a complex set of particle and gamma detectors. A Large Ion Collider Experiment (ALICE) is the only dedicated heavy-ion experiment of LHC study this extreme, high-temperature phase of matter and provide novel access to the question of how most of the mass of visible matter in the Universe was generated in the first microseconds after the Big Bang. During the first three years of LHC operation, ALICE has collected data for p-p collisions ($\sqrt{s} = 0.9, 2.76, 7$ and 8 TeV), p-Pb collisions ($\sqrt{s} = 5.02$ TeV) and Pb-Pb collisions ($\sqrt{s} = 2.76$ TeV/nucleon). The Direct photon studies indicates that the temperature reached in these Pb-Pb collisions was 304 MeV, i.e, about 5.5 trillion degrees, while charged particle correlation data fixes a volume of about 300 fm^3 (about the volume of an Argon nucleus). The charged particle multiplicity studies give the energy density of the matter to be about 10 GeV/fm^3 which is 70 times the normal nuclear density and the estimated lifetime of about 10 fm/c (i.e about 10^{-23} second). The flow properties of this matter indicate that it is an ideal fluid whose viscosity is more than three hundred times less than water. A recent theoretical calculation (AdS/CFT correspondence) has indicated that this is the lowest possible value for viscosity. Thus, the soft physics program of ALICE has been successful to determine the bulk properties of the matter created in the Pb-Pb collisions. On the other hand, the hard probes (particles with high transverse momentum, particle jets and heavy flavoured particles) are used to study the properties of the matter. The observation of jet quenching indicates the formation of very dense matter in heavy-ion collisions which is also supported by the observation of large suppression in the production of charged particles in central Pb-Pb collisions. The study of heavy quark resonances by the Muon Spectrometer of ALICE has established that the matter has deconfined quarks and gluons as these resonances are strongly suppressed in this medium. In summary, the first results from the Pb-Pb data collected in 2010-11 indicate that the matter created at LHC is an ideal fluid which is extremely dense and hot and the quarks and gluons are not confined within this fluid. It demonstrates our success in synthesising matter which mimics the state of our universe within few microseconds of the birth of our Universe. The coming years promise substantial increase in both statistics and centre of mass energy (from $\sqrt{s} = 2.76$ to 5.5 TeV/nucleon). These will open further windows to the wonderland to be explored by ALICE. The group at Saha Institute is closely associated with the analysis and physics of heavy quarks (charm and beauty) which are formed at early stages of collision and behaves like Brownian particles in the QGP. Thus, they are the unique probe for the deconfined state of matter. Saha Institute is a key member of the collaboration which is responsible for the Muon Spectrometer of ALICE which is the only detector at LHC capable of studying the heavy quarks formed in Pb-Pb collisions at extreme forward angles. Our group has been involved in the (a) development of the front end electronics chip (MANAS), (b) fabrication of the 2nd Tracking Station and its operation, (c) development of the Dimuon High Level Trigger, (d) fabrication of part of the Front Absorber (e) run co-ordination and data Quality Assurance checks in 2010-11, (f) Upsilon analysis of Pb-Pb and p-Pb collisions, (g) $\Psi(1S)$ and $\Psi(2S)$ analysis of p-p (7 TeV), p-Pb and Pb-Pb data and (h) phenomenological studies on anisotropic plasma and heavy quark energy loss.

The physics analyses of the SINP-CMS group spans all major areas of the LHC Physics program. The group has made notable contributions in the area of search for Standard Model (SM) Higgs boson, test of Standard Model and search for physics beyond the Standard Model. Group members have taken up leadership roles, serving as contact persons for analyses, and members of internal review committees.

In the area of SM physics most notable contribution of the SINP group has been in studies of QCD. Studies of event shape variables in inclusive hadronic sample and in multijet states have revealed dynamics of strong interaction [CMS-PAS-SMP-12-022, CMS-PAS-QCD-11-006].

In the area of SM Higgs boson search the group has made significant contribution in high mass region search, in which the Higgs boson decays to a pair of Z bosons with the Z's decaying further to an e^+e^- (or a $\mu^+\mu^-$) pair and a τ lepton pair. The other Higgs search channel with significant contribution from SINP is associated production of Higgs with a W boson, where the Higgs decays to a pair of hadronically decaying τ leptons and the W decays to either a muon or an electron [CMS PAS HIG-12-053, arXiv:1202.3617v1].

The SINP group has played key role in the search for dark matter and search for existence of large extra dimensions using final states with a single photon and large missing transverse energy and in the search for substructure of leptons [CERN-PH-EP-2012-084, arXiv:1210.2422 [hep-ex]]. SINP group member received the best poster award in this area at the Lepton Photon conference in 2012. Detector calibration and particle identification are closely integrated with the pursuit of the physics analyses. The SINP group has made several important and challenging measurements in these areas, which include calibration of the hadron calorimeter, improvement in the energy flow measurement by including the components of the hadron calorimeter, understating calorimetric response of isolated charged hadrons, detailed study of anomalous signals in the electromagnetic calorimeter, measurement of jet faking photon and electron faking photon probabilities, numerous studies related to the identification of the tau lepton with the CMS detector.

3.1.3 Nuclear Physics

Research activities in Nuclear Physics Division include experimental study of nuclear structures and nuclear reaction mechanisms using different accelerator centres in India and a few abroad. In addition members of the division are actively involved in the setting up of the FRENA facility for nuclear astrophysics research. The other major activities are: theoretical research, developmental activities and EDXRF spectrometry.

Nuclear Structure: High spin states in ^{122}I , ^{195}Bi , ^{194}Tl , ^{89}Zr , ^{154}Ho were investigated by populating these isotopes using fusion evaporation reactions. All these studies were performed as a part of the INGA campaign. Several new structural information like new band structures, magnetic rotational bands, etc. were predicted. Another experiment was performed where presence of a super deformed band was predicted in ^{35}Cl ; theoretical interpretation using large basis shell model (LBSM) calculations was used and interpreted it to having an alpha cluster structure. Experiments were performed at GSI, ISOLDE and TIFR pelletron to understand failure of magic number in neutron rich nuclei, exotic decay mode near proton drip line, etc.

Nuclear Reactions: Experiment was performed to study the $^{12}\text{C}/^{16}\text{O}$ ratio using the $^{12}\text{C}(^6\text{Li},d)^{16}\text{O}$ reaction. Spectroscopic factors were extracted from the deuteron angular distribution using CDCC- CRC theory. ^{212}Po α -cluster states were experimentally studied using α elastic scattering in ^{208}Pb . Fusion and quasi elastic excitation functions for $^6\text{Li}+^{64}\text{Ni}$ were experimentally studied. Barrier distributions from both these methods are found to agree with each other. A model calculation within the CDCC-CRC framework is under progress. Coupled channel calculations to explain fusion cross-sections of $^6\text{Li}+^{24}\text{Mg}$, measured earlier, is being pursued. CDCC calculations

are being used to study the effect of breakup on elastic scattering & fusion for ${}^6,7\text{Li}+{}^{28}\text{Si}$ systems. R-matrix calculations for ${}^{13}\text{C}(\text{p},\gamma){}^{14}\text{N}^*$ capture reaction using the AZURE code has been performed. Results yielded a lower astrophysical S-factor compared with the NCARE database.

Developmental activities: Preparation of ${}^{22}\text{Ne}$ implanted targets has been achieved. XPS analysis was used to estimate the amount of impurities present on the target surface. A laboratory is being setup to study γ - spectroscopy of fission fragments. Developmental work on gas scintillation proportional counter has been pursued. A fast timing MMRPC was tested at SINP using cosmic muon and γ -rays. Preliminary estimates gave a time resolution of less than 100 ps.

XRF laboratory: Polarized EDXRF spectrometer EPSILON5 was used for the analysis of soil samples collected from municipal waste dumping site at Dhapa, Kolkata. The laboratory also successfully participated in the worldwide open proficiency test conducted by IAEA.

3.2 Research Activities

3.2.1 Applied Nuclear Physics

3.2.1.1 Resonance-enhanced multiple ionization of krypton at an x-ray free-electron laser

The sequential inner-shell multiple ionization of krypton was investigated at the Linac Coherent Light Source using ion time-of-flight spectroscopy at photon energies above (2 keV) and below (1.5 keV) the L edge with two x-ray pulse lengths (5 and 80 fs, nominally) and various pulse energies. At 2.5 mJ pulse energy, charge states up to Kr^{17+} were recorded for M-shell ionization and charge states up to Kr^{21+} for L-shell ionization. Comparing the experimental charge state distribution to Monte Carlo rate-equation calculations, we find a strong enhancement of higher charge states at 2 keV photon energy as compared to the theoretical predictions. This enhancement is explained with a resonant ionization pathway where multiple excitations into outer valence and Rydberg orbitals are followed by autoionization. These resonant pathways play an important role for the photoionization of ions with charge higher than Kr^{12+} , for which direct one-photon L-shell photoionization is energetically impossible at 2 keV photon energy. Only a small pulse-length dependence of the charge state yield is observed at an x-ray pulse energy of 0.4 mJ.

Benedikt Rudek, Daniel Rolles, Sang-Kil Son, Sankar De, et al

3.2.1.2 Ultrafast Charge Rearrangement and Nuclear Dynamics upon Inner-Shell Multiple Ionization of Small Polyatomic Molecules

Ionization and fragmentation of methylselenol (CH_3SeH) molecules by intense ($>10^{17}$ W/cm²) 5 fs x-ray pulses ($\hbar\omega = 2$ keV) are studied by coincident ion momentum spectroscopy. We contrast the measured charge state distribution with data on atomic Kr, determine kinetic energies of resulting ionic fragments, and compare them to the outcome of a Coulomb explosion model. We find signatures of ultrafast charge redistribution from the inner-shell ionized Se atom to its molecular partners, and observe significant displacement of the atomic constituents in the course of multiple ionization.

B Erk, D Rolles, L Foucar, S De et al

3.2.1.3 Structural transition in rare earth doped zirconium oxide: A positron annihilation study

A series of compounds with the general composition $\text{Sm}_{2-x}\text{Dy}_x\text{Zr}_2\text{O}_7$ (where $0 \leq x \leq 2.0$) were synthesized by chemical route and characterized by powder X-ray diffraction (XRD) analysis. The rare earth ion namely Sm^{+3} in the compound was gradually replaced with another smaller and heavier ion, Dy^{+3} of the 4f series, thereby resulting in order-disorder structural transition, which has been studied by positron annihilation lifetime and Doppler broadening spectroscopy. This study reveals the subtle electronic micro environmental changes in the pyrochlore lattice (prevalent due to the oxygen vacancy in anti-site defect structure of the compound) toward its transformation to defect fluorite structure as found in $\text{Dy}_2\text{Zr}_2\text{O}_7$. A comparison of the changes perceived with PAS as compared to XRD analysis is critically assayed.

Keka Chakraborty, Abhijit Bisoi, Bichitra Nandi Ganguly et al

3.2.1.4 Oxidation of Hafnium and Diffusion of Hafnium Atoms in Hexagonal Close-Packed Hafnium; Microscopic Investigations by Perturbed Angular Correlations

Time-differential perturbed angular correlation (TDPAC) studies in hafnium metal (similar to 5%Zr) have been carried out at different temperatures. It is found that hafnium metal on heating at 873 K continuously for two days in air, transforms partially and abruptly to HfO_2 while no component of oxide has been observed for heating up to 773 K and during initial heating at 873 K for 1 day. This result is strikingly different to that expected from the Arrhenius theory. Also, a strong nuclear relaxation effect has been observed at 873 K due to rapid fluctuation of hafnium atoms in hexagonal close-packed (hcp) hafnium. At this temperature, similar to 45% probe nuclei experience static perturbation due to monoclinic HfO_2 , similar to 50% experience fluctuating interaction, and similar to 5% produce static defect configuration of hcp hafnium. With lowering of temperature, defect configurations of hafnium increase at the cost of fluctuating interaction. An almost total fluctuating interaction observed in hcp hafnium at a temperature much lower than its melting point is another interesting phenomenon.

Chandi C Dey

3.2.1.5 Measurement of electrical properties of electrode materials for the bakelite Resistive Plate Chambers

Single gap (gas gap = 2mm) bakelite Resistive Plate Chamber (RPC) modules of various sizes from 10 cm x 10 cm to 1m x 1m have been fabricated, characterized and optimized for efficiency and time resolution. Thin layers of different grades of silicone compound are applied to the inner electrode surfaces to make them smooth and also to reduce the surface resistivity. In the silicone coated RPCs an efficiency similar to 96% and time resolution similar to 2 ns (FWHM) have been obtained for both the streamer and the avalanche modes of operation. Before fabrication of detectors the electrical properties such as bulk resistivity and surface resistivity of the electrode materials are measured carefully. Effectiveness of different silicone coating in modifying the surface resistivity was evaluated by an instrument developed for monitoring the I-V curve of a high resistive surface. The results indicate definite correlation of the detector efficiency for the atmospheric muons and

the RPC noise rates with the surface resistivity and its variation with the applied bias voltage. It was also found that the surface resistivity varies for different grades of silicone material applied as coating, and the results are found to be consistent with the detector efficiency and noise rate measurements done with these RPCs.

KK Meghna†, A Banerjee†, S Biswas†, S Bhattacharya, S Bose, C Marick, S Saha et al

3.2.1.6 The N/Z key role on the dynamics of medium mass nuclear systems near fragmentation threshold

Effects related to the neutron to proton ratio (N/Z) degree of freedom in nuclear collisions Ca-40 +(40) Ca, Ca-40 +(48) Ca and Ca-48 +(48) Ca at 25 MeV per nucleon, analyzed by means of the Chimera multi-detector, have been investigated. Strong isotopic effects are found in mass distributions of light isotopes. Moreover, the competition between various reaction mechanisms at semi-central impact parameters seems to be influenced by the neutron richness of the total system formed.

I Lombardo, L Acosta, C Agodi, MB Chatterjee et al

3.2.1.7 A comparative numerical study on GEM, MHSP and MSGC

In this work, we have tried to develop a detailed understanding of the physical processes occurring in those variants of Micro Pattern Gas Detectors (MPGDs) that share micro hole and micro strip geometry, like GEM, MHSP and MSGC etc. Some of the important and fundamental characteristics of these detectors such as gain, transparency, efficiency and their operational dependence on different device parameters have been estimated following detailed numerical simulation of the detector dynamics. We have used a relatively new simulation framework developed especially for the MPGDs that combines packages such as GARFIELD, neBEM, MAGBOLTZ and HEED. The results compare closely with the available experimental data. This suggests the efficacy of the framework to model the intricacies of these micro-structured detectors in addition to providing insight into their inherent complex dynamical processes.

P Bhattacharya, S Mukhopadhyay, N Majumdar, S Bhattacharya

3.2.1.8 Correlations between emission timescale of fragments and isospin dynamics in Sn-124+Ni-64 and Sn-112+Ni-58 reactions at 35A MeV

We present a new experimental method to correlate the isotopic composition of intermediate mass fragments (IMF) emitted at midrapidity in semiperipheral collisions with the emission timescale: IMFs emitted in the early stage of the reaction show larger values of $|N/Z|$ isospin asymmetry, stronger angular anisotropies, and reduced odd-even staggering effects in neutron to proton ratio $|N/Z|$ distributions than those produced in sequential statistical emission. All these effects support the concept of isospin "migration", that is sensitive to the density gradient between participant and quasip spectator nuclear matter, in the so called neck fragmentation mechanism. By comparing the data to a stochastic mean field (SMF) simulation we show that this method gives valuable constraints on the symmetry energy term of nuclear equation of state at subsaturation densities.

An indication emerges for a linear density dependence of the symmetry energy.

E De Filippo, A Pagano, P Russotto, MB Chatterjee et al

3.2.1.9 Characterization of ZnO nanoparticles grown in presence of Folic acid template

Background: ZnO nanoparticles (grown in the template of folic acid) are biologically useful, luminescent material. It can be used for multifunctional purposes, e.g., as biosensor, bioimaging, targeted drug delivery and as growth promoting medicine. Methods: Sol-gel chemical method was used to develop the uniform ZnO nanoparticles, in a folic acid template at room temperature and pH similar to 7.5. Agglomeration of the particles was prevented due to surface charge density of folic acid in the medium. ZnO nanoparticle was further characterized by different physical methods. Results: Nanocrystalline, wurtzite ZnO particles thus prepared show interesting structural as well as band gap properties due to capping with folic acid. Conclusions: A rapid, easy and chemical preparative method for the growth of ZnO nanoparticles with important surface physical properties is discussed. Emphatically, after capping with folic acid, its photoluminescence properties are in the visible region. Therefore, the same can be used for monitoring local environmental properties of biosystems.

Sreetama Dutta, Bichitra N Ganguly

3.2.2 High Energy Nuclear and Particle Physics

3.2.2.1 Wake in anisotropic quark-gluon plasma

We calculate the wake in charge density and the wake potential due to the passage of a fast parton in an anisotropic quark-gluon plasma. For the sake of simplicity, a small ξ (anisotropic parameter) limit has been considered. When the velocity (v) of the jet is parallel to the anisotropy direction ($\langle n \rangle$) and remains below the phase velocity ($v(p)$), the wake in induced charge density shows a little oscillatory behavior in anisotropic quark-gluon plasma, contrary to the isotropic case. With the jet velocity greater than the phase velocity, the oscillatory behavior increases with ξ . Also for $v \gtrless v(p)$ one observes a clear modification of the conelike structure in the presence of anisotropy. For the parallel direction in the backward region, the depth of the wake potential decreases with the increase of ξ for $v \gtrless v(p)$, and the potential becomes modified Coulomb-like for higher values of ξ . In the forward region, the potential remains modified Coulomb-like with the change in magnitude for nonzero ξ , for both $v \gtrless v(p)$ and $v \gtrless v(p)$. In the perpendicular direction, the wake potential is symmetric in the forward and backward regions. With the increase of ξ , the depth of negative minimum is moving away from the origin irrespective of the jet velocity. On the other hand, when the jet velocity is perpendicular to the anisotropy direction, we find significant changes in the case of both wake charge density and potential in comparison to the isotropic case. For nonzero ξ , the oscillatory nature of the color charge wake is reduced at $v \gtrless v(p)$. Also the oscillatory behavior of the wake potential along the direction of motion of the parton is attenuated in the backward direction for anisotropic plasma at parton velocity $v \gtrless v(p)$. In the presence of anisotropy, for $v \gtrless v(p)$, the screening potential along the perpendicular direction of the parton is

transformed from the Lennard-Jones type to a modified Coulomb-like potential.

Mahatsab Mandal, Pradip Roy

3.2.2.2 Gluon dissociation of J/ψ in anisotropic quark-gluon plasma

We calculate the gluon dissociation cross section in an anisotropic quark gluon plasma expected to be formed in relativistic nucleus-nucleus collisions. It is shown that the thermally weighted cross section of gluon dissociation undergoes modification in anisotropic plasma, affecting the J/ψ survival probability. The dependence of the cross section on the direction of propagation of the charmonium with respect to the anisotropy axis is presented. Survival probability of J/ψ in two different space-time models of anisotropic quark gluon plasma (AQGP) has been calculated. It is shown that, depending upon the initial conditions [corresponding to Relativistic Heavy Ion Collider (RHIC) energies], the survival probability in AQGP differs from that in isotropic QGP both in the central as well as forward rapidity regions. For initial conditions relevant for Large Hadron Collider (LHC) energies, a marginal difference between the the two space-time models has been observed with given initial conditions.

Mahatsab Mandal, Pradip Roy

3.2.2.3 Next-to-leading order non-Fermi-liquid corrections to the neutrino emissivity and cooling of the neutron star

In this work we derive the expressions of the neutrino mean free path (MFP) and emissivity with non-Fermi-liquid corrections up to next-to-leading order (NLO) in degenerate quark matter. The calculation has been performed for both the absorption and the scattering processes. Subsequently the role of these NLO corrections on the cooling of the neutron star has been demonstrated. The cooling curve shows moderate enhancement compared to the leading order non-Fermi-liquid result. Although the overall correction to the MFP and emissivity are larger compared to the free Fermi gas, the cooling behavior is not altered significantly.

Souvik Priyam Adhya, Pradip K Roy, Abhee K Dutt-Mazumder

3.2.2.4 Effect of running coupling on photon emission from quark gluon plasma

We discuss the role of running coupling on the thermal photon yield from quark gluon plasma. It is shown that the photon production rate from the partonic phase is considerably enhanced when running coupling is considered with respect to a fixed value. However, we show by explicit evaluation that although this difference survives the space-time evolution the experimental data cannot distinguish between the two once the hard contribution, which is an essential component of the photon production mechanism, is added.

Mahatsab Mandal, Pradip Roy, Sukanya Mitra, Sourav Sarkar

3.2.2.5 Emergence of principal axis rotation in ^{110}Ag

The negative-parity yrast band of ^{110}Ag has been extended significantly and the lifetimes of the high spin levels of this band have been measured. The experimentally observed level scheme and measured electromagnetic transition rates have been compared with the theoretical predictions of a model with two quasiparticles coupled to a triaxially deformed core. This calculation successfully reproduces the energy spectra and electromagnetic transition rates beyond $I^\pi=12\hbar$. These observations indicate that the principal axis of rotation is responsible for the generation of high angular momentum states along the yrast cascade in ^{110}Ag . In all the other lighter isotopes, these states are generated through tilted axis rotation. Thus, ^{110}Ag is the first nucleus where the boundary between tilted and principal axis rotation could be established.

In the last two decades, a large number of bands arising from Tilted Axis Rotation (TAR) [1] and [2] have been identified [3], [4], [5], [6], [7], [8], [9], [10], [11], [12], [13] and [14] in the A~140, 110 and 80 regions of the periodic table. In this mode of excitation, the angular momenta of the valence nucleons are along the rotational axis (low ω orbitals) and the symmetry axis (high ω orbitals) only and the contribution of the rotational angular momentum is small (low to moderate deformation). In this situation, the total angular momentum becomes tilted with respect to the rotational axis. Thus, the π -rotational symmetry is broken and the signature is no longer a good quantum number. So, the staggering in the magnetic transition rates (B(M1))(B(M1)), observed in cases of Principal Axis Rotation (PAR), are absent in TAR. In this case, the B(M1)B(M1) transition rates show a decrease with increasing angular momentum.

Among the different mass regions, A~110A has a unique feature that the neutrons are in the low- ω shape driving orbitals while in all other mass regions the protons occupy these orbitals. Thus, it is possible to gradually increase the deformation in the A~110A region by increasing the number of neutrons in the low- ω orbitals of $-11/2$ parentage. This opens up the possibility to study the competition between PAR and TAR in the heavier isotopes of a nucleus of this mass region through the measurements of level lifetimes.

Santosh Roy, N Rather, Pradip Datta†, S Chattopadhyaya, S Pal... S Bhattacharya... A Goswami et al

3.2.3 Nuclear Physics

3.2.3.1 From a single encapsulated detector to the spectrometer for INTEGRAL satellite: predicting the peak-to-total ratio at high gamma-energies

In two recent papers (R. Kshetri, JINST 2012 7 P04008; *ibid.*, P07006), a probabilistic formalism was introduced to predict the response of encapsulated type composite germanium detectors like the SPI (spectrometer for INTEGRAL satellite). Predictions for the peak-to-total and peak-to-background ratios are given at 1.3 MeV for the addback mode of operation. The application of the formalism to clover germanium detector is discussed in two separate papers (R. Kshetri, JINST 2012 7 P07008; *ibid.*, P08015). Using the basic approach developed in those papers, for the first time we present a procedure for calculating the peak-to-total ratio of the cluster detector for gamma-energies up to 8MeV. Results are shown for both bare and suppressed detectors as well as for the single crystal and addback modes of operation. We have considered the experimental data of (i) peak-to-total ratio at 1.3MeV, and (ii) single detector efficiency and addback factor for other energies up to 8MeV. Using this data, an approximate method of calculating the peak-to-total ratio of other composite detectors, is shown. Experimental validation of our approach (for energies up to 8MeV) has been confirmed considering the data of the SPI spectrometer. We have discussed

about comparisons between various modes of operation and suppression cases. The present paper is the fifth in the series of papers on composite germanium detectors and for the first time discusses about the change in fold distribution and peak-to-total ratio for sophisticated detectors consisting of several modules of miniball, cluster and SPI detectors. Our work could provide a guidance in designing new composite detectors and in performing experimental studies with the existing detectors for high energy gamma-rays.

R Kshetri

3.2.3.2 Structure of the N=50 As, Ge, Ga nuclei

The level structures of the N = 50 As-83, Ge-82, and Ga-81 isotones have been investigated by means of multi-nucleon transfer reactions. A first experiment was performed with the CLARA PRISMA setup to identify these nuclei. A second experiment was carried out with the GASP array in order to deduce the gamma-ray coincidence information. The results obtained on the high-spin states of such nuclei are used to test the stability of the N = 50 shell closure in the region of Ni-78 (Z=28). The comparison of the experimental level schemes with the shell-model calculations yields an N=50 energy gap value of 4.7(3) MeV at Z=28. This value, in a good agreement with the prediction of the finite-range liquid-drop model as well as with the recent large-scale shell model calculations, does not support a weakening of the N=50 shell gap down to Z=28.

E Sahin, G de Angelis, G Duchene, UD Pramanik et al

3.2.3.3 Structure of C-16: Testing shell model and ab initio approaches

Excited states in C-16 were populated via the Be-9(N-17,C-16+gamma)X one-proton knockout reaction. The lifetime of the 2(1)(+) state in C-16 was measured using the recoil distance method. The extracted lifetime of $\tau(2(1)(+)) = 11.4(-0.9)(+0.8)(\text{stat}) \pm 0.7(\text{syst(B rho)})(-1.5)(+0.0)(\text{syst(feeding)})$ ps yields a deduced $B(E2; 2(1)(+) \rightarrow 0(1)(+)) = 4.21(-0.26)(+0.34)(\text{stat})(-0.24)(+0.28)(\text{syst(B rho)})(-0.00)(+0.64)(\text{syst(feeding)})$ e(2)fm(4) value in good agreement with a previous measurement. The one-proton knockout cross section is used to extract the proton amplitude of the C-16 2(1)(+) state, which confirms the neutron dominant character of this state. Gamma-ray branching ratios between the 2(2)(+) state and the 2(1)(+) and ground states were also determined. The results are compared with p-sd shell model and no-core shell model (with NN and NN + NNN) calculations. The inclusion of three-body forces are essential in order for the no-core shell model calculations to reproduce the experimental findings on the gamma-ray branching ratios.

M Petri, S Paschalis, RM Clark, UD Pramanik et al

3.2.3.4 A first principle approach for clover detector

A simple model based on probability flow arguments has been presented for understanding the clover germanium detector. Using basic concepts of absorption and scattering of gamma-rays, the operation of the clover detector has been described in terms of six probability amplitudes and a parameter. Instead of using an empirical method or simulation, this work presents the first attempt

to calculate the peak-to-total and peak-to-background ratios of the clover detector using experimental data of relative single crystal efficiency and addback factor as an input. A unique feature of our approach is that these ratios could be calculated for energies where their direct measurement is impossible due to absence of a radioactive source having single monoenergetic gamma-ray of that energy. Results for four gamma-ray energies ($E_{\text{gamma}} = 1.408, 3.907, 7.029$ and 10.430MeV) have been discussed. Agreement between experimental data and analysis results has been observed. The present approach could describe clover-type detectors as well. As an example, the nine element detector has been considered. We have demonstrated that our formalism can describe both finite and infinite interactions of gamma-rays with the clover crystals. The work presented in this paper follows similar philosophy as presented in a recent paper (R. Kshetri, 2012 JINST 7 P04008), which deals with modeling of encapsulated type composite detectors like miniball, cluster and SPI (Spectrometer for INTEGRAL satellite).

R Kshetri

3.2.3.5 Modeling of clover detector in addback mode

Based on absorption and scattering of gamma-rays, a formalism has been presented for modeling the clover germanium detector in addback mode and to predict its response for high energy gamma-rays. In the present formalism, the operation of a bare clover detector could be described in terms of three quantities only. Considering an additional parameter, the formalism could be extended for suppressed clover. Using experimental data on relative single crystal efficiency and addback factor as input, the peak-to-total ratio has been calculated for three energies ($E_{\text{gamma}} = 3.401, 5.324$ and 10.430MeV) where direct measurement of peak-to-total ratio is impossible due to absence of a radioactive source having single monoenergetic gamma-ray of that energy. The experimental validation and consistency of the formalism have been shown considering data for TIGRESS clover detector. In a recent work (R. Kshetri, JINST 2012 7 P04008), we showed that for a given gamma-ray energy, the formalism could be used to predict the peak-to-total ratio as a function of number of detector modules. In the present paper, we have shown that for a given composite detector (clover detector is considered here), the formalism could be used to predict the peak-to-total ratio as a function of gamma-ray energy.

R Kshetri

3.2.3.6 A first principle approach for encapsulated type composite detectors

A first principle approach is presented for modeling a composite detector consisting of several high-purity germanium detector modules. Without making assumptions, if we consider the full energy peak counts from single and multiple detector module interactions, and the decomposition of background counts to counts corresponding to the escaping gamma-rays and counts for gamma-rays which could be recovered in addback mode, it is observed that the addback mode of a composite detector could be described in terms of four probability amplitudes only. Expressions for peak-to-total and peak-to-background ratios are obtained. Considering details of the scattering and absorption processes in a composite detector, a formalism is introduced for understanding the probability amplitudes. Detailed investigation has been performed on the effect of shape and size of composite detectors on peak-to-total and peak-to-background ratios. In accordance with

isoperimetric inequality for hexagonal shapes, we have discussed about the optimal design of detector layout for extremely large values of detector modules. Using experimental data on relative single crystal efficiency, addback factor and peak-to-total ratio at 1332 keV for cluster detector, the peak-to-total and peak-to-background ratios have been calculated for several composite detectors.

R Kshetri

3.2.3.7 Onset of deformation at $N=112$ in Bi nuclei

The high spin states in Bi-195 were studied by gamma-ray spectroscopic method using the Ta-181(Ne-20, 6n) fusion-evaporation reaction at 130 MeV. The gamma gamma coincidence data were taken using an array of eight clover high-purity germanium detectors. The spin and parity assignments of the excited states were made from the measured directional correlation from oriented states ratios and integrated polarization asymmetry ratios. The results show, for the first time, the evidence of a rotational-like band based on a $13/2(+)$ bandhead in this nucleus, indicating the onset of deformation at the neutron number $N = 112$ for the bismuth isotopes. The results obtained were found to be consistent with the prediction of the total Routhian surface calculations using the Woods-Saxon potential. The same calculations also predicted a change in shape from oblate to triaxial in Bi-195 at high rotational frequency.

H Pai, G Mukherjee, R Raut, A Goswami, Sudeb Bhattacharya, S Ganguly, R Kshetri, MK Pradhan

3.2.3.8 Modeling an array of encapsulated germanium detectors

A probability model has been presented for understanding the operation of an array of encapsulated germanium detectors generally known as composite detector. The addback mode of operation of a composite detector has been described considering the absorption and scattering of gamma-rays. Considering up to triple detector hit events, we have obtained expressions for peak-to-total and peak-to-background ratios of the cluster detector, which consists of seven hexagonal closely packed encapsulated HPGe detectors. Results have been obtained for the miniball detectors comprising of three and four seven hexagonal closely packed encapsulated HPGe detectors. The formalism has been extended to the SPI spectrometer which is a telescope of the INTEGRAL satellite and consists of nineteen hexagonal closely packed encapsulated HPGe detectors. This spectrometer comprises of twelve detector modules surrounding the cluster detector. For comparison, we have considered a spectrometer comprising of nine detector modules surrounding the three detector configuration of miniball detector. In the present formalism, the operation of these sophisticated detectors could be described in terms of six probability amplitudes only. Using experimental data on relative efficiency and fold distribution of cluster detector as input, the fold distribution and the peak-to-total, peak-to-background ratios have been calculated for the SPI spectrometer and other composite detectors at 1332 keV. Remarkable agreement between experimental data and results from the present formalism has been observed for the SPI spectrometer.

R Kshetri

3.3 Developmental Work

3.3.0.9 Study on the Performance of a Single Thick GEM Detector using Ar /CH₄ (95:5)

The study on the performance of Thick Gas electron-multiplier (THGEM) has already been done for single-THGEM configuration with pre-mixed Ar/CO₂ (80:20) at atmospheric pressure using ⁵⁵Fe source. The installation of a gas-mixing system based on thermal Mass Flow Controller (MFC) has been done. This MFC has been added with the existing experimental set up of THGEM detector. It consists of four output channel flow divider and one N₂ channel with bubbler comparator. The calibration of channels for gas Ar, Ar/CO₂ (80:20) and Ar /CH₄ (95:5) has been done. The gas mixing utilizing MFC has been tested for the performance of THGEM gas detector with Ar/CH₄(95:5). The two main properties energy resolution and gain of indigenous single THGEM, fabricated in HFL, Hyderabad are presented. The results are given below.

Tinku Sinha

3.3.0.10 Upgrade of the CMS Hadron Calorimeter

The Large hadron Collider at CERN has been working successfully at CERN delivering high luminosity data for proton-proton collision to the CMS experiment. It proposes to increase the energy as well as luminosity for the runs beyond 2015. To meet this more hostile environment, the hadron calorimeter proposes to increase the number of readout channels by re-grouping the layers in a number of depth segments. It also proposes to measure the timing to a high degree of accuracy. These requirements demand an upgrade of the instrumentation electronics for the hadron calorimeter. The ongoing research has established the μ TCA as a potential candidate to replace the existing VME for the back-end electronics upgrade. For efficient and phased installation of the upgrade, it is particularly crucial that all requirements related to the HCAL and 1.6 Gbps data links operation are fully demonstrated by μ TCA. It is also equally important to operate the μ TCA electronics in parallel with the present electronics. This has been achieved by a collaboration of the University of Minnesota and Saha Institute of Nuclear Physics.

In the initial stage several mCTR2d (AMC) cards have been manufactured in Indian industry under the supervision of SINP CMS team and have been thoroughly tested at SINP before taking them to CERN and installed in a Vadatech μ TCA crate along with CMS-MCH (MicroTCA Carrier Hub) and commercial MCH module and optical splitters. This set up covered a HCAL slice ($\Delta\Phi=40^\circ$) in the negative hemisphere of Q4 covering $i\Phi$ 59-66.

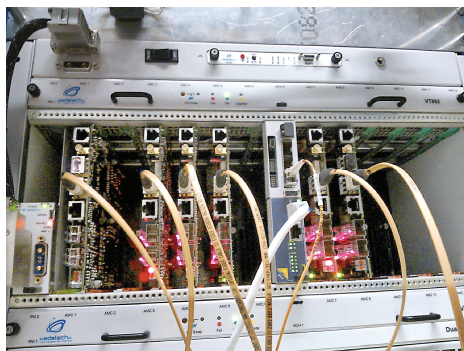


Fig 1: μ TCA (Vadatech) crate at the USC with 6 AMC cards and two MCH modules

During June 2012, the channel readouts of forward, barrel and endcap hadron calorimeter were monitored over (experimental set up shown in fig 1) a series of multiple long stable LHC fills. In order to keep the number of link-induced errors in the hadron calorimeter system at a level which does not affect overall CMS data quality, a bit error rate of 10^{15} will be required. Over stable long fills, the optically split signals from the detector are successfully received by a PPOD for all ribbons (fibers) in the tests and error rate is found to be zero integrated over few minutes. It establishes a good confidence of the performance of the receiver (PPOD) including its performance when used with the optical splitter. The signal from the forward hadron calorimeter is very narrow in time (confined within a time window of 25ns) as shown in figure 2. So looking at the fraction of samples after subtracting the pedestal ($ADC > 15$) for some channels of the forward hadron calorimeter one can see the bunch structure of the proton beams in the LHC. Also various channels are found to receive the different data occupancy as a function of their position from interaction point (IP). This has been an important benchmark for the new back-end electronics.

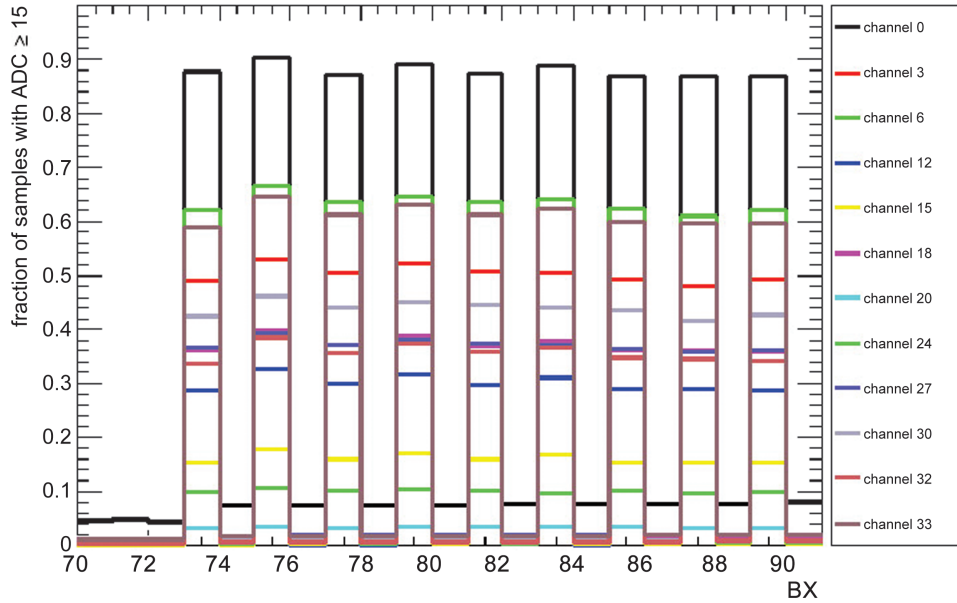


Fig 2: timing structure of the signal from the forward calorimeter

Preproduction of OHTR cards with final design has been carried out by Indian industry at Bangalore which successfully passed CMS preproduction review during June 2013. Necessary mechanical parts have been fabricated in the SINP workshop. Experimental facility to test such cards have been set up at SINP as well as in the factory by the supervision of SINP CMS team.

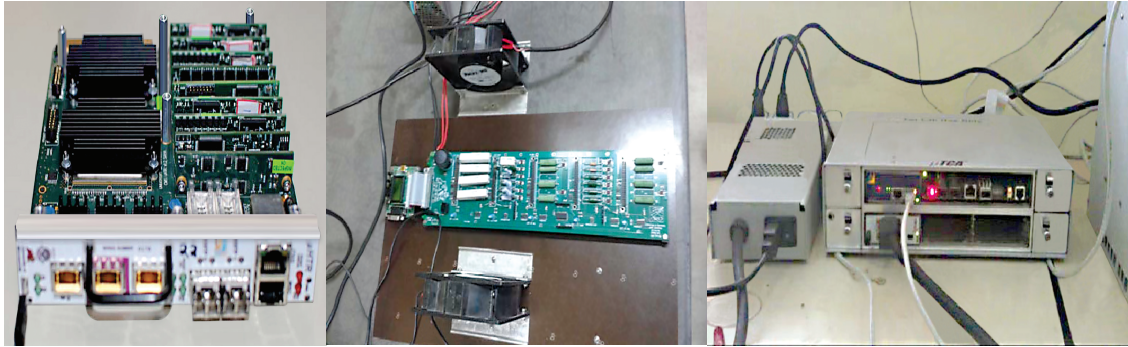


Fig 3: OHTR card (left) and the test set up at SINP (middle) and at the industry (right)

A OHTR card along-with the test setup is shown in Figure 3. We are committed to deliver 60 OHTR cards by February 2014 for forward hadron calorimeter which is a major responsibility. We are also working on prototyping of the readout cards for the barrel and endcap hadron calorimeters.

CMS Collaboration

3.3.0.11 Development of a Gas Scintillation Proportional Counter

A Gas Scintillation Proportional Counter is being developed for energy measurement of X rays. Measurement of low energy X rays are important in both astronomy and in nuclear fusion cross-section measurement. The detector is based on a gas medium (preferably Xenon) that produces VUV radiations due to interaction of the X-rays. We have fabricated the detector chamber that has a volume of approximately 1 litre and has several interfaces for vacuum, input radiation and the VUV photomultiplier. At present we are in the process of mounting the VUV photomultiplier that is a difficult and delicate process. The detector chamber has been already vacuum tested. A ^{55}Fe X ray source has been recently procured to test the detector and optimize the different



operating parameters such as operating voltage, gas pressure and the effective electric field.

Chinmay Basu

3.3.0.12 ISOLDE project No IS 544 Sept 12 at CERN

Aqueous sol-gel based ZnO nano-material offers important wide band gap semi conductor- structural characteristics. In order to know the nano structural evolution of the ZnO materials obtained through aqueous sol-gel route, the ZnO material obtained was irradiated with $^{111}\text{m Cd}$ atoms (beam current 150 pico amps , total dose : 3×10^{13} atoms at ISOLDE CERN), and annealed in stages to high temperature, up to 1000 C. The observed electronic and structural properties induced in the system due to this dopant, and evolution of ZnO nano material properties was surveyed through PAC technique. One such result is shown in figure 1

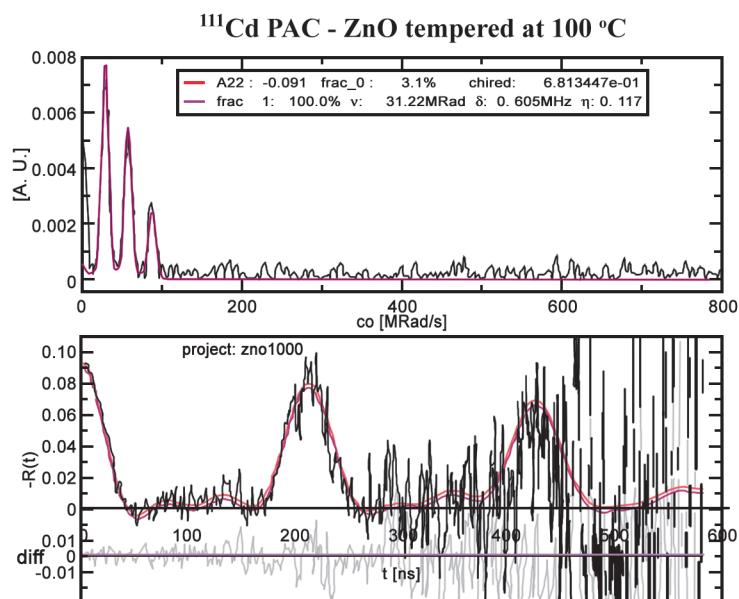


Figure Caption: ZnO nano crystalline material was doped with Cd111m in ISOLDE experiment and annealed at 1000C, measured in PAC . The experimental R(t) spectrum shows well defined hyperfine interaction and the Fourier transforms of the hyperfine parameters are also represented

Bichitra Nandi Ganguly

3.3.0.13 Use of LAMPS software for data acquisition of two-parameter Coincidence Doppler broadened spectra of positron annihilation gamma rays

LAMPS is the Linux version of Advanced Multi Parameter System software that has been in popular use in TIFR-BARC pelletron experiments for over a decade and is available for download at <http://www.tifr.res.in/pell/lamps.html>. It is a data acquisition and analysis package that supports VME, CAMAC-FERA and a number of CAMAC controllers and can also be used for offline data analysis. It runs under any recent version of Linux and is designed for large-scale experiments. For several years, we had used the earlier preliminary DOS version of the package for positron annihilation gamma ray experiments involving the acquisition of coincidence Doppler broadening spectroscopic (CDBS) data but the difficulties encountered by it could be overcome by the use of LAMPS. The CDBS experiments helps to shed light on the electron momentum distribution in samples and how positrons develop affinity to changes in it. After recording the annihilation gamma ray events E1 and E2 from two high sensitive high pure germanium detectors and noting their time correlations, a two-parameter spectrum is generated with E1 + E2 and E1 - E2 in the two coplanar axes and counts distributed accordingly. (See figure below). The projected one-dimensional spectrum parallel to the energy-difference axis within the energy-sum segment $(1022 - 2.4) \text{ keV} < (E1 + E2) < (1022 + 2.4) \text{ keV}$ of each sample is then divided by an area-normalized identical spectrum obtained for a pair of pure ($> 99.999\%$) single crystalline and defect-free reference samples. The quotient spectra so generated will indicate characteristic peaks at momentum values corresponding to the core electrons of the individual species of atoms involved in the constitution of the defect environment.

Figure : Typical coincidence Doppler broadened positron annihilation gamma ray spectrum

PMG Nambissan

3.4 Publications

3.4.1 Books/Monographs Publications & Edited Volumes

Bichitra Nandi Ganguly

Bichitra Nandi Ganguly and G Brauer (Eds), Near Surface Depth Profiling of Solids by Monoenergetic Positrons, (a special Series volume) Oct 2012, Trans Tech Publications, Switzerland

PMG Nambissan

Bulk structural changes in solids due to particle irradiation and their studies using positrons, Solid State Nuclear Track Detectors and Their Applications, Ed(s) NL Singh (Narosa, New Delhi pp 101)

Defect characterization in nanomaterials through positron annihilation spectroscopy, Nanotechnology: Synthesis and Characterization (Volume 2), Ed(s) Shishir Sinha, NK Navani and JN Govil (Studium Press LLC, Houston, USA, pp 455)

M Saha Sarkar

1. Study of neutron-rich nuclei near doubly magic ^{132}Sn , M Saha Sarkar, S Sarkar, Ed(s) N Mebarki, J Mimouni, N Belaloui, K Ait Moussa, AIP Conference Proceedings, 1444, (2012, pp 117)
2. Experimental study of upper sd shell nuclei and evolution of sd fp shell gap, M Saha Sarkar, Ed(s) N Mebarki, J Mimouni, N Belaloui, K Ait Moussa (Eds), AIP Conference Proceedings, 1444, (2012, pp190)
3. Characterisation of a Si-PIN diode detector and its usage in gamma spectroscopy, Abhijit Bisoi, A Nandi, M K Ray, NA Rather, S Ray, D Pramanik, M Saha Sarkar, Ed(s) PK Sarkar, Samita Basu, Maitreyee Nandy, Narosa, (2012, pp205)
4. Glimpses of new excitements in Nuclear Structure, Maitreyee Saha Sarkar, Physics Bulletin, Department of Physics, Aligarh Muslim University, Ed(s) Tauheed Ahmed, BP Singh, Abbas Ali, Shabbir Ahmed, Shahid Husain (Feb 2013, pp10)

3.4.2 Publications in Journals

ALICE Collaboration, Anisotropic flow of charged hadrons, pions and (anti-)protons measured at high transverse momentum in Pb-Pb collisions at $\sqrt{s_{NN}}=2.76$ TeV, Physics Letters **B719** (2013) 18

ALICE Collaboration, Charge separation relative to the reaction plane in Pb-Pb collisions at $\sqrt{s_{NN}}=2.76$ TeV, Physical Review Letters **110** (2013) Art No: 012301

ALICE Collaboration, D_s^+ meson production at central rapidity in proton-proton collisions at $\sqrt{s}=7$

TeV, Physics Letters **B718** (2012) 279

ALICE Collaboration, Inclusive J/ψ production in pp collisions at $\sqrt{S}=2.76$ TeV, Physics Letters **B718** (2012) 295

ALICE Collaboration (Debasish Das), Quarkonia production at forward rapidity in Pb plus Pb collisions at $\sqrt{S_{NN}}=2.76$ TeV with the ALICE detector, Pramana-Journal of Physics **79** (2012) 863

ALICE Collaboration, J/ψ production as a function of charged particle multiplicity in pp collisions at $\sqrt{S_{NN}}=7$ TeV, Physics Letters **B712** (2012) 165

ALICE Collaboration, J/ψ Suppression at Forward Rapidity in Pb-Pb Collisions at $\sqrt{S_{NN}}=2.76$ TeV, Physical Review Letters **109** (2012) Art No: 072301

ALICE Collaboration, $K_s^0 K_s^0$ correlations in pp collisions at $\sqrt{S}=7$ TeV from the LHC ALICE experiment, Physics Letters **B717** (2012) 151

ALICE Collaboration, Light vector meson production in pp collisions at $\sqrt{S}=7$ TeV ALICE Collaboration, Physics Letters **B710** (2012) 557

ALICE Collaboration, Long-range angular correlations on the near and away side in p-Pb collisions at $\sqrt{S_{NN}}=5.02$ TeV, Physics Letters **B719** (2013) 29

ALICE Collaboration, Measurement of electrons from semileptonic heavy-flavor hadron decays in pp collisions at $\sqrt{S}=7$ TeV, Physical Review **D86** (2012) Art No: 112007

ALICE Collaboration, Measurement of prompt J/ψ and beauty hadron production cross sections at mid-rapidity in pp collisions at $\sqrt{S}=7$ TeV, Journal of High Energy Physics, **Issue: 11**(2012) Art No: 065

ALICE Collaboration, Measurement of the Cross Section for Electromagnetic Dissociation with Neutron Emission in Pb-Pb Collisions at $\sqrt{S_{NN}}=2.76$ TeV, Physical Review Letters **109** (2012) Art No: 252302

ALICE Collaboration, Multi-strange baryon production in pp collisions at $\sqrt{S}=7$ TeV with ALICE, Physics Letters **B712** (2012) 309

ALICE Collaboration, Neutral pion and η meson production in proton-proton collisions at $\sqrt{S}=0.9$ TeV and $\sqrt{S}=7$ TeV, Physics Letters **B717** (2012) 162

ALICE Collaboration, Pion, Kaon, and Proton Production in Central Pb-Pb Collisions at $\sqrt{S_{NN}}=2.76$ TeV, Physical Review Letters **109** (2012) Art No: 252301

ALICE Collaboration, Production of $K^*(892)(0)$ and $\phi(1020)$ in pp collisions at $\sqrt{S_{NN}}=7$ TeV, European Physical Journal **C72** (2012) Art No: 2183

ALICE Collaboration, Production of Muons from Heavy Flavor Decays at Forward Rapidity in

pp and Pb-Pb Collisions at $\sqrt{s_{NN}}=2.76$ TeV, Physical Review Letters **109** (2012) Art No: 112301

ALICE Collaboration, Pseudorapidity Density of Charged Particles in p plus Pb Collisions at $\sqrt{s_{NN}}=5.02$ TeV, Physical Review Letters **110** (2013) Art No: 032301

ALICE Collaboration, Suppression of high transverse momentum D mesons in central Pb-Pb collisions at $\sqrt{s_{NN}}=2.76$ TeV, Journal of High Energy Physics, **Issue: 9** (2012) Art No: 112

ALICE Collaboration, Transverse Momentum Distribution and Nuclear Modification Factor of Charged Particles in p+Pb Collisions at $\sqrt{s_{NN}}=5.02$ TeV, Physical Review Letters **110** (2013) Art No: 082302

ALICE Collaboration, Transverse sphericity of primary charged particles in minimum bias proton-proton collisions at $\sqrt{s}=0.9, 2.76$ and 7 TeV, European Physical Journal **C72** (2012) Art No: 2124

ALICE Collaboration, Underlying Event measurements in pp collisions at $\sqrt{s}=0.9$ and 7 TeV with the ALICE experiment at the LHC, Journal of High Energy Physics, **Issue: 7** (2012) Art No: 116

Benedikt Rudek, Daniel Rolles, Sang-Kil Son Sankar De et al, Resonance-enhanced multiple ionization of krypton at an x-ray free-electron laser, Physical Review **A87** (2013) Art No: 023413

B Erk, D Rolles, L Foucar, S De et al, Ultrafast Charge Rearrangement and Nuclear Dynamics upon Inner-Shell Multiple Ionization of Small Polyatomic Molecules, Physical Review Letters **110** (2013) Art No:053003

Bichitra Nandi Ganguly, Positron Annihilation parameters in Connection to Surface Phenomenon of Liquids; Materials Science Forum **733** (2013) 121

Bichitra Nandi Ganguly, Positron annihilation spectroscopy: A prelude to modern aspects, Defect and diffusion Forum **331** (2012) 7

Chandi C Dey, Oxidation of Hafnium and Diffusion of Hafnium Atoms in Hexagonal Close-Packed Hafnium; Microscopic Investigations by Perturbed Angular Correlations, Zeitschrift Fur Naturforschung **A67** (2012) 633

CMS Collaboration, A search for a doubly-charged Higgs boson in pp collisions at $\sqrt{s}=7$ TeV, European Physical Journal **C72** (2012) Art No: 2189

CMS Collaboration, Azimuthal Anisotropy of Charged Particles at High Transverse Momenta in Pb-Pb Collisions at $\sqrt{s_{NN}}=2.76$ TeV, Physical Review Letters **109** (2012) Art No: 022301

CMS Collaboration, Centrality dependence of dihadron correlations and azimuthal anisotropy harmonics in PbPb collisions at $\sqrt{s_{NN}}=2.76$ TeV, European Physical Journal **C72** (2012) Art No: 2012

CMS Collaboration, Combined search for the quarks of a sequential fourth generation, Physical Review **D86** (2012) Art No: 112003

77. *CMS Collaboration*, Evidence for Associated Production of a Single Top Quark and W Boson in pp Collisions at $\sqrt{S}=7$ TeV, Physical Review Letters **110** (2013)

CMS Collaboration, Forward-backward asymmetry of Drell-Yan lepton pairs in pp collisions at $\sqrt{S}=7$ TeV, Physics Letters **B718** (2013) 752

CMS Collaboration, Inclusive and differential measurements of the $t\bar{t}$ over-bar charge asymmetry in proton-proton collisions $\sqrt{s}=7$ TeV, Physics Letters **B717** (2012) 129

CMS Collaboration, Inclusive b-jet production in pp collisions at $\sqrt{s}=7$ TeV, Journal of High Energy Physics, **Issue: 4** (2012) Art No: 084

CMS Collaboration, Jet momentum dependence of jet quenching in PbPb collisions at $\sqrt{s_{NN}}=2.76$ TeV, Physics Letters **B712** (2012) 176

CMS Collaboration, Limits on anomalous trilinear gauge couplings at the CMS with 7 TeV Large Hadron Collider data, Pramana-Journal of Physics **79** (2012) 899

CMS Collaboration, Measurement of isolated photon production in pp and PbPb collisions at $\sqrt{s_{NN}}=2.76$ TeV, Physics Letters **B710** (2012) 256

CMS Collaboration, Measurement of jet fragmentation into charged particles in pp and PbPb collisions at $\sqrt{s_{NN}}=2.76$ TeV, Journal of High Energy Physics, **Issue: 10** (2012) Art No: 087

CMS Collaboration, Measurement of the Azimuthal Anisotropy of Neutral Pions in Pb-Pb Collisions at $\sqrt{S_{NN}}=2.76$ TeV, Physical Review Letters **110** (2013) Art No: 042301

CMS Collaboration, Measurement of the cross section for production of b(b)over-barX decaying to muons in pp collisions at $\sqrt{s}=7$ TeV, Journal of High Energy Physics, **Issue: 6** (2012) Art No: 110

CMS Collaboration, Measurement of the cross-section of $Z \gamma$ and limits on ADD models at the CMS with 7 TeV Large Hadron Collider data, Pramana-Journal of Physics **79** (2012) 925

CMS Collaboration, Measurement of the Electron Charge Asymmetry in Inclusive W Production in pp Collisions at $\sqrt{s}=7$ TeV, Physical Review Letters **109** (2012) Art No: 111806

CMS Collaboration, Measurement of the elliptic anisotropy of charged particles produced in PbPb collisions at $\sqrt{s_{NN}}=2.76$ TeV, Physical Review **C87** (2013) Art No: 014902

CMS Collaboration, Measurement of the inclusive production cross sections for forward jets and for dijet events with one forward and one central jet in pp collisions at $\sqrt{s}=7$ TeV, Journal of High Energy Physics, **Issue: 6** (2012) Art No: 036

CMS Collaboration, Measurement of the Λ_b cross section and the Λ_b to Λ_b ratio with $J/\psi\Lambda$ decays in pp collisions at $\sqrt{s}=7$ TeV CMS Collaboration, Physics Letters **B714** (2012) 136

CMS Collaboration, Measurement of the mass difference between top and antitop quarks, Journal of High Energy Physics, **Issue: 6** (2012) Art No: 109

CMS Collaboration, Measurement of the Pseudorapidity and Centrality Dependence of the Transverse Energy Density in Pb-Pb Collisions at $\sqrt{s_N N}=2.76$ TeV, Physical Review Letters **109** (2012) Art No: 152303

CMS Collaboration, Measurement of the relative prompt production rate of χ_{c2} and χ_{c1} in pp collisions at $\sqrt{s}=7$ TeV, European Physical Journal **C72** (2012) Art No: 2251

CMS Collaboration, Measurement of the single-top-quark t-channel cross section in pp collisions at $\sqrt{s}=7$ TeV, Journal of High Energy Physics, **Issue: 12** (2012) Art No: 035

CMS Collaboration, Measurement of the $t\bar{t}$ over-bar production cross section in the dilepton channel in pp collisions at $\sqrt{s}=7$ TeV, Journal of High Energy Physics, **Issue: 11** (2012) Article Number: 067

CMS Collaboration, Measurement of the $t\bar{t}$ production cross section in pp collisions at $\sqrt{s}=7$ TeV in dilepton final states containing a tau, Physical Review **D85** (2012) Art No: 112007

CMS Collaboration, Measurement of the top-quark mass in $t\bar{t}$ events with dilepton final states in pp collisions at $\sqrt{s}=7$ TeV, European Physical Journal **C72** (2012) Art No: 2202

CMS Collaboration, Measurement of the top-quark mass in $t\bar{t}$ over-bar events with lepton plus jets final states in pp collisions at $\sqrt{s}=7$ TeV, Journal of High Energy Physics, **Issue: 12** (2012) Art No: 105

CMS Collaboration, Measurement of the underlying event activity in pp collisions at $\sqrt{s}=0.9$ and 7 TeV with the novel jet-area/median approach, Journal of High Energy Physics, **Issue: 8** (2012) Art No: 130

CMS Collaboration, Measurement of the underlying event in the Drell-Yan process in proton-proton collisions at $\sqrt{s}=7$ TeV, European Physical Journal **C72** (2012) Art No: 2080

CMS Collaboration, Measurement of the $\Upsilon(1S)$, $\Upsilon(2S)$, and $\Upsilon(3S)$ Polarizations in pp Collisions at $\sqrt{S}=7$ TeV, Physical Review Letters **110** (2013) Art No: 081802

CMS Collaboration, Measurement of the Z/γ^* plus b-jet cross section in pp collisions at $\sqrt{s}=7$ TeV, Journal of High Energy Physics, **Issue: 6** (2012) Art No: 126

CMS Collaboration, Measurement of the ZZ production cross section and search for anomalous couplings in $2l2l'$ final states in pp collisions at $\sqrt{s}=7$ TeV, Journal of High Energy Physics, **Issue: 1** (2013) Art No: 063

CMS Collaboration, Observation of a diffractive contribution to dijet production in proton-proton collisions at $\sqrt{s}=7$ TeV, Physical Review **D87** (2013) Art No: 012006

CMS Collaboration, Observation of a new boson at a mass of 125 GeV with the CMS experi-

ment at the LHC, Physics Letters **B716** (2012) 30

CMS Collaboration, Observation of a New Ξ_b Baryon, Physical Review Letters **108** (2012) Art No: 252002

CMS Collaboration, Observation of long-range, near-side angular correlations in pPb collisions at the LHC, Physics Letters **B718** (2013) 795

CMS Collaboration, Observation of Sequential upilon Suppression in PbPb Collisions, Physical Review Letters **109** (2012) Art No: 222301

CMS Collaboration, Observation of Z decays to four leptons with the CMS detector at the LHC, Journal of High Energy Physics, **Issue: 12** (2012) Art No: 034

CMS Collaboration, Performance of CMS muon reconstruction in pp collision events at $\sqrt{s}=7$ TeV, Journal of Instrumentation **7** (2012) Art No: P10002

CMS Collaboration, Ratios of dijet production cross sections as a function of the absolute difference in rapidity between jets in proton-proton collisions at $\sqrt{s}=7$ TeV, European Physical Journal **C72** (2012) Art No: 2216

CMS Collaboration, Search for a fermiophobic Higgs boson in pp collisions at $\sqrt{s}=7$ TeV, Journal of High Energy Physics, **Issue: 9** (2012) Art No: 111

CMS Collaboration, Search for a Higgs boson in the decay channel $H \rightarrow ZZ^{(*)} \rightarrow q(q)\overline{\text{bar}}l^{-}l^{+}$ in pp collisions at $\sqrt{s}=7$ TeV, Journal of High Energy Physics, **Issue: 4** (2012) Art No: 036

CMS Collaboration, Search for a light charged Higgs boson in top quark decays in pp collisions at $\sqrt{s}=7$ TeV, Journal of High Energy Physics, **Issue: 7** (2012) Art No: 143

CMS Collaboration, Search for a Light Pseudoscalar Higgs Boson in the Dimuon Decay Channel in pp Collisions at $\sqrt{s}=7$ TeV, Physical Review Letters **109** (2012) Art No: 121801

CMS Collaboration, Search for anomalous production of multilepton events in pp collisions at $\sqrt{s}=7$ TeV, Journal of High Energy Physics, **Issue: 6** (2012) Art No: 169

CMS Collaboration, Search for anomalous $t\bar{t}$ production in the highly-boosted all-hadronic final state, Journal of High Energy Physics **9** (2012) Art No: 029

CMS Collaboration, Search for a W' or Techni-rho Decaying into WZ in pp Collisions at $\sqrt{s}=7$ TeV, Physical Review Letters **109** (2012) Art No: 141801

CMS Collaboration, Search for $B - S^0 \rightarrow \mu^+\mu^-$ and $B^0 \rightarrow \mu^+\mu^-$ decays, Journal of High Energy Physics, **Issue: 4** (2012) Art No: 033

CMS Collaboration, Search for charge-asymmetric production of W' bosons in $t\bar{t} + \text{jet}$ events from pp collisions at $\sqrt{s}=7$ TeV, Physics Letters **B717** (2012) 351

CMS Collaboration, Search for contact interactions in $\mu^+\mu^-$ events in pp collisions at $\sqrt{s}=7$ TeV, Physical Review **D 87** (2013) Art No: 032001

CMS Collaboration, Search for dark matter and large extra dimensions in monojet events in pp collisions at $\sqrt{s}=7$ TeV, Journal of High Energy Physics, **Issue: 9**(2012) Art No: 094

CMS Collaboration, Search for Dark Matter and Large Extra Dimensions in pp Collisions Yielding a Photon and Missing Transverse Energy, Physical Review Letters **108** (2012) Art No: 261803

CMS Collaboration, Search for electroweak production of charginos and neutralinos using leptonic final states in pp collisions at $\sqrt{s}=7$ TeV, Journal of High Energy Physics, **Issue: 11** (2012) Art No: 147

CMS Collaboration, Search for excited leptons in pp collisions at $\sqrt{s}=7$ TeV, Pramana-Journal of Physics **79** (2012) 929

CMS Collaboration, Search for exclusive or semi-exclusive $\gamma\gamma$ production and observation of exclusive and semi-exclusive e^+e^- production in pp collisions at $\sqrt{s}=7$ TeV, Journal of High Energy Physics, **Issue: 11** (2012) Art No: 080

CMS Collaboration, Search for heavy bottom-like quarks in 4.9 fb^{-1} of pp collisions at $\sqrt{s}=7$ TeV, Journal of High Energy Physics, **Issue: 5** (2012) Art No: 123

CMS Collaboration, Search for heavy lepton partners of neutrinos in proton-proton collisions in the context of the type III seesaw mechanism, Physics Letters **B718** (2012) 348

CMS Collaboration, Search for heavy long-lived charged particles in pp collisions at $\sqrt{s}=7$ TeV, Physics Letters **B713** (2012) 408

CMS Collaboration, Search for heavy Majorana neutrinos in $\mu^\pm\mu^\pm + \text{jets}$ and $e^\pm e^\pm + \text{jets}$ events in pp collisions at $\sqrt{s}=7$ TeV, Physics Letters **B717** (2012) 109

CMS Collaboration, Search for Heavy Neutrinos and W-R Bosons with Right-Handed Couplings in a Left-Right Symmetric Model in pp Collisions at $\sqrt{S}=7$ TeV, Physical Review Letters **109** (2012) Art No: 261802

CMS Collaboration, Search for heavy quarks decaying into a top quark and a W or Z boson using lepton plus jets events in pp collisions at $\sqrt{s}=7$ TeV, Journal of High Energy Physics, **Issue no: 1** (2013) Art No: 154

CMS Collaboration, Search for heavy, top-like quark pair production in the dilepton final state in pp collisions at $\sqrt{s}=7$ TeV, Physics Letters **B716** (2012) 103

CMS Collaboration, Search for high-mass resonances decaying into tau-lepton pairs in pp collisions at $\sqrt{s}=7$ TeV, Physics Letters **B716** (2012) 82

CMS Collaboration, Search for large extra dimensions in dimuon and dielectron events in pp collisions

sions at $\sqrt{s}=7$ TeV, Physics Letters **B711** (2012) 15

CMS Collaboration, Search for leptonic decays of W^\pm bosons in pp collisions at $\sqrt{s}=7$ TeV, Journal of High Energy Physics, **Issue: 8** (2012)

CMS Collaboration, Search for microscopic black holes in pp collisions at $\sqrt{s}=7$ TeV, Journal of High Energy Physics, **Issue: 4** (2012) Art No: 061

CMS Collaboration, Search for narrow resonances and quantum black holes in inclusive and b-tagged dijet mass spectra from pp collisions at $\sqrt{s}=7$ TeV, Journal of High Energy Physics, **Issue: 1** (2013) Art No: 013

CMS Collaboration, Search for narrow resonances in dilepton mass spectra in pp collisions at $\sqrt{s}=7$ TeV CMS Collaboration, Physics Letters **B714** (2012) 158

CMS Collaboration, Search for neutral Higgs bosons decaying to tau pairs in pp collisions at $\sqrt{s}=7$ TeV, Physics Letters **B713** (2012) 68

CMS Collaboration, Search for new physics in events with opposite-sign leptons, jets, and missing transverse energy in pp collisions at $\sqrt{s}=7$ TeV, Physics Letters **B718** (2013) 815

CMS Collaboration, Search for new physics in events with same-sign dileptons and b-tagged jets in pp collisions at $\sqrt{s}=7$ TeV, Journal of High Energy Physics, **Issue: 8** (2012) Art No: 110

CMS Collaboration, Search for New Physics in the Multijet and Missing Transverse Momentum Final State in Proton-Proton Collisions at $\sqrt{s}=7$ TeV, Physical Review Letters **109** (2012) Art No: 171803

CMS Collaboration, Search for new physics with long-lived particles decaying to photons and missing energy in pp collisions at $\sqrt{s}=7$ TeV, Journal of High Energy Physics, **Issue: 11** (2012) Art No: 172

CMS Collaboration, Search for New Physics with Same-Sign Isolated Dilepton Events with Jets and Missing Transverse Energy, Physical Review Letters **109** (2012) Art No: 071803

CMS Collaboration, Search for pair produced fourth-generation up-type quarks in pp collisions at $\sqrt{s}=7$ TeV with a lepton in the final state, Physics Letters **B718** (2012) 307

CMS Collaboration, Search for pair production of first- and second-generation scalar leptoquarks in pp collisions at $\sqrt{s}=7$ TeV, Physical Review **D86** (2012) Art No: 052013

CMS Collaboration, Search for Pair Production of Third-Generation Leptoquarks and Top Squarks in pp Collisions at $\sqrt{s}=7$ TeV, Physical Review Letters **110** (2013) Art No: 081801

CMS Collaboration, Search for physics beyond the standard model in events with a Z boson, jets, and missing transverse energy in pp collisions at $\sqrt{s}=7$ TeV, Physics Letters **B716** (2012) 260

CMS Collaboration, Search for quark compositeness in dijet angular distributions from pp colli-

sions at $\sqrt{s}=7$ TeV, Journal of High Energy Physics, **Issue: 5** (2012) Art No: 055

CMS Collaboration, Search for resonant $t\bar{t}$ over-bar production in lepton plus jets events in pp collisions at $\sqrt{s}=7$ TeV, Journal of High Energy Physics, **Issue: 12** (2012) Art No: 015

CMS Collaboration, Search for stopped long-lived particles produced in pp collisions at $\sqrt{s}=7$ TeV, Journal of High Energy Physics, **Issue: 8** (2012) Art No: 026

CMS Collaboration, Search for supersymmetry in events with b-quark jets and missing transverse energy in pp collisions at 7 TeV, Physical Review **D86** (2012) Art No: 072010

CMS Collaboration, Search for supersymmetry in events with photons and low missing transverse energy in pp collisions at $\sqrt{S}=7$ TeV, Physics Letters **B719** (2013) 42

CMS Collaboration, Search for supersymmetry in final states with a single lepton, b-quark jets, and missing transverse energy in proton-proton collisions at $\sqrt{S}=7$ TeV, Physical Review **D87**(2013) Art No: 052006

CMS Collaboration, Search for supersymmetry in final states with missing transverse energy and 0, 1, 2, or ≥ 3 b-quark jets in 7 TeV pp collisions using the variable α_T , Journal of High Energy Physics, **Issue no:1** (2013) Art No: 077

CMS Collaboration, Search for supersymmetry in hadronic final states using M-T2 in pp collisions at $\sqrt{s}=7$ TeV, Journal of High Energy Physics, **Issue: 10** (2012) Art No: 018

CMS Collaboration, Search for the standard model Higgs boson decaying into two photons in pp collisions at $\sqrt{s}=7$ TeV, Physics Letters **B710** (2012) 403

CMS Collaboration, Search for the standard model Higgs boson decaying to bottom quarks in pp collisions at $\sqrt{s}=7$ TeV, Physics Letters **B710** (2012) 284

CMS Collaboration, Search for the standard model Higgs boson produced in association with W and Z bosons in pp collisions at $\sqrt{s}=7$ TeV, Journal of High Energy Physics, **Issue: 11** Article Number: 088

CMS Collaboration, Search for third-generation leptoquarks and scalar bottom quarks in pp collisions at $\sqrt{s}=7$ TeV, Journal of High Energy Physics, **Issue: 12** (2012) Art No: 055

CMS Collaboration, Search for three-jet resonances in pp collisions at $\sqrt{S}=7$ TeV, Physics Letters **B718** (2012) 329

CMS Collaboration, Shape, transverse size, and charged-hadron multiplicity of jets in pp collisions at $\sqrt{s}=7$ TeV, Journal of High Energy Physics, **Issue: 6** (2012) Art No: 160

CMS Collaboration, Studies of jet quenching using isolated-photon plus jet correlations in PbPb and pp collisions at $\sqrt{s_{NN}}=2.76$ TeV, Physics Letters **B718** (2013) 773

CMS Collaboration, Study of the Dijet Mass Spectrum in $pp \rightarrow W + \text{jets}$ Events at $\sqrt{S}=7$ TeV,

Physical Review Letters **109** (2012) Art No: 251801

CMS Collaboration, Study of the inclusive production of charged pions, kaons, and protons in pp collisions at $\sqrt{s}=0.9, 2.76$, and 7 TeV, European Physical Journal **C72** (2012) Art No: 2164

CMS Collaboration, Study of the Mass and Spin-Parity of the Higgs Boson Candidate via Its Decays to Z Boson Pairs, Physical Review Letters **110** (2013) Art No: 081803

CMS Collaboration, Study of W boson production in PbPb and pp collisions at $\sqrt{s_{NN}}=2.76$ TeV, Physics Letters **B715** (2012) 66

CMS Collaboration, Suppression of non-prompt J/ψ , prompt J/ψ , and $\Upsilon(1S)$ in PbPb collisions at $\sqrt{s_{NN}}=2.76$ TeV, Journal of High Energy Physics, **Issue: 5** (2012) Art No: 063

CMS Collaboration, Tau reconstruction and identification algorithm, Pramana-Journal of Physics **79** (2012)1235

CMS HCAL Collaboration, Tests of CMS hadron forward calorimeter upgrade readout box prototype, Journal of Instrumentation **7** (2012) Art No: P10015

E De Filippo, A Pagano, P Russotto, MB Chatterjee et al, Correlations between emission timescale of fragments and isospin dynamics in Sn-124+Ni-64 and Sn-112+Ni-58 reactions at 35A MeV, Physical Review **C86** (2012) Art No: 014610

E Sahin, G de Angelis, G DucheneU Datta Pramanik et al, Structure of the N=50 As, Ge, Ga nuclei, Nuclear Physics **A893**(2012) 1

G Cardella†, G Giuliani†, I Lombardo† MB Chatterjee, et al, Effects of neutron richness on the behavior of nuclear systems at intermediate energies, Physical Review **C85** (2012) Art No: 064609

H Pai, G Mukherjee, R Raut, A Goswami Sudeb Bhattacharya, S Ganguly, R Kshetri, MK Pradhan, Onset of deformation at N=112 in Bi nuclei, Physical Review **C85** (2012) Art No: 064317

HS Hans, Gulzar Singh, A Kumar, Sudip Ghosh, Theoretical interpretation of the systematics of effective single-particle level densities from (n, p) reactions at 14.8 MeV energy, Physical Review **C85** (2012) Art No:054614

I Lombardo, L Acosta, C Agodi, MB Chatterjee et al, The N/Z key role on the dynamics of medium mass nuclear systems near fragmentation threshold, Physica Scripta **T150** (2012) Art No:014023

Keka Chakraborty, Abhijit Bisoi, Bichitra Nandi Ganguly et al, Structural Transition in Rare Earth Doped Zirconium Oxide: A positron annihilation Study, Material Research Bulletin **47** (2012) 360

Keka Chakraborty, Abhijit Bisoi, Bichitra Nandi Ganguly et al, Structural transition in rare earth doped zirconium oxide: A positron annihilation study, Materials Research Bulletin **47** (2012) 3660

KK Meghna†, A Banerjee†, S Biswas†, S Bhattacharya, S Bose, C Marick, S Saha et al, Measurement of electrical properties of electrode materials for the bakelite Resistive Plate Chambers,

Journal of Instrumentation **7**(2012) Art No: P10003

Mahatsab Mandal, Pradip Roy, Gluon dissociation of J/ψ in anisotropic quark-gluon plasma, Physical Review **C86** (2012) Art No: 024915

Mahatsab Mandal, Pradip Roy, Sukanya Mitra, et al, Effect of running coupling on photon emission from quark gluon plasma, Physical Review **C85** (2012) Art No: 067901

Mahatsab Mandal, Pradip Roy, Wake in anisotropic quark-gluon plasma, Physical Review **D86** (2012) Art No: 114002

M Petri, S Paschalis, RM Clark, U Datta Pramanik et al, Structure of C-16: Testing shell model and ab initio approaches, Physical Review **C86** (2012) Art No: 044329

P Bhattacharya, S Mukhopadhyay, N Majumdar et al, A comparative numerical study on GEM, MHSP and MSGC, Journal of Instrumentation **7** (2012) Art No:P09007

Purnima Singh, Somnath Nag, K Selvakumar, Abhijit Bisoi, A Goswami, S Bhattacharya, et al, High-spin spectroscopy of I-122, Physical Review **C85** (2012) Art No:054311

R Kshetri, A first principle approach for clover detector, Journal of Instrumentation **7** (2012) Art No: P08015

R Kshetri, A first principle approach for encapsulated type composite detectors, Journal of Instrumentation **7** (2012) Art No: P07006

R Kshetri, From a single encapsulated detector to the spectrometer for INTEGRAL satellite: predicting the peak-to-total ratio at high gamma-energies, Journal of Instrumentation **7** (2012) Art No: P12007

R Kshetri, Modeling an array of encapsulated germanium detectors, Journal of Instrumentation **7** (2012) Art No:P04008

R Kshetri, Modeling of clover detector in addback mode, Journal of Instrumentation **7** (2012) Art No: P07008

Santosh Roy, N Rather, Pradip Datta et al, Emergence of principal axis rotation in ^{110}Ag , Physics Letters **B710** (2012) 587

S Muralithar, G Rodrigues, RP Singh et al, Nuclear structure of Ra-216 at high spin, Pramana-Journal of Physics **79**(2012) 403

Souvik Priyam Adhya, Pradip K Roy, Abhee K Dutt-Mazumder, Next-to-leading order non-Fermi-liquid corrections to the neutrino emissivity and cooling of the neutron star, Physical Review **D86** (2012) Art No: 034012

Sreetama Dutta, Bichitra Nandi Ganguly, Characterization of ZnO nano particles grown in presence of Folic Acid Template, J Nanobiotechnology **10** (2012)10

Sreetama Dutta, Bichitra N Ganguly, Characterization of ZnO nanoparticles grown in presence of Folic acid template, *Journal of Nanobiotechnology* **10** (2012) Art No: 29

S Saha, R Palit, J Sethi, A Goswami S Saha et al, Experimental investigation of shell-model excitations of Zr-89 up to high spin, *Physical Review* **C86** (2012) Art No: 034315

3.5 Seminars/Lectures given in Conference/Symposium/Schools

Debasish Das

1. Quarkonia production at forward rapidities with the ALICE Experiment, DAE Symposium on Nuclear Physics, New Delhi, Dec 3-7, 2012

Sankar De

1. Following wave packet dynamics in diatomic molecules with few-cycle infrared laser pulses One-day seminar on Laser and its Applications, Department of Instrumentation Science, Jadavpur University, Feb 6, 2013
2. Signature of vibrational flopping in dissociative acetylene - Joint Symposium on Collisions of Highly-Charged Ions with Molecules and Related Topics, Tokyo Metropolitan College of Industrial Technology, Shinagawa, Tokyo, Japan, Oct 18, 2012
3. Ion-induced Molecular Fragmentation Engineering and Applied Science Colloquium, Sophia University, Chiyoda, Tokyo, Japan, Oct 16, 2012

Bichitra Nandi Ganguly

Positron annihilation study of ZnO nano-particles grown under folic acid template, 16th International Conference on Positron Annihilation, University of Bristol, Aug 19-24, 2012 (Sreetama Dutta, Bichitra Nandi Ganguly)

M Saha Sarkar

1. Pairing and shell evolution in neutron rich nuclei, 5th International Conference on Fission and Properties of Neutron-Rich Nuclei, Sanibel Island, Florida, USA, Nov 4-10, 2012
2. Shell structure and evolution of collectivity in nuclei above the ^{132}Sn core, NUSTAR WEEK 2012 meeting at the Variable Energy Cyclotron Centre (VECC), Kolkata, INDIA, Oct 8-12, 2012
3. Study of neutron - rich nuclei near doubly magic ^{132}Sn and its implication in other neutron rich domains, Physics Department, Argonne National Laboratory, Argonne, USA, Oct 28-31, 2012
4. Understanding Nuclei in the upper sd shell, John D Fox Superconducting Accelerator Laboratory, Physics Department, The Florida State University, Tallahassee, Florida, USA, Oct 30-Nov 4, 2012
5. Study of neutron - rich nuclei near doubly magic ^{132}Sn and its implication in other neutron rich domains, Department of Physics and Astronomy, University of Tennessee, Knoxville, TN, USA, Nov 12-14, 2012
6. Seminar on Pairing and shell evolution in neutron rich nuclei, Department of Physics and Astronomy at Rutgers, The State University of New Jersey, Nov 14-16, 2012
7. Studies in Nuclear Astrophysics: experimental and theoretical efforts, DAE-BRNS theme meet-

ing on the physics aspects of accelerator radiation protection, BARC, Mumbai, Feb 20-22, 2013

Sunanda Banerjee

Geant4 and CMS Simulation Software, XX DAE-BRNS High Energy Physics Symposium, Visva-Bharati, Santiniketan

Satyaki Bhattacharyya

Statistical Issues in High Energy Physics, XX DAE-BRNS High Energy Physics Symposium, Visva-Bharati, Santiniketan

Kalyanmoy Chatterjee

Associated Higgs production with W boson in pp collision of CMS where $W \rightarrow e\nu$ and $H \rightarrow \tau^+\tau^-$ at XX DAE-BRNS High Energy Physics Symposium, Visva-Bharati, Santiniketan

Bhawna Gomer

Search for Dark Matter and Large Extra Dimensions in pp Collisions yielding a photon and missing transverse energy, XXII Physics in Collision 2012, Strbske Pleso, Slovakia, 2012

Search for Dark Matter and ADD gravitons in the gamma+MET final state, CMS Exotica Workshop in Rome, 2012

Searches for Dark Matter in pp collisions yielding a photon and missing transverse energy, XX DAE-BRNS High Energy Physics Symposium, Visva-Bharati, Santiniketan

Sandhya Jain

CMS results on Dark Matter physics, the International Workshop on the Interconnection between Particle Physics and Cosmology, 05-09 Nov 2012, KIAS, Seoul, Korea

Anomalous APD signals in CMS Electromagnetic Calorimeter, XX DAE-BRNS High Energy Physics Symposium, Visva-Bharati, Santiniketan

Shilpi Jain

Search for excited leptons, CMS Exotica Workshop in Rome, Nov 2012

Search for excited leptons in pp collisions at $\sqrt{s} = 7$ TeV, XX DAE-BRNS High Energy Physics Symposium, Visva-Bharati, Santiniketan

Raman Khurana

Search for Higgs Boson in CMS in the Decay Channel $H \rightarrow ZZ \rightarrow 4\ell$ or 4τ , XX DAE-BRNS High Energy Physics Symposium, Visva-Bharati, Santiniketan

Atanu Modak

Performance of CMS Track Trigger for Phase-II Upgrade, XX DAE-BRNS High Energy Physics Symposium, Visva-Bharati, Santiniketan

Swagata Mukherjee

Inclusion of Outer Hadron Calorimeter Information in Particle Flow Reconstruction Method of CMS, XX DAE-BRNS High Energy Physics Symposium, Visva-Bharati, Santiniketan

Debarati Roy

Status of BackEnd Electronics for CMS Hadron Calorimeter Upgrade in the Large Hadron Collider, XX DAE-BRNS High Energy Physics Symposium, Visva-Bharati, Santiniketan

Chinmay Basu

1. University of Calcutta on Breakup induced alpha transfer process, National Conference on Nuclear Dynamics and Nuclear Astrophysics, Feb 5-6, 2013
2. Title of the TALK?, International Conference on Nuclear Structure and Dynamics 2012, Opatija, Croatia, July 9-13, 2012

PMG Nambissan

1. Nano sulfide and oxide semiconductors as promising materials for studies by positron annihilation, 16th International Conference on Positron Annihilation (ICPA - 16), University of Bristol, Bristol, United Kingdom, Aug 19-24, 2012
2. Positron annihilation as an erudite member in the family of spectroscopies, Three Day Workshop on Spectroscopy and Microscopy, Mahatma Gandhi University, Kottayam, Kerala, Sept 10-12, 2012
3. Nanosciences and promises, SN Bose Lecture Series, The Zamorin Guruvayurappan College, Kozhikode, Kerala, Jan 05, 2013
4. Structural defects investigation in nanocrystalline semiconductors, National Conference on Nanoscience & Nanotechnology (ALIGARH NANO III), Department of Applied Physics, Aligarh Muslim University, Aligarh, Mar 16 17, 2013

3.6 Teaching elsewhere

Bichitra Nandi Ganguly

Course of 10 lectures taught: Positronium Chemistry M Sc IVth Sem, Nuclear and Analytical Special Paper, University of Bardwan

Chinmay Basu

25 Lectures (2 hrs per lecture) on Nuclear Reactions, M.Sc (Physics) special paper, Jan-Mar 2013, Department of Physics, Rajabazar Science College, University of Calcutta

Chapter 4

Plasma Physics

4.1 Summary of Research Activities of Divisions

4.1.1 Plasma Physics

Theoretical studies of electromagnetic wave propagation in magnetized plasma has been actively considered in this period. Our focus has been the study of relativistically strong plasma waves with extremely strong electric field generation and the associated wave breaking phenomenon in magnetized plasmas. By using Lagrangian co-ordinates, we have presented an exact non-stationary solution in parametric form of a fully nonlinear time dependent problem. It is demonstrated that bursts in the electron density appear in a finite time as a result of relativistic mass variation of electrons, indicating phase mixing / breaking of relativistic upper hybrid modes. In comparison with relativistic plasma waves, basic differences in the phase mixing / breaking process are pointed out regarding the issue of particle acceleration, plasma heating etc.

Investigations on shear flow driven instabilities, coupled acoustic and shear modes are being carried out in strongly coupled dusty plasmas to understand the effects of viscoelastic and non-Newtonian properties.

Kinetic models to understand plasma equilibria are more fundamental since they contain information on particle distribution functions. Studies of Vlasov equilibria associated with current sheets as well as potential structures in quantum plasmas have been studied.

In the experimental front, in our existing device MaPLE (Magnetized Plasma Linear Experimental)

we have studied in detail the selective excitation of low frequency drift mode. Existence of parallel flow of electrons causes the drift modes to have strong growth rate over a band of frequencies. However, the frequency selection for excitation is done in the experiment by driving a strong modulation of electron density with a frequency that is resonant in this region. Parallel velocity component of the excited $m = 2$ mode couples nonlinearly with the externally created density fluctuation to produce a parallel current fluctuation with twice the frequency. This selectively drives a second

drift mode resonant in a nearby location. In this experiment the $m = 4$ drift mode is stable and hence not excited. Interestingly, this mode starts appearing as the modulation parameters cross a threshold value to drive parametric mode-mode coupling in the plasma. The excited mode satisfies the frequency and wave number matching conditions. A parametric mode-mode coupling of drift waves was reported before where the pump drift mode excites two lower frequency modes which are normally stable. In contrast, we demonstrate that the pump drift wave can parametrically excite the higher frequency drift mode with a substantial growth rate of the lower frequency mode.

The Double Layer Experiment device has been constructed to study formation of double layers in a plasma created by an inductive RF discharge and allowed to expand along a diverging magnetic field.

Measurement of the axial profile of plasma potential shows that a DL is spontaneously formed near the throat of the expansion chamber. A 2-D mapping of the plasma potential has been done showing that the contours form a convex structure with a strong crowding at the corner point.

This indicates therefore a very strong electric field almost perpendicular to the local magnetic field. The contours exhibit secondary lobes with maxima on both sides of the axis. Field aligned electric fields have been observed along the most divergent magnetic field line. An accelerated ion beam has been detected in the downstream region, confirming the presence of the double layer.

Efforts are being made to maintain the high vacuum and clean conditions of the tokamak vessel. Existing diagnostics are being improved to carry out runaway related transport characteristics. SINP tokamak can be operated at very low q_a (edge safety factor) values. In this regime, turbulence level goes up significantly. Our current interest is to explore these fluctuations using nonlinear time series analysis. The tokamak facility is also being used for carrying out projects by students from various institutions.

Several types of nonlinear dynamic experiments like homoclinic bifurcations, intermittent chaos, parametric effects of external forcing on the dynamics of oscillations etc have been carried out in the glow discharge plasma set up.

4.2 Research Activities

4.2.1 Plasma Physics

4.2.1.1 Drift wave in pair-ion plasma

The conditions for the existence of low-frequency electrostatic drift wave in pair-ion plasma are discussed. It is shown that the temperature and/or mass difference of both species could produce drift wave in a pair-ion plasma. The results are discussed in the context of the fullerene pair-ion plasma experiment.

Samiran Ghosh, Nikhil Chakrabarti, Manoranjan Khan, MR Gupta

4.2.1.2 Electron acoustic shock waves in a collisional plasma

A nonlinear analysis for the finite amplitude electron acoustic wave (EAW) is considered in a collisional plasma. The fluid model is used to describe the two-temperature electron species in a fixed ion background. In general, in electron-ion plasma, the presence of wave nonlinearity, dispersion, and dissipation (arising from fluid viscosity) give rise to the Korteweg-de Vries Burgers (KdVB) equation which exhibits shock wave. In this work, it is shown that the dissipation due to the collision between electron and ion in the presence of collective phenomena (plasma current) can also introduce an anomalous dissipation that causes the Burgers term and thus leads to the generation of electron acoustic shock wave. Both analytical and numerical analysis show the formation of transient shock wave. Relevance of the results are discussed in the context of space plasma.

Manjitha Dutta, Samiran Ghosh, Nikhil Chakrabarti

4.2.1.3 A two-fluid model of the bifurcated current sheet

Recent satellite observations show that current sheets in the space plasma environment are often characterized by bifurcated structures. The majority of the available models of the bifurcated current sheet in the literature are based upon equilibrium Vlasov-Maxwell kinetic theory. While in principle, kinetic models are more fundamental, investigations based on fluid theory can sometimes be advantageous. For instance, because of its inherent simplicity, fluid models of the current sheet can be used in the detailed nonlocal or global analysis of fluid stability. The present paper puts forth a two-fluid model of the bifurcated current sheet on the basis of the pseudo-potential method. According to the present model, double peaked current sheet is characterized by a transverse non-uniform flow and a profile of plasma density that has a plateau in the region between the current peaks. Further, the plasma pressure tensor associated with such a bifurcated current sheet is shown to be anisotropic and non-gyrotropic. Citation: Janaki, M. S., B. Dasgupta, and P. H. Yoon (2012), A two-fluid model of the bifurcated current sheet, *J. Geophys. Res.*, 117, A12201

MS Janaki, Brahmananda Dasgupta, Peter H Yoon

4.2.1.4 Density distribution for an inhomogeneous finite gravitational system

An attempt is made to develop an equilibrium kinetic equation for a weakly non ideal inhomogeneous gravitational system utilizing the Bogoliubov-Born-Green-Kirkwood-Yvon (BBGKY) hierarchy of equations. It is shown that the pair correlational function explicitly depends upon the nature of binary interaction between particles. The corresponding kinetic equation containing pair correlation corrections is devoid of the degeneracy present in the collisionless Boltzmann equation with respect to the nature of the two particle interactions, unlike the Vlasov equation that cannot recognize the nature of two particle interaction. A net effect of the particle correlations can be realized only if the spatial symmetry of the correlation interaction is broken due to a spatial inhomogeneity. Such an inhomogeneity is inherently present in a bulk gravitational system in view of the unshielded long range nature of the two-particle interactions. In a finite gravitational system, the effects of pair correlations in the first order kinetic equation can be expressed in terms of the macroscopic gravitational potential to obtain a modified Boltzmann distribution that includes the

effects of correlations.

A Bose, MS Janaki

4.2.1.5 Wave breaking phenomenon of lower-hybrid oscillations induced by a background inhomogeneous magnetic field

In a fluid description, we study space-time evolution of lower hybrid modes in a cold quasi-neutral homogeneous plasma in presence of a background inhomogeneous magnetic field. Within a linear analysis, a dispersion relation with inhomogeneous magnetic field shows "phase mixing" of such oscillations. A manifestation of "phase mixing" is shown in "mode coupling." By using Lagrangian variables, an exact solution is presented in parametric form of this nonlinear time dependent problem. It is demonstrated that initially excited lower hybrid modes always break via phase mixing phenomenon in presence of an inhomogeneous magnetic field. Breaking of such oscillations is revealed by the appearance of spikes in the plasma density profile.

Chandan Maity, Nikhil Chakrabarti, Sudip Sengupta

4.2.1.6 Molecular discriminators using single wall carbon nanotubes

The interaction between single wall carbon nanotubes (SWNTs) and amphiphilic molecules has been studied in a solid phase. SWNTs are allowed to interact with different amphiphilic probes (e. g. lipids) in a narrow capillary interface. Contact between strong hydrophobic and amphiphilic interfaces leads to a molecular restructuring of the lipids at the interface. The geometry of the diffusion front and the rate and the extent of diffusion of the interface are dependent on the structure of the lipid at the interface. Lecithin having a linear tail showed greater mobility of the interface as compared to a branched tail lipid like dipalmitoyl phosphatidylcholine, indicating the hydrophobic interaction between single wall carbon nanotube core and the hydrophobic tail of the lipid. Solid phase interactions between SWNT and lipids can thus become a very simple but efficient means of discriminating amphiphilic molecules in general and lipids in particular.

Tamoghna Bhattacharyya, Anjan Kr Dasgupta, Nihar Ranjan Ray, Sabyasachi Sarkar

4.2.1.7 The electron geodesic acoustic mode

In this report, a novel new mode, named the electron geodesic acoustic mode, is presented. This mode can occur in toroidal plasmas like the conventional geodesic acoustic mode (GAM). The frequency of this new mode is much larger than that of the conventional GAM by a factor equal to the square root of the ion to electron mass ratio.

N Chakrabarti, PN Guzdar, PK Kaw

4.2.1.8 Two-dimensional double layer in plasma in a diverging magnetic field

Plasma created by an inductive RF discharge is allowed to expand along a diverging magnetic field. Measurement of the axial plasma potential profile reveals the formation of an electric double

layer near the throat of the expansion chamber. An accelerated ion beam has been detected in the downstream region, confirming the presence of the double layer. The 2-D nature of the ion energy distribution function of the downstream plasma has been studied by a movable ion energy analyser, which shows that the beam radius increases along the axial distance. The 2-D structure of the plasma potential has been studied by a movable emissive probe. The existence of a secondary lobe in the contour plot of plasma equipotential is a new observation. It is also an interesting observation that the most diverging magnetic field line not intercepting the junction of the discharge tube and the expansion chamber has an electric field aligned with it.

SK Saha, S Raychaudhuri, S Chowdhury, MS Janaki, AK Hui

4.2.1.9 Long range temporal correlation in the chaotic oscillations of a dc glow discharge plasma

Long range temporal correlations in the fluctuations of the plasma floating potentials (measured using a Langmuir probe) are investigated in a dc glow discharge plasma. Keeping the neutral pressure constant, the discharge voltage was varied and at the formation of the plasma, quasi periodic oscillations were excited and on further increase of the discharge voltage they became chaotic (irregular) beyond a threshold voltage. We compared the Lyapunov exponent with the Hurst exponent obtained from R/S statistics which showed an opposite behaviour at the transition point. These results are perhaps new since we have not come across such comparative analysis for chaotic oscillations in a glow discharge plasma before.

S Lahiri, D Roychowdhury, ANS Iyengar

4.2.1.10 Breaking of upper hybrid oscillations in the presence of an inhomogeneous magnetic field

We present space-time evolution of large-amplitude upper hybrid modes in a cold homogeneous plasma in the presence of an inhomogeneous magnetic field. Using the method of Lagrange variables, an exact space-time- dependent solution is obtained in parametric form. It is found that the magnetic field inhomogeneity causes various nonlinearly excited modes to couple, resulting in phase mixing and eventual breaking of the initially excited mode. The occurrence of wave breaking is seen by the appearance of spikes in the density profile. These results will be of relevance to laboratory and space plasma situations in which the external magnetic field is inhomogeneous.

Chandan Maity, Nikhil Chakrabarti, Sudip Sengupta

4.2.1.11 Suppression of electric and magnetic fluctuations and improvement of confinement due to current profile modification by biased electrode in Saha Institute of Nuclear Physics tokamak

Improvement of plasma confinement is achieved in normal q(a) discharges of SINP-tokamak by introducing a biased electrode inside the last closed flux surface. All the important features of high confinement mode are observed biasing the electrode negatively with respect to the vacuum vessel. Arrays of electric and magnetic probes introduced in the edge plasma region reveal suppression

of electric and magnetic fluctuations over distinct frequency ranges as well as modification of the toroidal current profile due to biasing. Further analysis identifies the electrostatic fluctuations to be due to drift mode and the magnetic fluctuations may be of slow compressional Alfvén waves. Both get suppressed due to current profile modification during biasing, hence leading to the improvement of plasma confinement.

Debjyoti Basu, Rabindranath Pal, Joydeep Ghosh, Prabal K Chattopadhyay

4.2.1.12 A different approach to obtain Mayer’s extension to stationary single particle Wigner distribution

It is shown that the stationary collisionless single-particle Wigner equation in one dimension containing quantum corrections at the lowest order is satisfied by a distribution function that is similar in form to the Maxwellian distribution with an effective mass and a generalized potential. The distribution is used to study quantum corrections to electron hole solutions.

Anirban Bose, MS Janaki

4.2.1.13 Linear and nonlinear electrostatic modes in a strongly coupled quantum plasma

The properties of linear and nonlinear electrostatic waves in a strongly coupled electron-ion quantum plasma are investigated. In this study, the inertialess electrons are degenerate, while non-degenerate inertial ions are strongly correlated. The ion dynamics is governed by the continuity and the generalized viscoelastic momentum equations. The quantum forces associated with the quantum statistical pressure and the quantum recoil effect act on the degenerate electron fluid, whereas strong ion correlation effects are embedded in generalized viscoelastic momentum equation through the viscoelastic relaxation of ion correlations and ion fluid shear viscosities. Hence, the spectra of linear electrostatic modes are significantly affected by the strong ion coupling effect. In the weakly nonlinear limit, due to ion-ion correlations, the quantum plasma supports a dispersive shock wave, the dynamics of which is governed by the Korteweg-de Vries Burgers’ equation. For a particular value of the quantum recoil effect, only monotonic shock structure is observed. Possible applications of our investigation are briefly mentioned.

Samiran Ghosh, Nikhil Chakrabarti, PK Shukla

4.2.1.14 Signature of Misoriented Bilayer Graphenelike and Graphanelike Structure in the Hydrogenated Diamond-Like Carbon Film

In the present experimental work, we have described the signature of misoriented bilayer graphene-like and graphane-like structure in the hydrogenated diamond-like carbon film having interlayer disorder region and high specific surface area. Our new results have implications for bilayer graphene/graphane electronic devices.

Nihar R Ray, Jagannath Datta, Hari S Biswas, Someswar Datta

4.2.1.15 Shear flow instability in a strongly coupled dusty plasma

Linear stability analysis of strongly coupled incompressible dusty plasma in presence of shear flow has been carried out using the generalized hydrodynamical (GH) model. With the proper Galilean invariant GH model, a nonlocal eigenvalue analysis has been done using different velocity profiles. It is shown that the effect of elasticity enhances the growth rate of shear flow driven Kelvin-Helmholtz (KH) instability. The interplay between viscosity and elasticity not only enhances the growth rate but the spatial domain of the instability is also widened. The growth rate in various parameter space and the corresponding eigenfunctions are presented.

D Banerjee, MS Janaki, N Chakrabarti

4.2.1.16 Nonlinear shear wave in a non Newtonian visco-elastic medium

An analysis of nonlinear transverse shear wave has been carried out on non-Newtonian viscoelastic liquid using generalized hydrodynamic model. The nonlinear viscoelastic behavior is introduced through velocity shear dependence of viscosity coefficient by well known Carreau-Bird model. The dynamical feature of this shear wave leads to the celebrated Fermi-Pasta-Ulam problem. Numerical solution has been obtained which shows that initial periodic solutions reoccur after passing through several patterns of periodic waves. A possible explanation for this periodic solution is given by constructing modified Korteweg de Vries equation. This model has application from laboratory to astrophysical plasmas as well as in biological systems.

D Banerjee, MS Janaki, N Chakrabarti, M Chaudhuri

4.2.1.17 Collisional drag may lead to disappearance of wave-breaking phenomenon of lower hybrid oscillations

The inhomogeneity in the magnetic field in a cold electron-ion non-dissipative homogeneous plasma leads to the breaking of lower hybrid modes via phase mixing phenomenon [Maity et al. Phys. Plasmas 19, 102302 (2012)]. In this work, we show that an inclusion of collisional drag force in fluid equations may lead to the disappearance of the wave-breaking phenomenon of lower hybrid oscillations. The nonlinear analysis in Lagrangian variables provides an expression for a critical value of damping rate, above which spikes in the plasma density profile may disappear. The critical damping rate depends on the perturbation and magnetic field inhomogeneity amplitudes as well as the ratio of the magnetic field inhomogeneity and perturbation scale lengths.

Chandan Maity, Nikhil Chakrabarti

4.2.1.18 Small amplitude nonlinear electron acoustic solitary waves in weakly magnetized plasma

Nonlinear propagation of electron acoustic waves in homogeneous, dispersive plasma medium with two temperature electron species is studied in presence of externally applied magnetic field. The linear dispersion relation is found to be modified by the externally applied magnetic field. Lagrangian transformation technique is applied to carry out nonlinear analysis. For small amplitude limit, a modified KdV equation is obtained, the modification arising due to presence of magnetic

field. For weakly magnetized plasma, the modified KdV equation possesses stable solitary solutions with speed and amplitude increasing temporally. The solutions are valid upto some finite time period beyond which the nonlinear wave tends to wave breaking.

Manjitha Dutta†, Samiran Ghosh†, Rajkumar Roychoudhury†, Manoranjan Khan†, Nikhil Chakrabarti

4.2.1.19 Shock wave structures in a dissipative quantum plasma

Weak nonlinear low-frequency modes in a two-component electron-ion dissipative quantum plasma are investigated. The dissipation arises due to the electron-ion collision. It is found that a standard perturbative approach leads to a new nonlinear equation for the dynamics of the finite amplitude wave. The quantum diffraction effect in the presence of collisions introduces a dissipative effect. The numerical solutions of this novel equation predict the existence of weak shock structures

Samiran Ghosh, Nikhil Chakrabarti

4.3 Developmental Work

4.3.0.20 Installation of different diagnostics system for Tokamak and process of getting vacuum vessel in clean condition to get long duration plasma shot

We have installed two ion energy analyser systems, one has been put at radial port and the other in tangential port. One will detect ions coming via toroidal path and other coming directly from core region. Soft x-ray detection system (using PIN photo-diode array) is to be modified for vacuum attachment and electrical insulation. We have already installed vacuum system for that purpose and soft x-ray detection system by PIN diode array. Hard x-ray detection system is being installed. These hard xrays are emitted by runaway electrons and limiter. These diagnostics will enable us to analyse generation of runaway electrons in the core, probably by magnetic turbulence, different processes of ion heating and transport of ions and runaway electrons. Langmuir probes and magnetic probes are also installed. Now we are facing new trouble to get clean plasma so that it can be told that plasma resistivity is low and loop voltage after break down and at the peak of the plasma is low enough so that slowbank can take over and stretch the plasma. Baking system is operational and audio frequency discharge cleaning system is running methodically to get the desired result.

S Chowdhury, ANS Iyengar, MS Janaki, S Raychaudhuri, AK Hui, SK Saha

4.4 Publications

4.4.1 Publications in Journal

A Bose, MS Janaki, Density distribution for an inhomogeneous finite gravitational system, European Physical Journal **B85** (2012) Art No: 360

Anirban Bose, MS Janaki, A different approach to obtain Mayer's extension to stationary single particle Wigner distribution, Physics of Plasmas **19** (2012) Art No: 072101

Chandan Maity, Nikhil Chakrabarti, Collisional drag may lead to disappearance of wave-breaking phenomenon of lower hybrid oscillations, *Phys Plasmas* **20** (2013) 014501

Chandan Maity, Nikhil Chakrabarti, Sudip Sengupta, Breaking of upper hybrid oscillations in the presence of an inhomogeneous magnetic field, *Physical Review* **E86** (2012) Art No: 016408

Chandan Maity, Nikhil Chakrabarti, Sudip Sengupta, Wave breaking phenomenon of lower-hybrid oscillations induced by a background inhomogeneous magnetic field, *Physics of Plasmas* **19** (2012) Art No: 102302

D Banerjee, MS Janaki, N Chakrabarti, M Chaudhuri, Nonlinear shear wave in a non Newtonian visco-elastic medium, *Physics of Plasmas* **19** (2012) Art No: 062301

D Banerjee, MS Janaki, N Chakrabarti, Shear flow instability in a strongly coupled dusty plasma, *Physical Review* **E85** (2012) Art No: 066408

Debjyoti Basu, Rabindranath Pal, Joydeep Ghosh et al, Suppression of electric and magnetic fluctuations and improvement of confinement due to current profile modification by biased electrode in Saha Institute of Nuclear Physics tokamak, *Physics of Plasmas* **19** (2012) Art No: 072510

Manjitha Dutta†, Samiran Ghosh†, Rajkumar Roychoudhury†... Nikhil Chakrabarti, Small amplitude nonlinear electron acoustic solitary waves in weakly magnetized plasma, *Phys Plasmas* **20** (2013) 012113

Manjitha Dutta, Samiran Ghosh, Nikhil Chakrabarti, Electron acoustic shock waves in a collisional plasma, *Physical Review* **E86** (2012) Art No:066408

MS Janaki, Brahmananda Dasgupta, Peter H Yoon, A two-fluid model of the bifurcated current sheet, *Journal of Geophysical Research-Space Physics* **117** (2012) Art No: A12201

N Chakrabarti, PN Guzdar, PK Kaw, The electron geodesic acoustic mode, *Physics of Plasmas* **19** (2012) Art No: 092113

Nihar R Ray, Jagannath Datta, Hari S Biswas, et al, Signature of Misoriented Bilayer Graphenelike and Graphanelike Structure in the Hydrogenated Diamond-Like Carbon Film, *IEEE Transactions on Plasma Science* **40** (2012) 1789

Samiran Ghosh, Nikhil Chakrabarti, Magnetic electron drift solitons in electron magnetohydrodynamic plasmas, *Plasma Phys Controlled Fusion* **55** (2013) 035008

Samiran Ghosh, Nikhil Chakrabarti, Manoranjan Khan et al, Drift wave in pair-ion plasma, *Pramana-Journal of Physics* **80** (2013) 283

Samiran Ghosh, Nikhil Chakrabarti, PK Shukla, Linear and nonlinear electrostatic modes in a strongly coupled quantum plasma, *Physics of Plasmas* **19** (2012) Art No: 072123

Samiran Ghosh, Nikhil Chakrabarti, Shock wave structures in a dissipative quantum plasma, *Phys Rev* **E87** (2013) Art No: 033102

SK Saha, S Raychaudhuri, S Chowdhury et al, Two-dimensional double layer in plasma in a diverging magnetic field, *Physics of Plasmas* **19** (2012) Art No: 092502

S Lahiri, D Roychowdhury, AN Sekar Iyengar, Long range temporal correlation in the chaotic oscillations of a dc glow discharge plasma, *Physics of Plasmas* **19** (2012) Art No: 082313

Tamoghna Bhattacharyya, Anjan Kr Dasgupta, Nihar Ranjan Ray, et al, Molecular discriminators using single wall carbon nanotubes, *Nanotechnology* **23** (2012) Art No: 385304

4.5 Seminars/Lectures given in Conference/Symposium/Schools

Nikhil Chakrabarti

1. Waves in strongly coupled plasma, International conference on Complex processes in Plasmas and Nonlinear dynamical systems, organized by Institute for Plasma Research, Gandhinagar, Nov 6-9, 2012
2. Vortex solution in a density gradient driven drift wave, National workshop on Nonlinear waves: Theory and simulation, organized by NIT, Durgapur, WB, Jan 14-18, 2013
3. Nonlinear cold plasma Oscillation: nonrelativistic vs. relativistic, One day seminar on Nonlinear Phenomena organized by Centre for Plasma Studies, Jadavpur University, Jan 31, 2013
4. Nonlinear Oscillations in un-magnetized and magnetized plasma, National conference on Theoretical Physics (NCTP -2013), organized by Tezpur University, Assam Gandhinagar, Feb 8-12, 2013
5. Basic plasma physics (2 lectures), SERC school organized by Physics Department Jadavpur University, Dec 8, 2012
6. Basic plasma physics (2 lectures), M Tech, Instrumentation Science Dept, Jadavpur University, Feb 18, 2013

MS Janaki

1. MHD phenomena in plasmas (8 lectures), Department of Applied Mathematics, Calcutta University, Jun 2012
2. Nonlinear dynamical modelling of electrostatic ion cyclotron oscillations, International Conference on Frontiers of Mathematical Sciences with Applications (ICFMSA-2012), Calcutta Mathematical Society, Kolkata, Dec 9, 2012
3. Waves in Strongly Coupled Dusty Plasmas, one day workshop on Plasmas and its Applications, Kharagpur College, Kharagpur, Dec 18, 2012
4. Kelvin-Helmholtz Instability in a shear thinning dusty plasma, National Conference on Emerging Trends in Physics of Fluids and Solids (NCETPFS- 2013), Department of Mathematics, Jadavpur University, Feb 27-28, 2013

4.6 Teaching elsewhere

Nikhil Chakrabarti

Basic Quantum Mechanics, M Sc, Narendrapur Ramkrishana Mission College (University of Calcutta), 2012

Chapter 5

Theoretical Physics

5.1 Summary of Research Activities of Divisions

5.1.1 Astroparticle Physics and Cosmology

The Astroparticle Physics and Cosmology (APC) Division pursues research in the interface areas spanning Astrophysics, Cosmology, and high energy particle and nuclear physics. During the year under review, members of the Division have carried out research on a variety of topics in AstroParticle Physics. Some highlights are given below.

(i) Weakly Interacting Massive Particle (WIMP) Dark Matter search experiment using Superheated Drop Detectors (SDD):

The work on WIMP Dark Matter (DM) search using SDDs as part of the PICASSO collaboration has been continued. The SINP group has initiated major R&D activity towards large drop-size detectors, and has contributed significantly towards detector fabrication, data analysis, simulations and physics results. The latest results from the PICASSO collaboration gave the most stringent upper limit so far on the cross section of spin-dependent interactions of WIMPs with nuclei.

Towards the end of XI-th Plan period, another new initiative had been made to set up a Dark Matter search experiment the DINO experiment in India. This will be vigorously pursued in the XII-th Plan period, primarily in collaboration with Texas A&M University, USA, and will be a Si/Ge-based cryogenic experiment, the first phase of which is proposed to be located in the UCIL, Jaduguda underground facility. The R&D work for this has already started.

(ii) Observational High Energy Gamma Ray Astronomy

Being a member of the High Altitude GAMMA Ray (HAGAR) Cherenkov telescope system located at Hanle, Ladakh, J&K, the SINP group has made major contributions in observations, simulations as well as data analysis. Recently, the SINP group has joined the international Cherenkov Telescope Array (CTA)-India consortium. Currently extensive computer simulations are being performed in the powerful blade server of Astroparticle Physics and Cosmology (APC) Division to understand the performance of the telescope array at different altitudes.

Observational Optical Astronomy:

A programme of Observational Optical Astronomy was started under the XIth plan period. A 14-inch diameter optical telescope was procured for teaching and demonstration of fundamental concepts of astronomy and for outreach activities. Also, an observatory dome the Meghnad Saha Observatory was set up atop a specially constructed concrete platform on the roof of the Institute building for housing the telescope. This facility was inaugurated by Professor Milan K. Sanyal, Director, SINP in presence of Professor J.V. Narlikar on 5 April, 2012. This is the first facility of this kind in Eastern India.

(iii) Physics and Astrophysics of Neutron Stars and Supernovas:

The melting of Bose-Einstein condensate of antikaons in hot and lepton-trapped nuclear matter in protoneutron stars was studied in a relativistic model. The critical temperature of antikaon condensation in a protoneutron star was smaller than that of a neutron star. The phase diagram of a protoneutron star with an antikaon condensate was constructed and its implication was discussed.

Torsional shear mode oscillations were investigated in general relativity. In particular, the effects of magnetised crusts on torsional shear mode frequencies were studied. Torsional shear mode frequencies calculated using the magnetised crusts were in good agreement with the observed frequencies of Quasi Periodic Oscillations (QPOs) of magnetars.

An exact expression for the rate of frame dragging of inertial frames (Lense-Thirring (LT) precession) in strong gravitational fields was derived. This expression of LT was calculated using various axisymmetric spacetimes such as Kerr, Kerr-Newman. Numerical values of the precession rate was estimated for a few known pulsars as well as the double-pulsar system. The research on the challenging problem of the Supernova Explosion mechanism was carried out during this period. The simulation of this problem including hyperons was carried out in the blade server of APC Division. The main goal of this investigation was to find out the role of hyperons on the core collapse supernova. The inclusion of hyperons did not give rise to any second shock leading to a successful supernova explosion and it rather accelerated the black hole formation. Neutrino signals which might be used as a probe to the core collapse supernova, were explored.

(iv) Theoretical research on Dark Matter:

The velocity distribution function (VDF) of the dark matter particles in the Galaxy has been derived directly from the observed rotation curve data using Eddingtons inversion method. The resulting VDF differs significantly from the Maxwellian distribution used in the so-called Standard Halo Model (SHM) to describe the dark matter halo of the Galaxy. This has major impact on analysis and interpretation of the results of both direct as well as indirect detection experiments for the search for dark matter.

Two-component dark matter models by adding a scalar singlet and an extra Higgs inert doublet or two scalar singlets, were constructed to explain gamma-ray lines due to dark matter annihilation in the galactic centre. Probable neutrino flux from dark matter annihilation in the galactic region was also studied in a supersymmetric dark matter model.

(v) Neutrino mass models:

Within the type-I seesaw and in the basis where charged lepton and heavy neutrino mass matrices are real and diagonal, $\mu\tau$ symmetric four and three zero neutrino Yukawa textures are perturbed by lowest order $\mu\tau$ symmetry breaking terms. These perturbations are taken to be the *most general ones for those textures*. For quite small values of those symmetry breaking parameters, permitting a lowest order analysis, current best-fit ranges of neutrino mass squared differences and mixing angles

were shown to be accommodable, including a value of θ_{13} in the observed range, provided all the light neutrinos have an inverted mass ordering. General Majorana neutrino mass matrix is complex symmetric and for three generations of neutrinos it contains 12 real parameters. This general neutrino mass matrix was diagonalised and the three neutrino masses, three mixing angles, one Dirac CP phase and two Majorana phases (removing three unphysical phases) were expressed in terms of the neutrino mass matrix elements. The results were applied in the context of a neutrino mass matrix derived from a broken cyclic symmetry invoking type-I seesaw mechanism. Phenomenological study of the above mass matrix allowed enough parameter space to satisfy the neutrino oscillation data with only 10% breaking of this symmetry. In this model only normal mass hierarchy was allowed. In addition, Dirac CP phase and Majorana phases were numerically estimated. $\sum m_i$ and $|m\nu_{ee}|$ were also calculated.

(vi) Classical & Quantum Gravity:

Research in Gravitational collapse problem, Loop quantum gravity, gauge-gravity connection, Black-hole entropy was pursued and significant progress was made in those areas.

5.1.2 Theory

Particle Physics Phenomenology:

Fixed order calculation truncated to NLO, at best yields results for sufficiently inclusive observable. Combining fixed order NLO and parton shower Monte Carlo (PS), would extend the coverage of the kinematical region to consistently include resummation in the collinear limit and also make a more exclusive description of the final state and get as realistic as possible to the experimental situation.

MC@NLO formalism has been used for the diphoton process in the ADD model and it is expected to significantly help extra dimension searches at the LHC to constrain the ADD model parameters. Diphoton final state in the large extra dimension model to NLO in QCD and matching to parton shower is implemented using the aMC@NLO framework. All the subprocesses that contribute to the diphoton final state from both the SM and ADD model are considered to NLO in QCD. Using a set of generic cuts we demonstrated the importance of NLO+PS over the fixed order NLO computations, by considering the $p_T^{\gamma\gamma}$ distribution. We have presented our results to NLO+PS accuracy for various observable. It is important to note that there is substantial enhancement of the various distributions due to the inclusion of NLO corrections and both the theoretical and PDF uncertainties have been estimated. There is a significant decrease in the theoretical uncertainties in going from LO to NLO order.

Another main direction of work is prompted by the discovery of the 125 GeV Higgs-like particle at the LHC. This can be broadly classified under two categories: (1) Study of extended scalar sector motivated from discrete flavor symmetry groups; also, model independent study of modified scalar couplings to fermions and gauge bosons. (2) Investigation of brane-world induced supersymmetry breaking which can accommodate ‘naturally’ heavy superparticles.

Gravity:

In completely local settings, we have shown that a dynamically evolving black hole horizon can be assigned a Hawking temperature. We could also calculate the Hawking flux and show that the horizon radius shrinks; we established a relation between the two.

We studied some general properties of black hole entropy in loop quantum gravity from the perspective of local stationary observers at distance l from the horizon. The black hole entropy differs from the low energy (IR) expected value $A/(4G)$ in natural units, in the deep Planckian regime

(UV). The partition function is well defined if the number of non-geometric degrees of freedom (associated with the area eigenvalue at a puncture) satisfy some local holographic bound. Our framework provided a natural renormalization mechanism from UV to IR as the scale l flows from zero to larger values.

The entropy of black holes was studied in loop quantum gravity. It was discovered that the logarithmic correction term, which is usually supposed to involve the logarithm of the eigenvalue of the area operator, actually involves the logarithm of the classical area of the horizon, which can be very different.

Cosmology:

We have initiated few new projects. One of them involves the construction of inflationary or dark-energy models in String Theory set-up. It turns out that constructing radiatively stable potentials under quantum corrections are difficult to achieve except for the pseudo-Nambu Goldstone Bosons (pNGBs). In String Theory, it is natural to get many axionic scalar fields, and those can be potentially inflaton or dark energy field. A new work has been initiated in the Large Volume Scenario of type IIB String Theory, where large number of pNGBs collectively drive inflation, or present day cosmic acceleration. In addition, we are also investigating the observational consequences of some variations of natural quintessence model. Another project involves the likeliness of chaotic inflation in the landscape paradigm of multiple vacua theories like String Theory. A new work has been initiated that involves the classical instabilities of the higher curvature theories and its connection to the so called Ostrogradski instabilities.

Strings:

Certain properties of the non-commutative Yang-Mills (NCYM) plasma has been studied from the holographic gravity dual (a decoupling limit of non-extremal D1/D3 bound state) using gauge/gravity duality. The velocity dependent quark-antiquark potential, the screening length and the jet quenching parameter have been computed in this theory and were compared with the known commutative results. Also during this time some new string theory solutions have been found. They are certain intersecting solutions of the form F-Dp (for $0 \leq p \leq 5$), D0-D4, D2-D6, D1-D3, D2-D4, D3-D5, D2-D2', D4-D4' and NS5-Dp (for $1 \leq p \leq 6$) having $1/4$ space-time supersymmetry and are threshold bound states. The novelty of these bound states is that they give non-relativistic space-time in the near horizon limit. In fact the metrics in that case have Lifshitz scaling symmetry with hyperscaling violation. Field theories having such scaling symmetry have been known to correspond to some condensed matter systems near their quantum critical point. So, these string theory solutions are possibly the holographic dual of such condensed matter systems. Thus studying these solutions may lead to some understanding of some strongly coupled quantum condensed matter systems which are otherwise hard to study from perturbative field theory point of view.

Recent success in understanding M2-brane Chern-Simons matter theories, like the ABJM or BLG model, has generated a renewed interest in understanding the holographic theory describing multiple M5-branes. The usual examples are the interacting (2,0) conformal field theory involving chiral tensor fields. We have studied a novel approach in constructing local M5 brane action by using the Yang-Mills fields and auxiliary U(1) field. The string solutions with non-relativistic Lifshitz and Schroedinger symmetries have been studied recently from the point of view of their applications in holographic theories, particularly condensed matter physics. We have found some elegant examples of such string vacua which have asymmetric scaling of space and time coordinates, but are supersymmetric also. Recently we introduced anspacial class of smooth interpolating Lifshitz-AdS solutions too. The entanglement entropy functional is well defined in these cases. All of these

solutions exhibit hyperscaling violation.

Nuclear Theory:

The nuclear symmetry energy at a given density measures the energy transferred in converting symmetric nuclear matter into the pure neutron matter. The density dependence of nuclear symmetry energy remains poorly constrained. We have provided some constraint on the behaviour of the nuclear symmetry energy around the saturation density on the basis of experimental data for nuclear masses, iso-vector giant quadrupole resonances and neutron-skin thickness in heavy nuclei.

QCD at Finite Temperature and Density:

We have been involved in both perturbative and non-perturbative aspects of QCD. We have computed 2-loop and 3-loop thermodynamic quantities (pressure, susceptibilities, speed of sound, trace anomaly etc) of a plasma of quarks and gluons at finite temperature and chemical potential using the state-of-the-art hard thermal loop perturbation theory (HTLpt), a reorganization of finite temperature/density quantum chromodynamics. The results have been compared with available LQCD data. We also worked on non-perturbative aspect of QGP using nonperturbative model based on QCD. A very recent study involves the consequence of center domains, i.e., $Z(3)$ domains on the phenomenology of QGP formed in heavy-ion collisions.

Mathematical Physics:

The spectrum of the $SU(m)$ spin Sutherland model associated with the B_N root system has been computed, including the exact degeneracy of all energy levels. An expression for the partition function of the corresponding Haldane-Shastry like spin chain has been obtained by using the freezing trick. A class of one-dimensional vertex models, whose energy functions depend on the vertices through polynomials of any possible degree, has been analysed. It is shown that the level density distribution of all such vertex models asymptotically follow the Gaussian pattern for large number of vertices.

We consider different realizations for the momentum sector of kappa-Poincare Hopf algebra, which is associated with a curved momentum space. We show that the notion of the particle mass as introduced recently by Amelino-Camelia et al. in the context of relative-locality is realization independent for a wide class of realizations, up to linear order in deformation parameter l . On the other hand, the time delay formula clearly shows a dependence on the choice of realization.

We study the combined effect of a conical topological defect and a Coulomb charge impurity on the dynamics of Dirac fermions in gapped graphene. Beyond a certain strength of the Coulomb charge, quantum instability sets in, which demarcates the boundary between sub and supercritical values of the charge. In the subcritical regime, for certain values of the system parameters, the allowed boundary conditions in gapped graphene cone can be classified in terms of a single real parameter. We propose a Dirac type modification of the xp -model to a Xp -model on a semi-infinite cylinder. This model is inspired by recent work by Sierra et al on the xp -model on the half-line. Our model realizes the Berry-Keating conjecture on the Riemann zeros. We indicate the connection of our model to that of gapped graphene with a supercritical Coulomb charge, which might provide a physical system for the study of the zeros of the Riemann Zeta function.

Quantum Fields on Lattice:

In the context of additive mass renormalization and chiral anomaly in Wilson lattice QCD, we showed that by appropriately averaging over suitably chosen branches one can reduce cut-off artifacts. Comparing the central branch with all other branches, we found that the central branch, among all the avatars of the Wilson fermion, is the most suitable candidate for exploring near conformal lattice field theories.

We also investigated topological charge density correlator in Lattice QCD with two flavours of unimproved Wilson fermions, pion and nucleon in two flavour lattice QCD with unimproved Wilson fermion and explored two flavour Wilson Lattice QCD using DD-HMC algorithm.

Quantum Fields on Light-Front

In the area of polarized deep inelastic scattering, we pointed out that the identifications of transverse boost and rotation operators in light-front theory done in Phys. Rev. Lett. 109, 152005 (2012) are incorrect and the simple parton interpretation claimed is, in fact, for the transverse boost operator. The correct identifications and the associated sum rules in light-front QCD were investigated and published by us a decade ago.

5.2 Research Activities

5.2.1 Astroparticle Physics and Cosmology

5.2.1.1 Stability of quantum isolated horizon: a local observer's view

It is shown that a quantum isolated horizon (QIH), as observed by a local observer, is locally unstable as a thermodynamic system. The result is derived in two different ways. Firstly, the specific heat of the QIH is shown to be negative definite through a quantum statistical analysis. Then, it is shown, in the thermal holographic approach, that the canonical partition function of the QIH diverges under Gaussian thermal fluctuations of such energy spectrum, implying local instability of such a QIH as a thermodynamic system.

Abhishek Majhi

5.2.1.2 Stability of quantum isolated horizon: a local observer's view

It is shown that a quantum isolated horizon (QIH), as observed by a local observer, is locally unstable as a thermodynamic system. The result is derived in two different ways. Firstly, the specific heat of the QIH is shown to be negative definite through a quantum statistical analysis. Then, it is shown, in the thermal holographic approach, that the canonical partition function of the QIH diverges under Gaussian thermal fluctuations of such an energy spectrum, implying local instability of such a QIH as a thermodynamic system.

Abhishek Majhi

5.2.1.3 A study of the performance parameters of the High Altitude Gamma Ray (HAGAR) telescope system at Ladakh in India

We present results of Monte Carlo simulations for the High Altitude Gamma Ray (HAGAR) telescope array which detects very high energy gamma rays from astronomical sources. This telescope array, located at Hanle at an altitude of 4270 m in the Ladakh region of the Himalayas in India, is the highest altitude atmospheric Cherenkov experiment in the world. Taking advantage of the high altitude, this experiment could achieve relatively low energy threshold with a modest mirror area coverage. To understand the performance parameters of this telescope system, we have simulated large samples of extensive air showers initiated by gamma rays and various species of cosmic

rays, using the CORSIKA package. Cherenkov photons produced in the atmosphere are sampled at ground level. These photons are then passed through the detector simulation program, which takes into account various design details and the data acquisition system of HAGAR. Night sky photons are also considered in the detector simulation program as performance of the telescope depends strongly on the level of night sky background (NSB) at the observation site. We have estimated various performance parameters like energy threshold and effective area for vertically incident showers as well as inclined showers. Details of these parameters, results obtained from simulations and comparison with the observed data are presented. It is shown that the energy threshold of the HAGAR telescope system is about 208 GeV, a factor of similar to 4 less than for a similar set up at about 1000 m altitude, and it is able to detect Crab like sources at 50 sigma significance in 17 h of observation without imposing additional criteria, like gamma-hadron separation, for further rejection of cosmic rays.

L Saha, VR Chitnis, PR Vishwanath... P Bhattacharjee, RJ Britto et al

5.2.1.4 Neutrino Yukawa Textures within Type-I Seesaw

We review neutrino Yukawa textures with zeros within the framework of the type-I seesaw with three heavy right chiral neutrinos and in the basis where the latter and the charged leptons are mass diagonal. An assumed nonvanishing mass of every ultralight neutrino and the observed nondecoupling of any neutrino generation allow a maximum of four zeros in the Yukawa coupling matrix in family space. We show that the requirement of an exact μt symmetry, coupled with the observational constraints, reduces seventy-two allowed such textures to only four corresponding to just two different forms of the light neutrino mass matrix: one with an inverted and the other with a normal mass ordering. The masses and Majorana phases of ultralight neutrinos are predicted within definite ranges with laboratory and cosmological observational inputs. Within the same framework, we also study Yukawa textures with a fewer number of zeros, but with exact μt symmetry. We further formulate the detailed scheme of the explicit breaking of μt symmetry in terms of three small parameters for allowed four zero textures. The observed sizable mixing between the first and third generations of neutrinos is shown to follow for a suitable choice of these symmetry breaking parameters.

Biswajit Adhikary†, Probir Roy

5.2.1.5 Light mass galileons: Cosmological dynamics, mass screening and observational constraints

In this Letter, we examine the cosmological viability of a light mass galileon field consistent with local gravity constraints. The minimal, $L_3 = (\Box)^2 L_3 = (\Box)^2$, massless galileon field requires an additional term in order to give rise to a viable ghost free late time acceleration of Universe. The desired cosmological dynamics can either be achieved by incorporating an additional terms in the action such as $(L_4, L_5)(L_4, L_5)$ the higher order galileon Lagrangians or by considering a light mass field la galileon field potential. We analyze the second possibility and find that: (1) The model produces a viable cosmology in the regime where the non-linear galileon field is subdominant, (2) the Vainshtein mechanism operates at small scales where the non-linear effects become important and contribution of the field potential ceases to be significant. Also the small mass of the field under consideration is protected against strong quantum corrections thereby providing quantum

stability to the system.

Amna Ali, Radouane Gannouji[†], Md Wali Hossain[†] et al

5.2.1.6 Melting of antikaon condensate in protoneutron stars

We study the melting of a K- condensate in hot and neutrino-trapped protoneutron stars. In this connection, we adopt relativistic field theoretical models to describe the hadronic and condensed phases. It is observed that the critical temperature of antikaon condensation is enhanced as baryon density increases. For a fixed baryon density, the critical temperature of antikaon condensation in a protoneutron star is smaller than that of a neutron star. We also exhibit the phase diagram of a protoneutron star with a K- condensate.

Sarmistha Banik, Rana Nandi, Debades Bandyopadhyay

5.2.1.7 Scaling ansatz, four zero Yukawa textures, and large $\theta(13)$

We investigate the "scaling Ansatz" in the neutrino sector within the framework of a type-I seesaw mechanism with diagonal charged lepton and right-handed Majorana neutrino mass matrices (M-R). We also assume the four zero texture of Dirac neutrino mass matrices ($m(D)$) which severely constrain the phenomenological outcomes of such schemes. The scaling Ansatz and the present neutrino data allow only six such matrices out of 126 four zero Yukawa matrices. In this scheme, in order to generate large $\theta(13)$, we break the scaling Ansatz in $m(D)$ through a perturbation parameter and we also show that our breaking scheme is radiatively stable. We further investigate CP violation and baryogenesis via leptogenesis in those surviving textures.

Biswajit Adhikary, Mainak Chakraborty, Ambar Ghosal

5.2.1.8 Charged quantum black holes: thermal stability criterion

A criterion of thermal stability is derived for electrically charged quantum black holes having a large horizon area (compared to the Planck area), as an inequality between the mass of the black hole and its microcanonical entropy. The derivation is based on the key results of loop quantum gravity and equilibrium statistical mechanics of a grand canonical ensemble, with Gaussian fluctuations around an equilibrium thermal configuration assumed here to be a quantum isolated horizon. No aspect of classical black hole geometry is used to deduce the stability criterion. Since no particular form of the mass function is used a priori, our stability criterion provides a platform to test the thermal stability of a black hole with a given mass function. The mass functions of the two most familiar charged black hole solutions are tested as a fiducial check. We also discuss the validity of the saddle-point approximation used to incorporate thermal fluctuations. Moreover, the equilibrium Hawking temperature is shown to have an additional quantum correction over the semiclassical value.

Abhishek Majhi, Parthasarathi Majumdar

5.2.1.9 Neutrinos from WIMP annihilation in the Sun: Implications of a self-consistent model of the Milky Way's dark matter halo

Upper limits on the spin-independent as well as spin-dependent elastic scattering cross sections of low mass (similar to 2-20 GeV) weakly interacting massive particles (WIMPs) with protons, imposed by the upper limit on the neutrino flux from WIMP annihilation in the Sun given by the Super-Kamiokande (S-K) experiment, and their compatibility with the "DAMA-compatible" regions of the WIMP parameter space-the regions of the WIMP mass versus cross-section parameter space within which the annual modulation signal observed by the DAMA/LIBRA experiment is compatible with the null results of other direct-detection experiments-are studied within the framework of a self-consistent model of the finite-size dark matter halo of the Galaxy. The halo model includes the gravitational influence of the observed visible matter of the Galaxy on the phase-space distribution function of the WIMPs constituting the Galaxy's dark matter halo in a self-consistent manner. Unlike in the "standard halo model" used in earlier analyses, the velocity distribution of the WIMPs in our model is non-Maxwellian, with a high-velocity cutoff determined self-consistently by the model itself. The parameters of the model are determined from a fit to the rotation curve data of the Galaxy. We find that, for our best-fit halo model, for spin-independent interaction, while the S-K upper limits do not place additional restrictions on the DAMA-compatible region of the WIMP parameter space if the WIMPs annihilate dominantly to (b) over barb and/or (c) over barc, portions of the DAMA-compatible region can be excluded if WIMP annihilations to $T+T$ - and ν ($\bar{\nu}$) over bar occur at larger than 35% and 0.4% levels, respectively. For spin-dependent interaction, on the other hand, the restrictions on the possible annihilation channels are much more stringent: they rule out the entire DAMA region if WIMPs annihilate to (b) over barb and (c) over barc final states at greater than similar to 0.05% and 0.0005% levels, respectively, and/or to (b) over barb and (c) over barc at greater than similar to 0.5% levels. The very latest results from the S-K Collaboration [T. Tanaka et al., *Astrophys. J.* 742, 78 (2011)] make the above constraints on the branching fractions of various WIMP annihilation channels even more stringent by roughly a factor of 3-4.

Susmita Kundu, Pijushpani Bhattacharjee

5.2.1.10 Four lepton flavor violating signals at the LHC

Some yet unknown dynamics is expected to be at work behind the flavor puzzles of the Standard Model. Speculations exist that this may manifest itself in significant strength at the terascale. One consequence may be lepton flavor violation with total lepton number conserved. Already observed in neutrino oscillation experiments, such a phenomenon may show up more prominently at TeV energies, thus signaling a completely new physics. Proposed flavor violating charged dilepton states have already been studied with reference to the LHC. Here we study the production and detection at the LHC of flavor violating charged quadrileptons which are shown to have certain advantages over dileptons in searching for lepton flavor violation. A classification of all six-fermionic operators, in the chiral basis and contributing to such processes, is made and the corresponding cross section for each in 14 TeV pp collisions is computed under the hypothesis of single operator dominance. We further present the sensitivity reach of the new physics scale in terms of the integrated luminosity.

Dilip Kumar Ghosh[†], Probir Roy, Sourov Roy[†]

5.2.1.11 Multiwavelength study of the TeV blazar Mrk 421 during a giant flare

Aims. The nearby ($z = 0.031$) TeV blazar Mrk 421 was reported to be in a high state of flux activity since November, 2009. We aim to investigate possible changes in the physical parameters of Mrk 421 during its high state of activity using multiwavelength data.

Methods. We have observed this source in the bright state using the High Altitude GAMMA Ray (HAGAR) telescope array at energies above 250 GeV during February 13-19, 2010. Optical, X-ray and gamma-ray archival data were also used to obtain the spectral energy distribution and light curves.

Results. Mrk 421 was found to undergo one of its brightest flaring episodes on February 17, 2010 by various observations in X-rays and gamma-rays. HAGAR observations during February 13-19, 2010 at energies above 250 GeV show an enhancement in the flux level, with a maximum flux of similar to 7 Crab units being detected on February 17, 2010. We present the spectral energy distributions during this flaring episode and investigate the correlation of the variability in X-ray and gamma-ray bands.

Conclusions. Our multiwavelength study suggests that the flare detected during February 16 and 17, 2010 may have been caused by a passing shock in the jet.

A Shukla; VR Chitnis†; PR Vishwanath†...P Bhattacharjee; L Saha et al

5.2.2 Theory

5.2.2.1 Giant quadrupole resonances in Pb-208, the nuclear symmetry energy, and the neutron skin thickness

Recent improvements in the experimental determination of properties of the isovector giant quadrupole resonance (IVGQR), as demonstrated in the $A = 208$ mass region, may be instrumental for characterizing the isovector channel of the effective nuclear interaction. We analyze properties of the IVGQR in Pb-208, using both macroscopic and microscopic approaches. The microscopic method is based on families of nonrelativistic and covariant energy density functionals (EDF), characterized by a systematic variation of isoscalar and isovector properties of the corresponding nuclear matter equations of state. The macroscopic approach yields an explicit dependence of the nuclear symmetry energy at some subsaturation density, for instance $S(\rho = 0.1 \text{ fm}^{-3})$, or the neutron skin thickness $\Delta r(\text{np})$ of a heavy nucleus, on the excitation energies of isoscalar and isovector GQRs. Using available data it is found that $S(\rho = 0.1 \text{ fm}^{-3}) = 23.3 \pm 0.6 \text{ MeV}$. Results obtained with the microscopic framework confirm the correlation of the $\Delta r(\text{np})$ to the isoscalar and isovector GQR energies, as predicted by the macroscopic model. By exploiting this correlation together with the experimental values for the isoscalar and isovector GQR energies, we estimate $\Delta r(\text{np}) = 0.14 \pm 0.03 \text{ fm}$ for Pb-208, and the slope parameter of the symmetry energy: $L = 37 \pm 18 \text{ MeV}$.

X Roca-Maza, M Brenna, BK Agrawal et al

5.2.2.2 Holographic entanglement entropy of the near horizon 1/4 BPS F-Dp bound states

It was shown in Dey and Roy [J. High Energy Phys. 06 (2012) 129] that the near-horizon limit of the 1/4 Bogomol'nyi-Prasad-Sommerfield, threshold F-Dp (for $0 \leq p \leq 5$, $p \neq 4$) bound-state solutions of type-II string theories give rise to space-time metrics endowed with Lifshitz scaling along with hyperscaling violation. Here we compute the holographic entanglement entropy of this system for all $p \neq 4$ (for $p = 4$ the space-time has AdS(2) structure). For $p = 3, 5$, we get the expected area-law behavior of the entanglement entropy. For $p = 0, 1$, the entanglement entropy has new area-law violations and exhibits behavior which is in between the linear and logarithmic behaviors. For $p = 2$, we get a logarithmic violation of the area law. We also compute the entanglement entropy at finite temperature and show that as the temperature rises, the entanglement entropy makes a crossover to the thermal entropy of the system. We thus obtain the string-theoretic realization of the holographic entanglement entropy and its various aspects, which were noted earlier for a generic metric with hyperscaling violation.

Parijat Dey, Shibaji Roy

5.2.2.3 Influence of the Effective Mass Modification of Weak Interacting Light Boson on the Properties of Neutron Stars

The influence of modification of the effective mass of weakly interacting light boson (WILB) present in the compact hyperonic stars are investigated within the framework of the extended relativistic mean field model. It is found that the bulk properties of the hyperonic stars are compatible with the provided recent observational constraints, if the presence of the WILBs with appropriate effective mass is considered.

A Sulaksono, BK Agrawal

5.2.2.4 Jet-parton inelastic interaction beyond eikonal approximation

Most of the models of jet quenching generally assumes that a jet always travels in a straight eikonal path, which is indeed true for sufficiently hard jet but may not be a good one for moderate and low momentum jet. In this article an attempt has been made to relax part of this approximation for $2 \rightarrow 3$ processes and found a (15-20)% suppression in the differential cross section for moderately hard jets because of the noneikonal effects. In particular, for the process $qq' \rightarrow qq'g$ in the centre of momentum frame the scattering with an angle wider than $\pm 0.52 \pi$ is literally forbidden unlike the process $gg \rightarrow ggg$ that allows an angular range $\pm \pi$. This may have consequence on the suppression of hadronic spectra at low transverse momenta.

Raktim Abir

5.2.2.5 Effect of topological defects and Coulomb charge on the low energy quantum dynamics of gapped grapheme

We study the combined effect of a conical topological defect and a Coulomb charge impurity on the dynamics of Dirac fermions in gapped graphene. Beyond a certain strength of the Coulomb

charge, quantum instability sets in, which demarcates the boundary between sub- and supercritical values of the charge. In the subcritical regime, for certain values of the system parameters, the allowed boundary conditions in a gapped graphene cone can be classified in terms of a single real parameter. We show that the observables such as local density of states, scattering phase shifts and the bound state spectra are sensitive to the value of this real parameter, which is interesting from an empirical point of view. For a supercritical Coulomb charge, we analyze the system with a regularized potential as well as with a zigzag boundary condition and find the effect of the sample topology on the observable features of the system.

Baishali Chakraborty, Kumar S Gupta, Siddhartha Sen

5.2.2.6 Modified Higgs couplings and unitarity violation

Prompted by the recent observation of a Higgs-like particle at the CERN Large Hadron Collider, we investigate a quantitative correlation between possible departures of the gauge and Yukawa couplings of this particle from their Standard Model expectations and the scale of unitarity violation in the processes $WW \rightarrow WW$ and $t(\bar{t}) \rightarrow WW$.

Gautam Bhattacharyya, Dipankar Das, Palash B Pal

5.2.2.7 The exactly solvable spin Sutherland model of B-N type and its related spin chain

We compute the spectrum of the $su(m)$ spin Sutherland model of B-N type, including the exact degeneracy of all energy levels. By studying the large coupling constant limit of this model and of its scalar counterpart, we evaluate the partition function of their associated spin chain of Haldane-Shastry type in closed form. With the help of the formula for the partition function thus obtained we study the chain's spectrum, showing that it cannot be obtained as a limiting case of its BCN counterpart. The structure of the partition function also suggests that the spectrum of the Haldane-Shastry spin chain of BN type is equivalent to that of a suitable vertex model, as is the case for its $A(N-1)$ counterpart, and that the density of its eigenvalues is normally distributed when the number of sites N tends to infinity. We analyze this last conjecture numerically using again the explicit formula for the partition function, and check its validity for several values of N and at.

B Basu-Mallick, F Finkel, A Gonzalez-Lopez

5.2.2.8 Pushing the SUSY Higgs mass towards 125 GeV with a color adjoint

We show that inclusion of a TeV scale chiral superfield transforming in the adjoint representation of the color $SU(3)$ to the minimal supersymmetric standard model particle content modifies the renormalization group running of some parameters in such a way that a 125 GeV mass of the light Higgs boson is accommodated more comfortably than in the constrained minimal supersymmetric standard model or minimal supergravity. Put differently, the introduction of a color adjoint TeV scale superfield helps resurrect lighter choices for the top squark and gluino which are otherwise

disfavored in the constrained minimal supersymmetric standard model or minimal supergravity.

Gautam Bhattacharyya, Tirtha Sankar Ray

5.2.2.9 Statistical spectroscopy for neutron-rich sd-shell nuclei

Statistical spectroscopic results using the spectral distribution theory are obtained for the structure of neutron-rich light nuclei going towards the drip line and compared to experimental values available. It is seen that the spectral distribution methods work reasonably well for light nuclei with large neutron excess. These methods are useful for problems in nuclear astrophysics where often averaged nuclear properties are adequate.

Kamales Kar

5.2.2.10 Determining the Density Content of Symmetry Energy and Neutron Skin: An Empirical Approach

The density dependence of nuclear symmetry energy remains poorly constrained. Starting from precise empirical values of the nuclear volume and surface symmetry energy coefficients and the nuclear saturation density, we show how in the ambit of microscopic calculations with different energy density functionals, the value of the symmetry energy slope parameter L along with that for neutron skin can be put in tighter bounds. The value of L is found to be $L = 64 \pm 5$ MeV. For Pb-208, the neutron skin thickness comes out to be 0.188 ± 0.014 fm. Knowing L , the method can be applied to predict neutron skin thicknesses of other nuclei.

BK Agrawal, JN De, SK Samaddar

5.2.2.11 Common Origin of Fermion Mixing and Geometrical CP Violation, and Its Test Through Higgs Physics at the LHC

We construct for the first time a flavor model, based on the smallest discrete symmetry $\Delta(27)$ that implements spontaneous CP violation with a complex phase of geometric origin, which can actually reproduce all quark masses and mixing data. We show that its scalar sector has exotic properties that can be tested at the LHC.

Gautam Bhattacharyya, Ivo de Medeiros Varzielas, Philipp Leser

5.2.2.12 Local symmetries of non-expanding horizons

Local symmetries of a non-expanding horizon have been investigated in the first-order formulation of gravity. When applied to spherically symmetric horizons, only a $U(1)$ subgroup of the Lorentz group survives as a residual local symmetry that one can make use of in constructing an effective theory on the horizon.

Rudranil Basu, Ayan Chatterjee, Amit Ghosh

5.2.2.13 Diphoton production in the ADD model to NLO plus parton shower accuracy at the LHC

In this paper, we present the next-to-leading order predictions for diphoton production in the ADD model, matched to the HERWIG parton shower using the MC@NLO formalism. A selection of the results is presented for $d = 2-6$ extra dimensions, using generic cuts as well as analysis cuts mimicking the search strategies as pursued by the ATLAS and CMS experiments.

R Frederix, Manoj K Mandal, Prakash Mathews et al

5.2.2.14 Existence of hyperons in the pulsar PSRJ1614-2230

The possibility of existence of hyperons in the recently measured 2M(circle dot) pulsar PSRJ1614-2230 is explored using a diverse set of nuclear equations of state calculated within the relativistic mean-field models. Our results indicate that the nuclear equations of state compatible with heavy-ion data allow the hyperons to exist in the PSRJ1614-2230 only for significantly larger values for the meson-hyperon coupling strengths. The maximum mass configurations for these cases contain sizable hyperon fractions (similar to 60%) and yet masqued their counterpart composed of only nucleonic matter.

A Sulaksono, BK Agrawal

5.2.2.15 Topological charge density correlator in Lattice QCD with two flavours of unimproved Wilson fermions

We study the two-point Topological Charge Density Correlator (TCDC) in lattice QCD with two degenerate flavours of unimproved Wilson fermions and Wilson gauge action at two values of lattice spacings and different volumes, for a range of quark masses. Configurations are generated with DDHMC algorithm and smoothed with HYP smearing. In order to shed light on the mechanisms leading to the observed suppression of topological susceptibility with respect to the decreasing quark mass and decreasing volume, in this work, we carry out a detailed study of the two-point TCDC. We have shown that, (1) the TCDC is negative beyond a positive core and radius of the core shrinks as lattice spacing decreases, (2) as the volume decreases, the magnitude of the contact term and the radius of the positive core decrease and the magnitude of the negative peak increases resulting in the suppression of the topological susceptibility as the volume decreases, (3) the contact term and radius of the positive core decrease with decreasing quark mass at a given lattice spacing and the negative peak increases with decreasing quark mass resulting in the suppression of the topological susceptibility with decreasing quark mass, (4) increasing levels of smearing suppresses the contact term and the negative peak keeping the susceptibility intact and (5) both the contact term and the negative peak diverge in nonintegrable fashion as lattice spacing decreases. It is gratifying to note that observations similar to 1 and 5 have been made using topological charge density operator based on chiral fermion. The observations 2 and 3 may be confirmed more precisely by using formulations based on chiral fermions.

Abhishek Chowdhury, Asit K De, A Harindranath, Jyotirmoy Maiti, Santanu Mondal

5.2.2.16 Motion of a test particle in the transverse space of dp-branes

We investigate the motion of a test particle in higher dimensions due to the presence of extended sources like Dp-branes by studying the motion in the transverse space of the brane. This is contrasted with the motion of a point particle in the Schwarzschild background in higher dimensions. Since Dp-branes are specific to 10-dimensional spacetime and exact solutions of geodesic equations for this particular spacetime has not been possible so far for the Schwarzschild background, we focus here to find the leading order solution of the geodesic equation (for motion of light rays). This enables us to compute the bending of light in both the backgrounds. We show that contrary to the well known result of no noncircular bound orbits for a massive particle, in Schwarzschild background, for $d \geq 5$, the Dp-brane background does allow bound elliptic motion only for $p = 6$ and the perihelion of the ellipse regresses instead of advancement. We also find that circular orbits for photon are allowed only for $p \leq 3$.

Anindita Bhattacharjee, Ashok Das, Levi Greenwood, Sudhakar Panda

5.2.2.17 Electroweak symmetry breaking beyond the Standard Model

In this paper, two key issues related to electroweak symmetry breaking are addressed. First, how fine-tuned different models are that trigger this phenomenon? Second, even if a light Higgs boson exists, does it have to be necessarily elementary? After a brief introduction, the fine-tuning aspects of the MSSM, NMSSM, generalized NMSSM and GMSB scenarios shall be reviewed, then the little Higgs, composite Higgs and the Higgsless models shall be compared. Finally, a broad overview will be given on where we stand at the end of 2011.

Gautam Bhattacharyya

5.2.2.18 166. A natural connection between neutrino mass generation and the lightness of a next-to-minimal supersymmetric Standard Model pseudoscalar

One of the attractive properties of the NMSSM is that it can accommodate a light pseudoscalar of order 10 GeV. However, such scenarios are constrained by several experimental results, especially those related to the fermionic decays of the pseudoscalar. In this work, extending the NMSSM field content by two gauge singlets, with lepton number $+1$ and -1 , we generate neutrino masses via the inverse see-saw mechanism at one hand and on the other hand a very light pseudoscalar becomes experimentally viable by having dominant invisible decay channels which help it to evade the existing bounds.

Debottam Das, Asmaa Abada, Gautam Bhattacharyya et al

5.2.2.19 Intersecting D-branes and Lifshitz-like space-time

In a previous paper [P. Dey and S. Roy, J. High Energy Phys. 06 (2012) 129] we have shown how Lifshitz-like space-times (space-times having Lifshitz scaling with hyperscaling violation) arise from $1/4$ Bogomol'nyi-Prasad-Sommerfield, threshold F - Dp-bound state solutions of type II string theories in the near horizon limit. In this paper we show that similar structures also arise from the near horizon limit of $1/4$ Bogomol'nyi-Prasad-Sommerfield, threshold-intersecting D-brane solutions of

type II string theories. Some of these solutions are standard ($D_p - D(p + 4)$ for $p = 0, 2$) and some are nonstandard ($D_p - D(p + 2)$ for $p = 1, 2, 3$), including $D2 - D2'$, $D3 - D3'$, and $D4 - D4'$ solutions. The dilatons of these solutions, in general, run (except in $D2-D4$ and $D3 - D3'$ cases) and produce renormalization group flows. We discuss the phase structures of these solutions. $D2-D4$ and $D3 - D3'$ in the near horizon limit do not produce Lifshitz-like space-time but give $AdS(3)$ spaces.

Parijat Dey, Shibaji Roy

5.2.2.20 Wilson loops in noncommutative Yang-Mills theory using gauge/gravity duality

By using the gauge/gravity duality and the Maldacena prescription we compute the expectation values of the Wilson loops in hot, noncommutative Yang-Mills (NCYM) theory in $(3 + 1)$ dimensions. We consider both the time-like and the light-like Wilson loops. The gravity dual background is given by a particular decoupling limit of non-extremal $(D1, D3)$ bound state of type IIB string theory. We obtain the velocity dependent quark antiquark potential and numerically study how the dipole length and the potential change with velocity (for $0 < \nu < 1$, i.e., the Wilson loop is time-like) of the dipole as well as noncommutativity. We discuss and compare the results with the known commutative results. We also obtain an analytic expression for the screening length when the rapidity is large and the noncommutativity parameter is small with the product remaining small. When $\nu \rightarrow 1$, the time-like Wilson loop becomes light-like and in that case we obtain the form of the jet quenching parameter for the strongly coupled noncommutative Yang Mills plasma which matches with our earlier results obtained using different approach.

Somdeb Chakraborty, Najmul Haque, Shibaji Roy

5.2.2.21 Temperature dependence of volume and surface symmetry energy coefficients of nuclei

The thermal evolution of the energies and free energies of a set of spherical and near-spherical nuclei spanning the whole periodic table are calculated in the subtracted finite-temperature Thomas-Fermi framework with the zero-range Skyrme-type KDE0 and the finite-range modified Seyler-Blanchard interaction. The calculated energies are subjected to a global fit in the spirit of the liquid-drop model. The extracted parameters in this model reflect the temperature dependence of the volume symmetry and surface symmetry coefficients of finite nuclei, in addition to that of the volume and surface energy coefficients. The temperature dependence of the surface symmetry energy is found to be very substantial whereas that of the volume symmetry energy turns out to be comparatively mild.

JN De, SK Samaddar, BK Agrawal

5.2.2.22 Regularizing tunnelling calculations of Hawking temperature

Attempts to understand Hawking radiation as tunnelling across a black hole horizon require the consideration of singular integrals. Although Schwarzschild coordinates lead to the standard Hawking temperature, isotropic radial coordinates may appear to produce an incorrect value. It is demonstrated here how the proper regularization of singular integrals leads to the standard temperature

for the isotropic radial coordinates as well as for other smooth transformations of the radial variable, which of course describe the same black hole.

Bhramar Chatterjee, P Mitra

5.2.2.23 Multifragmentation model for astrophysical strangelets

A model for the possible size distribution of astrophysical strangelets. that fragment out of the warm strange quark matter ejected during the merger of binary strange stars in the Galaxy, is presented here by invoking the statistical multifragmentation model. A simplified assumption of zero quark mass has been considered to obtain such mass-spectrum for the strangelets. An approximate estimate for the intensity of such strangelets in the galactic cosmic rays is also attempted by using a diffusion approximation.

Sayan Biswas, JN De, Partha S Joarder

5.2.2.24 Heavy quark energy loss and D-mesons in RHIC and LHC energies

We obtain the radiative energy loss of a heavy quark in a deconfined medium due to radiation of gluons off them using a recently derived generalised gluon emission spectrum. We find that the heavy flavour loses energy almost in a similar fashion like light quarks through this process. With this, we further analyse the nuclear modification factor for D-meson at LHC and RHIC energies. In particular, the obtained result is found to be in close agreement with the most recent data from ALICE collaboration at 2.76 ATeV Pb-Pb collisions. We also discuss the nuclear modification factor due to the collisional energy loss. Furthermore, the result of non-photonic single electron from the decay of both D- and B-mesons is compared with the RHIC data at 200 AGeV Au-Au collisions, which is also in close agreement.

Raktim Abir, Umme Jamil, Munshi G Mustafa et al

5.2.2.25 Supersymmetry, shape invariance and the Legendre equations

In three space dimensions, when a physical system possesses spherical symmetry, the dynamical equations automatically lead to the Legendre and the associated Legendre equations, with the respective orthogonal polynomials as their standard solutions. This is a very general and important result and appears in many problems in physics (for example, the multipole expansion. etc.). We study these equations from an operator point of view, much like the harmonic oscillator, and show that there is an underlying shape invariance symmetry in these systems responsible for their solubility. We bring out various interesting features resulting from this analysis from the shape invariance point of view.

D Bazeia, Ashok Das

5.2.2.26 Novel signatures of the Higgs sector from S-3 flavor symmetry

In an earlier work we analyzed the CP-even scalar sector of an S-3 flavor model, where we identified some novel decay signatures of an exotic scalar. In this work we extend our analysis by including the complete set of scalars/pseudoscalars, revisiting the potential minimization conditions in a more general setup, setting the spectrum in conformity with the current LHC limits on the scalar mass, and identifying yet another spectacularly novel decay channel which might be revealed from an intense study of rare top decays at the LHC into modes containing multileptons of different flavors.

Gautam Bhattacharyya, Philipp Leser, Heinrich Paes

5.2.2.27 Effects of medium on nuclear properties in multifragmentation

In multifragmentation of hot nuclear matter, properties of fragments embedded in a soup of nucleonic gas and other fragments should be modified as compared with isolated nuclei. Such modifications are studied within a simple model where only nucleons and one kind of heavy nuclei are considered. The interaction between different species is described with a momentum-dependent two-body potential whose parameters are fitted to reproduce properties of cold isolated nuclei. The internal energy of heavy fragments is parametrized according to a liquid-drop model with density- and temperature-dependent parameters. Calculations are carried out for several subnuclear densities and moderate temperatures, for isospin-symmetric and asymmetric systems. We find that the fragments get stretched due to interactions with the medium and their binding energies decrease with increasing temperature and density of nuclear matter.

JN De, SK Samaddar, X Vinas et al

5.2.2.28 Causal amplitudes in the Schwinger model at finite temperature

We show, in the imaginary time formalism, that the temperature dependent parts of all the retarded (advanced) amplitudes vanish in the Schwinger model. We trace this behavior to the CPT invariance of the theory and give a physical interpretation of this result in terms of forward scattering amplitudes of on-shell thermal particles.

Ashok Das, RR Francisco, J Frenkel

5.2.2.29 Level density distribution for one-dimensional vertex models related to Haldane-Shastry like spin chains

The energy level density distributions of some Haldane-Shastry like spin chains associated with the $A(N)$ $(-)$ (1) root system have been computed recently by Enciso et al., exploiting the connection of these spin systems with inhomogeneous one-dimensional vertex models whose energy functions depend on the vertices through specific polynomials of first or second degree. Here we consider a much broader class of one-dimensional vertex models whose energy functions depend on the vertices through arbitrary polynomials of any possible degree. We estimate the order of mean and variance for such energy functions and show that the level density distribution of all vertex models belonging to this class asymptotically follow the Gaussian pattern for large number of vertices. We

also present some numerical evidence in support of this analytical result.

Pratyay Banerjee, B Basu-Mallick

5.2.2.30 A study of Lambda hypernuclei within the Skyrme-Hartree-Fock model

We investigate the properties of the single Lambda hypernuclei within a Skyrme-Hartree-Fock (SHF) model. The parameters of the Skyrme type effective lambda-nucleon (Lambda N) interaction are obtained by fitting to the experimental Lambda binding energies of hypernuclei with masses spanning a wide range of the periodic table. Alternative parameter sets are also obtained by omitting nuclei below mass number 16 from the fitting procedure. The SHF calculations are performed for the binding energies of the Lambda single-particle states over a full mass range using the best fit parameter sets obtained in these fitting procedures and the results are compared with the available experimental data. The data show some sensitivity to the parameter sets obtained with or without including the nuclei below mass 16. The radii of the Lambda orbits in the hypernuclear ground states and the Lambda effective mass in nuclear matter show some dependence on different parameter sets. We present results for the total binding energy per baryon of the hypernuclei over a large mass region to elucidate their stability as a function of the baryon number. We have also employed the our best fit Lambda N parameter sets to investigate the role of hyperons in some key properties of neutron stars.

Neelam Guleria , Shashi K Dhiman, Radhey Shyam

5.2.2.31 Lifshitz/Schrodinger Dp-branes and dynamical exponents

We extend our earlier study of special double limits of 'boosted' AdS(5) black hole solutions to include all black Dp-branes of type II strings. We find that Lifshitz solutions can be obtained in generality, with varied dynamical exponents, by employing these limits. We then study such double limits for 'boosted' Dp-brane bubble solutions and find that the resulting non-relativistic solutions instead describe Schrodinger like space-times, having varied dynamical exponents. We get a simple map between these Lifshitz & Schrodinger solutions and a relationship between two types of dynamical exponents. We also discuss about the singularities of the Lifshitz solutions and an intriguing thermodynamic duality.

Harvendra Singh

5.2.2.32 Lifshitz-like space-time from intersecting branes in string/M theory

We construct $1/4$ BPS, threshold F-Dp bound states (with $0 \leq p \leq 5$) of type II string theories by applying S- and T-dualities to the D1-D5 system of type IIB string theory. These are different from the known $1/2$ BPS, non-threshold F-Dp bound states. The near horizon limits of these solutions yield Lifshitz-like space-times with varying dynamical critical exponent $z = 2(5 - p)/(4 - p)$, for p not equal 4, along with the hyperscaling violation exponent $\theta = p - (p - 2)/(4 - p)$, showing how Lifshitz-like space-time can be obtained from string theory. The dilatons are in general non-constant (except for $p = 1$). We discuss the holographic RG flows and the phase structures of these solutions. For $p = 4$, we do not get a Lifshitz-like space-time, but the near horizon limit in

this case leads to an $\text{AdS}(2)$ space.

Parijat Dey, Shibaji Roy

5.2.2.33 Non-holonomic deformation of the DNLS equation for controlling optical soliton in doped fibre media

Optical signal propagating through a non-linear fibre medium when coupled to an Erbium-doped resonant medium is known to produce a cleaner solitonic pulse, described by the self-induced transparency (SIT) coupled to the non-linear Schrodinger (NLS) equation. Extending this idea to ultra short pulses when description through derivative NLS (DNLS) becomes relevant, we propose and investigate a new model of a coupled DNLS-SIT system for greater efficiency. It is shown that, the broadening of the optical pulse, a well-known problem in fibre transmission, can be controlled by regulating a certain initial profile related to the population inversion. This effect can be enhanced by using the constrained integrable hierarchy of the DNLS-SIT system.

Anjan Kundu

5.2.2.34 Synchronized oscillations on a Kuramoto ring and their entrainment under periodic driving

We consider a finite number of coupled oscillators on a ring as an adaptation of the Kuramoto model of populations of oscillators. The synchronized solutions are characterized by an integer m , the winding number, and a second integer l , with solutions of type $(m, l = 0)$ being all stable. Following a number of recent works (see below) we indicate how the various solutions emerge as the coupling strength K is varied, presenting a perturbative expression for these for large K . The low K scenario is also briefly outlined, where the onset of synchronization by a tangent bifurcation is explained. The simplest situation involving three oscillators is described, where more than one tangent bifurcations are involved. Immediately before the tangent bifurcation leading to synchronization, the system exhibits the phenomenon of frequency- (or phase) splitting where more than one (usually two) phase clusters are involved. All the synchronized solutions are seen to be entrained by an external periodic driving, provided that the driving frequency is sufficiently close to the frequency of the synchronized population. A perturbative approach is outlined for the construction of the entrained solutions. Under a periodic driving with an appropriately limited detuning, there occurs entrainment of the phase-split solutions as well.

Tarun Kanti Roy, Avijit Lahiri

5.2.2.35 Neutral triple electroweak gauge boson production in the large extra-dimension model at the LHC

We study the prospects of probing large extra-dimension models at the LHC through neutral triple gauge boson production processes. In theories with extra dimensions these processes result from the exchange of a tower of massive graviton modes between the SM particles. We consider $\gamma\gamma\gamma$, $\gamma\gamma Z$, γZZ , and ZZZ production processes, and present our

results for various kinematic distributions at the LHC for root $S = 14$ TeV.

MC Kumar, Prakash Mathews, V Ravindran, Satyajit Seth

5.2.2.36 Optimization of relativistic mean field model for finite nuclei to neutron star matter

We have optimized the parameters of extended relativistic mean-field model using a selected set of global observables which includes binding energies and charge radii for nuclei along several isotopic and isotonic chains and the iso-scalar giant monopole resonance energies for the Zr-90 and Pb-208 nuclei. The model parameters are further constrained by the available informations on the energy per neutron for the dilute neutron matter and bounds on the equations of state of the symmetric and asymmetric nuclear matter at supra-nuclear densities. Two new parameter sets BSP and IUFSU* are obtained, later one being the variant of recently proposed IUFSU parameter set. The BSP parametrization uses the contributions from the quartic order cross-coupling between omega, and sigma mesons to model the high density behaviour of the equation of state instead of the omega meson self-coupling as in the case of IUFSU* or IUFSU. Our parameter sets yield appreciable improvements in the binding energy systematics and the equation of state for the dilute neutron matter. The importance of the quartic order omega-sigma cross coupling term of the extended RMF model, as often ignored, is realized.

BK Agrawal, A Sulaksono, PG Reinhard

5.2.2.37 Area law for black hole entropy in the SU(2) quantum geometry approach

Black hole thermodynamics suggests that a black hole should have an entropy given by a quarter of the area of its horizon. Earlier calculations in U(1) loop quantum gravity have led to a dominant term proportional to the area, but there was a correction involving the logarithm of the area. We find however that SU(2) loop quantum gravity can provide an entropy that is strictly proportional to the area as expected from black hole thermodynamics.

P Mitra

5.2.2.38 Naturally split supersymmetry

Nonobservation of superparticles till date, new Higgs mass limits from the CMS and ATLAS experiments, WMAP constraints on relic density, various other low energy data, and the naturalness consideration, all considered simultaneously imply a paradigm shift of supersymmetric model building. In this paper we perform, for the first time, a detailed numerical study of brane-world induced supersymmetry breaking for both minimal and next-to-minimal scenarios. We observe that a naturally hierarchical spectrum emerges through an interplay of bulk, brane-localized and quasi-localized fields, which can gain more relevance in the subsequent phases of the LHC run.

Gautam Bhattacharyya, Tirtha Sankar Ray

5.2.2.39 Zeta function regularization, anomaly and complex mass term

If zeta function regularization is used and a complex mass term considered for fermions, the phase does not appear in the fermion determinant. This is not a drawback of the regularization, which can recognize the phase through source terms, as demonstrated by the anomaly equation which is explicitly derived here for a complex mass term.

P Mitra

5.2.2.40 Production of cascade hypernuclei via the (K-, K+) reaction within a quark-meson coupling model

We study the production of bound hypernuclei Be-12(Xi-) and Mg-28(Xi-) via the (K-, K+) reaction on C-12 and Si-28 targets, respectively, within a covariant effective Lagrangian model, employing Xi bound state spinors derived from the latest quark-meson coupling model as well as Dirac single-particle wave functions. The K+ Xi(-) production vertex is described by excitation, propagation and decay of Lambda and Sigma resonance states in the initial collision of a K- meson with a target proton in the incident channel. The parameters of the resonance vertices are fixed by describing the available data on total and differential cross sections for the p(K-, K+)Xi(-) reaction. We find that both the elementary and hypemuclear production cross sections are dominated by the contributions from the Lambda(1520) intermediate resonant state. The 0 degrees differential cross sections for the formation of simple s-state Xi(-) particle-hole states peak at a beam momentum around 1.0 GeV/c, with a value in excess of 1 mu b.

R Shyam, K Tsushima, AW Thomas

5.2.2.41 Electric dipole polarizability and the neutron skin

The recent high-resolution measurement of the electric dipole (E1) polarizability $\alpha(D)$ in Pb-208 [A. Tamii et al., Phys. Rev. Lett. 107, 062502 (2011)] provides a unique constraint on the neutron-skin thickness of this nucleus. The neutron-skin thickness $r(\text{skin})$ of Pb-208 is a quantity of critical importance for our understanding of a variety of nuclear and astrophysical phenomena. To assess the model dependence of the correlation between $\alpha(D)$ and $r(\text{skin})$, we carry out systematic calculations for Pb-208, Sn-132, and Ca-48 based on the nuclear density functional theory using both nonrelativistic and relativistic energy density functionals. Our analysis indicates that whereas individual models exhibit a linear dependence between $\alpha(D)$ and $r(\text{skin})$, this correlation is not universal when one combines predictions from a host of different models. By averaging over these model predictions, we provide estimates with associated systematic errors for $r(\text{skin})$ and $\alpha(D)$ for the nuclei under consideration. We conclude that precise measurements of $r(\text{skin})$ in both Ca-48 and Pb-208-combined with the recent measurement of $\alpha(D)$ -should significantly constrain the isovector sector of the nuclear energy density functional.

J Piekarewicz, BK Agrawal, G Colo et al

5.2.2.42 Near-extremal black holes

We present a new formulation of deriving Hawking temperature for near-extremal black holes using distributions. In this paper the near-extremal Reissner-Nordstrom and Kerr black holes are

discussed. It is shown that the extremal solution as a limit of non-extremal metric is well-defined. The pure extremal case is also discussed separately.

Bhramar Chatterjee, Amit Ghosh

5.2.2.43 Lifshitz metric with hyperscaling violation from NS5-Dp states in string theory

In previous papers Dey and Roy (2012) [1] and [2] we have shown how Lifshitz-like spacetime (space-time having a Lifshitz scaling along with a hyperscaling violation) can arise by taking near horizon limits of certain intersecting solutions (F-string with Dp-branes and also with two D-branes) of string theory. In this Letter we construct intersecting bound state solutions in the form of NS5-Dp-branes (with $1 \leq p \leq 6$) of type II string theories. These are $1/4$ BPS and threshold bound states unlike the known NS5-Dp bound states which are $1/2$ BPS and non-threshold. We show that the near horizon limits of these solutions also lead to Lifshitz-like spacetime with the dynamical scaling exponent $z=0$ and the hyperscaling violation exponent $\nu=9-p$. The spatial dimension of the boundary theory is $d=7-p$. The dilatons in these theories are not constant in general (except for $p=5$) and therefore produce RG flows. So, we also consider the strong coupling phases of these theories and find that these phases also have similar Lifshitz-like structures, except for $p=2$, where it has an AdS3 structure.

Parijat Dey, Shibaji Roy

5.2.2.44 Many avatars of the Wilson fermion: a perturbative analysis

We explore different branches of the fermion doublers with Wilson fermion in perturbation theory, in the context of additive mass renormalization and chiral anomaly, and show that by appropriately averaging over suitably chosen branches one can reduce cut-off artifacts. Comparing the central branch with all other branches, we find that the central branch, among all the avatars of the Wilson fermion, is the most suitable candidate for exploring near conformal lattice field theories.

Abhishek Chowdhury, A Harindranath, Jyotirmoy Maiti[†], Santanu Mondal

5.2.2.45 The Yang-Mills and chiral fields in six dimensions

In previous work [15], we constructed an action in six dimensions using Yang-Mills fields and an auxiliary Abelian field. Here we first write down all the equations of motion and the constraints which arise from such an action. From these equations we reproduce all dynamical equations and the constraints required for self-dual tensor field theory constructed by Lambert-Papageorgakis, which describes $(2,0)$ supersymmetric CFT in 6D. This is an indication of the fact that our 6D gauge theory contains all the same information as the on-shell theory of chiral tensor fields.

Harvendra Singh

5.3 Developmental Work

5.3.1 Astroparticle Physics and Cosmology

5.3.1.1 Software and Monte Carlo Simulations

I have installed the Cerenkov Telescope Array (CTA) Simulation package in APC cluster (actually this is the first time the full simulation package has been installed and successfully run outside Europe anywhere within the CTA collaboration and also SINP is the first institute to run this package in India within India-CTA consortium). We are currently running extensive simulations to understand the performance of the telescope array for different altitudes. This is particularly important as inputs to the site survey group in finalizing the site for CTA installation.

Pratik Mazumder

5.4 Publications

5.4.1 Publications in Books/Monographs & Volumes Edited

Debades Bandyopadhyay

Nuclei in Strongly Magnetised Neutron Star Crusts, R Nandi and D Bandyopadhyay, in Exciting Interdisciplinary Physics, FIAS Interdisciplinary Science Series, Ed Walter Greiner, 2013, Springer, pp 333-343

Pratik Majumdar

Locating the TeV γ - rays from shell regions of Cassiopeia A, L Saha, T Ergin, P Majumdar and M Bozkurt, Proceedings of International Astronomical Union (IAU) Symposium No 296, Eds A Ray & D McCray, 2013

5.4.2 Publications in Journal

Abhishek Chowdhury, A Harindranath, Jyotirmoy Maiti, Santanu Mondal, Many avatars of the Wilson fermion: a perturbative analysis, J of High Energy Phys **1302** (2013) 037

Abhishek Chowdhury, Asit K De, A Harindranath et al, Topological charge density correlator in Lattice QCD with two flavours of unimproved Wilson fermions, Journal of High Energy Physics **Issue: 11** (2012) Art No: 029

Abhishek Chowdhury, Asit K De, A Harindranath, Jyotirmoy Maiti, Santanu Mondal, Quark mass, scale and volume dependence of topological charge density correlator in Lattice QCD, PoS Lattice **2012** (2012) 200

Abhishek Chowdhury, Asit K De, Sangita De Sarkar, A Harindranath, Jyotirmoy Maiti, Santanu Mondal, Anwesha Sarkar, Autocorrelation studies in two-flavour Wilson Lattice QCD using DD-HMC algorithm, PoS Lattice *2012* (2012) 189

Abhishek Chowdhury, Asit K De, Sangita De Sarkar, A Harindranath, Jyotirmoy Maiti, Santanu Mondal, Anwesa Sarkar, Low lying hadron spectrum and chiral condensate with two flavors of naive Wilson fermions, *PoS Lattice* **2012** (2012) 208

Abhishek Majhi, Parthasarathi Majumdar, Charged quantum black holes: thermal stability criterion, *Classical and Quantum Gravity* **29** (2012) Art No: 135013

Abhishek Majhi, Stability of quantum isolated horizon: a local observer's view, *Classical and Quantum Gravity* **30** (2013) Art No: 055001

Abhishek Majhi, Stability of quantum isolated horizon: a local observer's view, *Classical and Quantum Gravity* **30** (2013) Art No: 055020

Amna Ali, Radouane Gannouji, Md Wall Hossain et al, Light mass galileons: Cosmological dynamics, mass screening and observational constraints, *Physics Letters* **B718** (2012) 5

Anindita Bhattacharjee, Ashok Das, Levi Greenwood et al, Motion of a test particle in the transverse space of Dp-Branes, *International Journal of Modern Physics* **D21** (2012) Art No: 1250056

Ashok Das, RR Francisco, J Frenkel, Causal amplitudes in the Schwinger model at finite temperature, *Physical Review* **D86** (2012) Art No. 047702

A Shukla, VR Chitnis, PR Vishwanath, P Bhattacharjee, RJ Britto, L Saha et al, Multiwavelength study of the TeV blazar Mrk 421 during a giant flare, *Astronomy & Astrophysics* **541** (2012) Art No: A140

A Sulaksono, BK Agrawal, Existence of hyperons in the pulsar PSRJ1614-2230, *Nuclear Physics* **A895** (2012) 44

A Sulaksono, BK Agrawal, Influence of the Effective Mass Modification of Weak Interacting Light Boson on the Properties of Neutron Stars, Few-Body Systems **54** Special Issue: SI (2013) 501

Anjan Kundu, Non-holonomic deformation of the DNLS equation for controlling optical soliton in doped fibre media, *IMA Journal of Applied Mathematics* **77** (2012) 382

L Saha, VR Chitnis, PR Vishwanath...P Bhattacharjee, RJ Britto et al, A study of the performance parameters of the High Altitude Gamma Ray (HAGAR) telescope system at Ladakh in India, *Astroparticle Physics* **42** (2013) 33

Baishali Chakraborty, Kumar S Gupta, Siddhartha Sen, Effect of topological defects and Coulomb charge on the low energy quantum dynamics of gapped graphene, *Journal of Physics* **A46** (2013) Art No: 055303

B Basu-Mallick, F Finkel, A Gonzalez-Lopez, The exactly solvable spin Sutherland model of B-N type and its related spin chain, *Nuclear Physics* **B866** (2013) 391

Bhramar Chatterjee, Amit Ghosh, Near-extremal black holes, *Journal of High Energy Physics* **Issue: 4** (2012) Art No: 125

Bhramar Chatterjee, P Mitra, Regularizing tunnelling calculations of Hawking temperature, General Relativity and Gravitation **44**(2012) 2365

Biswajit Adhikary, Mainak Chakraborty, Ambar Ghosal, Scaling ansatz, four zero Yukawa textures, and large theta(13), Physical Review **D86** (2012) Art No:013015

Biswajit Adhikary, Probir Roy, Neutrino Yukawa Textures within Type-I Seesaw, ADVANCES IN HIGH ENERGY PHYSICS (2013) Art No:324756

BK Agrawal, A Sulaksono, PG Reinhard, Optimization of relativistic mean field model for finite nuclei to neutron star matter, Nuclear Physics **A882** (2012) 1

BK Agrawal, JN De, SK Samaddar, Determining the Density Content of Symmetry Energy and Neutron Skin: An Empirical Approach, Physical Review Letters **109** (2012) Art No: 262501

D Bazeia, Ashok Das, Supersymmetry, shape invariance and the Legendre equations, Physics Letters **B715** (2012) 256

Debottam Das, Asmaa Abada, Gautam Bhattacharyya, et al, A natural connection between neutrino mass generation and the lightness of a next-to-minimal supersymmetric Standard Model pseudoscalar, Pramana-Journal of Physics **79** (2012) 867

Dilip Kumar Ghosh, Probir Roy, Sourov Roy, Four lepton flavor violating signals at the LHC, Journal of High Energy Physics **Issue: 5** (2012) Art No:067

Gautam Bhattacharyya, Dipankar Das, Palash B Pal, Modified Higgs couplings and unitarity violation, Physical Review **D87** (2013) Art No: 011702

Gautam Bhattacharyya, Electroweak symmetry breaking beyond the Standard Model, Pramana-Journal of Physics **79** (2012) 675

Gautam Bhattacharyya, Ivo de Medeiros Varzielas, Philipp Leser, Common Origin of Fermion Mixing and Geometrical CP Violation, and Its Test Through Higgs Physics at the LHC, Physical Review Letters **109** (2012) Art No: 241603

Gautam Bhattacharyya, Philipp Leser, Heinrich Paes, Novel signatures of the Higgs sector from S-3 flavor symmetry, Physical Review **D86** (2012) Art No: 036009

Gautam Bhattacharyya, Tirtha Sankar Ray, Naturally split supersymmetry, Journal of High Energy Physics **Issue: 5** (2012) Art No: 022

Gautam Bhattacharyya, Tirtha Sankar Ray, Pushing the SUSY Higgs mass towards 125 GeV with a color adjoint, Physical Review **D87** (2013) Art No: 015017

Harvendra Singh, Lifshitz/Schrodinger Dp-branes and dynamical exponents, Journal of High Energy Physics **Issue: 7** (2012) Art No: 082

Harvendra Singh, The Yang-Mills and chiral fields in six dimensions, JHEP **1302** (2013) 056

JN De , SK Samaddar, BK Agrawal, Temperature dependence of volume and surface symmetry energy coefficients of nuclei, Physics Letters **B716** (2012) 361

JN De, SK Samaddar, X Vinas et al, Effects of medium on nuclear properties in multifragmentation, Physical Review **C86** 92012) Art No: 024606

J Piekarewicz, BK Agrawal, G Colo, et al, Electric dipole polarizability and the neutron skin, Physical Review **C85** (2012) Art No: 041302

Kamales Kar, Statistical spectroscopy for neutron-rich sd-shell nuclei, Journal of Physics **G40** (2013) Art No: 015105

Mala Das, Universal energy calibration for neutron detection and WIMPs search for superheated droplet detector, PSTR_12.006 (PICASSO Scientific & Technical Report), Aug 2012

MC Kumar, Prakash Mathews, V Ravindran, et al, Neutral triple electroweak gauge boson production in the large extra-dimension model at the LHC, Physical Review **D85** (2012) Art No: 094507

M Das (PICASSO collaboration), Dark matter search with PICASSO, Journal of Physics: Conference series **375** (2012) 012023

Neelam Guleria, Shashi K Dhiman, Radhey Shyam, A study of Lambda hypernuclei within the Skyrme-Hartree-Fock model, Nuclear Physics **A886** (2012) 71

Parijat Dey, Shibaji Roy, Holographic entanglement entropy of the near horizon 1/4 BPS F-Dp bound states, Physical Review **D87**(2013) Art No: 066001

Parijat Dey, Shibaji Roy, Intersecting D-branes and Lifshitz-like space-time, Physical Review **D86** (2012) Art No: 066009

Parijat Dey, Shibaji Roy, Lifshitz-like space-time from intersecting branes in string/M theory, Journal of High Energy Physics **Issue: 6** (2012) Art No: 129

Parijat Dey, Shibaji Roy, Lifshitz metric with hyperscaling violation from NS5-Dp states in string theory, Phys Lett **B720**(2013) 419 *P Mitra*, Area law for black hole entropy in the SU(2) quantum geometry approach, Physical Review **D85** (2012) Art No: 104025

P Mitra, Zeta function regularization, anomaly and complex mass term, European Physical Journal **C72** (2012) Art No: 2024

Pratik Mazumder (CTA Collaboration), Introducing the CTA Concept, BS Acharya et al, Astroparticle Physics **43** (2013) 3

Pratyay Banerjee, B Basu-Mallick, Level density distribution for one-dimensional vertex models related to Haldane-Shastry like spin chains, Journal of Mathematical Physics **53** (2012) Art No: 083301

Purnendu Chakraborty, Munshi G Mustafa, D=2 gluon condensate and QCD propagators at finite temperature, Physics Letters **B711** (2012) 390

Raktim Abir, Jet-parton inelastic interaction beyond eikonal approximation, Physical Review **D87** Art No: 034036

Raktim Abir, Umme Jamil, Munshi G Mustafa et al, Heavy quark energy loss and D-mesons in RHIC and LHC energies, Physics Letters **B715** (2012) 183

R Frederix, Manoj K Mandal, Prakash Mathews, et al, Diphoton production in the ADD model to NLO plus parton shower accuracy at the LHC, Journal of High Energy Physics **Issue: 12** (2012) Art No: 102

R Nandi, D Bandyopadhyay, Magnetised neutron star crusts and torsional shear modes of magnetars, J Phys Conf Ser **420** (2013) 012144

R Shyam, K Tsushima, AW Thomas, Production of cascade hypernuclei via the (K-, K+) reaction within a quark-meson coupling model, Nuclear Physics **A881** (2012) 255

Rudranil Basu, Ayan Chatterjee, Amit Ghosh, Local symmetries of non-expanding horizons, Classical and Quantum Gravity **29** (2012) Art No: 235010

S Archambault, E Behnke, P Bhattacharjee et al, Constraints on low-mass WIMP interactions on F-19 from PICASSO, Physics Letters **B711** (2012) 153

Sarmistha Banik, Rana Nandi, Debades Bandyopadhyay, Melting of antikaon condensate in proton-neutron stars, Physical Review **C86** (2012) Art No: 045803

Sarmistha Banik, Rana Nandi, Nucleation of antikaon condensed matter in proto neutron stars, AIP Conf Proc **1441** (2012) 286

Sarmistha Banik, Role of hyperons in black hole formation, J Phys Conf Ser **426** (2013) 012004

Sayan Biswas, JN De, Partha S Joarder, et al, Multifragmentation model for astrophysical strangelets, Physics Letters **B715** (2012) 30

Somdeb Chakraborty, Najmul Haque, Shibaji Roy, Wilson loops in noncommutative Yang-Mills theory using gauge/gravity duality, Nuclear Physics **B862** (2012) 650

Susmita Kundu, Pijushpani Bhattacharjee, Neutrinos from WIMP annihilation in the Sun: Implications of a self-consistent model of the Milky Way's dark matter halo, Physical Review **D85** (2012) Art No: 123533

Tarun Kanti Roy, Avijit Lahiri, Synchronized oscillations on a Kuramoto ring and their entrainment under periodic driving, Chaos Solitons & Fractals **45** (2012) 888

X Roca-Maza, M Brenna, BK Agrawal, et al, Giant quadrupole resonances in Pb-208, the nuclear

symmetry energy, and the neutron skin thickness, Physical Review **C87** (2013) Art No: 034301

5.5 Ph D Awarded

Rana Nandi [Debades Bandyopadhyay], HBNI, Mumbai, November, 2012

5.6 Seminars/Lectures given in Conference/Symposium/Schools

Debades Bandyopadhyay

1. Phase diagram of antikaon condensed matter in compact stars, the conference on Frontiers in Nuclear Physics 2013, Guadeloupe, France, Mar 15, 2013
2. Shear mode oscillations of magnetars and strongly magnetised neutron star crusts, seminar at Institute for Theoretical Physics, Heidelberg University, Jun 5, 2012
3. Strongly magnetised neutron star crusts and shear mode oscillations of magnetars, Nucleus-Nucleus Conference 2012, San Antonio, USA, May 27-Jun 1, 2012

Sarmistha Banik

1. Equation of state for core collapse supernova simulation and neutron star core, Workshop on Young Scientists with Research Interest focused on Physics at FAIR, Hersonissos, Greece, Sept 3-8, 2012
2. Role of hyperon equation of state in core collapse supernova simulation, Workshop on Nuclear Equation of State for Compact Stars and Supernovae, Frankfurt Institute of Advanced Studies (FIAS), Germany, Nov 28-30, 2012

Rana Nandi

1. Shear mode oscillations of magnetars, Workshop on "Nuclear Equation of State for Compact Stars and Supernovae, Frankfurt Institute of Advanced Studies (FIAS), Germany, Nov 28-30, 2012

Pratik Mazumder

1. Cosmic Rays: An Experimental Perspective, XX DAE-BRNS High Energy Physics Symposium, Shantiniketan, Jan 2013
2. Very High Energy Gamma ray Astronomy: A tool to Study the High Energy Universe, IAGRG, Hemwati Nandan Bahuguna University, Garhwal, Mar 2013

Mala Das

International conference on TeV Particle Astrophysics (TeVPA-2012), TIFR, Mumbai, Dec 10-14, 2012

PICASSO collaboration meeting, Queen University Biological station, Kingston, Canada, Jul 31-Aug 1, 2012

Anjan Kundu

1. Unraveling Hidden Possibilities in Integrable Systems, Institute of Theoretical Physics, Hannover University, Germany, June 5, 2012

2. Hidden Directions in Integrable Systems: Classical and Quantum NLSE, Theoretical Physics, University of Wuppertal, Germany, May 24, 2012
3. Modelling rogue waves through exact dynamical lump soliton controlled by ocean currents, Indian Institute of Geo-Magnetism, Mumbai, March 25, 2013
4. Novel Hierarchies & Hidden Dimensions in Integrable Field Models and modelling rogue waves, Theory Group, TIFR, Mumbai, March 28, 2013

Gautam Bhattacharyya

1. Electroweak Symmetry Breaking Beyond the Standard Model: i. Physics Department, TU Dortmund, Germany, May 2012;
ii. Max-Planck-Institut für Kernphysik, Heidelberg, May 2012;
iii. Physics Department, TU Munich, Jun 2012;
iv. Frankfurt Institute for Advanced Studies (FIAS), Frankfurt, Jun 2012;
v. Instituto Superior Técnico, Lisbon, Jul 2012;
vi. Dept of Physics and Technology, Univ of Bergen, Norway, Aug 2012;
vii. Department of Physics, University of Helsinki, Aug 2012;
viii. Department of Physics, TU Dresden, Sep 2012
2. Novel Higgs signatures from S3 flavor symmetry, FLASY12-Workshop on Flavor Symmetries, Dortmund, Jun-Jul 2012
3. Geometrical CP violation and nonstandard Higgs decays: i. International Conference on From Strings to LHC-III, Puri, Dec 2012;
ii. International Conference, KEK-PH 2013, KEK, Japan, Mar 2013;
iii. Physics Department, Niigata University, Niigata, Japan, Mar 2013;
iv. Kavli IPMU, University of Tokyo, Japan, Mar 2013

P Mitra

1. Black Hole Entropy in Quantum Gravity, New Trends in Field Theories III, BHU, Varanasi, Nov 23-26, 2012
2. Black Hole Entropy with and without Log Correction, Light Cone 2012, Delhi University, Delhi, Dec 10-15, 2012

Palash Baran Pal

1. The structure of gauge theories, Workshop on The role of mathematics in theoretical physics, organized by Mathematics Department, Jadavpur University, Jan 11, 2013
2. History and mystery of calendars, Physics colloquium, Instituto Superior Técnico, Lisbon, Nov 21, 2012
3. Bangla Horoph (Bengali Typefaces), 2-day conference on Bengali printing and publishing of 19th and 20th centuries, organized jointly by the Department of Bengali, Jadavpur University and Publication Department, Visva-Bharati University, Mar 19-20, 2013
4. Linguistic consciousness: good or bad?, Conference on Current directions in Linguistics, organized by Department of Linguistics, University of Calcutta, Jan 15, 2013
5. Moulou kona (Elementary particles), Prashanta Chandra Mahalanobish Memorial Lecture given at the Annual Meeting of Science and Technology, organized by the Government of West Bengal, Feb 28, 2013
6. The history and mystery of calendars, Talk at the Children's pavilion of the Indian Science Congress, Jan 5, 2013
7. What is the Higgs boson?:

- i. Talk arranged by the "Gainsayers" and "Samanway" in Nalikul, Hooghly, Sep 22, 2012
- ii. Talk arranged by the "Bhabna" science society in Amta, Howrah, Sep 2, 2012
- iii. Talk given at a public seminar organized jointly by Science City and Saha Institute of Nuclear Physics, held at the Science City, Calcutta, Jul 31, 2012
- iv. Talk given at a public seminar organized by the "Breakthrough Science Society" at Jadavpur University, 28 Jul 2012
- v. Talk given at a public seminar organized by "Howrah Bigyan Bhavna Samanwoy" at Sharat Sadan, Howrah, 22 Jul 2012

Polular Talk:

- 1. Upendrokishor and Sukumar, Public talk at the Annual Science Fair, Jan 31, 2013

Harvendra Singh

Uplifting 5D SYM to 6D and M5-, Isaac Newton Institute, University of Cambridge, Cambridge, UK, Apr 2012

Asit Kumar De

Low lying hadron spectrum and chiral condensate with two flavors of naive Wilson fermions, 30th International Symposium on Lattice Field Theory (Lattice 2012), Cairns, Australia, Jun 24-29, 2012

Bireswar Basu-Mallick

Level density distribution for a class of vertex models related to Haldane-Shastry like spin chains, XXth International Conference on Integrable Systems and Quantum symmetries (ISQS-20), Prague, Czech Republic, Jun 17-23, 2012

Shibaji Roy

Lifshitz metric with hyperscaling violation from string/M theory, International string conference 'ISM 2012', Puri, India, Dec 16-21, 2012

Munshi Golam Mustafa

- 1. Equation of state of hot and dense matter, 20th CBM International Collaboration Meeting, VECC, Kolkata, Sept 24-28, 2012
- 2. Heavy Quark Production and Propagation in heavy-ion collisionss, DAE Symposium on Nuclear Physics, Dec 3-7, 2012, Physics Department, Delhi University, Delhi

5.7 Honours and Distinctions

Gautam Bhattacharyya

- 1. Elected Fellow of Indian National Science Academy, New Delhi (2013)

5.8 Teaching elsewhere

Gautam Bhattacharyya

Special lectures on Electroweak Symmetry Breaking Physics as Mercator Visiting Professor for Masters and Ph D students at TU Dortmund, Jul 2012 (5 lectures)

Palash Baran Pal

1. Neutrino oscillation and level crossing, Refresher course on "Mathematical physics", organized by the Applied Mathematics Department, University of Calcutta, Feb 27, 2013
2. Approximation methods in Statistical mechanics, A series of 4 lectures (90 minutes each) at a refresher course organized by Calcutta University, Jul 17 & Jul 18, 2012
3. The story of calendars, A series of 2 lectures at a refresher course organized by Jadavpur University, Jul 9 & Jul 13, 2012
4. Neutrino physics, A series of 3 lectures (2 hours each) at the Instituto Superior Tecnico, Lisbon 8, 10 and 15 May 2012; part of a course on the Standard Model and beyond

5.9 Miscellany

Anjan Kundu

1. Elected as Member of the Editorial Board of the "Proceedings of the Royal Society (Ser. A), London" for the year : 2012-2014
2. As Humboldt Foundation Scholar visited Germany from 1 May- 30 June, 2012
3. Senior Associate of ICTP, Trieste, Italy (up to 2013)

Gautam Bhattacharyya

MERCATOR Visiting Professor at T.U. Dortmund (funded by DFG, Germany) during 01.04.12 - 30.09.12

5.10 Computational Science

5.11 Summary of Research Activities of Divisions

5.11.1 Computational Science

Studies in the areas of theoretical biophysics and bioinformatics are as follows. Stacking interactions are the most important ones in stabilizing double helical structures of nucleic acids, DNA as well as RNA, however, it is quite poorly understood from the perspective of interatomic/intermolecular interactions. Detailed studies of base pair stacking interactions, in DNA and RNA using Dispersion Corrected Density Functional Theory have been done. This method can reproduce the experimental observations to some extent. In this study variation of three degrees of freedom describing relative orientations of four bases with respect to each other were performed. Monte Carlo simulation using phase space, with classical force-field, to characterize the complete energy landscape are found to be a better representative and are suitable for study of RNA systems with non-Watson-Crick base pairs.

5.11.2 Research Activities

5.11.2.1 125. Modeling the Closed and Open State Conformations of the GABA(A) Ion Channel - Plausible Structural Insights for Channel Gating

Recent disclosure of high resolution crystal structures of *Gloeobacter violaceus* (GLIC) in open state and *Erwinia chrysanthemii* (ELIC) in closed state provides newer avenues to advance our knowledge and understanding of the physiologically and pharmacologically important ionotropic GABA(A) ion channel. The present modeling study envisions understanding the complex molecular transitions involved in.. ionic conductance, which were not evident in earlier disclosed homology models. In particular, emphasis was put on understanding the structural basis of gating, gating transition from the closed to the open state on an atomic scale. Homology modeling of two different physiological states of GABA(A) was carried out using their respective templates. The ability of induced fit, docking in breaking the critical inter residue salt bridge (Glu155 beta(2) and Arg207 beta(2)) upon endogenous GABA docking reflects the side chain rearrangements that occur at the orthosteric site and consolidate the quality of the model. Biophysical calculations like electrostatic mapping, pore radius calculation, ion solvation profile, and normal mode analysis (NMA) were undertaken to address pertinent questions like. the following : How the change in state of the ion channel alters the electrostatic environment across the lumen; How accessible is the Cl⁻ ion in the open state and closed state; What structural changes regulate Channel gating. A "Twist to Turn" global motion evinced at the quaternary level accompanied by tilting and rotation of the M2 helices along the membrane normal rationalizes the structural transition involved in gating. This perceived global motion hints toward a conserved gating mechanism among pLGIC. To paraphrase, this Modeling Study proves to be a reliable framework for understanding the structure function relationship of the hitherto unresolved GABA(A) ion channel. The modeled structures presented herein not only reveal the structurally distinct conformational states of the GABA(A) ion channel but also explain the biophysical difference between the respective states.

RSK Vijayan, Neha Trivedi, Sudipendra Nath Roy, Indrani Bera...Dhananjay Bhattacharyya, Nanda Ghoshal

5.11.2.2 147. Structural Variations of Single and Tandem Mismatches in RNA Duplexes: A Joint MD Simulation and Crystal Structure Database Analysis

Internal loops within RNA duplex regions are formed by single or tandem basepairing mismatches with flanking canonical Watson Crick basepairs on both sides. They are the most common motif observed in RNA secondary structures and play integral functional and structural roles. In this report, we have studied the structural features of 1 x 1, 2 x 2, and 3 x 3 internal loops using all-atom molecular dynamics (MD) simulation technique with explicit solvent model. As MD simulation is intricately dependent on the choice of force-field and these are often rather approximate, we have used both the most popular force-fields for nucleic acids-CHARMM27 and AMBER94- for a comparative analysis. We find that tandem noncanonical basepairs forming 2 x 2 and 3 x 3 internal loops are considerably more stable than the single mismatches forming 1 x 1 internal loops, irrespective of the force field. We have also analyzed crystal structure database to study the conservation of these helical fragments in the corresponding sets of RNA structures. We observe that the nature of stability in MD simulations mimic their fluctuating natures in crystal data sets also, probably indicating reliable natures of both the force fields to reproduce experimental results. We also notice significant structural changes in the wobble G:U basepairs present in these double helical stretches, leading to a biphasic stability for these wobble pairs to release the deformational

strains introduced by internal loops within duplex regions.

Sukanya Halder, Dhananjay Bhattacharyya

5.11.2.3 229. Unraveling siRNA unzipping kinetics with graphene

Using all atom molecular dynamics simulations, we report spontaneous unzipping and strong binding of small interfering RNA (siRNA) on graphene. Our dispersion corrected density functional theory based calculations suggest that nucleosides of RNA have stronger attractive interactions with graphene as compared to DNA residues. These stronger interactions force the double stranded siRNA to spontaneously unzip and bind to the graphene surface. Unzipping always nucleates at one end of the siRNA and propagates to the other end after few base-pairs get unzipped. While both the ends get unzipped, the middle part remains in double stranded form because of torsional constraint. Unzipping probability distributions fitted to single exponential function give unzipping time (τ) of the order of few nanoseconds which decrease exponentially with temperature. From the temperature variation of unzipping time we estimate the energy barrier to unzipping

Santosh Mogurampelly, Swati Panigrahi, Dhananjay Bhattacharyya, AK Sood, Prabal K Maiti

5.11.2.4 275. Effect of temperature on DNA double helix: An insight from molecular dynamics simulation

The three-dimensional structure of DNA contains various sequence-dependent structural information, which control many cellular processes in life, such as replication, transcription, DNA repair, etc. For the above functions, DNA double helices need to unwind or melt locally, which is different from terminal melting, as often seen in molecular dynamics (MD) simulations or even in many DNA crystal structures. We have carried out detailed MD simulations of DNA double helices of regular oligonucleotide fragments as well as in polymeric constructs with water and charge-neutralizing counter-ions at several different temperatures. We wanted to eliminate the end-effect or terminal melting propensity by employing MD simulation of DNA oligonucleotides in such a manner that gives rise to properties of polymeric DNA of infinite length. The polymeric construct is expected to allow us to see local melting at elevated temperatures. Comparative structural analysis of oligonucleotides and its corresponding virtual polymer at various temperatures ranging from 300 K to 400 K is discussed. The general behaviour, such as volume expansion coefficients of both the simulations show high similarity, indicating polymeric construct, does not give many artificial constraints. Local melting of a polymer, even at elevated temperature, may need a high nucleation energy that was not available in the short (7 ns) simulations. We expected to observe such nucleation followed by cooperative melting of the polymers in longer MD runs. Such simulations of different polymeric sequences would facilitate us to predict probable melting origins in a polymeric DNA.

Sangeeta Kundu, Sanchita Mukherjee, Dhananjay Bhattacharyya

5.11.2.5 361. Deciphering the binding mode of Zolpidem to GABA(A) $\alpha(1)$ receptor - insights from molecular dynamics simulation

To investigate the binding mode of Zolpidem to GABA(A) and to delineate the conformational changes induced upon agonist binding, we carried out atomistic molecular dynamics simulation

using the ligand binding domain of GABA(A) alpha(1) receptor. Comparative molecular dynamics simulation of the apo and the holo form of GABA(A) receptor revealed that gamma(2)/alpha(1) interface housing the benzodiazepine binding site undergoes distinct conformational changes upon Zolpidem binding. We notice that C loop of the alpha(1) subunit experiences an inward motion toward the vestibule and the F loop of gamma(2) sways away from the vestibule, an observation that rationalizes Zolpidem as an alpha1 selective agonist. Energy decomposition analysis carried out was able to highlight the important residues implicated in Zolpidem binding, which were largely in congruence with the experimental data. The simulation study disclosed herein provides a meaningful insight into Zolpidem-GABA(A)R interactions and helps to arrive at a binding mode hypothesis with implications for drug design.

RSK Vijayan, Dhananjay Bhattacharyya, Nanda Ghoshal

5.11.3 Developmental Work

5.11.3.1 Hybridized Method by Combining Two Optimization Techniques

We have developed a hybridized method by combining two optimization techniques. One of them is a local search optimization method and the other one is a global search optimization approach namely CAscaded Genetic Algorithm (CAGA). Thus the hybrid genetic method namely Hybrid CAscaded Genetic Algorithm (H-CAGA) which is faster than either of the optimization techniques used for hybridization. The hybrid genetic method (H-GAGA) incorporates slow reduction of the search space according to the user's choice. The algorithm provides the users to choose whether they want to reduce the search space along all dimensions or along a few dimensions at a time. This slow reduction process ultimately improves the convergence rate of the algorithm to a global optimum even for very high dimensional (100) mathematical functions. We have applied H-CAGA in data mining and pattern matching. In both cases we have got competitive results. The genetic algorithm based method has also been used for sequence alignment without incorporation of backtracking for DNA and Proteins. The results comparing with relevant sequence alignment approaches are either similar or better. The algorithm will also be applicable with minor modification for multi-sequence analysis.

Gautam Garai

5.11.4 Publications in Journal

G Garai, Biswanath Chowdhury, A novel genetic approach for optimized biological sequence alignment, *Journal of Biophysical Chemistry* **3** (2012) 201

RSK Vijayan, Dhananjay Bhattacharyya, Nanda Ghoshal, Deciphering the binding mode of Zolpidem to GABA(A) alpha(1) receptor - insights from molecular dynamics simulation, *Journal of Molecular Modeling* **18** (2012) 1345

RSK Vijayan, Neha Trivedi, Sudipendra Nath Roy, Indrani Bera...Dhananjay Bhattacharyya, Nanda Ghoshal, Modeling the Closed and Open State Conformations of the GABA(A) Ion Channel - Plausible Structural Insights for Channel Gating, *Journal of Chemical Information and Modeling* **52** (2012) 2958

Sukanya Halder, Dhananjay Bhattacharyya, Structural Variations of Single and Tandem Mismatches in RNA Duplexes: A Joint MD Simulation and Crystal Structure Database Analysis, *Journal of Physical Chemistry* **B116** (2012) 11845

Santosh Mogurampelly, Swati Panigrahi, Dhananjay Bhattacharyya, AK Sood, Prabal K Maiti, Unraveling siRNA unzipping kinetics with graphene, *Journal of Chemical Physics* **137** (2012) Art No: 054903

Sangeeta Kundu, Sanchita Mukherjee, Dhananjay Bhattacharyya, Effect of temperature on DNA double helix: An insight from molecular dynamics simulation, *Journal of Biosciences* **37** (2012) 445

5.11.5 Seminars/Lectures given in Conference/Symposium/Schools

G Garai, Biswanath Chowdhury, The 3rd International Conference in Engineering Applications of Information Technology (EAIT), Kolkata, India, Nov 29-Dec 1, 2012

Chapter 6

Research Fellows/Visiting Fellows/Research Associates

Computational Sciences Division

- 1 Smt Sanchita Mukherjee : Senior Research Fellow
- 2 Sri Manas Mondal : Senior Research Fellow
- 3 Smt Angana Ray : Senior Research Fellow

Chemical Sciences Division

- 1 Smt Mousumi Banerjee : Senior Research Fellow
- 2 Smt Binita Dutta : Senior Research Fellow
- 3 Smt Moupriya Nag : Senior Research Fellow
- 4 Sm Chaitrali Sengupta : Junior Research Fellow
- 5 Sm Nidhi Agnihotri : Junior Research Fellow
- 6 Sm Sathi Goswami : Junior Research Fellow
- 7 Smt Sreeja Chakraborty : Senior Research Fellow

Biophysics & Structural Genomics Division

- 1 Sri Biswapathik Pahari : Senior Research Fellow
- 2 Smt Saptaparni Ghosh : Senior Research Fellow
- 3 Smt Amrita Banerjee : Senior Research Fellow
- 4 Smt Pritha Bhattacharjee : Senior Research Fellow
- 5 Sm Arijita Mukherjee : Junior Research Fellow
- 6 Sri Manindra Bera : Junior Research Fellow
- 7 Sm Shreyasi Dutta, : Senior Research Fellow
- 8 Smt Nandini Pal Basak : Senior Research Fellow
- 9 Smt Kasturi Roy : Senior Research Fellow
- 10 Smt Suchismita Halder : Senior Research Fellow
- 11 Sri Shounak Baksi : Senior Research Fellow
- 12 Smt Madhurima Mitra : Senior Research Fellow
- 13 Smt Shilpita Karmakar : Senior Research Fellow
- 14 Sri Srijan Haldar : Senior Research Fellow
- 15 Smt Debashree Das : Senior Research Fellow
- 16 Smt Devika Srivastava : Senior Research Fellow
- 17 Sm Rukmini Mukherjee : Junior Research Fellow
- 18 Sm Anita Roy : Senior Research Fellow

Crystallography & Molecular Biology Division

- 1 Smt Jayeeta Ghosh : Senior Research Fellow
- 2 Smt Kamalika RoyChoudhury : Senior Research Fellow
- 3 Smt Eashita Das : Senior Research Fellow
- 4 Smt Kasturi Sengupta (Guha) : Senior Research Fellow
- 5 Sri Sankar Ch. Basu : Senior Research Fellow
- 6 Sri Saurav Roy : Senior Research Fellow
- 7 Smt Barnali Waugh : Senior Research Fellow

- 8 Smt Seema Nath : Senior Research Fellow
- 9 Sri Mahan Ray : Senior Research Fellow
- 10 Smt Rakhi Paul : Senior Research Fellow
- 11 Smt Arpita Saha : Senior Research Fellow
- 12 Sri Supratim Ghatak : Senior Research Fellow
- 13 Sri Pradip Das : Junior Research Fellow
- 14 Sm Sanghati Roy Choudhuri : Junior Research Fellow
- 15 Sm Soumita Mukherjee : Junior Research Fellow

Condensed Matter Physics Division

- 1 Sri Dilip Kumar Bhoi : Senior Research Fellow
- 2 Sri Nazir Khan : Senior Research Fellow
- 3 Sri Arindam Midya : Senior Research Fellow
- 4 Sri Sudipta Mandal : Senior Research Fellow
- 5 Smt Susmita Dhara : Senior Research Fellow
- 6 Smt Moumita Nandi : Senior Research Fellow
- 7 Smt Rajeswari Roy Chowdhury : Senior Research Fellow
- 8 Sri Tapas Paramanik : Senior Research Fellow
- 9 Sri Santanu Pakhira : Junior Research Fellow
- 10 Sri Debashis Samanta : Senior Research Fellow
- 11 Sri Rakesh Chatterjee : Senior Research Fellow
- 12 Sri Asim Ghosh : Senior Research Fellow
- 13 Sri Debarshee Bagchi : Senior Research Fellow
- 14 Smt Mahashweta Basu : Senior Research Fellow
- 15 Smt Paramita Dutta : Senior Research Fellow
- 16 Sri Niladri Sarkar : Senior Research Fellow
- 17 Smt Moumita Dey : Senior Research Fellow
- 18 Smt Srilekha Saha : Senior Research Fellow
- 19 Sri Soumyajyoti Biswas : Senior Research Fellow
- 20 Sourish Bandyopadhyay : Senior Research Fellow
- 21 Sri Amit Dey : Senior Research Fellow
- 22 Sri Atanu Rajak : Senior Research Fellow
- 23 Sri Arijit Chatterjee : Junior Research Fellow
- 24 Sri Gourab Majumder : Junior Research Fellow
- 25 Sri Sabyasachi Nag : Junior Research Fellow
- 26 Sri Sourav Kundu : Junior Research Fellow

Nuclear Physics Division

- 1 Sri Santosh Chakraborty : Senior Research Fellow
- 2 Md Anisur Rahaman : Senior Research Fellow
- 3 Sm Minakshi Roy : Junior Research Fellow

Applied Nuclear Physics Division

- 1 Smt Purba Bhattacharya : Senior Research Fellow
- 2 Sri Hitesh Vijay Rahangdale : Senior Research Fellow
- 3 Sri Rajani Raman : Senior Research Fellow

High Energy Nuclear & Particle Physics Division

- 1 Smt Sreemoyee Sarkar : Senior Research Fellow
- 2 Sri Mahatsab Mandal : Senior Research Fellow
- 3 Ms Debarati Roy : Senior Research Fellow
- 4 Ms Swagata Mukherjee : Senior Research Fellow
- 5 Ms Shilpi Jain : Senior Research Fellow
- 6 Ms Sandhya Jain : Senior Research Fellow
- 7 Sri Sourav Dey : Junior Research Fellow
- 8 Sri Kalyanmoy Chatterjee : Senior Research Fellow
- 9 Sri Atanu Modak : Senior Research Fellow
- 10 Sri Debasish Saha : Senior Research Fellow

Surface Physics Division & Material Science Division

- 1 Sri Sirshendu Gayen : Senior Research Fellow
- 2 Sri Abhisakh Sarma : Senior Research Fellow
- 3 Smt Paramita Chatterjee : Senior Research Fellow
- 4 Sri Safiul Alam Mollick : Senior Research Fellow
- 5 Smt Tanusree Samanta : Senior Research Fellow
- 6 Sri Pabitra Das : Senior Research Fellow
- 7 Smt Manjula Sharma : Senior Research Fellow
- 8 Sri Amaresh Metya : Senior Research Fellow
- 9 Sri Santanu Maiti : Senior Research Fellow
- 10 Sri Jayanta Das : Senior Research Fellow
- 11 Sri Shyamal Mondal : Senior Research Fellow
- 12 Smt Ishani Roy : Senior Research Fellow
- 13 Sri Suvankar Chakraborty : Senior Research Fellow
- 14 Sri Bishnudas Ghosh : Senior Research Fellow
- 15 Sri Kousik Bagani : Senior Research Fellow
- 16 Smt Mala Mukhopadhyay : Senior Research Fellow
- 17 Sri Tanmay Ghosh : Senior Research Fellow
- 18 Smt Debashree Chowdhury : Senior Research Fellow
- 19 Sri Arka Bikash Dey : Junior Research Fellow
- 20 Sri Asish Kumar Kundu : Junior Research Fellow
- 21 Sri Kaustabh Dan : Senior Research Fellow
- 22 Sri Debaleen Biswas : Junior Research Fellow
- 23 Sri Rajendra Prasad Giri : Junior Research Fellow
- 24 Sk Abdul Kader Md. Faruque : Junior Research Fellow

Plasma Physics Division

- 1 Sri Subir Biswas : Senior Research Fellow
- 2 Sri Debabrata Banerjee : Senior Research Fellow
- 3 Smt Anwesa Sarkar : Senior Research Fellow
- 4 Sri Chandan Maity : Senior Research Fellow
- 5 Sri Sudip Garai : Senior Research Fellow
- 6 Sri Abhijit Ghosh : Junior Research Fellow
- 7 Mr Alpha Michael : Junior Research Fellow
- 8 Sri Sourav Pramanik : Junior Research Fellow

Theory Division

- 1 Sri Priti Bhajan Byakti : Senior Research Fellow
- 2 Sri Raktim Abir : Senior Research Fellow
- 3 Sri Santanu Mondal : Senior Research Fellow
- 4 Md Najmul Haque : Senior Research Fellow
- 5 Smt Baishali Chakraborty : Senior Research Fellow
- 6 Sri Arindam Mazumdar : Senior Research Fellow
- 7 Sri Somdeb Chakraborty : Senior Research Fellow
- 8 Sri Pratyay Banerjee : Senior Research Fellow

- 9 Sri Avirup Ghosh : Senior Research Fellow
- 10 Sri Abhishek Chowdhury : Senior Research Fellow
- 11 Sri Dipankar Das : Senior Research Fellow
- 12 Sri Abhik Mukherjee : Senior Research Fellow
- 13 Sri Goutam Das : Junior Research Fellow

Astro Particle Physics & Cosmology Division

- 1 Smt Soumini Chaudhury : Senior Research Fellow
- 2 Smt Susnata Seth : Senior Research Fellow
- 3 Sri Lab Saha : Senior Research Fellow
- 4 Smt Susmita Kundu : Senior Research Fellow
- 5 Sri Mainak Chakraborty : Senior Research Fellow
- 6 Sri Abhishek Majhi : Senior Research Fellow
- 7 Sri Anirban Biswas : Senior Research Fellow
- 8 Sri Debabrata Adak : Senior Research Fellow
- 9 Sri Chandrachur Chakraborty : Senior Research Fellow
- 10 Sri Kamakshya Prasad Modak : Senior Research Fellow
- 11 Sri Amit Dutta Banik : Senior Research Fellow
- 12 Sri Apurba Kheto : Junior Research Fellow
- 13 Sri Prasanta Char : Junior Research Fellow

Senior Research Fellow (EX), Post Doctoral Fellow, Research Associate

- 1 Ratan kumar saha: AMS PDF
- 2 Sreetama Dutta: ANP RA-2
- 3 Mr Subhajit Karmakar: ANP SRF (Extended)
- 4 Debasmita kanjilal: ANP SRF(Extended)
- 5 Prasanna Kumar Mondal: APC PDF
- 6 Dr Richard J Britto: APC PDF
- 7 Amna Ali APC: PDF
- 8 Dr Sangeeta Kundu: BIOPHYSICS RA-II
- 9 Dr Pradipta Kundu: BIOPHYSICS RA-I
- 10 Moumita Gangopadhyay: Biophysics RA-3
- 11 Paramita Bhattacharyya: C&MB PDF
- 12 Mr Ambarnil Ghosh: C&MB PDF
- 13 Prabal Kumar Chakraborty: C&MB RA-1
- 14 Dr Nirmalya Dey: C&MB PDF
- 15 Sudip Majumder: C&MB SRF(Extended)
- 16 Anup Kumar Maity: C&MB SRF(Extended)
- 17 Mr Arnab Basu: CSD SRF(Extended)
- 18 Mr Swadesh Mandal: CSD SRF(Extended)
- 19 Arpita Dutta: CSD RA-1
- 20 Dr Papri Dasgupta: ECMP RA-III
- 21 Rangana Bhattacharyya; ECMP RA-3
- 22 Dr Soumen Das: ECMP RA-3
- 23 Dr Kaushik Sengupta: ECMP PDF
- 24 Biswanath Samantaray: ECMP RA-1
- 25 Mayukh Majumder: ECMP SRF(Extended)
- 26 Deep Talukdar: ECMP RA-1
- 27 Ms Payal Mohanti: HENPP RA-1
- 28 Dr Kushal Das: HENPP PDF
- 29 Anil Pratap Singh: HENPPD RA-3
- 30 Dr Mandira Sinha: NPD RA-II
- 31 Dr Mukhesh Kumar Pradhan: NPD SRF(Extended)
- 32 Krishichayan: NPD RA-3
- 33 Arunabha Chakraborty: SGD SRF(Extended)
- 34 Sourav Kanti Jana: SPD PDF
- 35 Dr Sananda Jana: SPD PDF
- 36 Velaga Srihari: SPD Visiting Fellow
- 37 Rupali kundu: SPD SRF(Extended)
- 38 Subarna Mitra: SPD RA-3
- 39 Sayan Bayan: SPD RA-1
- 40 Sanjoy Kr. Mahata: SPD SRF(ExTd)
- 41 Bibekananda Maji: SPD RA-1
- 42 Satyaki Kar: TCMP RA-3
- 43 Subrat Kumar Das: TCMP visiting scientiest

44 Bhramar Chatterjee: Theory SRF(Extended)
 45 Dr Santosh Kr Singh: Theory RA-2
 46 Munmun Bardhan: CSD RA-3
 47 Mr Manas Kumar Sarangi: CSD SRF(Extended)

UGC Fellow working at SINP

1 Mr Ajoy Mandal: CSD
 2 Ms Ajanta Kundu: ANP
 3 Mr Satyajit Seth: THEORY
 4 Mr Rabindra Seth: CMP
 5 Mr Palash Khan: HENPP
 6 Ms Sumana Sinha: SP&MS
 7 Sm Anupa Majumdar: CSD
 8 Mr Mayukh Kr. Roy: SP&MS
 9 Ch Aminul Islam: THEORY
 10 Sm Banabithi Koley Seth: CSD
 11 Mr Uttam Kr Basak: SP&MS
 12 Mr Souvik Priyam Adhya: HENPP
 13 Md Niyaz Ahmed Rather: HENPP
 14 Mr Subhash Ch Bera: CSD
 15 Ms Avinanda Banerjee: B&SG

CSIR Fellows working at SINP

1 Ms Anuradha Bhattacharya: SPD
 2 Mr Ramanuj Banerjee: C&MB
 3 Mr Srijit Das: C&MB

4 Mr Kaustab Ghosh: CSD
 5 Mr Kallol Bera: CSD
 6 Mr Ankan Dutta Chowdhury: CSD
 7 Mr Sujay Ghosh: CSD
 8 Mr Samik Dutta Gupta: ECMP
 9 Mr Kalipada Das: CMP
 10 Mr Ujjal Kr Gayen: CMP
 11 Mr Avijit Bisoi: NPD
 12 Mr Atanu Kumar: THEORY
 13 Ms Anindita Deb Pal: B&SG
 14 Mr Arpan Bhattacharyya: SPD
 15 Ms Bhawna Gomber: HENPP
 16 Mr Raman Khurana: HENPP
 17 Ms Parijat Dey: (SPM) THEORY
 18 Mr Bijoy Kr. Daga: CMP
 19 Md Moin Shaikh: NPD
 20 Mr Subhendu Rajbanshi NPD
 21 Mr Biswarup Paul: HENPP
 22 Ms Jayati Roy: NPD
 23 Sm Sanchayita Mondal: CMP
 24 Sm Madhumita Choudhuri: SP&MS
 25 Mr Prithwish Dutta: CMP
 26 Sm Priyanka Majumder: B&SG
 27 Sm Sayantani Ghosh: B&SG
 28 Sm Mohar Biplab Sengupta: B&SG
 29 Sm Piyali Mitra: CSD
 30 Sm Neha Rai: C&MB
 31 Sm Sudha Bucha: C&MB
 32 Avik Basu: B&SG

Chapter 7

Facilities

7.1 Centre for Advanced Research & Education

The Centre for Advanced Research & Education (CARE) has been playing a significant role to the academic community of the Institute and to the different parts of West Bengal at large. The CARE was established in the Xth Plan period, with the purpose of initiating motivated and talented students of physics and the biophysical sciences into advanced research. The undergraduate associate (UGA) program involves bright science undergraduates coming to the Institute during vacation periods, taking advanced level courses and doing actual research projects. These programs are continued at substantially higher levels also initiating a program of undergraduate research by the UG associates. Phase III of the CARE plans to cater the growing needs of the outreach programs on different aspects of science to young students and training of the science teachers across the country along with continuation with the existing Summer Students' program, UGA, pre-PhD Post M Sc associateship course, maintenance of the MN Saha Archive, a museum to house old equipments, home-made and custom fabricated in SINP which are of historic values. Since past 55 years or more, Saha Institute of Nuclear Physics (SINP) has been running a one-year long course in Physics and later since past 40 years or more in Biophysical Sciences, at the post M Sc level for students before joining a research for Ph.D degree. This pre-PhD course work has been now made compulsory by the University Grants Commission for every students interested in pursuing research.

The SINP Auditorium Complex is mainly used for holding various programmes, seminars, symposium, conferences national and international stature, etc. 216 Programmes held during 2012-13.

Activities:

1. Post M Sc Teaching Program
2. The Publication & Documentation activities
3. Maintaining and managing the Auditorium complex & the Science Gallery
4. The Meghnad Saha Archive
5. Outreach Programs
6. Undergraduate Associateship Program
7. Summer Students Program
8. Schools/ Workshops/Symposiums/ Colloquiums/Conferences and CARE Seminar
9. Science Day Celebration with Visits to / of Undergraduate Colleges, High Schools

Some of the programs organized by the CARE in 2012-13

Science Exhibition/Fair:

National Integrity Festival and Gandhi Mela 2012, Ramlila Maidan, organized by Ekabinsha, April 7-13, 2012

16th National Exhibition, Nazrul Maidan, Baguiati, organized by Central Calcutta Science & Culture Organization for Youth, Sept 7-11, 2012

9th Jatiya Sanhati Utsav-o-Bharat Mela, 2012, Gobinda Nagar High School Ground, Canning, South 24 Parganas, Dec 8-15, 2012

Sundarban Kristi Mela O Loko Sanskriti Utsab, Kultali Milon Tirtha Society, Kultali, P.S. Basanti, South 24 parganas, Dec 20-29, 2012

Sundarban Lokopriya Utsav by Sundarban Unnayan Niketan at Sonakhali Bazar, Vill & PO- Sonakhali, PS- Basanti, South 24 parganas, Jan 23-30, 2013

Outreach Program:

Outreach on Water & Life organized jointly by CARE & Bangiya Bijnan Prasar Mancha (BBPM), Sept 25, 2012

Theme talks on water by Prof Milan K Sanyal, Director, SINP and Dr Kalyan Rudra, River Scientist. There were prizes for Creative Poster and Extempore Speech Competition for school students. Students of Prafulla Kanan Deshapriya Vidyamandir, Lake Town Govt, Sponsored Girls High School, Bamunpara Anchalik High School, Laban Hrada Vidyapith, Deshapriya Balika Vidyamandir, Krishnapur Adarsha Vidyamandir were the participants.

Awareness Programme:

Program on Cancer Awareness organized by CARE and Indian Cancer Society on Oct 5, 2012
Speakers: Dr Arunava Sengupta, Dr Sanjoy Kr Das, Dr T Mandal

Institute Laboratory Visited by the Students of Other Institute/University

Students of Kathmandu Univ, Dhulikhel, Kavre, Nepal, Dept of Natural Science (Physics) visited SINP Labs with their Professor Dr Dipak Raj Adhikari, Oct 30, 2012

18 students and 3 teachers of Kamrup College (P.O. Baihata Chariali Kamrup, Assam) visited SINP Labs, Nov 5, 2012

Seminar/Lecture/School Organised:

International School on Nanoscience with X-ray and Neutron Sources organized jointly by CEN-SUP and CARE, July 23-24, 2012

CARE Seminar on Kinesin-2 based transports in the axons and cilia by Krishanu Ray, Nov 30, 2012

Bengal Science Lecture & Sattalite Conference on 100 years of Science in India, organized by West Bengal State Council of Science and Technology & CARE, SINP, Jan 9-10, 2013

The satellite programme includes:

- (1) Lectures by eminent scientists
- (2) Panel Discussion

(3) Contributed papers (oral & poster)

7.1.1 The Post-M Sc Associateship Course

PHYSICS:

59th Session (2011-12) **THIRD TERM:** [Student, Review Title (Supervisor)]

1. Abhijit Ghosh, Solitons and Branes in string/M theory (Harvendra Singh)
2. Alpha Michael Wharton, Nonlinear Dynamical modelling and Time series Analysis of Plasma Oscillations (ANS Sekar Iyengar)
3. Apurba Kheto, Superfluidity in neutron star matter (Debades Bandyopadhyay)
4. Arijit Chatterjee, Universality classes in Non-equilibrium phase transitions (PK Mohanty)
5. Arka Bikash Dey, Electron Ordering in low-dimensional materials (Milan K Sanyal)
6. Arnab Roy, Shell Model studies of neutron rich nuclei (Theoretical Project) (Maitreyee Saha-Sarkar)
7. Arup Singha Roy, Study of electro deposited polyelectrolyte thin films (Manabendra Mukherjee)
8. Asish Kumar Kundu, Growth, Structure and Electronic Structure of Epitaxial Cr(100) Ultra-thin Films on Ag(100) substrate (Krishnakumar SR Menon)
9. Debaleen Biswas, Application of ultra-thin gate dielectric materials to metal-oxide-semiconductor (MOS) devices (Supratic Chakraborty)
10. Gourab Majumder, Search for Topological Mott Insulators (Arti Garg)
11. Goutam Das, Next-to-leading order in QCD (Prakash Mathews)
12. Minakshi Roy, Decay properties of exotic nuclei near drip line (Ushasi Datta Pramanik)
13. Prasanta Char, Physics of core collapse supernova (Debades Bandyopadhyay)
14. Rajendra Prasad Giri, Study of Quantum Spin Liquids (Arti Garg)
15. Sabyasachi Nag, Localization of Dirac Particles in Honey comb Lattice (Arti Garg)
16. Sagnik Chakraborty, Identification of Electrons/Photons in the CMS detector (Satyaki Bhattacharya, Subir Sarkar, Sunanda Banerjee)
17. Santanu Pakhira, Geometrically frustrated magnetism in intermetallic system (Chandan Mazumdar)
18. Santu Manna, Spin Caloric Transport (Indranil Das)
19. Sk Abdul Kader Md Faruque, Influence of composition of gate dielectric materials on the interface properties of metal-oxide-semiconductor (MOS) devices (Supratic Chakraborty)
20. Sourav Dey, Study of simplified Parametrization of Hadronic Showers in the Fast Simulation Software of CMS (Satyaki Bhattacharya, Subir Sarkar, Sunanda Banerjee)
21. Sourav Kundu, Non Local electrical transport and non local magnetoresistance in nanostructure (Indranil Das)
22. Sourav Pramanik, Parametric Instability: An application in Plasma Physics (Nikhil Chakrabarti)
23. Suraj Kumar Karmakar, Surface Plasmon based Photonics (Tapas Kumar Chini)

The following 23 Physics students have successfully completed the course:

1. Abhijit Ghosh, 2. Alpha Michael Wharton, 3. Apurba Kheto, 4. Arijit Chatterjee, 5. Arka Bikash Dey, 6. Arnab Roy, 7. Arup Singha Roy, 8. Asish Kumar Kundu, 9. Debaleen Biswas, 10. Gourab Majumder, 11. Goutam Das, 12. Minakshi Roy, 13. Prasanta Char, 14. Rajendra Prasad Giri, 15. Sabyasachi Nag, 16. Sagnik Chakraborty, 17. Santanu Pakhira, 18. Santu Manna, 19. Sk

Abdul Kader Md Faruque, 20. Sourav Dey, 21. Sourav Kundu, 22. Sourav Pramanik, 23. Suraj Kumar Karmakar

7.1.1.1 60th Session (2012-13)

The following (Physics) students have joined on 1st August 2012 for the session 2012-13: 1. Achyut Maity, 2. Amrita Ghosh, 3. Anshu Chatterjee, 4. Aritra bandyopadhyay, 5. Arpan Maiti, 6. Ashim Roy, 7. Barnamala Saha, 8. Binita Mandal, 9. Chiranjib Mandal, 10. Chitraklekha Datta, 11. Debajyoti Saha, 12. Gouranga Manna, 13. Kumar Das, 14. Kuntal Mondal, 15. Kuntal Nayek, 16. Md. Ali Asgar (Release on 31-08-2012), 17. Mily Kundu, 18. Naosad Alam, 19. Pankaj Kumar Shaw, 20. Sabuj Ghosh, 21. Sanjib Banik, 22. Sanjukta Paul, 23. Satyajit Chowdhury, 24. Sayanee Jana, 25. Sruti Datta, 26. Sudip Mukherjee, 27. Sukanta Barman, 28. Sultana Tajmili Hasnahena, 29. Suvankar Roy Chowdhury, 30. Tapash Ghosh, 31. Tirthankar Banerjee

First Term

Courses: Teachers

Statistical Mechanics: Abhee Kanti Dutt-Mazumder

Condensed Matter Physics: Sangam Banerjee & Sachin Karmakar

Plasma Physics: Nikhil Chakrabarti & Janaki Sita Mylavarapu

Nuclear Physics: Chinmay Basu

Quantum Mechanics: Asit K De

Field Theory: Parthasarathi Mitra

Second Term

1. A course on C++ (Satyaki Bhattacharya & Subir Sarkar), 2. Experimental techniques (Palash Baran Pal), 3. Particle physics (Prakash Mathews), 4. Condensed matter physics (Sudhakar Yarlagaadda), 5. Surface techniques (Milan Kumar Sanyal), 6. Quantum Field Theory (Harvendra Singh), 7. Differential & Riemannian Geometry (Amit Ghosh), 8. Soft Matter (Alokmay Datta), 9. Astroparticle physics (Pratik Majumdar & Debashis Majumdar), 10. Non-linear Dynamics (I.N. Sekar Iyenger), 11. Plasma physics (M Sita Janaki & Nikhil Chakrabarti)

Biophysical Sciences

59th Session 2011-12 Third Term

REVIEW: [Students, Review Title (Supervisor)]

Sathi Goswami, B-cyclodextrin: Inclusion complexes with Non Steroidal Anti-Inflammatory drugs (NSAIDs) and uses as drug delivery system (Munna Sarkar)

Soumita Mukherjee, Role of Post-translational modifications in initiation of DNA replication, (Partha Saha)

Manindra Bera, Biomechanics and Proteomics of Lamine A (Kaushik Sengupta)

Arijita Mukherjee, Exosomes and their emerging roles in cancer immunosuppression (Subrata Banerjee)

Chaitrali Sengupta, Ultrafast fluorescence spectroscopy in photo-induced charge transfer reaction in biological macromolecules (Samita Basu)

Nidhi Agnihotri, Synthesis and characterization of Graphene based Conducting Polymer Composites for their Application in Electrochemical Capacitors and Biosensors (Amitabha De)

Rukmini Mukherjee, Mitochondrial Dysfunction in Neurodegenerative Disease (Oishee Chakrabarti)

Sanghati Roy Choudhuri, A Peptidyl prolyl isomerase SurA having chaperone activity: Structural and functional Studies (Udayaditya Sen)

Pradip Das, Role of Non-Coding RNAs in DNA Replication (Partha Saha)

Sudha Bucha, REST/NRSF mediated transcriptional regulation in Huntington disease (Nitai Pada Bhattacharya)

The following Ten (10) students have successfully completed the Post-M Sc Biophysical Sciences course in the 2011-2012 session:

1. Arijita Mukherjee 2. Chaitrali Sengupta 3. Manindra Bera 4. Nidhi Agnihotri 5. Pradip Das 6. Rukmini Mukherjee 7. Sanghati Roy Choudhuri 8. Sathi Goswami 9. Soumita Mukherjee 10. Sudha Bucha.

The following (Biophysical sciences) students have joined on 1st August 2012 for the session 2012-13:

1. Archisman Ghosh 2. Debasish Mukherjee 3. Isha Sengupta 4. Kamalendu Pal 5. Malti Yadav 6. Piyali Majumder 7. Sabyasachi Sen 8. Sourav Ghoshal 9. Tapas Paul 10. Zenia Kaul

1. Biomolecular structure (20 lectures by Munna Sarkar, Rahul Banerjee and Dhananjay Bhattacharyya):

Biomembrane: structure & dynamics, biomembrane transport External and internal coordinate system, non-covalent interactions stabilizing biomolecules, Proteins, amino acids, peptide, secondary tertiary, quaternary structure of protein, Nucleic acids, Watson-Crick and non-Watson Crick base-pair, DNA double helical and multistranded structures, RNA structural features

2. Chemical Biology (20 lectures by Dipak Dasgupta and Abhijit Chakrabarti):

Basic Biochemistry - glycolysis, lipid synthesis, amino-acid synthesis, chemical thermodynamics and enzyme kinetics

3. Basic Molecular Biology (20 lectures by Partha Saha and Kaushik Sengupta):

Biological Processes: Replication, Transcription, Translation, and related things Technique in molecular biology: DNA detection, RNA detection, Protein detection, cloning, PCR, and related methods

4. Cell Biology (20 lectures by Subrata Banerjee and Oishee Chakrabarti):

Cell as unit, identification, characterisation, function of cellular organelles, Golgi, ER, lysozome, mitochondria, cell-membrane, cell-cell communication, cell-signalling, basic of immune system (20 lectures)

5. Biophysical Techniques (30 lectures by Samita Basu, Padmaja Misra, Mantu Hazra, Udyaditya Sen and Sampa Biswas):

Spectroscopy: absorption, emission, excited state properties, acidity, basicity, polarization, anisotropy, solvent relaxation, quenching, energy transfer, electron transfer, Circular dichroism, Infrared spectroscopy, FTIR, Raman spectroscopy

Microscopy: light microscopy, confocal microscopy, atomic force microscopy, electron microscopy

Basics of Crystallography: Crystals, lattice, symmetry, Braggs law, Reciprocal lattice, Ewald sphere; Structure factors: Atomic scattering factor, temperature factor, structure factor calculation;

Data collection: Technique & strategy, data processing, extinctions & space group determination;

Phase problem and electron density calculation: phasing techniques like MR, MIR, MAD, etc;

Fiber Diffraction & Virus Crystallography and Model building & refinement.

6. Computer Programming and Application (40 lectures by Pulak Ray and Dhananjay Bhattacharyya):

Algorithm and flow-chart, FORTRAN programming, Molecular modelling software, basic statistics, regression and curve-fitting

7. Radiation Physics and Chemistry (20 lectures by Maitryee Nandy and Sushanta Lahiri):

Rad, Rem, LET, etc, Interaction of radiation with matter/biological materials, Bethe-Bloch, dosimetry, etc. Free-radicals, quantum yield, G-value, etc.

8. Molecular Genetics (20 lectures by Nitai Pada Bhattacharya, Debashis Mukhopadhyay and Chandrima Das):

DNA as genetic material, Mendelian genetics, Bacterial genetics, recombination, DNA damage and repair, mutation, transposon, Human genetics, genetic markers and epigenetics

B) Advanced optional course:

1. Topics in Cell Biology (Oishee Chakrabarti and Kaushik Sengupta)
2. Cell Cycle, Signaling & Stem Cell Biology (Sanghamitra Raha/ Partha Saha/Subrata Banerjee)
3. Chemical Biology of Chromatin & Epigenetics (Dipak Dasgupta/Chandrima Das)
4. Modern Spectroscopic Methods and Applications (Mantu Hazra/ Samita Basu)
5. Neurobiology (Debashis Mukhopadhyay/ Nitai Pada Bhattacharyya)
6. Advanced Imaging Techniques (Padmaja Misra/Pulak Ray)
7. Biomolecular Simulations (Dhananjay Bhattacharyya)
8. Polymer Chemistry (Amithabha De)
9. Protein Folding (Soumen Basak)
10. Chemical Biology of Chromatin & Epigenetics (Dipak Dasgupta/Chandrima Das)
11. Drug Design (Munna Sarkar)
12. Macromolecular Crystallography (Udayaditya Sen/ Samita Basu)

7.1.2 Summer Students' Programme

Summer Students in 2012 [Name, Affiliation (Supervisor/Mentor)]

1. Kaushik Roy, IISER Bhopal (Harvendra Singh)
2. Kushagra Nigam, BITS Pilani, Goa (Debasish Majumdar)
3. Abhisek Samanta, IIT Kanpur (Ambar Ghosal)
4. Amartya Dutta, IIT Kanpur (Sunanda Banerjee)
5. Puja Banerjee, IIT Kanpur (Padmaja Mishra)
6. Manoj K. Hansda, IIT Bombay (Alokmay Datta)
7. Jitendra Gurjar, IISER Bhopal (Partha Saha)
8. Apurba Bera, IIT Kharagpur (Satyaki Bhattacharya)
9. Anirudh Chandra, NIT Trichy (Maitreyee Saha Sarkar)
10. Khyati Malhan, University of Delhi (ANS Iyenger)
11. Pallabi Das, IIT Kharagpur (Nikhil Chakraborty)

12. Rahul Nag, IIT Kanpur (Padmaja Mishra)
13. Animik Ghosh, University of Delhi (Subir Sarkar)
14. Smruti R. Shao, ISM Dhanbad (Dhananjay Bhattacharyya)
15. Nikhil N. Narain, Pondicherry University (Subir Sarkar)
16. Arindam Nandi, IISER Kolkata (Sankar De)
17. Cuckoo Varkey K, Loyola College, Chennai (Mala Das)
18. Arindam Ray, University of Calcutta (Debasish Mukhopadhyay)
19. Pragati Mitra, IIT Hyderabad (Debasish Majumdar)

7.1.3 Under Graduate Students' Programme

Undergraduate Associates in 2012 [Name, Affiliation (Supervisor/Mentor)]

1. Ms Krithika Raman, Stella Maris College, Chennai (Maitreyee Saha Sarkar)
2. Ms Namrata Dutta Majumdar, St. Stephen's College, Delhi (Satyaranjan Bhattacharyya)
3. Mr Saikat Bera, IISER Pune (Biswarup Satpati)
4. Mr Upamanyu Moitra, Jadavpur University (Pradeep K Mohanty)
5. Ms Payel Mukhopadhyay, IISER Kolkata (Debades Bandyopadhyay)

7.2 Electron Microscope Facility

The Electron Microscope Facility is working as a central facility and equipped with a 200keV Transmission Electron Microscope and a 300keV Field Emission Gun Transmission Electron Microscope. The facility caters to the researchers from Biological Sciences and Material Sciences both. Biophysics Div., Chemical Sc. Div., C & MB Div. and Structural Genomic Div. used the facility to study biological samples like bacteria & their thin section, lipid vesicles, detergent micelles, lipid-protein complexes, peptide aggregation etc. 14 faculty members of our Institute used the facility for Biological samples. ECMP, Surface Physics, Applied Material Sciences and Applied Nuclear Physics Div. used the facility to study material sciences samples like nanomaterials, metal oxides, nanocrystalline solids etc. 11 faculty members of our Institute used the facility for Material science related samples. 6 scientists from VECC also used the facility during this period. Other research institutes and universities e.g. NIT-Rourkela, UGC-DAE, IACS, BIT-Meshra, ISI, Jadavpur University, S.N.Bose, NIT-Durgapur, Kalyani University, St. Xaviers College, Presidency College, Benaras Hindu University, IICB and IISER-Kolkata used the E.M. Facility extensively. The 200kV TEM has been utilized more than 70 % of the available days. More than 11 publications have come out in the reputed scientific journals, contributed by different scientists using the 200keV Transmission Electron Microscope during this period.

7.3 Library

Main activities:

The Library of SINP is one of the major information resource centres within Eastern India in the field of Physical and Biophysical Sciences. It is privilege to support the institutes march towards its vision- to be the pioneer research Institute of India. Through our well equipped and digitized library, the members of our institution and the other members associated with our research and

development program are being benefited and this will assist towards scientific development of our Institute and the country at large.

The Library not only acquires, organizes and disseminates knowledge; it has put its foot ahead towards policies and procedures, systems and services. The details of our library are given below.

Collection: The library of SINP is one of the leading science-library within Eastern Region. In addition to huge collection of books and e-books on science and technology it also subscribe more than 264 leading journals in the field of physical, chemical and biophysical sciences. Library has a huge collection of books, e-books and non-book materials. The details are given below:

Books: 35435 (technical - 31481 + non-technical- 3954 [182 books are added in this year]

E- books: 1000+

Bound volumes of journals: 51463

Current subscribed journals: 264 (Foreign 207 + Indian 57)[12 titles added in this year]

Online journals: 3000+

Reports: 26000+

Number of CD/DVD Rom: 1021

Thesis: 200

Major items/equipments available:

Library has two IBM servers where Libsys 4 (Rel 6.2 upgraded version) database is running.

30 Pcs are in the library out of 20 are for library user.

One hp Design jet plotter printer & one Canon plotter printer.

One hp colour printer

3 hp black & white printers.

Six Xerox machines cum printers (black & white).

One colour Xerox cum network printer (Sharp).

Three lamination machines.

Three scanner & one spiral binding machine.

Membership:

In addition to our 785 institute members (faculties, fellows and non academic), library has the privilege to serve near about six hundred (593) users coming from different scientific and educational institutes of Eastern India. The list of external users includes Calcutta University, Jadavpur University, Viswa Bharati, IACS, IICB, ISI, Bengal Engineering and Science University, WBUT, CMERI, Guwahati University, North East Hilly University, Patna University etc. apart from numerous Under-Graduate/Post-Graduate colleges and project students Number of members & types of facilities are available for each category of members: (A) SINP members (Total No. 681 academic 446, others 235) (1) Borrowing facility (2) Xerox facility (3) Inter-library-loan (4) Online searching & downloading.

(B) VECC members (No. 104) (1) Borrowing facility (2) Online searching & downloading

(C) External members (No. 593) (1) Reading room facility for reference use (2) Xerox facility against payment (3) Online searching & downloading

(D) Institutional Members (1) Reading room facility for reference use (2) Borrowing facility (3) Online searching & downloading (4) Poster printing facility Online facilities implemented through XI plan project: Successfully our library has implemented the online and archival facilities of various journals of the following publishers from XI plan project grant (LDER). More than 3000 online journals as well as online archives (full-text pdf) from our site:

1. Institute of Physics, London 2. American Institute of Physics 3. American Physical Society 4. American Chemical Society 5. John Wiley online library 6. World Scientific 7. Springer 8. Taylor

& Francis 9. Science Classic 10. Nature Publishing Group 11. Cambridge University Press 12. Royal Society of Chemistry 13. Royal Society of London 14. Oxford Library has the online e-books collection of Annual Reviews, Lecture Notes in Physics (volume 1 - 475) and 500 e-books of T&F, CUP, Wiley and World Scientific. Currently the library is subscribing Web of Knowledge & Science Citation Index from 1945 to current, JSTOR (Mathematics & Statistics), Scopus from Elsevier and Springer protocols database.

7.4 Central Workshop

A technical team from the Workshop is closely associated with Institute scientists working in LHC, CERN, Geneva. SINP Workshop has modified the Cradle movement system of the Second Muon Tracking Station of ALICE. Specially designed platform for detector assembly and other accessories have also been developed and installed at CERN by the said team. Workshop has installed a 5.0 meter diameter Observatory (Sirius make College model) on the rooftop of the Institute main building for Astroparticle Physics and Cosmology Division. A large number of precision machining jobs have been completed in Computerized Numerical Control (CNC) machining environment and conventional machining section of the Workshop. Nano x-ray beam deflector cell, Ion-beam focusing column, Dielectric cell with cryostat and Motorized probe movement arrangement for plasma device are some of the interesting jobs designed and fabricated in the said period. Altogether Machining and fitting section completed 355 jobs, Welding section completed 42 jobs and Glass blowing section fabricated 190 jobs during this period. Drawing and design section completed 34 jobs including various designs, computer aided drawings, tracing graphs and posters. Five trade apprentices passed the All India Trade Test after completion of their training from the Workshop. As and when approved by the Institute authority, Workshop has also provided technical services to Variable Energy Cyclotron Centre, Bose Institute and other premier research organizations in and around Kolkata.

Chapter 8

Administration

8.1 Governing Council

Chairman:

Dr RK Sinha
Chairman, Atomic Energy Commission &
Secretary to the Government of India
Department of Atomic Energy, Mumbai

Members:

Prof Dhrubajyoti Chattopadhyay
Pro Vice-Chancellor (Academic)
University of Calcutta
Kolkata

Prof PK Kaw
Director
Institute for Plasma Research
Near Indira Bridge Ghat
Gandhinagar

Shri Satish Chandra Tewary, IAS
Principal Secretary,
Higher Education Department
Government of West Bengal
Kolkata

Prof Mustansir Barma
Director
Tata Institute of Fundamental Research
Mumbai

Shri PR Baviskar
Joint Secretary (R&D) to the
Government of India
Department of Atomic Energy
Mumbai

Shri VR Sadasivam
Joint Secretary (Finance)
Govt of India and
Department of Atomic Energy
Mumbai

Prof Susanta Sen
Professor
Institute of Radiophysics & Electronics,
Deputy Director
Centre for Research in Nanoscience & Nanotechnology
University of Calcutta
Kolkata

Prof Amitava Raychaudhuri
Palit Professor of Physics
University of Calcutta
Kolkata

Prof Milan K Sanyal
Director
Saha Institute of Nuclear Physics
Kolkata

Mr VV Mallikarjuna Rao (Ex-Officio Secretary)
Registrar
Saha Institute of Nuclear Physics
Kolkata

8.2 Audited Accounts

8.3 Balancesheet

SAHA INSTITUTE OF NUCLEAR PHYSICS

Balance Sheet as at 31st March, 2013

	Schedule	2012-13	2011-12
<u>CAPITAL FUND & LIABILITIES</u>			
CAPITAL FUND	1	708815201.33	447,050,420.38
CAPITAL RESERVE	2	7116996.30	7,116,996.30
EARMARKED FUNDS	3	10498421.00	28,407,395.00
CURRENT LIABILITIES AND PROVISIONS	4	2798198561.07	2,880,426,010.92
TOTAL		3524629179.70	3363000822.60
<u>ASSETS</u>			
FIXED ASSETS			
Gross Block	5	3703492767.23	3,371,943,886.26
Less : Accumulated Depreciation	5	1617512127.35	1339150305.66
		2085980639.88	2032793580.60
INVESTMENT	6	63510000.00	20824200.00
CURRENT ASSETS, LOANS & ADVANCES	7	1375138539.82	1309383042.00
TOTAL		3524629179.70	3363000822.60
SIGNIFICANT ACCOUNTING POLICES	15		
CONTINGENT LIABILITIES AND NOTES ON ACCOUNTS	16		

The Schedules referred to above form part of these Accounts



(V. P. Mishra)
Accounts Officer



(N. Sanyal)
Dy. Controller of Accounts



(V.V. Mallikarjuna Rao)
Registrar

In terms of our attached Report of even date
For K. Sharma & Co
Chartered Accountants

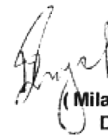


(K. K. Sharma)
Partner

Membership No. 005313

1/B, Old Post Office Street, Room No.8, (First Floor),
Kolkata - 700 001

Dated :- 10th October, 2013



(Milan K. Sanyal)
Director


8.4 Income & Expenditure Account for the year ended March 31, 2013

SAHA INSTITUTE OF NUCLEAR PHYSICS

Income & Expenditure Account for the year ended 31st March, 2013

	<u>Schedule</u>	<u>2012-13</u>	<u>2011-12</u>
INCOME : -			
Income from Sales/Services	8	347270.00	735190.00
Grants	9	982922773.03	465910761.25
Interest Earned	10	23013196.00	57279374.00
Other Income	11	5766192.20	3984941.00
Excess of Expenditure over Income transferred to Capital Fund			620420956.35
		<u>1012049431.23</u>	<u>1148331222.60</u>
EXPENDITURE : -			
Establishment Expenses	12	353321367.80	641413051.00
Administrative Expenses	13	270184179.51	228466429.32
Interest/Bank charges	14	34844.25	52893.00
Depreciation	5	278361821.69	278398849.28
Excess of Income over Expenditure transferred to Capital Fund		110147217.98	
		<u>1012049431.23</u>	<u>1148331222.60</u>

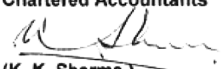
The Schedules referred to above form part of these Accounts


(V. P. Mishra)
Accounts Officer


(N. Sanyal)
Dy. Controller of Accounts


(V.V. Mallikarjuna Rao)
Registrar

In terms of our attached Report of even date
For K. Sharma & Co
Chartered Accountants


(K. K. Sharma)
Partner


Membership No. 005313
1/B, Old Post Office Street, Room No.8, (First Floor),
Kolkata - 700 001
Dated :- 10th October, 2013

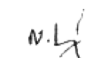

(Milan K. Sanyal)
Director

8.5 Receipts & Payments for the year ended March 31, 2013

SAHA INSTITUTE OF NUCLEAR PHYSICS

Receipts & Payments Account for the year ended 31st March, 2012					
Receipts	2011-12	2012-13	Payments	2011-12	2012-13
Opening Balance b/f :-					
Cash in hand	198,788.00	68,284.00	Establishment Expenses	499,997,051.00	555,245,249.80
Current Account Balances	418,018,075.30	652,190,811.03	Administrative Expenses	226,093,003.32	266,990,602.51
			Bank Charges	30,878.00	34,844.25
Grant-in-aid received from DAE :-			Assets	590,484,702.36	331,548,880.97
Recurring	587,700,000.00	611,200,000.00	Expenses paid for ongoing projects of other agencies	100,300,489.80	61,491,706.35
Non-Recurring	514,200,000.00	325,000,000.00	HBA & Other Advances paid	1,267,166.00	1,555,885.00
			Investment	4,915,644.00	60,000,000.00
Grant received from other agencies			Margin Money deposit	506,103,600.00	134,923,177.00
for on going projects	119,296,672.14	376,446,264.00	Other Deposit	211,500.00	250,143,000.00
HBA & Other Advance recovery	3,614,089.00	2,976,262.00	Advances paid	57,347,015.93	
Realisation of Margin Money Deposit	551,613,770.00	322,225,095.00	Last Year's provision paid	2,009,267.00	2,845,316.00
Realisation from other Deposit	355,000,000.00	17,314,200.00	Last Year's current liabilities paid		3,654,621.00
Realisation of other advances		68,255,191.33	Pension Fund Payments		9,627,100.00
Interest Received	57,279,374.00	23,013,196.00	Closing Balance c/f :-		
Income Receipts	4,720,131.00	6,113,462.20	Cash in hand	68,284.00	7,784.00
Current Liabilities	23,916,337.00		Current Account Balances	652,190,811.03	727,285,084.68
Pension Fund Receipts	5,462,176.00	550,486.00			
	2,641,019,412.44	2,405,353,251.56		2,641,019,412.44	2,405,353,251.56


(V. P. Mishra)
Accounts Officer



(N. Sanyal)
Dy. Controller of Accounts


(V.V. Mallikarjuna Rao)
Registrar


(Mijan K. Sanyal)
Director

In terms of our attached Report of even date

For K. Sharma & Co
Chartered Accountants


(K. K. Sharma)
Partner

Membership No. 005313

1/B, Old Post Office Street, Room No.8, (First Floor),
Kolkata - 700 001

Dated :- 10th October, 2013

8.6 Purchase Section

Order Placed by Purchase Section

Year	Domestic Order
2012-13	1021
Year	Foreign Order
2012-13	55

8.7 Members of the Institute [As on March 31, 2013]

Prof Milan Kumar Sanyal: Director

DIRECTOR'S OFFICE

- 1 Sri Amalesh Chandra Saha: AO(DO)
- 2 Sri Jeevan Shaw: AAO (DO)
- 3 Sri Subhasish Ghoshal: Superintendent
- 4 Sri Goutam Mandal: Superintendent
- 5 Sri Babu Rajak: Helper 'C'

REGISTRAR'S OFFICE

- 1 Sri VV Mallikarjuna Rao: Registrar
- 2 Shri Biplab Kumar Ray: AAO(E-I)
- 3 Sri Bimlesh Kr Tripathi: Senior Hindi Translator
- 4 Shri Bibekbijay Bandyopadhyay: Superintendent
- 5 Shri Aditya Dhara: Lower Division Clerk
- 6 Sri Rudal Prasad Ram: Technician 'D'
7. Sri Mahadev Das: Caretaker-'E'

Academic Departments and Divisions

ASTROPARTICLE PHYSICS & COSMOLOGY (APC)

- 1 Prof Pijushpani Bhattacharjee: Sr Professor 'H' & HOD
- 2 Prof Debades Bandyopadhyay: Professor 'G'
- 3 Prof Debasish Majumdar: Professor 'G'
- 4 Prof Ambar Ghosal: Professor 'G'
- 5 Dr Mala Das: Associate Professor 'E'
- 6 Dr Pratik Majumder: Associate Professor 'E'
- 7 Shri Nilanjan Biswas: Scientific Assistant 'B'

THEORY DIVISION

- 1 Prof Anjan Kundu: Sr Professor 'H+'
- 3 Prof Parthasarathi Mitra: Sr Professor 'H+'
- 4 Prof Avaroth Harindranath: Sr Professor 'H+'
- 5 Prof Polash B Pal: Sr Professor 'H+'
- 6 Prof Asit Kr De: Sr Professor 'H' & HOD
- 7 Prof Kumar Sankar Gupta: Sr Professor 'H'
- 8 Prof Sibaji Roy: Sr Professor 'H'
- 9 Prof Gautam Bhattacharyya: Sr Professor 'H'
- 10 Prof Munshi Golam Mustafa: Professor 'G'
- 11 Prof Bireswar Basu Mallick: Professor 'G'
- 12 Prof Prakash Mathews: Professor 'G'
- 13 Prof Harvendra Singh: Professor 'G'
- 14 Prof Bijay Kr Agrawal: Professor 'G'
- 15 Prof Amit Ghosh: Professor 'G'
- 16 Smt Sangita Pande: Scientific Assistant 'B'
- 17 Sri Prodyut Kr Mitra: Technician 'E'
- 18 Sri Sudarshan Hazra: Technician 'A'
- 19 Sm. Dola Mallick: Superintendent
- 20 Sri Arun Kr Bose: Helper 'E'

PLASMA PHYSICS DIVISION

- 1 Prof ANS Iyengar: Sr Professor 'H'
- 2 Prof Mylavarapu Sita Janaki: Professor 'G' & HOD
- 3 Prof Nikhil Chakraborty: Professor 'G'
- 5 Sri Shantanu Chowdhury: Engineer 'F'
- 6 Sri Parthasarathi Bhattacharya: Scientific Officer 'C'
- 7 Sri Subhasis Basu: Scientific Officer 'C'
- 8 Sri Monobir Chattopadhyay: Scientific Officer 'C'
- 9 Sri Amalendu Bal: Scientific Assistant-E
- 10 Sri Abhijit Betal: Scientific Assistant-D
- 11 Sri Dulal Chatterjee: Superintendent
- 12 Sri Sib Sankar Sil: Technician 'E'
- 13 Sri Dipankar Das: Technician 'D'

- 14 Sri Ashok Kr Ram: Helper 'C'

SURFACE PHYSICS DIVISION

- 1 Prof Purushottam Chakraborty: Sr Professor 'H+' & HOD
- 2 Prof Debabrata Ghosh: Sr Professor 'H'
- 3 Prof SR Bhattacharyya: Professor 'G'
- 4 Prof Tapas Kr Chini: Professor 'G'
- 5 Prof Sangam Banerjee: Professor 'G'
- 6 Prof Manabendra Mukherjee: Professor 'G'
- 7 Prof Srinanda Kundu: Professor 'F'
- 8 Prof Satyajit Hazra: Professor 'G'
- 9 Prof Satyaban Bhunia: Professor 'F'
- 10 Prof Krishnakumar SR Menon: Professor 'F'
- 11 Dr Biswarup Satpati: Scientist 'E'
- 12 Sri Avijit Das: Scientific Officer 'C'
- 13 Sri Subir Roy: Scientific Officer 'C'
- 14 Sri Susanta Bandyopadhyay: Scientific Officer 'C'
- 15 Sri Souvik Banerjee: Scientific Assistant-C
- 16 Shri Debraj Dey: Scientific Assistant 'B'
- 17 Sri Goutam Sarkar: Scientific Assistant-C
- 18 Sri Manoj Biswas: Lower Division Clerk
- 19 Sri Harendra Nath Jana: Caretaker
- 20 Sri Gobardhan Jana: Helper 'C'

APPLIED NUCLEAR PHYSICS DIVISION

- 1 Prof Satyajit Saha: Sr Professor 'H' & HOD
- 2 Prof (Smt) Bichitra Ganguly: Professor 'G'
- 3 Prof PMG Nambissan: Professor 'G'
- 4 Prof Supratik Mukhopadhyay: Professor 'G'
- 5 Prof Chandi Charan Dey: Professor 'F'
- 6 Prof (Sm) Nayana Majumdar: Professor 'F'
- 7 Prof Sandip Sarkar: Professor 'F'
- 8 Dr. Sankar De: Associate Professor 'E'
- 9 Sri Pradipta Kumar Das: Scientific Officer 'C'
- 10 Sri Saibal Saha: Scientific Officer 'C'
- 11 Sri Haradhan Dhar: Scientific Assistant-E
- 12 Sri Chandra Nath Marik: Scientific Assistant-D
- 13 Smt Soma Roy: Scientific Assistant-C
- 14 Sri Asim Kumar Sarkar: AAO
- 15 Sri Dilip Kr Sardar: Technician 'C'
- 16 Sri Kuntal Sarkhel: Helper 'C'
- 17 Sri Prabir Das: Helper 'C'

NUCLEAR PHYSICS DIVISION

- 1 Prof Polash Banerjee: Sr Professor 'H' & HOD
- 2 Prof Padmanava Basu: Professor 'G'
- 3 Prof Maitreyee Saha Sarkar: Professor 'G'
- 4 Prof Subinit Roy: Professor 'G'
- 5 Prof Ashimananda Goswami: Professor 'G'
- 6 Prof Ushasi Datta Pramanik: Professor 'F'
- 7 Prof Chinmay Basu: Professor 'F'
- 8 Prof (Smt) Anjali Mukherjee: Professor 'F'
- 9 Sri Sujib Ch Chattopadhyay: Scientific Officer 'C'
- 10 Sri Kaushik Chatterjee: Scientific Officer 'C'
- 11 Smt Jonaki Panja: Scientific Officer 'C'
- 12 Sri Ajoy Kr Mitra: Scientific Officer 'C'
- 13 Smt Rita Ghosh: Scientific Assistant-E
- 14 Sri Dilip Sil: Scientific Assistant-D
- 15 Sri Pradip Barua: Technician 'C'
- 16 Sri Sankar Prasad Singh: Technician 'C'
- 17 Smt Tultul Dutta: Superintendent
- 18 Sri Siladitya Chakraborty: Helper 'C'

HIGH ENERGY NUCLEAR AND PARTICLE PHYSICS DIVISION

- 1 Prof Sunanda Banerjee: Professor & Head
- 2 Prof Pratap Bhattacharya: Professor 'G'
- 3 Prof Sukalyan Chattopadhyay: Professor 'G'
- 4 Prof Pradip Kr Roy: Professor 'G'
- 5 Prof Abhee Kanti Dutt-Mazumdar: Professor 'F'
- 6 Prof Manoj K Sharan: Professor 'F'
- 7 Dr (Smt) Tinku Sinha: Scientist 'F'
- 8 Dr Satyaki Bhattacharya: Associate Professor 'F'
- 9 Dr Subir Sarkar: Associate Professor 'F'
- 10 Dr Suchandra Dutta: Associate Professor 'F'
- 11 Dr Debasish Das Associate: Professor 'E'
- 12 Sri Debasish Bandyopadhyay: Scientific Assistant-E
- 13 Sri Dwijendra Das: Scientific Assistant-C
- 14 Sri Dipankar Das: Scientific Assistant-C
- 15 Smt Lipy Das Bose: Scientific Assistant-C
- 16 Sri Sanjib Kr Mondal: Superintendent
- 17 Sri Rakesh Kr Ram: Helper 'C'
- 18 Sri Sudam Bagdi: Helper 'C'
- 19 Sri Singh Bahadur Thapa: Helper 'C'

APPLIED MATERIAL SCIENCE DIVISION

Division

- 1 Prof Alokmay Datta: Sr Professor 'H' & HOD
- 2 Dr Madhusudan Roy: Associate Professor 'F'
- 3 Dr Supratic Chakraborty: Associate Professor 'E'
- 4 Dr Mrinmay Kr. Mukhopadhyay: Associate Professor 'E'
- 5 Sri Abhijit Sanyal: Engineer 'G'
- 6 Sri Shyama Prasad Mallick: Technician 'F'
- 7 Sri Ramkrishna Deb Das: Scientific Assistant 'B'
- 8 Sri Subhasish Sanyal: Superintendent
- 9 Sri Provash Halder: Helper 'E'

THEORETICAL CONDENSED MATTER PHYSICS DIVISION

- 1 Prof Bikas Kanta Chakrabarti: Sr Professor 'I'
- 2 Prof Atindra Nath Das: Sr Professor 'H'
- 3 Prof SN Karmakar: Professor 'G' & HOD
- 4 Prof Sudhakar Yarlagaadda: Professor 'G'
- 5 Prof Pradeep Kr Mohanty: Professor 'G'
- 6 Prof Abhik Basu: Professor 'F'
- 7 Prof Arti Garg: Associate Professor 'E'
- 8 Sri Kausik Das: Scientific Assistant-C

9 Smt Suparna Das: Superintendent

10 Sri Jhantu Mallick: Helper 'C'

11 Sri Asish Ram: Helper 'C'

EXPERIMENTAL CONDENSED MATTER PHYSICS DIVISION

- 1 Prof R Ranganathan: Sr Professor 'H+' & HOD
- 2 Prof (Smt) Kajal Ghosh Ray: Sr Professor 'H'
- 3 Prof Chandidas Mukherjee: Professor 'G'
- 4 Prof Indranil Das: Professor 'G'
- 5 Prof Prabhat Kr Mandal: Professor 'G'
- 6 Prof Barnana Pal: Professor 'F'
- 7 Prof Asok Podder: Professor 'F'
- 8 Prof Bilwadal Bandyopadhyay: Professor 'F'
- 9 Prof Chandan Mazumdar: Professor 'G'
- 10 Sri Ajoy Kr Bhattacharya: Scientific Officer 'D'
- 11 Sri Tapan Kr Pyne: Scientific Officer 'C'
- 12 Sri Arun Kumar Pal: Technician 'H'
- 13 Smt Sankari Chakrabarti: Scientific Assistant-D
- 14 Sri Arindam Chakraborti: Scientific Assistant-C
- 15 Sri Dhruvajyoti Seth: Scientific Assistant-C
- 16 Smt Papia Bhowmik (Mondal): Scientific Assistant-C
- 17 Sri Anish Karmahapatra: Technician 'E'
- 18 Sri Tapan Kr Sarkar: Superintendent
- 19 Sri Sambu Hembrom: Technician 'C'
- 20 Sri Prabir Das: Technician 'B'
- 21 Sri Patit Paban Ranjit: Helper 'E'
- 22 Shri Rajeshwar Dubey: Helper 'A'

CRYSTALLOGRAPHY & MOLECULAR BIOLOGY DIVISION

- 1 Prof Nitai Pada Bhattacharyya: Sr Professor 'H' & HOD
- 2 Prof Rahul Banerjee: Professor 'F'
- 3 Prof Sampa Biswas: Professor 'F'
- 4 Prof Partha Saha: Professor 'F'
- 5 Prof Udayaditya Sen: Professor 'F'
- 6 Sri Utpal Basu: Scientific Officer 'C'
- 7 Sri Abhijit Bhattacharya: Scientific Assistant-D
- 8 Sri Bikram Nath: Scientific Assistant-C
- 9 Sri Sushanta Debnath: Scientific Assistant-C
- 10 Sri Saikat Mukhopadhyay: Scientific Assistant-C
- 11 Sri Ashis Kumar Dutta: Scientific Assistant-C
- 12 Smt Durga Hazra: Superintendent
- 13 Sri Samir Kr Majumdar: Technician 'C'
- 14 Sri Chinmoy Chatterjee: Helper 'E'
- 15 Sri Sakal Dev Ram: Helper 'C'
- 16 Sri Bipin Bose: Helper 'C'

STRUCTURAL GENOMICS DIVISION

- 1 Prof Subrata Banerjee: Professor 'G' & HOD
- 2 Prof Abhijit Chakrabarti: Sr Professor 'H'
- 3 Prof Debashis Mukhopadhyay: Professor 'F'
- 4 Dr (Smt) Oishee Chakrabarti: Associate Professor 'E'
- 5 Smt Mahuya Dutta: Lower Division Clerk
- 6 Sri Raju Dutta: Technician 'B'
- 7 Sri Sanjay Shaw: Helper 'C'
- 8 Shri Madhu Sudan Samal: Asstt Halwai-cum-Cook

BIOPHYSICS DIVISION

- 1 Prof Dipak Dasgupta: Sr Professor 'H+' & HOD
- 2 Prof Arun Kr Pal: Professor 'F'
- 3 Dr Kaushik Sengupta: Associate Professor 'E'
- 4 Dr Chandrima Das: Associate Professor 'E'
- 5 Sri Shekhar Bhattacharya: Scientific Officer 'C'

6 Sri Arijit Pal: Scientific Assistant-D
 7 Sri Bijay Kr Das: Superintendent
 8 Sri Nirmal Ch Das: Technician 'B'
 9 Sri Shyamal Ch Digar: Helper 'C'

CHEMICAL SCIENCES DIVISION

1 Prof Soumen Basak: Sr Professor 'H'
 2 Prof Amitabha De: Professor 'G'
 3 Prof Susanta Lahiri: Sr Professor 'H'
 4 Prof Samita Basu: Professor 'G' & HOD
 5 Prof Maitreyee Nandy: Professor 'F'
 6 Prof Munna Sarkar: Professor 'G'
 7 Dr Padmaja Prasad Mishra: Associate Professor 'E'
 8 Dr Montu K Hazra: Associate Professor 'E'
 9 Dr Dulal Senapati: Associate Professor 'E'
 10 Sri Ajay Das: Scientific Assistant-E
 11 Smt Chitra Raha: Scientific Assistant-E

12 Sri Avijit Shome: Scientific Assistant-C
 13 Sri Subir Bandyopadhyay: Superintendent
 14 Sri Bablu Ram: Technician 'C'
 15 Sri Deepak Kr Ram: Technician 'A'
 16 Sri Jitendra Nath Roy: Technician 'A'

COMPUTATIONAL SCIENCES DIVISION

1 Prof Dhananjay Bhattacharyya: Professor 'G' & HOD
 2 Dr Gautam Garai: Scientist 'G'
 3 Sri Deeptish Dey: Engineer 'F'
 4 Sri Gautam Datta: Scientific Assistant-E
 5 Sri Sumit Basu: Scientific Assistant-C
 6 Sri Nanda Lal Sanpui: Technician 'C'
 7 Sri Soumya Majumdar: Technician 'C'

Central Facilities

CENTRE FOR ADVANCED RESEARCH & EDUCATION

Prof Abhijit Chakrabarti: Sr Professor 'H' & Head
 Smt Seema Bhattacharyya: Officer-In-Charge
 1 Sri Amit Kumar Saha: Scientific Officer 'C'
 2 Smt Dipa Dasgupta: Scientific Officer 'C'
 3 Sri Sushanta Chakraborty: Scientific Assistant-E
 4 Sri Jayant Kr Mukherjee: Scientific Assistant-C
 5 Sri Pradip Das: Scientific Assistant-A
 6 Sri Sudarshan Mondal: Superintendent
 7 Sri Nirmal Ch Biswas: Technician 'B'
 8 Sri Sanjib Kr Roy: Helper 'C'

LIBRARY

Prof R Ranganathan: Chairman
 1 Smt Ratna Raychaudhuri: Scientific Officer 'C'
 2 Sri Abhijit Kumar Malakar: Scientific Assistant-E
 3 Sri Samit De: Scientific Assistant-E
 4 Shri Mahesh Hembram: Scientific Assistant 'B'
 5 Smt Manlunching: Scientific Assistant 'B'
 6 Sri Subrata Chowdhury: Technician 'E'
 7 Smt Anupama Saha: Technician 'C'
 8 Sri Manoj Karmakar: Technician 'C'
 9 Sri Kishori Lal Ram: Technician 'C'
 10 Sri Kartick Ch Panigrahi: Helper 'C'

WORKSHOP

1 Prof Manabendra Mukherjee: Professor 'G' & Chairman
 2 Dr Jisnu Basu: Engineer 'F' & Officer-In-Charge
 3 Sri Sadananda Dutta: Technician 'G'
 4 Sri Ramen Jana: Technician 'G'
 5 Sri Sudipta Barman: Scientific Assistant 'C' (Fitter)
 6 Sri Narayan Chandra Dey: Scientific Assistant-C (CNC Operator)
 7 Sri Debasish Sen: Technician 'G'
 8 Sri Supriya Mondal: Technician 'G'
 9 Sri Biplab Kr Dey: Technician 'E'
 10 Sri Partha Sarathi Karmakar: Technician 'F' (Turner)
 11 Sri Tarun Tapan Biswas: Technician 'E' (Fitter)
 12 Sri Gopal Kr Chatterjee: Technician 'E' (Eng.Stores)
 13 Sri Ramkrishna Roy: Technician 'E' (Machinist)

14 Sri Bhairab Ch Nath: Technician 'D' (Mil. Fitter)
 15 Sri Sunil Das: Technician 'D' (Mil. Fitter)
 16 Sri Durlav Tudu: Technician 'D' (Turner)
 17 Sri Subrata Baidya: Technician 'D' (Machinist)
 18 Sri Sadip Patra: Technician 'D' (Welder)
 19 Sri Himadri Chakraborty: Technician 'D' (Machinist)
 20 Sri Subal Ch Bindi: Technician 'C'
 21 Shri C Palanivel: Technician 'C' (Glass Blower)
 22 Sri Adhir Sarkar: Technician 'B'
 23 Sri Santosh Kr Barman: Caretaker
 24 Sri Deb Prasad Sardar: Helper 'E'
 25 Sri Gopal Das: Helper 'C'

BUILDING MAINTENANCE (ELECTRICAL)

Prof Debabrata Ghosh: Chairman, BM(Elec) Committee
 1 Sri Debi Prasad Ghosh: Engineer 'G'
 2 Sri Soumendra Pal: Engineer 'D'
 3 Sri Swapan Kr Mandal: Scientific Assistant-E
 4 Sri Somenath Ghosh: Scientific Assistant-D
 5 Sri Saral Guha: Technician 'G'
 6 Sri Kali Kanto Dey: Technician 'G'
 7 Sri Madhusudan Kaity: Technician 'G'
 8 Sri Asok Kr Majumdar: Technician 'E'
 9 Sri Kalyan Paul Roy: Technician 'D'
 10 Sri Gautam Kr Sabui: Technician 'C'
 11 Sri Pratap Dhanuk: Technician 'C'
 12 Sri Dilip Kr Chakraborty: Technician 'C'
 13 Shri Jai Prakash Tiwari: Technician 'C'
 14 Sri Jagannath Mondal: Technician 'C'
 15 Sri Mahendra M Khapekar: Technician 'C'
 16 Sri Dilip Ram: Caretaker
 17 Sri Bijay Ram: Helper 'C'
 18 Sri Sankar Adhikari: Helper 'C'

BUILDING MAINTENANCE (CIVIL)

Prof Asimananda Goswami: Chairman, BM(Civil) Committee
 1 Sri Rajkumar Sengupta: Engineer 'E'
 2 Sri Siddhartha Saha: Engineer 'D'
 3 Sri Subha Sankar Kundu: Technician 'G'
 4 Sri Arup Polley Technician: 'G'
 5 Sri Nil Kanta Sinha: Scientific Assistant-D
 6 Sri Gobinda Pal: Scientific Assistant-C

7 Shri Sujoy Halder: Scientific Assistant 'B'
 8 Sri Asok Kumar Das: Technician 'G'
 9 Sri Sisir Kumar Mondal: Technician 'E' (Structural Draftsman)
 10 Sri Sunil Murmu: Technician 'C'
 11 Sri Subir Modak: Superintendent

12 Sri Samir Kr Chakraborty: Caretaker (Mali)
 13 Sri Dulal Dey: Helper 'E' (Mali)
 14 Sri Shyamal Kr Bose: Helper 'E'

Administrative Departments

ESTABLISHMENT

1 Sri Suchintya Kumar Gupta: Establishment Officer
 2 Sri Alok Mitra: AO(Establishment)
 3 Smt Chandana Basu: A.A.O.
 4 Sri Biswajit Dutta: Accountant
 5 Shri Subhendu Naskar: Lower Division Clerk
 6 Smt Paramita Pal: Lower Division Clerk
 7 Sri Subhash Ch Gayen: Technician 'B'

DESPATCH

1 Smt Chandana Mitra: A.A.O.
 2 Sri Tapan Chakraborty: A.A.O.
 3 Sri Swadesh Ch Deb: Upper Division Clerk
 4 Sri Tarak Nath Bhattacharya: Technician 'B'
 5 Sri Gouri Sankar Singh: Driver - V
 6 Shri Pintu Ram: Helper 'C'

ACCOUNTS

1 Sri Niladri Sanyal: Dy Controller of Accounts
 2 Shri Ved Prakash Mishra: Accounts Officer
 3 Sri Asit Ranjan Deb: AO(Accounts)
 4 Sri Prasanta Kr Das: AAO
 5 Sri Mukul Ch Das: AAO
 6 Sri Tapan Kr Bhattacharyya: A.A.O.
 7 Sri Goutam Ghosh: Superintendent
 8 Shri Nand Kishor Gond: Lower Division Clerk
 9 Shri Pourjok Majumder: Lower Division Clerk
 10 Shri Manoj Lakra: Lower Division Clerk
 11 Sri Biswanath Paul: Helper 'E'
 12 Shri Pradip Ram: Asst Halwai-cum-cook

ACCOUNTS (BUDGET & AUDIT)

1 Sri Mrityunjoy Dey: AO(Accounts)
 2 Sri Somnath Sarkar: AAO(Cash)
 3 Sri Pradip Dutta Sharma: Lower Division Clerk

ACCOUNTS (CASH)

1 Sri Swarup Kr Bose: AO(Accounts),Cash Section
 2 Shri Raghunath Naskar: Superintendent
 3 Sri Avijit Saha: Superintendent
 4 Smt Seethalakshmi Rath: Superintendent
 5 Sri Sanat Kumar Kotal: Technician 'B'

ACCOUNTS (SALARY)

1 Sri Rammohan Moitra: AAO(Salary)
 2 Sri Debasish Das: AAO
 3 Sri Ashoke Maity: Sr Superintendent
 4 Sm. Nirupama Halder: Superintendent
 5 Smt. Monika Bhattacharya: Lower Division Clerk
 6 Sri Madhu Bose: Helper 'E'

ACCOUNTS (PF & PENSION)

1 Sri Niranjan Sarkar: AAO(PF & Pension)
 2 Sri Ranjit Dutta: AAO
 3 Sri Pradip Kr Das: Driver - V

PURCHASE

1 Smt Seema Bhattacharyya: AO-III & Off-In-Charge of Purchase Cell

Purchase (Domestic)

2 Sri Sanjoy Chakraborty: AO(Purchase-Domestic)
 3 Sri Gautam Das: Superintendent
 4 Sri Ajoy Kumar Biswas: Superintendent
 5 Sri Asim Halder: Superintendent
 6 Ms. Rekha Ram: Upper Division Clerk
 7 Sri Soumyajit Karmakar: Lower Division Clerk
 8 Sri Ashoke Kr Roy: Technician 'A'

Purchase (Foreign Cell)

1 Sri JS Raychaudhuri: AO(Purchase-Foreign)
 2 Sri Sankar Nath Dewan: Sr Superintendent
 3 Sri Ranjit Roy: Superintendent
 4 Mr James Wilson Kerketta: Lower Division Clerk
 5 Sri Gour Hari Das: Caretaker

STORE

1 Sri Shyamal Ch Biswas: Superintendent
 2 Sri Ramesh Hari: Helper 'D'

MEDICAL UNIT

1 Prof Abhijit Chakrabarti: Chairman, MAC
 2 Dr Sumalay Kar: Part-time Attending Physician
 3 Dr Arup Kumar Sahu: Part-time Attending Physician
 4 Sri Gobinda Chakraborty: AAO
 5 Smt Dipali Saha: AAO
 6 Sri Gautam Dutta: Technician 'E'
 7 Sri Dipak Kr Das: Superintendent
 8 Smt Chandana Nayak: Lower Division Clerk
 9 Shri Avishek Pal: Lower Division Clerk
 10. Sri Nabin Kumar Halder: Technician 'B'

GUEST HOUSE & HOSTEL

Prof Sukalyan Chattopadhyay: "Prof-in-Charge, Guest House & Hostel, SINP Housing Com.(MSA-II)"
 Prof Chandi Das Mukherjee: "Prof-In-Charge, Guest House & Hostel, Salt Lake Campus (MSA-I)"
 1 Shri Ramesh Singh: Helper 'C'
 2 Sri Somenath Das: Helper 'C'
 3 Smt Suro Mahato: Helper 'C'
 4 Sri Suresh Ch Das: Asst Halwai-cum-cook
 5 Sri Sakti Pada Bisui: Asst Halwai-cum-cook

CANTEEN

Prof Dhananjay Bhattacharyya: Chairman, Canteen Committee

- 1 Sri Asok Kumar Roy: Asstt Manager-cum-Storekeeper
- 2 Sri Prabhat Maity: Halwai-cum-cook
- 3 Sri Kartick Ch Maity: Asst Halwai-cum-cook
- 4 Sri Sujan Ch Mistri: Asst Halwai-cum-cook
- 5 Sri Shankar Andia: Asst Halwai-cum-cook
- 6 Sri Sailen Halder: Bearer-II
- 7 Sri Nema Ch Das: Bearer-II
- 8 Sri Amar Das: Bearer-II
- 9 Sri Barun Kr Barua: Bearer-II
- 10 Sri Subodh Kr Pradhan: Bearer-I
- 11 Sri Sunil Ram: Bearer-II

TELEPHONE

- 1 Prof (Smt) Samita Basu: Prof & In-Charge
- 2 Smt Sunanda Chakraborty: Technician 'G'
- 3 Smt Bithi Biswas: Technician 'E'
- 4 Smt Pampa Bhattacharjee: Technician 'D'

SECURITY

- 1 Sri Supriya Gangopadhyay: Sr Security Officer
- 2 Sri Ratan Kr Bose: Security Officer
- 3 Sri Tapas Kr Dalal: Security Officer
- 4 Sri Swaraj Nath Sarkar: Security Officer
- 5 Sri Ashok Kr Singh: Security Supervisor 'B'
- 6 Sri Ganesh Prasad Sharma: Security Supervisor 'B'
- 7 Sri Tarak Chandra Nath: Security Supervisor 'B'
- 8 Sri Gobinda Ch Roy: Lower Division Clerk
- 9 Sri Balli Rana: Technician 'A'
- 10 Sri Dukha Krishna Reddy: Technician 'A'
- 11 Sri Subrata Kr Chowdhury: Technician 'A'
- 12 Sri PB Thapa: Helper 'E' (Watchman)
- 13 Sri Joyram Murmu: Helper 'E' (Watchman)
- 14 Sri Madhusudan Bhakta: Helper 'E' (Watchman)
- 15 Sri Sudhangsu Sekhar Mondal: Helper 'E' (Watchman)
- 16 Sri Swapan Mukherjee: Helper 'E'
- 17 Sri Mongol Oraon: Helper 'D' (Watchman)
- 18 Sri Sibu Oraon: Helper 'D' (Watchman)
- 19 Sri Tapan Kr Singha: Helper 'D' (Watchman)
- 20 Sri Sudhir Kr Debnath: Helper 'C' (Watchman)
- 21 Md Manayar Hasan Mondal: Technician 'A'
- 22 Sri Ranjit Kr Roy: Helper 'C' (Watchman)

- 23 Sri Arun Kumar Dutta: Helper 'B' (Watchman)
- 24 Sri Pran Gopal Das: Helper 'C' (Watchman)
- 25 Sri Gopal Chandra Saren: Helper 'C' (Watchman)

SECURITY (COSMETIC)

- 1 Sri Badal Hari: Helper 'E' (Sweeper)
- 2 Sri Sakhi Chand Hari: Helper 'E' (Sweeper)
- 3 Sri Banarshi Mallick: Helper 'E' (Sweeper)
- 4 Sri Siblal Hari: Helper 'D' (Sweeper)
- 5 Smt Anjali Hari: Helper 'C' (Sweeper)
- 6 Sri Gobinda Ch Das: Helper 'D' (Sweeper)
- 7 Sri Santosh Hari: Helper 'C' (Sweeper)
- 8 Sri Ashok Mallick: Helper 'C'
- 9 Sri Kala Chand Hela: Helper 'C' (Sweeper)
- 10 Sri Amit Hari: Helper 'A'
- 11 Sri Gangadhar Maity: Tech 'E' (Supervisor Mali)
- 12 Sri Sushil Kr De: Helper 'E' (Mali)
- 13 Sri Santosh Kr Sarkar: Helper 'E' (Mali)
- 14 Sri Kamala Kanta Sarkar: Helper 'E' (Mali)
- 15 Sri Santosh Kr Bachar: Helper 'E' (Mali)
- 16 Sri Swapan Kr Mondal: Helper 'E' (Mali)
- 17 Sk Mostakin: Helper 'C'

TRANSPORT

Prof Subrata Banerjee: Chairman, Transport Committee
Sri Kaushik Chatterjee: Officer-in-Charge, Transport Sec

- 1 Sri Dharmendra Prasad: Scientific Assistant-C
- 2 Sri Aloke Kr Sarkar: Transport Supervisor
- 3 Sri Swapan Kumar Mondal: Technician 'G'
- 4 Sri Trinath Maharana: Technician 'E' (Vehi Mech)
- 5 Sri Surai Mandi: Technician 'C' (Vehi Mech)
- 6 Sri Kanai Lal Malakar: Technician 'C'
- 7 Sri Tarak Nath Ghosh: Driver - IV
- 8 Sri Dilip Baidya: Driver - IV
- 9 Sri Madhusudan Mondal: Driver - IV
- 10 Sri Gopal Ch Ghosh: Driver - III
- 11 Sri Uttam Kr Roy: Driver - III
- 12 Sri Kartick Ch Pal: Driver - III
- 13 Sri Prabir Kr Mistri: Driver - III
- 14 Sri Prabir Biswas: Driver - II
- 15 Sri Asit Kr Mahapatra: Technician 'B'
- 16 Sri Mongol Ch Mondal: Helper 'E'
- 17 Sri Shankar Ram: Helper 'C'

List of Retirement: April 01, 2012 to March 31, 2013

1. Dr Nihar Ranjan Ray, PPD: 30.04.2012
2. Sri Swapan Kumar Banerjee, Library: 30.06.2012
3. Dr Rabindranath Pal, PPD: 31.07.2012
4. Dr AI Jaman, ECMP: 31.08.2012
5. Dr Tarun Kanti Roy, Theory: 31.08.2012
6. Dr Kamales Kar, Theory: 31.08.2012
7. Sri Paresh Chandra Mazumdar, BM(E): 30.09.2012
8. Dr (Smt) Santwana Roychowdhury, PPD: 30.09.2012
9. Sri Asit Kumar Mondal, Wks: 31.10.2012
10. Dr Sujit Kumar Saha, PPD: 31.10.2012
11. Dr (Smt) Sanghamitra Raha, C&MB: 30.11.2012
12. Dr Amitabha Ghosh Ray, ECMP: 31.12.2012
13. Dr Radhey Shyam, Theory: 31.01.2013
14. Dr Debabrata Mukhopadhyay, Theory: 28.02.2013
15. Sri Amal Ghosal, ANP: 28.02.2013

Voluntary Retirement List: April 01, 2012 to March 31, 2013

1. Late Kartick Hari, Accounts: 20.07.2012
2. Prof Partha Sarathi Majumdar, Theory: 31.10.2012

List of Demise: April 01, 2012 to March 31, 2013

1. Late Ratan Lal Ram, 02.03.2013

Chapter 9

External Collaborators

Basak, Trayambak, Genomics and Molecular Medicine, CSIR-Institute of Genomics and Integrative Biology, Delhi, India
Nayak, Mukti Kant, Department of Zoology, University of Calcutta, Kolkata, India
Saha, Priyanka, Univ Calcutta, Dept Biophys Mol Biol & Bioinformat, Calcutta, India
Das, Debasis, Univ Calcutta, Dept Biophys Mol Biol & Bioinformat, Calcutta, India
Bhowmick, Rahul, Natl Inst Cholera & Enter Dis, Div Virol, Calcutta, India
Halder, Umesh Chandra, Natl Inst Cholera & Enter Dis, Div Virol, Calcutta, India
Chattopadhyay, Shiladitya, Natl Inst Cholera & Enter Dis, Div Virol, Calcutta, India
Kawamura, Hikaru, Department of Earth & Space Science, Osaka University, Osaka, Japan
Hatano, Takahiro, Earthquake Research Institute, University of Tokyo, Japan
Kato, Naoyuki, Earthquake Research Institute, University of Tokyo, Japan
Das, Sumistha, Indian Stat Inst, Div Biol Sci, Calcutta 700108, W Bengal, India
Debnath, Nitai, Indian Stat Inst, Div Biol Sci, Calcutta 700108, W Bengal, India
Mitra, Shouvik, Indian Stat Inst, Div Biol Sci, Calcutta 700108, W Bengal, India
Mandal, Arun Kumar, Bengal Engn & Sci Univ, Sch Mat Sci & Engn, Howrah 711103, W Bengal, India
Ray, Mallar, Bengal Engn & Sci Univ, Sch Mat Sci & Engn, Howrah 711103, W Bengal, India
Rajapaksa, Indrajith, Univ Calif Irvine, Dept Elect Engn & Comp Sci, Irvine, CA 92697 USA
Kundu, Souvik, Materials Science Centre, Indian Institute of Technology, Kharagpur 721 302, India
Halder, Nripendra N, Advanced Technology Development Centre, Indian Institute of Technology, Kharagpur 721 302, India
Biswas, D, Department of Electronics & Electrical Communication Engineering, Indian Institute of Technology, Kharagpur 721302, India
Das, Sumistha, Indian Stat Inst, Div Biol Sci, Calcutta 700108, W Bengal, India
Debnath, Nitai, Indian Stat Inst, Div Biol Sci, Calcutta 700108, W Bengal, India
Mitra, Shouvik, Indian Stat Inst, Div Biol Sci, Calcutta 700108, W Bengal, India
Rudek, Benedikt, Max-Planck-Advanced Study Group at CFEL, DESY, Notkestra 85, 22607 Hamburg, Germany

Rolles, Daniel, Max-Planck-Advanced Study Group at CFEL, DESY, Notkestra 85, 22607 Hamburg, Germany
Son, Sang-Kil, Center for Free-Electron Laser Science CFEL, DESY, Notkestra 85, 22607 Hamburg, Germany
Hans, HS, Department of Physics, Panjab University, Chandigarh, India
Singh, Gulzar, Department of Physics, Panjab University, Chandigarh, India
Kumar, A, Department of Physics, Panjab University, Chandigarh, India
Singh, Purnima, Department of Physics & Meteorology, Indian Institute of Technology Kharagpur, IN-721302, India
Nag, Somnath, Department of Physics & Meteorology, Indian Institute of Technology Kharagpur, IN-721302, India
Selvakumar, K, Department of Physics & Meteorology, Indian Institute of Technology Kharagpur, IN-721302, India
Cardella, G, INFN, Sezione di Catania, Via S. Sofia, 95123 Catania, Italy
Giuliani, G, INFN, Sezione di Catania, Via S. Sofia, 95123 Catania, Italy
Lombardo, I, Dip. di Scienze Fisiche, Universitdi Napoli Federico II, and INFN-Sezione di Napoli, Italy
Pai, H, Variable Energy Cyclotron Centre, 1/AF Bidhan Nagar, Kolkata 700064, India
Mukherjee, G, Variable Energy Cyclotron Centre, 1/AF Bidhan Nagar, Kolkata 700064, India
Erk, B, Max Planck Advanced Study Group (ASG) at CFEL, 22761 Hamburg, Germany
Rolles, D, Max Planck Advanced Study Group (ASG) at CFEL, 22761 Hamburg, Germany
Foucar, L, Max Planck Advanced Study Group (ASG) at CFEL, 22761 Hamburg, Germany
Sahin, E, Laboratori Nazionali di Legnaro dell'INFN, Legnaro, Italy
de Angelis, G, Laboratori Nazionali di Legnaro dell'INFN, Legnaro, Italy
Duchene, G, IPHC, IN2P3/CNRS et UniversitLouis Pasteur, Strasbourg, France
Petri, M, Nuclear Science Division, Lawrence Berkeley National Laboratory, Berkeley, California 94720, USA
Paschalis, S, Nuclear Science Division, Lawrence Berkeley National Laboratory, Berkeley, California 94720, USA
Clark, RM, Nuclear Science Division, Lawrence Berkeley National Laboratory, Berkeley, California 94720, USA
Banerjee, A, Ctr Variable Energy Cyclotron, Calcutta 700064, India
Biswas, S, Ctr Variable Energy Cyclotron, Calcutta 700064, India
Lombardo, I, Univ Naples Federico II, Dipartimento Sci Fis,

Naples, Italy

Acosta, L, Ist Nazl Fis Nucl, Lab Nazl Sud, I-95129 Catania, Italy

Agodi, C, Ist Nazl Fis Nucl, Lab Nazl Sud, I-95129 Catania, Italy

Saha, S, Department of Nuclear and Atomic Physics, Tata Institute of Fundamental Research, Mumbai 400005, India

Palit, R, Department of Nuclear and Atomic Physics, Tata Institute of Fundamental Research, Mumbai 400005, India

Sethi, J, Department of Nuclear and Atomic Physics, Tata Institute of Fundamental Research, Mumbai 400005, India

De Filippo, E, INFN, Sezione di Catania, Italy

Pagano, A, INFN, Sezione di Catania, Italy

Russotto, P, 2INFN, Laboratori Nazionali del Sud, Catania, Italy

Ghosh, Samiran, Univ Calcutta, Dept Appl Math, Kolkata Manjistha Dutta, Department of Instrumentation Science, Jadavpur University, Kolkata 700 032, India

Samiran Ghosh, Department of Applied Mathematics, University of Calcutta, 92, Acharya Prafulla Chandra Road, Kolkata-700 009, India

Rajkumar Roychoudhury, Indian Statistical Institute, Kolkata 700 108, India

Shukla, A, Indian Inst Astrophys, Bangalore 560034, Karnataka, India

Chitnis, VR, Tata Inst Fundamental Res, Bombay 400005, Maharashtra, India

Vishwanath, PR, Indian Inst Astrophys, Bangalore 560034, Karnataka, India

Ghosh, Uday Chand, Presidency Univ, Dept Chem & Biochem, Calcutta 700073, India

Nandi, Debabrata, Presidency Univ, Dept Chem & Biochem, Calcutta 700073, India

Gupta, Kaushik, Presidency Univ, Dept Chem & Biochem, Calcutta 700073, India

Ghosh, Arup Kumar, Presidency Univ, Dept Chem & Biochem, Calcutta 700073, India

Ghosh, Uday Chand, Presidency Univ, Dept Chem & Biochem, Calcutta 700073, India

Talukdar, Atanu, Presidency Univ, Dept Chem & Biochem, Calcutta 700073, India

Gangopadhyay, Rupali, Indian Assoc Cultivat Sci, Ctr Adv Mat, Calcutta 700032, India

Bhattacharjya, S, Cancer Biology and Inflammatory Disorder Division, Indian Institute of Chemical Biology, 4 Raja SC Mullick Road, Kolkata

Nath, S, Cancer Biology and Inflammatory Disorder Division, Indian Institute of Chemical Biology, 4 Raja SC Mullick Road, Kolkata

Maiti, Jyotirmoy, Department of Physics, Barasat Government College, 10, KNC Road, Kolkata 700124

Radheep, D Mohan, Centre for High Pressure Research, School of Physics, Bharathidasan University, Tiruchirappalli 620024, India

Arumugam, S, Centre for High Pressure Research, School of Physics, Bharathidasan University, Tiruchirappalli 620024, India

Sarkar, P, Department of Physics, Serampore College, Serampore 712201, India

Choudhury, P, Cent Glass & Ceram Res Inst, Calcutta 700032, W Bengal, India

Mydeen, K, Bharathidasan Univ, Ctr High Pressure Res, Sch Phys, Tiruchchirappalli 620024, India

J Sengupta, Sikkim Manipal Inst Technol, Dept Phys, Sikkim 737136, India

RK Sahoo, Indian Inst Technol, Ctr Mat Sci, Kharagpur 721302, W Bengal

Gannouji, Radouane; Department of Physics, Faculty of Sci-

ence, Tokyo University of Science, 1-3, Kagurazaka, Shinjuku-ku, Tokyo 162-8601, Japan

Hossain, Md Wali; Centre for Theoretical Physics, Jamia Millia Islamia, New Delhi 110025, India

Adhikary, Biswajit; Department of Physics, Gurudas College, Narkeldanga, Kolkata 700054, India

Ghosh, Dilip Kumar; Department of Theoretical Physics, IACS, 2A & 2B Raja SC Mullick Road, Kolkata, 700 032, India

Roy, Sourov; Department of Theoretical Physics, IACS, 2A & 2B Raja SC Mullick Road, Kolkata, 700 032, India

Shukla, A; Indian Inst Astrophys, Bangalore 560034, Karnataka, India

Chitnis, VR; Tata Inst Fundamental Res, Bombay 400005, Maharashtra, India

Vishwanath, PR; Indian Inst Astrophys, Bangalore 560034, Karnataka, India

Biswas, Pranab; Materials Science Centre, Indian Institute of Technology, Kharagpur 721 302, India

Kundu, Souvik; Materials Science Centre, Indian Institute of Technology, Kharagpur 721 302, India

Halder, Nripendra N; Advanced Technology Development Centre, Indian Institute of Technology, Kharagpur 721 302, India

Biswas, D; Department of Electronics & Electrical Communication Engineering, Indian Institute of Technology, Kharagpur 721302, India

Alessia Le Donne1, Milano-Bicocca Solar Energy Research Center (MIB-SOLAR), Department of Materials Science, University of Milano-Bicocca, via Cozzi 53, Milano, Italy

Sourav Kanti Jana1, Milano-Bicocca Solar Energy Research Center (MIB-SOLAR), Department of Materials Science, University of Milano-Bicocca, via Cozzi 53, Milano, Italy

Chebil, M Souheib; LUNAM Universit, IMMM, Facult de Sciences, Universit du Maine, UMR 6283 CNRS, Le Mans Ce dex 9, 72000, France

Vignaud, G; Laboratoire d'Ingénierie des MATériaux de Bretagne, Centre de Recherche, Rue de Saint Maud, BP 92 116, 56321 Lorient Cedex France

Grohens, Y; Laboratoire d'Ingénierie des MATériaux de Bretagne, Centre de Recherche, Rue de Saint Maud, BP 92 116, 56321 Lorient Cedex France

Laha, P; Department of Applied Physics, Birla Institute of Technology, Mesra, Ranchi 835215, India

Banerjee, I; Department of Applied Physics, Birla Institute of Technology, Mesra, Ranchi 835215, India

Bajaj, A; Department of Applied Physics, Birla Institute of Technology, Mesra, Ranchi 835215, India

Chatterjee, Arnab; Centre de Physique Thorique (CNRS UMR 6207), Universit de la Mditerranée Aix Marseille II, Luminy, 13288 Marseille cedex 9, France

Parongama, Sen; Department of Physics, University of Calcutta, 92 Acharya Prafulla Chandra Road, Kolkata 700009, India

Pradip Datta†, Ananda Mohan College, 102/1 Raja Rammohan Roy Sarani, Kolkata 700 009

Roy, S, Department of Biochemistry, University of Calcutta, 35 Ballygunge Circular Road, Kolkata 700019

Takao, T, Laboratory of Protein Profiling and Functional Proteomics, Institute for Protein Research (IPR), Osaka University, 3-2 Yamadaoka, Suita-shi, Osaka 565-0871, Japan

Chakraborty, B, Department of Chemistry, Adamas Institute of Technology, P.O. Jagannathpur, Barasat-Barrackpore Road, Barbaria, North 24, Parganas, Pin -700126, India

Tomar, BS, Radioanalytical Chemistry Division, Bhabha Atomic Research Centre, Mumbai 400085

Nandi, D, Department of Chemistry and Biochemistry, Presidency University, 86/1 College Street, Kolkata 700073

Gupta, K, Department of Chemistry and Biochemistry, Presidency University, 86/1 College Street, Kolkata 700073
 Ghosh, AK, Department of Chemistry and Biochemistry, Presidency University, 86/1 College Street, Kolkata 700073
 Sarkar, P, Department of Biochemistry, University of Calcutta,

35 Ballygunge Circular Road, Kolkata 700 019, India
 Yamasaki, S, Department of Veterinary Science, Graduate School of Life and Environmental Sciences, Osaka Prefecture University, Osaka, Japan

Chapter 10

Index

- Abada, Asmaa, 141, 152
Abir, Raktim, 137, 143, 154
Ackermann, D, 25
Acosta, L, 89, 110
Adhikary, Biswajit, 133, 134, 152
Adhya, Souvik Priyam, 91, 111
Agodi, C, 89, 110
Agrawal, BK, 136, 137, 139, 140, 142, 147, 148, 151–154
Aich, Pulakesh, 19
Ali, Amna, 134, 151
ALICE Collaboration, 101–103
Andersson, LL, 25
Anitha, Yelagam, 53, 78
Archambault, S, 154
Arumugam†, S, 57
Arumugam†, S, 75

Bagchi, Debarshee, 72–74
Bagla, Hemlata, 23
Bajaj, A, 66, 77
Bal, JK, 62, 63, 65, 75
Bandyopadhyay, Debades, 134, 150, 154, 155
Banerjee, A, 89, 110
Banerjee, Amrita, 14, 37
Banerjee, D, 121, 123
Banerjee, Debashis, 40
Banerjee, I, 66, 77
Banerjee, Mousumi, 29, 38
Banerjee, Pratyay, 145, 153
Banerjee, Rahul, 21, 39
Banerjee, Ramanuj, 17, 20, 39
Banerjee, S, 26, 35, 37
Banerjee, Sangam, 24, 65, 74
Banerjee, Sunanda, 113
Banerji, Pallab, 53, 78
Banik, Sarmistha, 134, 154, 155
Bardhan, KK, 56, 75
Barma, Prof Mustansir, 177
Basak, NP, 35, 37
Basak, Soumen, 14, 31, 38, 39
Basu, A, 68, 76
Basu, Abhik, 67, 68, 74, 76
Basu, Avik, 43
Basu, Chinmay, 99, 114
Basu, Debjoyti, 120, 123
Basu, JK, 50, 77
Basu, Mahashweta, 70, 75
Basu, Rudranil, 139, 154
Basu, Samita, 22, 26, 28, 29, 31, 38, 43

Basu, Sankar, 21, 39
Basu, Smita, 33
Basu, Urna, 68, 70, 75, 78
Basu-Mallick, B, 138, 145, 151, 153
Basu-Mallick, Bireswar, 157
Baviskar, Shri PR, 177
Bazeia, D, 143, 152
Behnke, E, 154
Bera, Indrani, 159, 161
Bhattacharjee, A, 53, 74
Bhattacharjee, Anindita, 141, 151
Bhattacharjee, Ashis, 52, 74
Bhattacharjee, J, 78
Bhattacharjee, P, 133, 136, 151, 154
Bhattacharjee, Pijushpani, 135, 154
Bhattacharjya†, S, 21
Bhattacharjya†, S, 39
Bhattacharya, Dipankar, 40
Bhattacharya, P, 89, 111
Bhattacharya, S, 89, 92, 110, 111
Bhattacharya, Sudeb, 95, 110
Bhattacharyya, Dhananjay, 162
Bhattacharyya, Satyaki, 113
Bhattacharyya, Dhananjay, 21, 22, 38, 39, 159–162
Bhattacharyya, Gautam, 138, 139, 141, 144, 147, 152, 156–158
Bhattacharyya, Nitai P, 17, 18, 37, 38
Bhattacharyya, NP, 21, 39
Bhattacharyya, SR, 60, 78
Bhattacharyya, Tamoghna, 118, 124
Bhoi, D, 57, 74, 77
Bhoi, P, 58
Bhowmick, Rahul, 34, 39
Bhunja, Satyaban, 32, 37, 50, 74
Bisoi, Abhijit, 88, 110, 111
Biswas, D, 78
Biswas, Hari S, 120, 123
Biswas, Nupur, 55, 76
Biswas, Pranab, 78
Biswas, S, 89, 110
Biswas, Sampa, 17, 19, 40
Biswas, Sayan, 143, 154
Biswas, Soumyajyoti, 71, 73, 78
Biswas, Soumyajyoti, 75
Biswas†, Pranab, 52, 54
Bondyopadhyay, Sourish, 70, 71, 75, 78
Bose, A, 118, 122
Bose, Anirban, 120, 122
Bose, S, 89, 110

Brenna, M, 136, 154
 Britto, RJ, 133, 151

Cardella, G, 110
 Chakrabarti Abhijit, 42
 Chakrabarti BK, 80
 Chakrabarti, Abhijit, 29, 33, 38, 40
 Chakrabarti, Arunabha, 38
 Chakrabarti, Atisdipankar, 73, 76
 Chakrabarti, Bikas K, 71
 Chakrabarti, Bikas K, 75
 Chakrabarti, BK, 73
 Chakrabarti, N, 118, 121, 123
 Chakrabarti, Nikhil, 116–125
 Chakrabarti, Oishee, 34, 39, 40
 Chakraborty, Purushottam, 80
 Chakraborty, Baishali, 138, 151
 Chakraborty, Brotati, 38
 Chakraborty, Keka, 88, 110
 Chakraborty, Mainak, 134, 152
 Chakraborty, Monodeep, 73, 76
 Chakraborty, P, 64, 66, 77
 Chakraborty, Purnendu, 154
 Chakraborty, Purushottam, 62, 74, 78
 Chakraborty, S, 52, 54, 78
 Chakraborty, Sandipan, 14, 15, 37, 39
 Chakraborty, Somdeb, 142, 154
 Chakraborty, Suchandra, 28, 33
 Chakraborty, Supratic, 53, 78
 Chakraborty†, Brotati, 22
 Chakraborty†, Sandipan, 15
 Chakravorty, Dipankar, 60, 75
 Chandran, Sivasurender, 50, 77
 Chatterjee, Arnab, 73
 Chatterjee, Ayan, 139, 154
 Chatterjee, Bhramar, 143, 149, 151, 152
 Chatterjee, Kalyanmoy, 113
 Chatterjee, MB, 89, 90, 110
 Chatterjee, Tanmay, 67, 75
 Chatterjee†, Arnab, 78
 Chattopadhyay, Prabal K, 120
 Chattopadhyay, Prof Dhrubajyoti, 177
 Chattopadhyay, Shiladitya, 34, 39, 40
 Chattopadhyaya, S, 92
 Chaudhuri, M, 121, 123
 Chaudhuri, Sudip, 15, 37, 39
 Chebil, M Souheib, 67
 Chebil†, M Souheib, 76
 Chini, Tapas Kumar, 64, 66, 76
 Chitnis, VR, 133, 151
 Chitnis†, VR, 136
 Choudhury, Debi, 19
 Choudhury, P, 77
 Choudhury†, P, 58
 Chowdhury, Abhishek, 140, 149–151
 Chowdhury, Ankan Dutta, 27
 Chowdhury, Biswanath, 161, 162
 Chowdhury, S, 119, 122, 124
 Clark, RM, 93, 111

CMS Collaboration, 98, 103–110
 CMS HCAL Collaboration, 110
 Colo, G, 148, 153
 CTA Collaboration, 153
 Das, AN, 71, 73, 74
 Das, Ashok, 141, 143, 144, 151, 152
 Das, Chandrima, 43
 Das, Debasis, 33, 37, 38
 Das, Debasish, 102, 112
 Das, Debottam, 141, 152
 Das, Dipankar, 138, 152
 Das, M, 153
 Das, Mala, 153, 155
 Das, Mili, 16, 40
 Das, NS, 40
 Das, Pabitra, 64, 66, 76
 Das, Samir, 34, 39
 Das, Saurabh, 30, 38
 Das, Sumistha, 53, 78
 Dasgupta, Amrita, 16, 39, 40
 Dasgupta, Anjan Kr, 14, 118, 124
 Dasgupta, Brahmananda, 117, 123
 Dasgupta, Dipak, 14, 16, 34, 37, 39, 40
 Dasgupta, Jhimli, 20, 40
 Datta Pramanik, U, 110, 111
 Datta, Alokmay, 53–55, 74, 76, 78, 80
 Datta, Jagannath, 120, 123
 Datta, Pradip, 92, 111
 Datta, Someswar, 120
 Dattagupta, Jiban K, 19, 20
 Dattagupta, JK, 17, 40
 de Angelis, G, 93, 110
 De Filippo, E, 90, 110
 De Sarkar, Sangita, 150, 151
 De, Asit Kumar, 157
 De, Amitabha, 24, 27, 28, 32, 36, 37, 39, 41
 De, Amitava, 36
 De, Asit K, 140, 150, 151
 De, Debapriya, 50, 74
 De, JN, 139, 142–144, 152–154
 De, S, 87, 103
 De, Sankar, 87, 112
 Debnath, Nitai, 53, 78
 Devi, Pukhrambam Grihanjali, 16, 39
 Dey, Chandi C, 88, 103
 Dey, Moumita, 70, 76
 Dey, Parijat, 137, 142, 146, 149, 153
 Dhiman, Shashi K, 145, 153
 Dubey, Nilesh B, 23, 38
 Duchene, G, 93, 110
 Dutt-Mazumder, Abhee K, 91, 111
 Dutta Chowdhury, Ankan, 27, 36, 39
 Dutta Pramanik, U, 93
 Dutta, B, 23, 37
 Dutta, Manjistha, 117, 123
 Dutta, P, 58, 77
 Dutta, Paramita, 69, 72, 76, 77
 Dutta, S, 77

- Dutta, Sreetama, 90, 111, 112
 Dutta, Sretama, 112
 Dutta†, Manjistha, 122
 Dutta†, Manjistha, 123

 Erk, B, 87, 103

 Finkel, F, 138, 151
 Foucar, L, 87, 103
 Francisco, RR, 144, 151
 Frederix, R, 140, 154
 Frenkel, J, 144, 151

 Gangopadhyay, Rupali, 27
 Gangopadhyay†, Rupali, 39
 Ganguly, Bichitra N, 112
 Ganguly, S, 95, 110
 Gannouji, Radouane, 151
 Gannouji†, Radouane, 134
 Garai, Gautam, 161, 162
 Ghosal, Ambar, 134, 152
 Ghose J, 21, 39
 Ghose, D, 65, 74
 Ghosh, Amit, 139, 149, 151, 154
 Ghosh, Arup Kumar, 24, 28
 Ghosh, Ayanjeet, 16, 39, 40
 Ghosh, B, 26, 37
 Ghosh, Binita, 74
 Ghosh, Dilip Kumar, 135, 152
 Ghosh, Joydeep, 120, 123
 Ghosh, K, 22, 38
 Ghosh, Kaustab, 21, 38
 Ghosh, M, 56, 75
 Ghosh, Samiran, 116, 117, 120, 122, 123
 Ghosh, Saptarni, 16, 34, 39
 Ghosh, Sudip, 110
 Ghosh, Sujay, 28, 33
 Ghosh, Uday Chand, 24
 Ghosh†, Arup Kumar, 32
 Ghosh†, Samiran, 122
 Ghosh†, Uday Chand, 32
 Ghosh†, Arup Kumar, 37
 Ghosh†, Samiran, 123
 Ghosh†, Uday Chand, 37
 Ghoshal, Nanda, 159, 161
 Ghoshray, A, 56, 76
 Ghoshray, Amitabha, 57, 75
 Ghoshray, K, 56, 75, 76
 Ghoshray, Kajal, 57, 75
 Giuliani, G, 110
 Gnaser, H, 64
 Gnaser, Hubert, 62, 74, 78
 Gomber, Bhawna, 113
 Gonzalez-Lopez, A, 138, 151
 Goswami, A, 92, 95, 110–112
 Goswami, Arunava, 53
 Greenwood, Levi, 141, 151
 Grohens, Y, 67
 Grohens†, Y, 76

 Guin, Partha S, 30, 38
 Guleria, Neelam, 145, 153
 Gupta, Kaushik, 24, 28
 Gupta, Kumar S, 138, 151
 Gupta, MR, 116
 Gupta, Sanjay, 71, 77
 Gupta, Tribikram, 71, 77
 Gupta†, Kaushik, 32
 Gupta†, Kaushik, 37
 Guzdar, PN, 118, 123

 Halder, Nripendra N, 78
 Halder, Nripendra N, 78
 Halder, Suchismita, 40
 Halder, Sukanya, 160, 162
 Halder, Umesh Chandra, 34, 39
 Halder†, Nripendra N, 52, 54
 Hans, HS, 110
 Haque, Najmul, 142, 154
 Harindranath, A, 140, 149–151
 Hasan, Salman, 33, 37
 Hatano, Takahiro, 71, 75
 Hazra, S, 62, 63, 65, 75
 Hossain, Md Wall, 151
 Hossain†, Md Wali, 134
 Hui, AK, 119, 122
 Hysi, Eno, 51, 54, 55, 75, 77

 Ichikawa, Masatoshi, 55, 76
 Iyengar, AN Sekar, 124
 Iyengar, ANS, 119, 122

 Jain, Shilpi, 113
 Jaman, Abu Ismail, 74
 Jaman, Abu Ismail, 50
 Jamil, Umme, 143, 154
 Jana, Sourav Kanti, 65
 Jana†, Sourav Kanti, 74
 Janaki, MS, 117–124
 Joanny, Jean-Francois, 67, 74
 Joarder, Partha S, 143, 154
 Juelicher, Fran, 74
 Juelicher, Frank, 67

 Kar, Kamales, 139, 153
 Karmakar, SN, 69, 70, 72, 76–78
 Karmakar, Subhajit, 51, 55, 77
 Kato, Naoyuki, 71, 75
 Kaw, PK, 118, 123
 Kaw, Prof PK, 177
 Kawamura, Hikaru, 71, 75
 Khamrui, Susmita, 17, 20, 39, 40
 Khan, Manoranjan, 116, 122, 123
 Khan, N, 57–59, 74, 76, 77
 Khurana, Raman, 113
 Khuyagbaatar, J, 25
 Kolios, Michael C, 51, 54, 55, 75
 Kozakiewicz, Anna, 74
 Kshetri, R, 93–95, 110, 111

- Kumar, A, 110
 Kumar, MC, 147, 153
 Kundu, Anjan, 146, 151, 155, 158
 Kundu, Sangeeta, 160, 162
 Kundu, Sarathi, 62, 63, 65, 75
 Kundu, Souvik, 53, 78
 Kundu, Susmita, 135, 154
 Kundu†, Souvik, 52, 54

 Laha, P, 66, 77
 Lahiri, Avijit, 146, 154
 Lahiri, Chirashree, 25, 38
 Lahiri, S, 22, 23, 26, 37, 38, 119, 124
 Lahiri, Shibojyoti, 16, 39
 Lahiri, Susanta, 21–24, 26, 30, 32, 36, 38, 40
 Le Donne, Alessia, 65
 Le Donne†, Alessia, 74
 Leser, Philipp, 139, 144, 152
 Littlewood, Peter B, 70, 77
 Lombardo, I, 89, 110

 Mahatha, SK, 59–61, 63, 77
 Maiti, Jyotirmoy, 140, 149–151
 Maiti, M, 22, 25, 38
 Maiti, Moumita, 21, 23, 24, 38
 Maiti, Prabal K, 160, 162
 Maiti, RP, 77
 Maiti, Santanu K, 69, 70, 72, 76–78
 Maity, Anup Kumar, 19, 37
 Maity, Chandan, 118, 119, 121, 123
 Majhi, Abhishek, 132, 134, 151
 Majumdar, A, 65
 Majumdar, N, 89, 111
 Majumdar, Parthasarathi, 134, 151
 Majumdar, Pratik, 150
 Majumder, M, 56, 76
 Majumder, Mayukh, 57, 75
 Majumder, Parijat, 14, 37
 Majumder, Sudip, 20, 40
 Mandal, Ajoy, 22, 24, 30, 32, 36, 38, 40
 Mandal, Arun Kumar, 54, 74
 Mandal, Mahatsab, 91, 111
 Mandal, Manoj K, 140, 154
 Mandal, P, 56–59, 74–77
 Mandal, Parikshit C, 30, 38
 Mandal, Swadesh, 22, 23, 26, 30, 40
 Mandal, TK, 40
 Mandal, Mahatsab, 91
 Manikandan, A, 36, 37
 Marick, C, 89, 110
 Mathews, Prakash, 140, 147, 153, 154
 Mazumdar, C, 56, 76
 Mazumder, Pratik, 150, 153, 155
 Meghna, KK, 89, 110
 Menon, Krishnakumar SR, 59–61, 63, 77
 Metya, A, 65, 74
 Midya, A, 57, 58, 74, 77
 Min, BI, 73, 76
 Mishra, Padmaja Prasad, 35

 Mitra, Amrit Krishna, 28, 33
 Mitra, Ankita, 26, 31, 38
 Mitra, P, 60, 78, 143, 147, 148, 152, 153, 156
 Mitra, Piyali, 22, 38
 Mitra, Shouvik, 53, 78
 Mitra, Sukanya, 91, 111
 Modak, Atanu, 113
 Mogurampelly, Santosh, 160, 162
 Mohanty, PK, 68, 70, 71, 73, 74, 78
 Mollick, SA, 65, 74
 Mondal, Mojammel H, 66, 76
 Mondal, S, 60, 64, 78
 Mondal, Santanu, 140, 149–151
 Mondal, Subhendu, 78
 Mukherjee, CD, 59, 75
 Mukherjee, G, 95, 110
 Mukherjee, M, 62, 66, 76–78
 Mukherjee, Manabendra, 60, 67, 75
 Mukherjee, Sanchita, 160, 162
 Mukherjee, Smita, 54, 74
 Mukherjee, Swagata, 113
 Mukhopadhyay, MK, 50, 77
 Mukhopadhyay, S, 89, 111
 Mukhopadhyay, Saikat, 18, 38
 Mukhopadhyaya, Debashis, 34, 39
 Mukti, Kant, 40
 Muralithar, S, 111
 Mustafa, Munshi G, 143, 154
 Mustafa, Munshi Golam, 157
 Mydeen†, K, 59
 Mydeen†, K, 76

 Nag, Somnath, 111
 Nambissan, PMG, 101, 114
 Nandi Ganguly, Bichitra, 88, 90, 100, 101, 103, 110–112, 114
 Nandi, Rana, 155
 Nandi, Debabrata, 24, 28
 Nandi, R, 154
 Nandi, Rana, 134, 154
 Nandi†, Debabrata, 32
 Nandi†, UN, 56
 Nandi†, Debabrata, 37
 Nandi†, UN, 75
 Nandy, M, 25, 29, 36, 37
 Nandy, Maitreyee, 25, 28, 36, 38, 42
 Nath, Seema, 17, 18, 20, 39
 Nath†, S, 21
 Nath†, S, 39
 Nayak, Trayambak, 40

 Paes, Heinrich, 144, 152
 Pagano, A, 90, 110
 Pahari, Biswapathik, 14, 15, 37, 39
 Pai, H, 95, 110
 Pal, Barnana, 80
 Pal, Palash B, 138, 152
 Pal, Palash Baran, 156, 158
 Pal, Rabindranath, 120, 123

- Pal, S, 92
 Pal, Sudipta, 16, 40
 Pal, Uttam, 29
 Palit, R, 112
 Panda, Prabir Kr, 50, 74
 Panda, Sudhakar, 141
 Pani, Bibhusita, 17
 Panigrahi, Swati, 160, 162
 Pankaj, Ravindra, 69, 77
 Paschalis, S, 93, 111
 Patel, KD, 60, 77
 Paul, Rakhi, 18, 39
 Petri, M, 93, 111
 PICASSO collaboration, 153
 Piekarewicz, J, 148, 153
 Poddar, A, 56, 75, 76
 Pond, James, 64, 76
 Pradhan, MK, 95, 110

 Radheep, D Mohan, 57, 75
 Rahman, Atikur, 63, 74
 Rajapaksa, Indrajith, 54, 74
 Ranjan, Amitabh, 17, 39
 Ranu, Brindaban C, 67
 Rao, Mr VV Mallikarjuna, 177
 Rather, N, 92, 111
 Raut, R, 95, 110
 Ravindran, V, 147, 153
 Ray, Mallar, 74
 Ray, Aurkie, 29
 Ray, Mallar, 54
 Ray, Nihar R, 120, 123
 Ray, Nihar Ranjan, 32, 37, 118, 124
 Ray, Pulak, 14, 39
 Ray, Tirtha Sankar, 139, 147, 152
 Raychaudhuri, Prof Amitava, 177
 Raychaudhuri, S, 119, 122, 124
 Raychaudhuri, Swasti, 17, 37
 Reinhard, PG, 147, 152
 Reja, Sahinur, 70, 77
 Roca-Maza, X, 136, 154
 Rodrigues, G, 111
 Rolles, D, 87, 103
 Rolles, Daniel, 87, 103
 Roy Chaudhuri, Chiroosree, 27, 36
 Roy Choudhury, Kamalika, 17, 37
 Roy, Pradip K, 111
 Roy, A, 35, 37
 Roy, D, 53, 74
 Roy, Debarati, 113
 Roy, Debasis, 52, 74
 Roy, M, 53, 74
 Roy, Madhusudan, 50–52, 55, 74, 77
 Roy, Pradip, 91, 111
 Roy, Pradip K, 91
 Roy, Probir, 133, 135, 152
 Roy, Santosh, 92, 111
 Roy, Sarita, 14, 39
 Roy, Shibaji, 137, 142, 146, 149, 153, 154, 157
 Roy, Sourov, 135, 152

 Roy, Sudipendra Nath, 159, 161
 Roy, Sumana, 17, 19, 38, 40
 Roy, Tarun Kanti, 146, 154
 Roychoudhury†, Rajkumar, 122
 Roychoudhury†, Rajkumar, 123
 Roychowdhury, D, 119, 124
 Rudek, Benedikt, 87, 103
 Russotto, P, 90, 110

 S Lahiri, 25
 Sadasivam, Shri VR, 177
 Saha Sarkar, M, 101, 112
 Saha, Biswajit, 62, 74
 Saha, Chandan, 28, 33
 Saha, Debasree, 67, 75
 Saha, Dhriti Ranjan, 60, 75
 Saha, L, 133, 136, 151
 Saha, Partha, 19, 37
 Saha, Priyanka, 38
 Saha, Ratan K, 51, 54, 55, 75, 77
 Saha, S, 89, 110, 112
 Saha, SK, 119, 122, 124
 Saha, Srilekha, 69, 78
 Saha, Sutapa, 40
 Sahin, E, 93, 110
 Sahoo, GS, 29
 Sahoo, RK, 59, 75
 Sain, S, 78
 Samaddar, SK, 139, 142, 144, 152, 153
 Samanta, Dibyendu, 33, 37
 Samanta, Tanusree, 62, 78
 Sandhya Jain, 113
 Sankar, De, 103
 Sanyal, Milan K, 62, 63, 74, 79
 Sanyal, MK, 67, 76
 Sanyal, Prof Milan K, 177
 Saran, PK, 28, 38
 Sarangi, Manas Kumar, 26, 28, 31, 33, 38
 Sardar, M, 26, 37
 Sarkar, Anwesha, 150, 151
 Sarkar, B, 36, 37
 Sarkar, N, 68, 76
 Sarkar, Niladri, 68, 76
 Sarkar, PK, 28, 38
 Sarkar, Prodipta, 38
 Sarkar, Sabyasachi, 118
 Sarkar, Sourav, 91
 Sarkar†, Prodipta, 31
 Sarkar†, P, 57
 Sarkar†, P, 75
 Sarma, Abhisakh, 63, 74
 Satpati, Biswarup, 63, 73
 Selvakumar, K, 111
 Sen, Parongama, 73
 Sen, Prof Susanta, 177
 Sen, Ranjan, 17
 Sen, Siddhartha, 138, 151
 Sen, Udayaditya, 17, 18, 20, 34, 39

Sen†, Parongama, 78
Sengupta, Bidisha, 14, 15, 37
Sengupta, Chaitrali, 33
Sengupta, Joydip, 59, 75
Sengupta, Kaushik, 42, 43
Sengupta, Pradeep K, 14, 15, 37, 39
Sengupta, Sudip, 118, 119, 123
Seth, Banabithi Koley, 29
Seth, Satyajit, 147
Sethi, J, 112
Shanbhag, A, 37
Shanbhag, AA, 25, 29
Sharma, Manjula, 62
Shukla, A, 151
Shukla, PK, 120, 123
Shukla†, A, 136
Shyam, R, 148, 154
Shyam, Radhey, 145, 153
Sil, S, 71, 74
Singh, Gulzar, 110
Singh, Harvendra, 145, 149, 152, 153, 157
Singh, Purnima, 111
Singh, RP, 111
Sinha, Dr RK, 177
Sinha, Mithun, 18, 38
Sinha, Tinku, 96
Son, Sang-Kil, 87, 103
Sood, AK, 160, 162
Sudhakar, Y, 81
Sulaksono, A, 137, 140, 147, 151, 152
Sunil, C, 25, 36, 37
Takao, Toshifumi, 39
Takao†, Toshifumi, 16
Talukdar, D, 56, 75
Talukdar†, Atanu, 32
Talukdar†, Atanu, 37
Tewary, Shri Satish Chandra, 177
Thomas, AW, 148, 154
Tiwari, Santosh R, 23, 38
Tomar, BS, 37
Tomar†, BS, 23
Tripathy, SP, 29
Trivedi, Neha, 159, 161
Tsushima, K, 148, 154
Varzielas, Ivo de Medeiros, 139, 152
Vignaud, G, 67
Vignaud†, G, 76
Vijayan, RSK, 159, 161
Vinas, X, 144, 153
Vishwanath, PR, 133, 151
Vishwanath†, PR, 136
Yamasaki, Shinji, 38
Yamasaki†, Shinji, 31
Yarlagadda, Sudhakar, 69, 70, 77
Yoon, Peter H, 117, 123

